EVALUATION OF STRENGTHENING SCHEMES FOR REINFORCED CONCRETE

MOMENT-RESISTING FRAME STRUCTURES

SUBJECTED TO SEISMIC LOADS

APPROVED BY

DISSERTATION COMMITTEE:

S. KYRIAKIDES.

A mi esposa, Maria Teresa

EVALUATION OF STRENGTHENING SCHEMES FOR REINFORCED CONCRETE

MOMENT-RESISTING FRAME STRUCTURES

SUBJECTED TO SEISMIC LOADS

by

RODRIGO MANUEL JORDAN, INGENIERO CIVIL

DISSERTATION

Presented to the Faculty of the Graduate School of

The University of Texas at Austin

in Partial Fulfillment

of the Requirements

for the Degree of

DOCTOR OF PHILOSOPHY

THE UNIVERSITY OF TEXAS AT AUSTIN

May, 1991

ACKNOWLEDGEMENTS

iv

TABLE OF CONTENTS

LIST OF FIGURES

LIST OF TABLES

CHAPTER 1

INTRODUCTION

1.1 General

Results of a significant amount of experimental and analytical research conducted

during recent decades have been incorporated in current code provisions and have improved

our understanding of the behavior of buildings subjected to strong earthquake motions.

Buildings designed and constructed according to current code provisions are required

to have more lateral strength, and most of all, more energy dissipation capacity than buildings

designed with obsolete codes.   Because there is a large inventory of buildings that were

designed and constructed following these dated code provisions, it is believed that many of

these structures may pose an unacceptable life-safety hazard in the event of a major

earthquake. This fact explains the basic need for identification of such buildings, the evaluation

of their expected seismic performance, and if needed, their seismic strengthening. Seismic

strengthening is a broad term that implies improving the lateral strength and/or ductility of an

existing building.

Existing buildings may need to be strengthened for a variety of reasons, including:

- Upgrading of seismic code provisions

- Damage in previous earthquakes

- Changes in building occupancy

- Design and/or construction errors

While the first point mentioned above is not, per se, an indication that an existing

building needs to be strengthened, it is believed to be strongly tied to why existing buildings

1

may represent a serious hazard to their occupants. The upgrading of seismic code provisions during recent years is a consequence of better understanding of the seismic behavior of structures. Response modification factors to consider the energy dissipation capabilities of the structural system were first incorporated in the 1988 edition of the Uniform Building Code (UBC) [31]. Moment-resisting reinforced concrete frame buildings designed according to the UBC-64 [19] (or earlier editions) are likely to fall in the category of "ordinary moment-resisting space frame buildings", which are now required to be designed for increased lateral force levels, and also, are not permitted in moderate to high-risk seismic zones (seismic zones 2, 3 and 4 defined in the UBC-88). Figure 1.1 shows how the design acceleration spectrum for moment-resisting reinforced concrete frame buildings has been upgraded during the past 26 years by the International Conference of Building Officials [19,30,31]. The differences in the design acceleration spectra illustrated in Fig. 1.1 occurred after recognizing that buildings designed with old versions of this code did not have adequate energy dissipation characteristics, and therefore, should have been designed to have more lateral strength.

Upgrading of seismic code provisions has not been limited to an increase in the design lateral force levels. Confinement requirements in critical zones of the structural elements have also been incorporated, as have provisions to avoid partial or undesired collapse mechanisms. The "strong column-weak beam" design philosophy for moment-resisting frames is strongly encouraged in current code provisions. Plastic hinging of columns is permitted only in the lowest story, while beam hinging is expected to occur at every story level (Fig 1.2). This type of mechanism allows for more rational and uniform ductility demands in the structural components of the building, in contrast to the "strong beam-weak column" concept in which large ductility demands are likely to be concentrated in only a few structural elements (Fig 1.3).
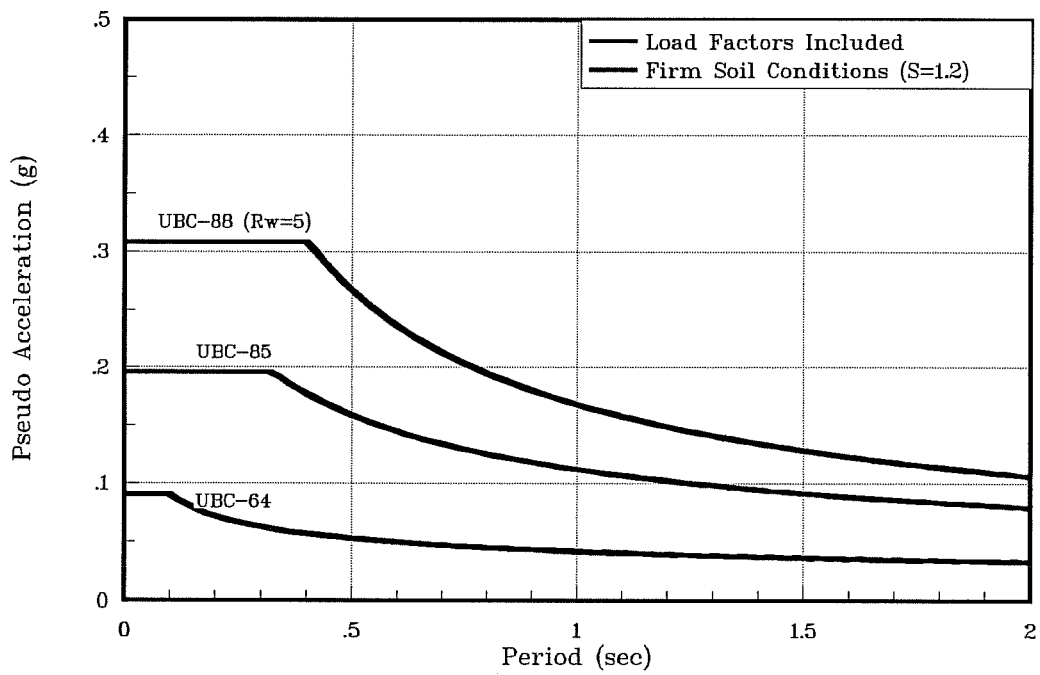
Figure 1.1 Design Spectrum Comparison
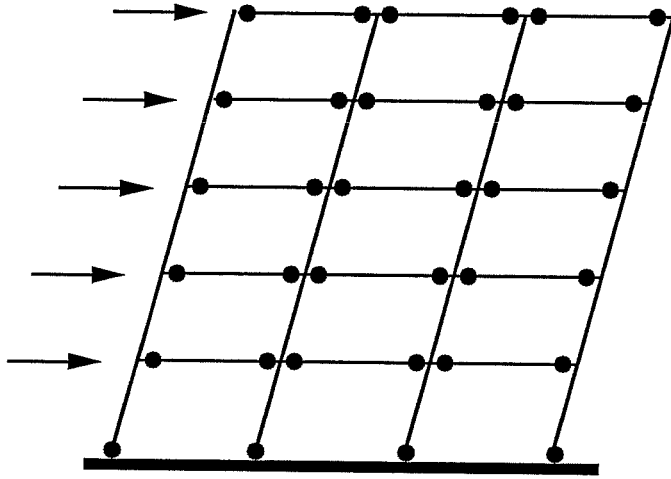
Figure 1.2 Strong Column-Weak Beam Sidesway Mechanism
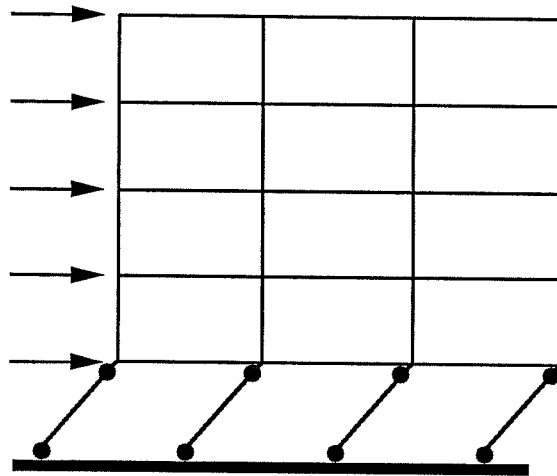
Figure 1.3 Strong Beam-Weak Column Mechanism

Damage experienced by buildings in previous earthquakes has been the primary reason for strengthening and repair operations that have taken place in existing structures. The rehabilitation of damaged buildings involves the assessment of damage suffered by the structural elements and the search for the reasons that caused such damage. The assessment of damage is usually accomplished by a visual inspection of the structure. Permanent deformations, crack widths, spalling of concrete cover, exposure, fracture and buckling of reinforcement are commonly used as guidance for judging the severity of damage. Other indicators of structural damage, such as bond deterioration, are very difficult, if not impossible to determine with a visual inspection.

Changes in building occupancy and design or construction errors are also cases where strengthening of an existing structure may be required.

Although all the points mentioned previously deserve attention, this investigation will be focused on buildings that have been designed using outdated codes, where problems such as low lateral strength and lack of detailing for ductility have been identified.

1.2 Strengthening Strategy

If a given building is found to be deficient in strength and ductility, and the building owner desires to upgrade the building to current code provisions (for example, UBC-88 and ACI 318-89 [16]) it is very likely that modifications to most of the structural elements will be required. This alternative is clearly impractical and not cost efficient. A deficient structure can be strengthened by upgrading a portion of its structural elements, for example, by jacketing beams and columns of the exterior frames, or by adding structural walls to the existing building. In this manner the construction process can be confined to certain areas of the building with

the advantage of reducing the interference with normal operations of the building during construction.

The primary problem that arises when strengthening only selected elements of a structure with limited ductility is that inelastic demands in the unstrengthened elements must be limited, and therefore, a criterion involving force or deformation demand limits for these elements must be established.

The design of any strengthening scheme in which some of the original structural elements will not be strengthened requires a decision about how much stiffness and strength should be provided to strengthened portions of the structure. Designing the strengthened portions of the structure to be able to resist the entire specified base shear by a given code does not guarantee that the resulting design will be adequate. This is due to the fact that unstrengthened elements will deform and be loaded as the structural system deforms, and failure of these elements can occur before the strengthened system reaches capacity.

1.3 Objectives

The main objectives of this study are:

- To extrapolate the experimental results of strengthening techniques to complete structural systems.

- To evaluate and compare the effectiveness of strengthening schemes that consider frame jacketing and/or addition of reinforced concrete walls for improving the seismic performance of lightly-reinforced concrete frame buildings.

- To determine what characteristics of stiffness, strength, and ductility are needed for strengthened portions of the building to obtain satisfactory response of the

retrofitted structure when subjected to a severe ground motion.

- To develop an analytical model to simulate the non-linear response of reinforced concrete structures.

1.4 Scope

A discussion of current procedures for evaluating the seismic performance of existing buildings, followed by a description of different strengthening techniques is presented in Chapter 2. A joint element to model the cyclic response of reinforced concrete beam-column connections is introduced in Chapter 3, along with a description of the analytical model used in this study. In Chapter 4 the main parameters used to define the analytical model are calibrated based on experimental results of reinforced concrete beam-column connection tests. Chapter 5 introduces details for a low and a medium-rise moment-resisting frame building, representative of construction practice in the U.S. in the 50's or 60's. The most significant weaknesses of the buildings are discussed and several strengthening schemes are proposed to improve their seismic response. The dynamic response of the strengthened buildings to selected ground motions, assuming the buildings to be fixed at the base, is used to assess the effectiveness of the strengthening schemes. Emphasis is placed on the behavior of the unstrengthened elements of the retrofitted buildings. A generalization of the results obtained in Chapter 5 is presented in Chapter 6. Design implications for strengthening existing buildings with limited ductility are discussed. Finally, a summary of the findings and conclusions resulting from this study and recommendations for future research are presented in Chapter 7.

CHAPTER 2

BACKGROUND

2.1 Introduction

The first step in evaluating an existing building that is a suspect for poor seismic performance during future earthquakes is an evaluation of the structural characteristics of the building. Collecting the necessary data may be a difficult task. Availability of the original drawings and calculations may considerably simplify the evaluation process. However, a detailed field inspection is always necessary to discover discrepancies between the original drawings and the building as constructed, and to asses the influence of non-structural elements in the dynamic response of the building.

In Japan, damage to many buildings during the 1968 Tokachi-Oki earthquake triggered the need for investigating different strengthening techniques and developing guidelines for evaluation, repair and strengthening of buildings. In 1977 the Japan Disaster Prevention Association published two standards: one for the evaluation of existing reinforced concrete buildings, and the other for design guidelines used in seismic retrofitting. Both standards have been recently revised and published [32,33]. Specific recommendations and formulas are provided to evaluate existing buildings and to asses the lateral load capacity of different strengthening techniques. The case where buildings contain structural elements with different deformation capacities is also addressed and taken into account by a performance index, I_o, that considers the lateral strength and ductility of different structural elements within the building, time deterioration effects, and the influence of stiffness and/or mass irregularities.

In the United States, the Applied Technology Council has recently published guidelines

8

to assist the structural engineer in the evaluation process. The evaluation methodology proposed in ATC-14 [28] and ATC-22 [23] is aimed to identify "hazardous buildings" that may endanger human lives in the event of a future earthquake. A building is considered to be hazardous if one or more of the following events occurs, or is likely to occur, during an earthquake [28]:

- The entire building collapses,

- Portions of the building collapse,

- Components of the building fail and fall,

- Exit and entry routes are blocked, preventing evacuation and rescue of the occupants.

The objective of the evaluation process is to determine whether any of these events is likely to occur during the lifetime of the building.

For evaluating moment-resisting cast-in-place concrete buildings, ATC-14 provides a list of performance characteristics that have been reported as the main cause of damage to this type of buildings during previous earthquakes. A part of this list from Ref. 28 is reproduced below.

- "Buildings with substantial plan irregularities, such as T, L, U, or cruciform shapes, can exhibit large torsional effects. Concentration of damage is likely to occur at re-entrant corners if special reinforcement or joint separation has not been provided.

- Buildings with abrupt vertical changes in stiffness and/or strength have performed poorly in past earthquakes.

- Large tie spacing in columns can lead to lack of confinement of the

concrete core and/or shear failures.

- If the column shear strength is insufficient to develop the full moment

  hinge capacity, the column can exhibit a brittle shear failure.

- Insufficient column lap lengths can cause the concrete to spall.

- Inadequate reinforcing of beam-column joints or location of beam bar

  splices at columns can lead to joint failures.

- Insufficient anchorage of shear tie reinforcement in column cores can

  prevent the column from developing its full shear capacity.

- Lack of continuous beam reinforcement can cause hinge formation during

  load reversals".

If as a result of the evaluation process there is sufficient evidence to believe that the

building under investigation may pose unacceptable life-safety hazards to the occupants, the

building should be strengthened. Several strengthening schemes can be visualized to improve

the seismic performance of the building. A schematic representation of possible strengthening

schemes is presented in Fig. 2.1.

Although the ATC-14 and ATC-22 recommendations specify the minimum lateral load

level that an existing building should be able to withstand (which depends on the response

modification factor, R_w [28] or R [23]), there are no explicit recommendations regarding the

lateral load level that the retrofitted building should be designed for. For example, if the

building to be strengthened has been classified as "Ordinary Moment Frames of Reinforced

Concrete" [23], and a strengthening scheme consisting of the addition of reinforced concrete

infill walls to some frames of the building is being considered, should the retrofitted building

be designed for a lateral force level consistent with the response modification factor associated
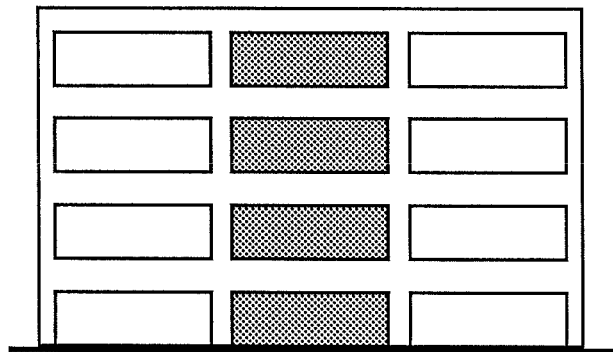
a) Infill Walls
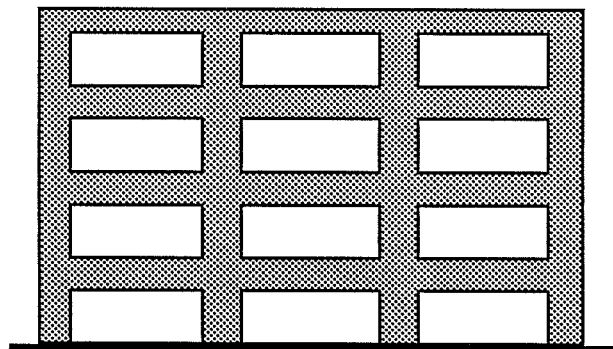
b) Frame Jacketing
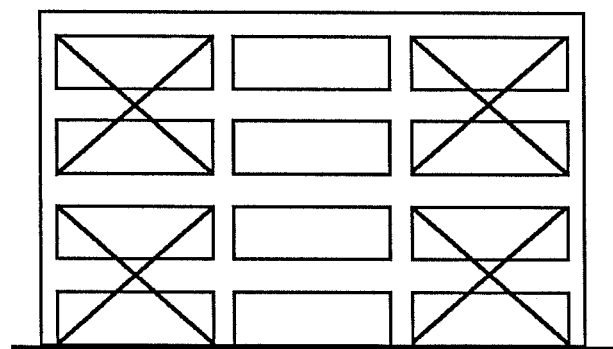
c) Steel Braces

Figure 2.1 Strengthening Schemes

with Ordinary Moment Frames of Reinforced Concrete buildings (R=2), or with the response factor associated with Reinforced Concrete Shear Wall buildings (R=5.5) ? One of the objectives of this study is to provide an answer to this question.

2.1.1 Strengthening with Concrete Infill Walls

Strengthening by using reinforced concrete infill walls can substantially increase the lateral strength and stiffness of a building. Ductility can also be improved if the infill wall-frame system is forced to fail in a flexural mode, and slip at the interface between the infill wall and existing frame is minimized. This can be accomplished by encasing (jacketing) the boundary columns and casting them at the same time as the infill wall [25] (Fig. 2.2). Wedge anchors, epoxy grouted dowels or other type of anchors placed around the existing frame are commonly used to transfer shear forces coming from the slab into the wall. Experimental results reported by Sugano [34] show that the lateral strength and hysteretic behavior of cast-in-place infill walls is about the same as similar monolithic specimens. The main problem that is likely to arise when using infill walls is that foundation modifications may be required to accommodate large seismic overturning moments.

2.1.2 Strengthening by Element Jacketing

Providing a concrete jacket around existing columns can considerably increase the shear strength and ductility of columns with inadequate shear capacity. If it is not desired to increase the flexural strength of the member, a gap should be left between the beam and column (Fig. 2.3).

Jacketing beams and columns (frame jacketing) of selected frames of a building system
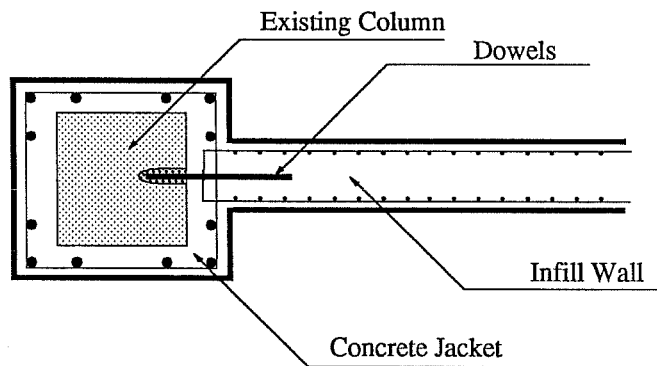
Figure 2.2 Infill Wall with Jacketed Boundary Column

a) Elevation

b) Column Cross Section
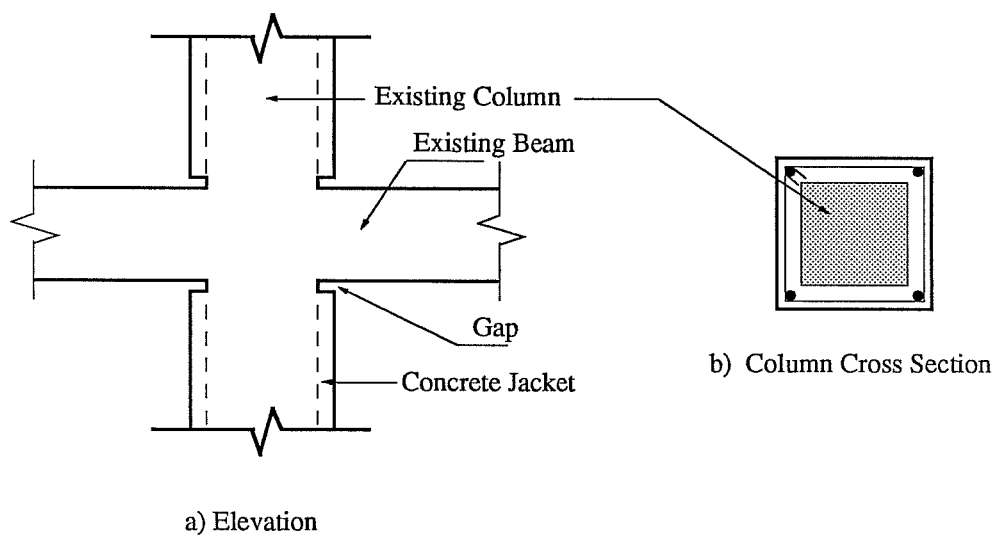
Figure 2.3 Column Jacketing

can increase the lateral strength of the building. Longitudinal steel reinforcement should be made continuous through the beam-column connection, and confinement of the joint must be assured. Confinement of the joint can be accomplished by placing hoops or a prefabricated steel cage around the joint (Fig. 2.4) [35]. Although the ductility of jacketed frames can be considerably improved by this technique, the increase in building ductility will depend on the characteristics of the unstrengthened frames of the building. Frame jacketing may be appropriate for a building in which the primary problem is a lack of lateral strength, but which has adequate ductility. This may be the case for an existing building designed with current code provisions in which a change in building occupancy may require strengthening of the building. For an existing building in which a lack of ductile detailing has been identified as the main problem, frame jacketing can increase the lateral strength, but increase in ductility of the retrofitted structure is likely to be limited by the deformation capacity of the unstrengthened elements of the building.

The main advantage of this technique is that few or minor foundation modifications are likely to be required. From an architectural standpoint, minor changes in the building layout can be anticipated. This technique is labor intensive, which is a disadvantage in countries where labor is expensive.

2.1.3 Strengthening with Steel Braces

The lateral strength of a building can be increased by the use of steel braces in selected bays of the existing frames. The connection between the braces and the surrounding frame can be achieved through the use of epoxy grouted dowels or other type of anchors. Because the bracing system will attract most of the seismic lateral forces, shear and axial

strength of the surrounding columns should be checked. The use of steel channels attached

to existing columns may be used [26] to confine existing columns and to increase their axial

capacity. Providing a concrete jacket to an existing column may also be an alternative.

Inelastic buckling of braces must be prevented to achieve good energy dissipation and to limit

large local deformations at brace connections that may lead to failure [36]. Inelastic buckling

can be prevented if the brace slenderness ratio is low enough to achieve yielding prior to

buckling. The other alternative is to design the bracing system so that buckling is elastic, as

for cables. In this last alternative the bracing system should be designed to respond in the

elastic range, since little energy dissipation can be expected in a system with braces that buckle

elastically.

2.2 Experimental Results

2.2.1 General

Three primary objectives can be identified as the goal of a strengthening operation:

(a) increase the lateral strength, (b) increase the ductility, or (c) increase both, strength and

ductility. A conceptual representation of these alternatives is presented in Fig. 2.5 [49].

Much of the research in the area of strengthening and repair of structures has been

done following destructive earthquakes. Emphasis has been placed on developing connection

techniques between existing and added structural elements, behavior of infill walls,

subassemblages, jacketing of beams and/or columns, and addition of steel braces.

Typical load-deflection relationships for different retrofitting alternatives for reinforced

concrete frames, obtained by Japanese researchers [37,38,39,40] on 1/3 scale specimens and

summarized by Sugano [49], are presented in Figure 2.6. Results obtained for cast-in-place
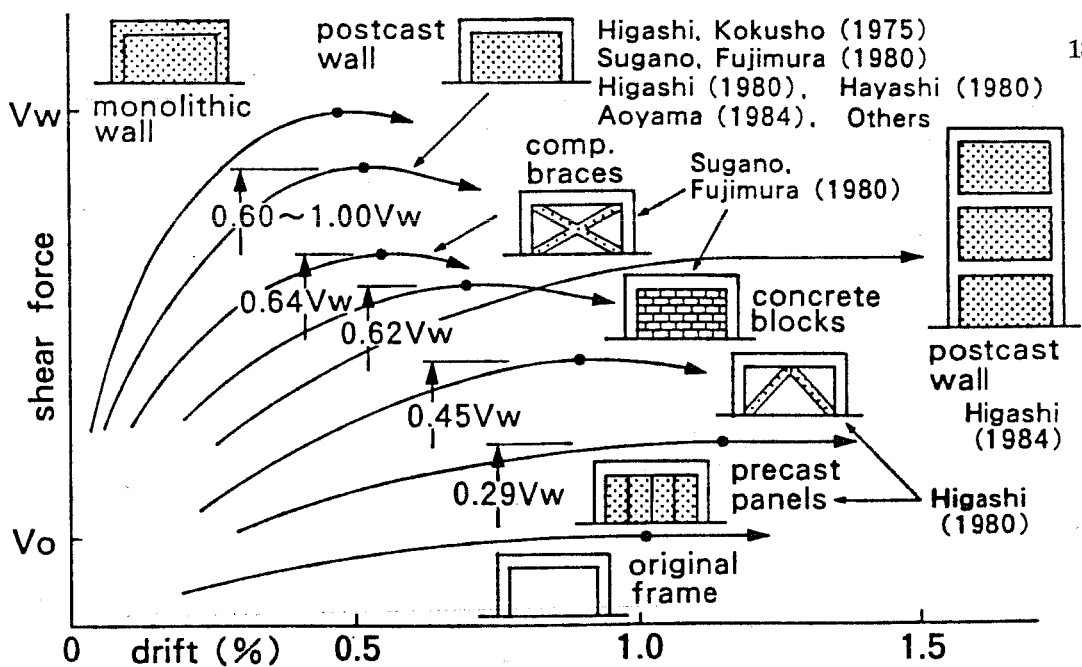
Figure 2.6 Typical Load-Deflection Relationships for Retrofitted Frames (from Ref. 49)
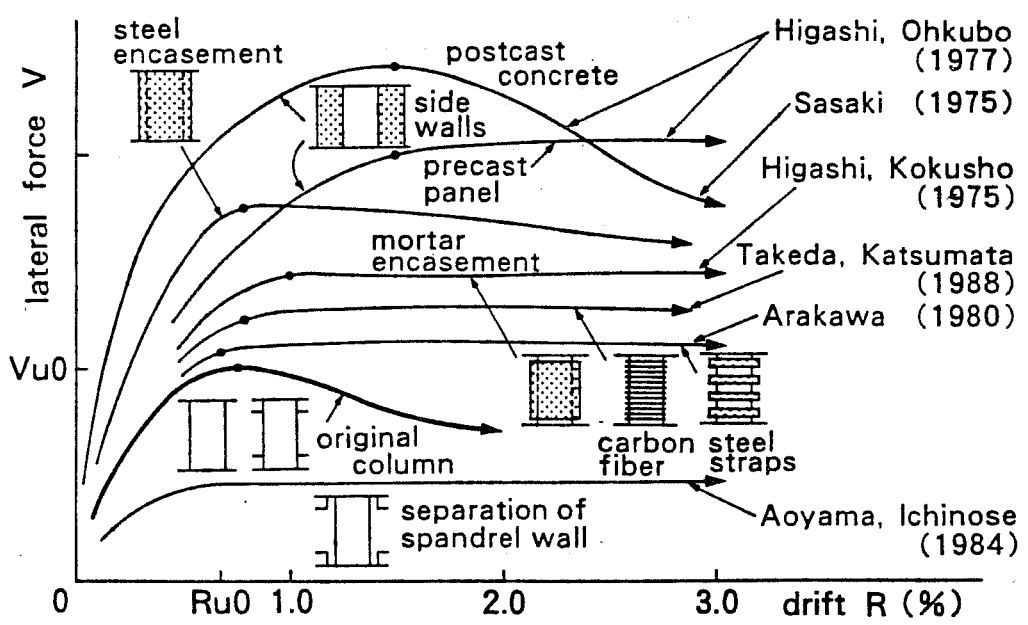
Figure 2.7 Typical Load-Deflection Relationships for Retrofitted Columns (from Ref. 49)

infill walls showed that providing an adequate connection between the existing frame and wall resulted in almost the same strength as monolithic walls. In a three-story frame retrofitted with infill walls by Higashi [41], lower lateral strength but considerably higher ductility associated with flexural behavior was observed, in contrast with the shear-dominated behavior exhibited by the one-story frames.

For columns weak in shear, the use of concrete or steel jackets, steel straps, or side walls can considerably improve their behavior by changing a brittle shear failure mode to a more ductile flexural failure. Typical load-deflection curves obtained by Japanese researchers [38,42,43,44,45,46] using these techniques (summarized by Sugano [49]), are presented in Fig. 2.7. A considerable increase in ductility can be observed, with low gain in lateral strength in most situations. Strengthening with side walls increased the strength too, but a reduction in the clear length may force an undesired shear failure of the beams.

Experimental studies conducted at the University of Texas at Austin to examine connection techniques, behavior of infilled walls, and jacketing of beam and/or column connections are briefly reviewed next. Finally, experimental results representing the behavior of lightly-reinforced beam-column connections are discussed.

2.2.2 Connections

Bass [47] conducted an experimental investigation to study the interface shear-transfer capacity between new concrete cast against an existing concrete surface. Thirty-three push-off specimens (Fig. 2.8) simulating an existing concrete column and an added shear wall or wing wall were tested in direct cyclic shear. Among the variables analyzed were: amount and embedment depth of the interface shear reinforcement, casting procedures, and preparation
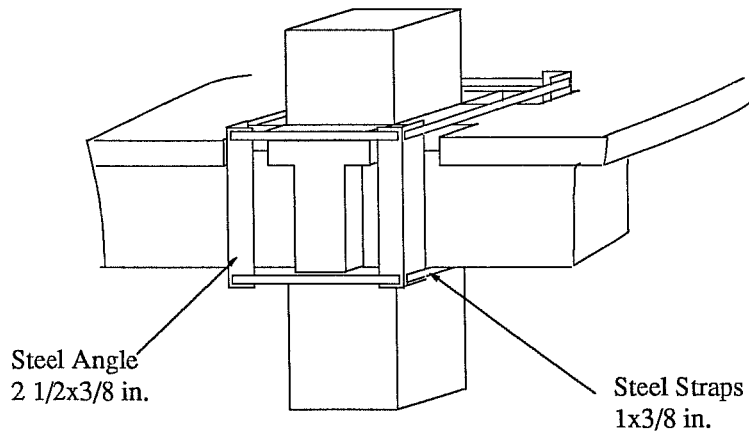
Figure 2.4   Steel Cage Assembled around Beam-Column Joint   (from Ref. 35)
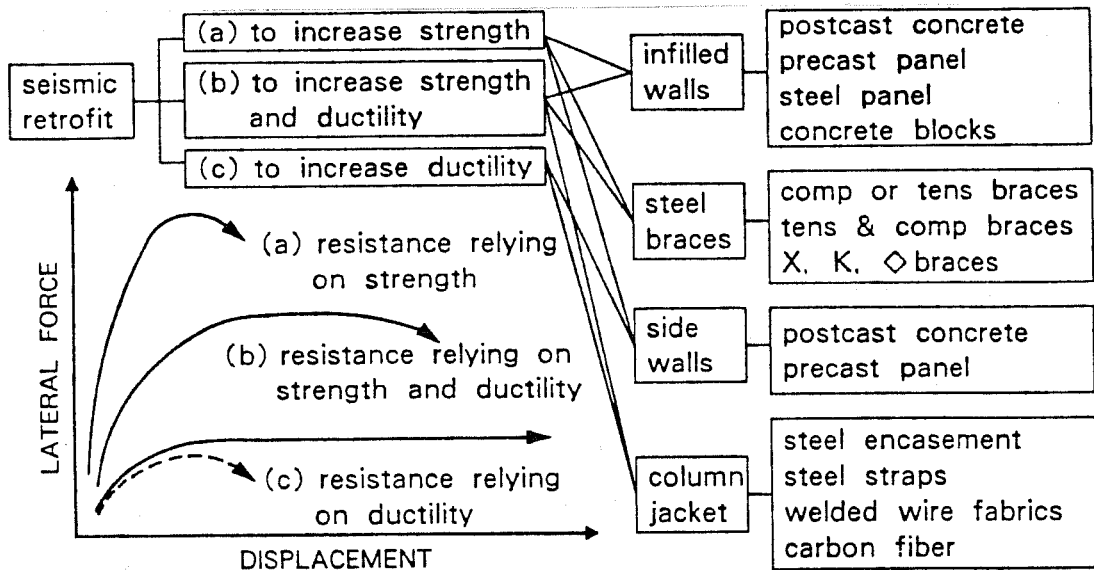
Figure 2.5 Concepts of Seismic Strengthening (from Ref. 49)
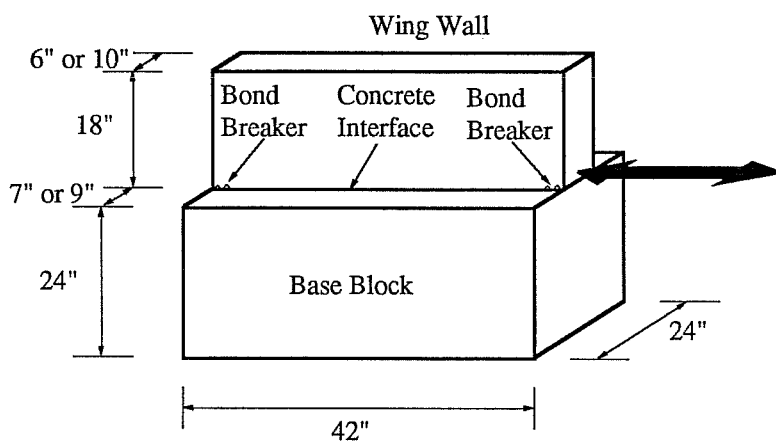
Figure 2.8 Basic Push-Off Specimen (from Ref. 47)

Elevation   Plan   Side
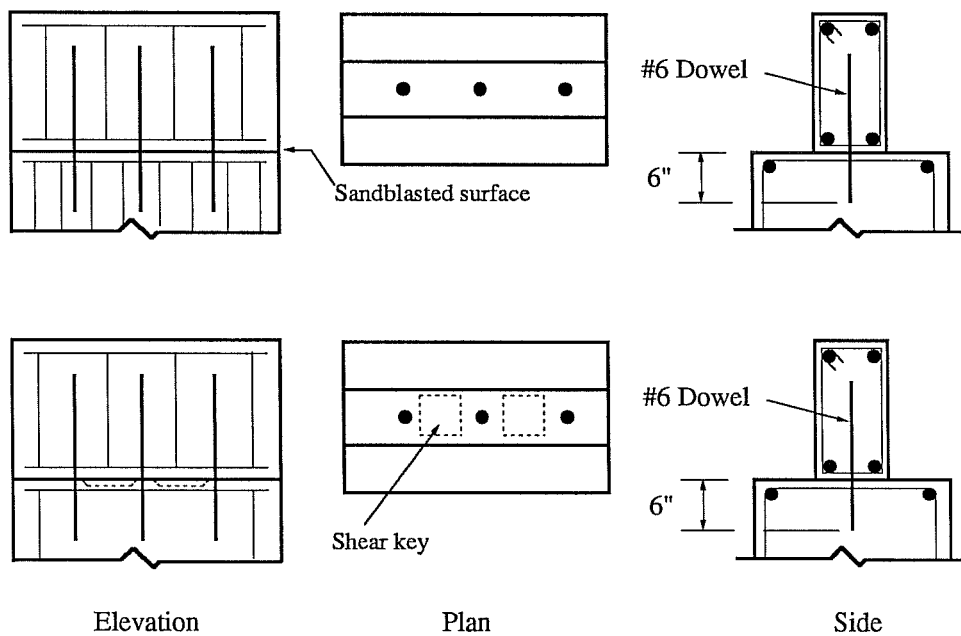
Figure 2.9 Push-Off Specimen Details (from Ref. 47)

of the concrete interface area.

Interface reinforcement typically consisted of Grade 60, #6 dowels spaced at 6", 10", and 12", with embedment lengths of 3", 6" or 12". Full development length of the dowels was provided in the wing walls. Vertical, horizontal, and overhead casting positions were considered. Interface surfaces were either untreated, sandblasted, chipped to 1/4" amplitude, or had shear keys. The use of bonding agents was also studied. Typical push-off specimen details are illustrated in Fig. 2.9.

The main results obtained by Bass can be summarized as follows:

- Generally, increasing the amount of interface reinforcement resulted in higher shear capacity.

- An increase in the embedment length of interface reinforcement resulted in an increase in the peak shear transfer capacity and higher shear capacities at large slip levels.

- Specimens in which some kind of interface surface preparation was performed showed no significant effects on the residual interface shear capacity at large slip levels. Specimens with an untreated surface exhibited the lowest peak shear capacity.

- Horizontal or vertical casting positions showed similar peak and residual shear capacities. The overhead casting position showed a lower peak shear capacity, which was attained at a larger slip level. However, the residual shear capacity was almost the same as for the horizontal or vertical casting positions.

- The design strength equations and the dowel embedment length of the ACI 318-83 shear friction provisions provided a conservative estimate of the peak shear transfer

capacity of all the specimens analyzed. For specimens with dowel embedment lengths of 3", the strength at low slip levels (0.04") dropped below ACI requirements. Specimens with dowels embedded 6" exhibited higher shear transfer capacity than their respective ACI 318-83 design strength for slip levels up to about 0.1", while specimens with 12" embedment depth maintained a capacity above the ACI design strength for the entire range of displacement (0.5").

2.2.3 Strengthening of Frames Using Infill Walls.

Three one-bay, single story, 2/3 scale non-ductile moment resisting frames infilled with reinforced concrete walls were tested by Gaynor [48]. One wall was solid, one had a door opening, and the other had a window opening. The frames were infilled with 5-1/4-in. shotcreted walls. The primary reinforcement of the walls consisted of #4 bars spaced at 12" in the horizontal and vertical directions. The connection between the wall and the existing frame was achieved with #6 dowels that were epoxy-grouted 9-in. into the existing columns, foundation and top beam. Additional reinforcement was placed around the window and door openings.

The frame design was typical of U.S. practice in the 1950's. The columns featured wide tie spacing and a short compression splice that was inadequate for developing the tensile yield of the spliced bars.

All three specimens exhibited a brittle failure when subjected to cyclic lateral loads. In the solid wall and the wall with a door opening, a tensile failure of the splice region in the existing columns precipitated a tension failure along the length of each wall. In the wall with a window opening, failure was controlled by crushing of concrete close to the corners of the

opening and shear failure of the boundary column. Slip between the infill wall and top beam was small in all cases. The infill with door opening exhibited the most slip (approximately 0.06") at peak resistance, revealing good behavior of the connection.

The results obtained by Gaynor showed that strength of the infill walls was limited by failure of the lightly-reinforced boundary frame. A splice failure is not ductile and is undesirable for seismic design where energy dissipation capacity of the structure is essential for good seismic performance.

Shah [24] and Jimenez [25] continued the work done by Gaynor. The same boundary frames tested by Gaynor were used, and the damaged infill with a door opening and solid infill were removed and replaced by cast-in-place 5-1/4-in. walls. A modified reinforcing scheme was considered in both cases.

In the infill with a door [24], a group of 3#8 bars were placed adjacent to the column to supplement the spliced column reinforcement. The bars were epoxy grouted to the top and foundation beams and spliced at midheight. Spiral reinforcement was provided to confine the splice region of the #8 bars. Reinforcement details for this specimen are presented in Fig. 2.10.

Test results indicated a 35% increase in the lateral strength of the specimen, with respect to the shotcreted infill with door opening. Maximum displacements at failure were also larger. However, still a column splice failure was the cause for failure in one loading direction, while crushing of the concrete near the door opening in the download pier was responsible for failure while loading in the opposite direction.

In the cast-in-place solid wall tested by Jimenez, reinforced concrete jackets around the existing columns were provided to improve the behavior of the column splice. The wall was
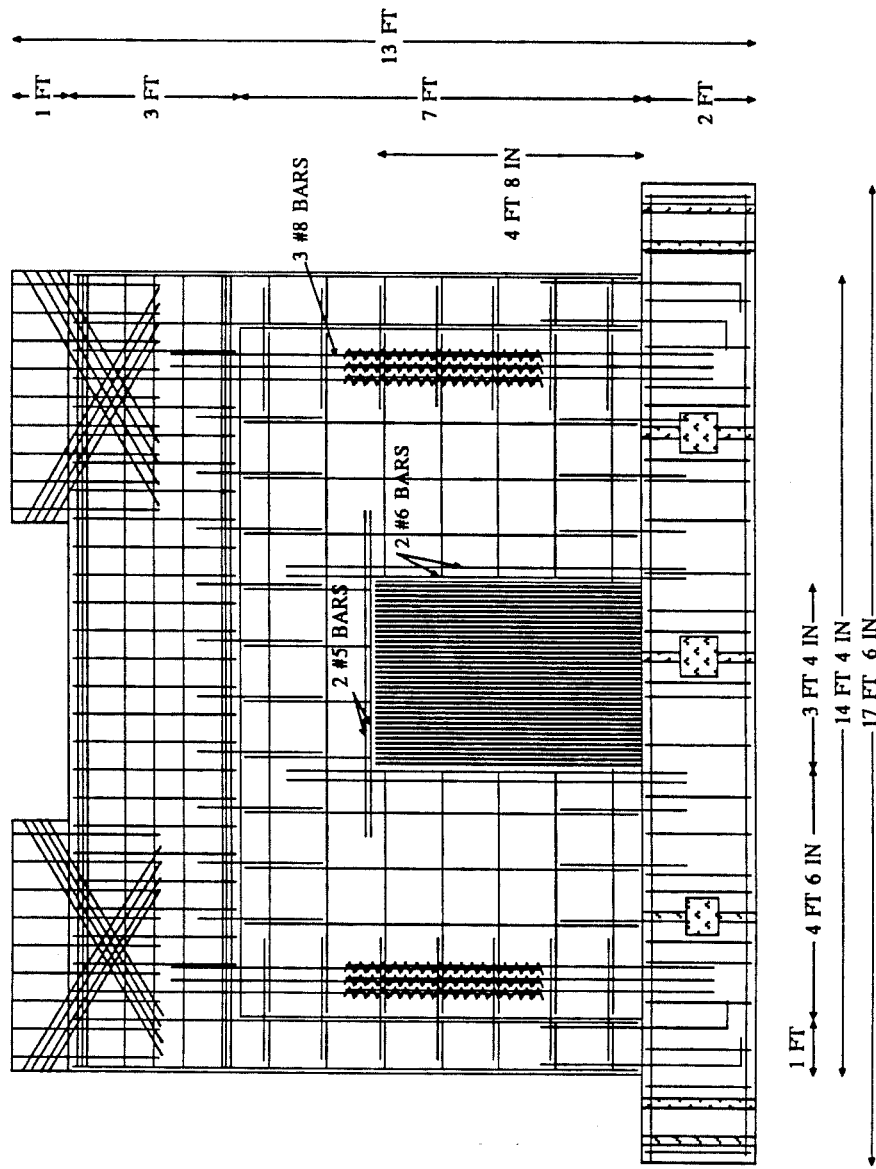
Figure 2.10 Infill with Door - Geometry and Steel Layout (from Ref. 24)
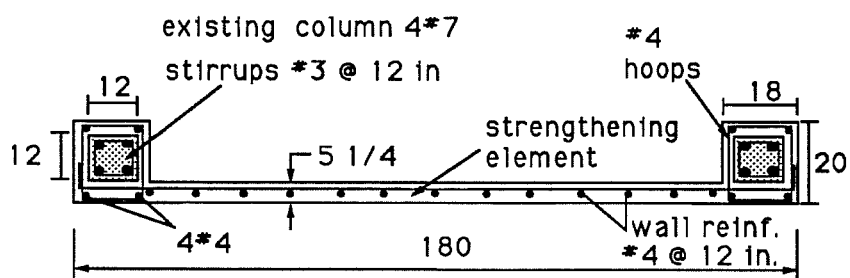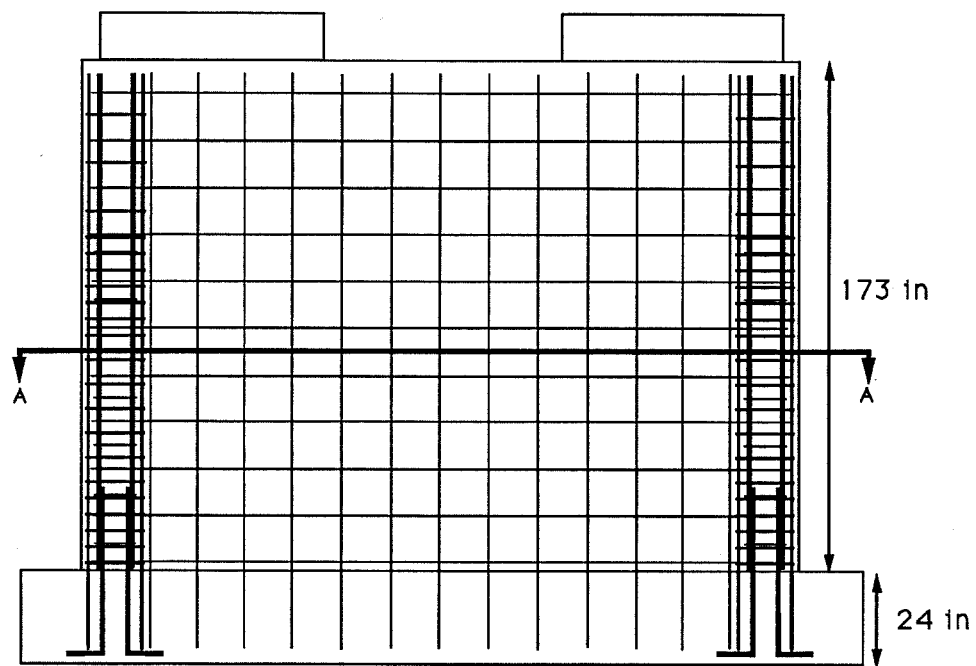
Figure 2.11 Cast-in-Place Solid Wall Details (from Ref. 25)

eccentric to the plane of the frame, and was connected through epoxy-grouted dowels inserted in the beams and columns. Specimen details are shown in Fig. 2.11.

Test results indicated that the concrete jackets considerably improved the behavior of the existing column splice, allowing steel strains well beyond yield (6.5 times the yield strain when the test was stopped) without indication of column distress. Measured strains in the wall reinforcement at the base also exceeded the yield strain. Because the capacity of the specimen exceeded that of the loading system, the specimen could not be failed. However, the load-deflection response was nearly flat when the test was stopped, indicating that the ultimate load in flexure was almost reached. A maximum nominal shear stress of $6.84\sqrt{f_c'}$ was computed at the end of the test. Negligible slip was observed between the wall and surrounding frame. Very low strains developed in the epoxy-grouted dowels suggested that wider spacing of the connecting dowels may be used when a jacketed column is provided as a boundary element for the infill wall. Further experimental results are needed to confirm this observation.

2.2.4 Strengthening of Frames Using Beam and/or Column Jacketing.

An interior beam-column connection subassemblage designed following U.S. practice in the 1950's was designed and tested to failure in bi-directional cyclic loading by Alcocer [6,35]. The specimen exemplified the strong beam-weak column concept. The damaged specimen was repaired with a concrete jacket around the existing column and tested to failure. Three similar specimens were also tested. Two of them considered jacketing of the column only with different arrangements of the longitudinal reinforcement (bundles and distributed reinforcement). The third one involved jacketing both beams and columns. In all the jacketed specimens a steel cage (Fig. 2.4) was provided to confine the joint region. This avoided the

Summary of Experimental Program

Test name	Specimen before test	Jacketing Columns	Beams	Bundled column bars
ME1	Undamaged	—	—	—
ME1-R	Damaged	x		x
ME2	Undamaged	x		x
ME3	Undamaged	x		
ME4	Undamaged	x	x	

Side view

Top view

165 in.

75 in.

70 in.

c= 12" ME1
c= 20" ME1-R
        ME2
        ME3
        ME4

c

70.4 in.

63.2 in.

70.4 in.

b

b= 8" ME1
      ME1-R
      ME2
      ME3
b= 15" ME4

b

17 ft.
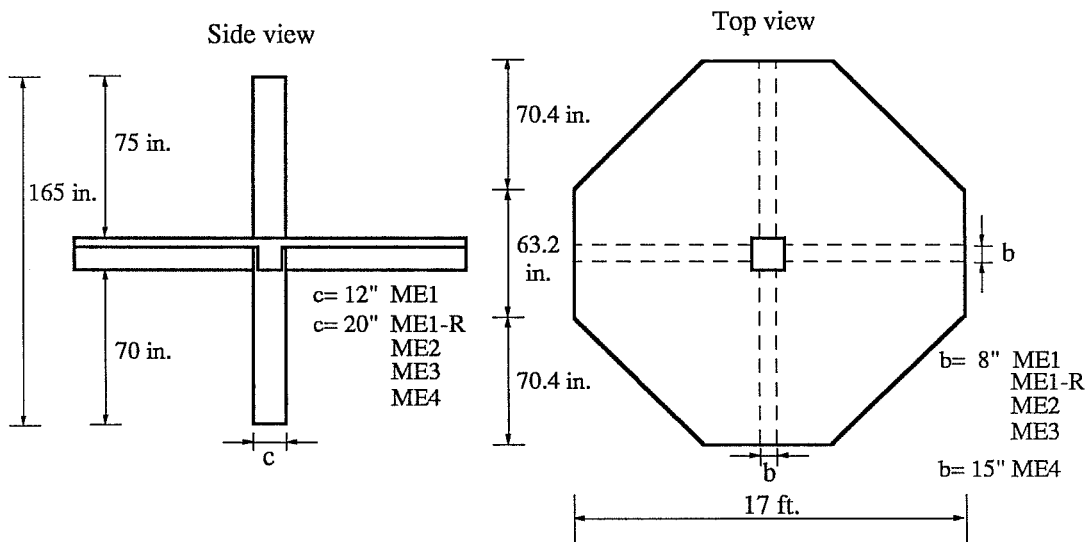
Figure 2.12 Experimental Program and Specimen Details (from Ref. 35)

need for drilling holes through the existing beams to place confining ties in the joint. A
summary of the test program and specimens tested by Alcocer is presented in Fig. 2.12.

Preliminary results obtained by Alcocer may be summarized as follows:

- The original beam-column connection (ME1) exhibited, as expected, very poor
  performance, with concentration of damage in the columns.

- The strength of the repaired specimen (ME1-R) was more than double its original
  strength, and its general response improved, in terms of energy dissipation and
  stiffness degradation, with respect to the original specimen. However, less stiffness
  and strength with respect to the jacketed, initially undamaged specimens (ME2 and
  ME3) could be observed.

- The specimen in which beams and columns were jacketed (ME4) exhibited the
  highest strength and stiffness. No negative effects of the perforations in the slab,
  through which the concrete of the jacketed beams was cast, was reported.

- No negative effects due to bundled column bars were reported. In fact, it was
  reported that the specimen with bundled bars exhibited better performance than the
  one with distributed reinforcement, primarily because bundled bars in the corners
  provide the greatest capacity for biaxial bending.

- Although eventually, all the strengthened specimens exhibited a shear failure of the
  joint at large amplitude cycles, the steel cage proved to be very effective in confining
  the joint region.

- Bond loss between the existing and new concrete was not detected in any of the
  tests.

- Story shear versus drift angle envelopes for the five specimens tested by Alcocer are
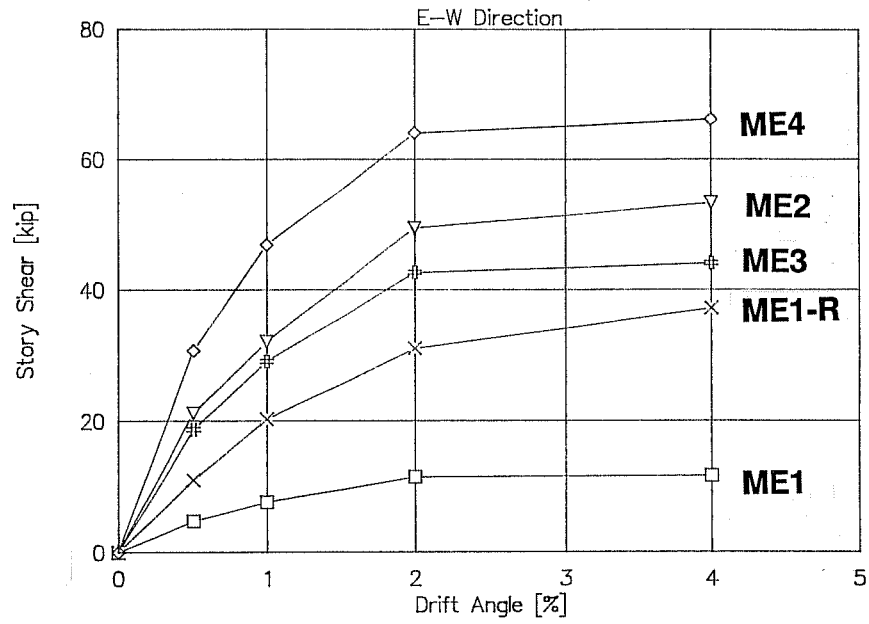
Figure 2.13 Envelopes of the Response of Frame Jacketing Specimens

EW Direction (from Ref. 35)

presented in Fig. 2.13. It is of interest to note that the shape of the load-deflection response is very similar for all the specimens (original and strengthened). As will be seen later, this characteristic in most cases will limit the extrapolation of performance of strengthened subassemblages to complete structural systems in which only some of the portions of the structure are retrofitted.

2.2.5 Tests of Lightly-Reinforced Beam-Column Connections

Very little information is available in the literature related to experimental results obtained from lightly-reinforced beam-column connections. Experimental work in this area is relevant because it can provide valuable information to assess the vulnerability of this type of structure.

Pessiki et al. [22] tested to failure, with cyclic loading, ten cruciform-shaped reinforced concrete beam-column joints detailed according to American practice in the 1950's. Columns were 16 inches square, and beams 14 in. wide by 24 in. deep. Typical transverse reinforcement in columns was #3 bars spaced at 16 or 14 in. Columns in all specimens were provided with about 2% longitudinal reinforcement with different bar arrangements (4#10, 6#8, or 8#7). The longitudinal reinforcement of the columns was spliced above the top of the beam, and a 30-bar diameter lap length was provided in all cases but one, in which the bars were made continuous. Beam bottom longitudinal reinforcement was anchored only six inches into the joints in four of the specimens. Joint ties were provided in only two of the specimens. Axial load in the columns was rather high (0.4 $f_c A_g$) for all specimens that featured a short compression splice and continuous beam bottom reinforcement.

The primary variables studied in Pessiki's tests were the effect of the splice in the

columns, amount of joint reinforcement, and behavior of the specimens with embedded bottom reinforcement.

Pessiki reported that the splice performed adequately in specimens that featured a short compression splice and continuous beam bottom reinforcement. This was attributed to the steep moment gradient on the columns. Additional experimental research is needed to confirm and generalize this observation. Three factors may be mentioned that do not allow easy extrapolation of these results to existing buildings:

a) The splice length provided in Pessiki's tests exceeds the 24-bar diameter lap length recommended in ACI 318-63 [17].

b) The heavy axial load acting on the column of these specimens may have prevented a splice failure.

c) It would have been interesting to know the actual tensile stress developed in the spliced column bars at failure of the specimens, and if failure of the specimen was controlled by the capacity of the beams.

Other observations reported by Pessiki follow:

Specimens with continuous beam bottom reinforcement resisted joint shear stresses of about $13 \sqrt{f_c'}$, while maximum joint shear stresses for specimens with embedded reinforcement (6 in.) averaged $10.4 \sqrt{f_c'}$. Pullout of the beam bottom reinforced is likely to have damaged the joint region.

Failure of the specimens with embedded reinforcement was always initiated by pullout of this reinforcement. No correlation was found between the peak pullout resistance and the level of axial force, the presence of transverse reinforcement within the joint region, or the diameter of the embedded bars.

CHAPTER 3

ANALYTICAL MODEL

3.1 Introduction

The analytical modeling of the non-linear behavior of reinforced concrete structures has been and still is the subject of extensive research. The need for developing such models arises from the well known fact that buildings designed for earthquake loading according to current code provisions are expected to undergo significant inelastic deformations when subjected to severe ground motions. As a result, the assessment of inelastic deformation demands is then crucial for the proper detailing of structural components.

The analytical representation of the dynamic response of buildings subjected to arbitrary ground motions can be separated into two phases. The first one is common to any structural system (reinforced concrete, steel, masonry, etc.), and involves the selection of the relevant degrees of freedom (DOF) of the structure, formulation of the stiffness matrix for the structural elements, identification of the numerical procedure for solving the equations of motion, and among others, the inclusion of equivalent viscous damping. The second phase, which is dependent on the material actually being used in the structure, involves the definition of hysteresis rules to account for stiffness and strength deterioration of the structural elements, pinching of the hysteresis loops and, for reinforced concrete members, the consideration of bond-slip deformations and bond deterioration due to cyclic loading.

These two aspects are discussed in this chapter. The calibration of the main parameters of the analytical model is discussed in Chapter 4.

3.2 General Considerations.

Numerical representation of a multi-story building subjected to earthquake-type loading must address the need to identify and reproduce essential behavior, while keeping the model as simple as possible.

The numerical model that was developed for this investigation, which is a modified version of the computer program LARZWD [3] developed at the University of Illinois, represents planar reinforced concrete buildings on a rigid base subjected to horizontal ground motions or lateral forces applied at the story levels. The main assumptions incorporated in the analytical model include the following:

- The building is idealized as a series of planar frames linked at the story levels by rigid diaphragms.

- One dynamic translational DOF per story level is considered.

- Masses are assumed to be lumped at each story level.

- Torsional response of the building is neglected.

- Vertical accelerations of the building due to vertical ground accelerations are not included.

- Axial deformation of columns and walls are included, but assumed to be in the elastic range.

- Elastic shear deformations of flexural elements (beams, columns, and walls) are included.

- Joint shear distortions are considered.

- Secondary moments due to gravity loads can be included (P-Δ effect).

- Non-linear response of beams, columns, and walls is assumed to be dominated by

flexure.

- Non-linear response of joint cores is assumed to be dominated by shear.

- Slip of reinforcement is considered at beam-column joints.

3.3 Equation of Motion

The equilibrium equations of a multidegree of freedom system (1 dynamic DOF per floor) subjected to a ground acceleration $\ddot{x}_g$, written in its incremental form is:

$$[M]\{\Delta\ddot{v}\} + [C]\{\Delta\dot{v}\} + [K]\{\Delta v\} = -[M]\{1\}\Delta\ddot{x}_g \qquad (3.1)$$

where [M], [C], and [K] are the mass, damping and tangent stiffness matrices. The vectors $\{\Delta\ddot{v}\}$, $\{\Delta\dot{v}\}$, and $\{\Delta v\}$ represent the incremental accelerations, velocities and displacements respectively.

The average constant acceleration method [1] was used to numerically solve the set of equations (3.1). If we assume that the acceleration $\{\ddot{v}_n\}$, velocity $\{\dot{v}_n\}$, and displacements $\{v_n\}$ are known at a time t_n, the incremental velocity and displacement can be computed as follows:

$$\Delta\dot{v} = \ddot{v}_n\Delta t + \frac{1}{2}\Delta\ddot{v}\Delta t \qquad (3.2)$$

$$\Delta v = \dot{v}_n\Delta t + \frac{1}{2}\ddot{v}_n(\Delta t)^2 + \frac{1}{4}\Delta\ddot{v}(\Delta t)^2 \qquad (3.3)$$

where Δt is the integration time step.

From Eq. (3.3) the incremental acceleration can be expressed as

Substituting Eq. (3.4) into Eq. (3.2) yields

Finally, substituting equations (3.4) and (3.5) into (3.1) gives a set of linear equations for the

$$\Delta \ddot{v} = 4\frac{\Delta v}{(\Delta t)^2} - 4\frac{\dot{v}_n}{\Delta t} - 2\ddot{v}_n \qquad (3.4)$$

$$\Delta \dot{v} = 2\frac{\Delta v}{\Delta t} - 2\dot{v}_n \qquad (3.5)$$

incremental displacements $\{\Delta v\}$ of the form

$$[\bar{K}]\{\Delta v\} = \{P\} \qquad (3.6)$$

where:

$$[\bar{K}] = \frac{4}{(\Delta t)^2}[M] + \frac{2}{\Delta t}[C] + [K] \qquad (3.7)$$

$$\{P\} = [M]\{ \frac{4}{\Delta t}\{\dot{v}_n\} + 2\{\ddot{v}_n\} - \{1\}\ddot{x}_g \} + 2[C]\{\dot{v}_n\} \qquad (3.8)$$

Once Eq. (3.6) is solved, the incremental velocities and accelerations are obtained from Eq. (3.4) and (3.5), and the initial values for the next integration step are known.

3.4 Equilibrium Imbalance

Equation (3.1) is solved for each integration time step by assuming that the tangent stiffness matrix does not change during the time step being considered. After the incremental lateral displacements $\{\Delta v\}$ are obtained, element forces are computed and a check is performed to determine whether the stiffness matrix of the structural components must be updated to consider possible changes in stiffness due to yielding or unloading.

Let's assume that at the beginning of a given time step the moment and rotation of a particular element are those defined by point P in Fig 3.1. Let ΔM be the computed incremental moment due to an incremental rotation $\Delta \theta$. Since the element response must

follow the primary moment-rotation curve OAC, a correction must be made in the incremental moment to the level defined by point P' in Fig 3.1. This correction produces an equilibrium imbalance at the element level of

$$\Delta M_u = \Delta M - \Delta M_c \qquad (3.9)$$

By proper transformation, and after summing over all the structural elements, an imbalanced force vector $\{\Delta R_u\}$ associated with the global DOF's of the structure can be computed. This force vector can be subsequently reduced by static condensation to an equivalent force vector $\{\Delta F_u\}$ associated with the lateral DOF's of the structure. The forces $\{\Delta F_u\}$ must be added to the load vector $\{P\}$ (Eq. 3.8) for the next time step.

Neglecting the equilibrium imbalance represented by $\{\Delta F_u\}$ may lead to a systematic accumulation of error unless a very small integration time step is used in the calculations. Figure 3.2 shows a comparison of the computed displacement response of an elasto-plastic stiffness degrading SDOF system with a yield level of 20% of its weight and an initial period of 0.4 sec. It can be observed that if the equilibrium imbalance is neglected, satisfactory results are obtained when an integration step of 0.001 sec is used, while the error accumulation is very large when integrating with 0.02 sec. On the other hand, the response is satisfactory when an integration step of 0.02 sec is used and the correction due to equilibrium imbalance is performed. It should be pointed out that the preceding example is an extreme case since the inelastic response of the system is controlled by a single element. In a real building where only part of the structural elements will enter in the inelastic range at a given integration step, this effect is likely to be diminished.
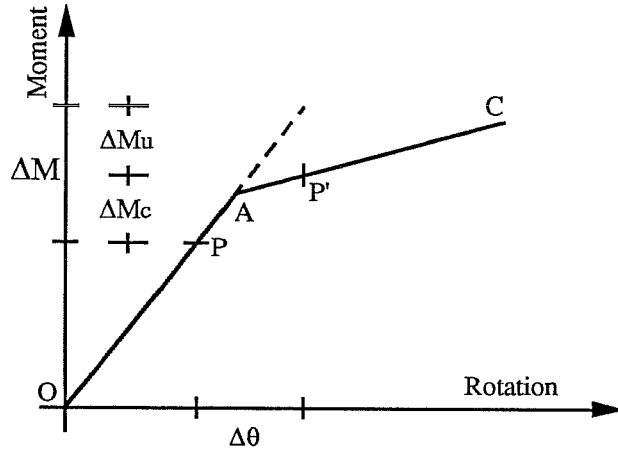
Figure 3.1 Equilibrium Imbalance
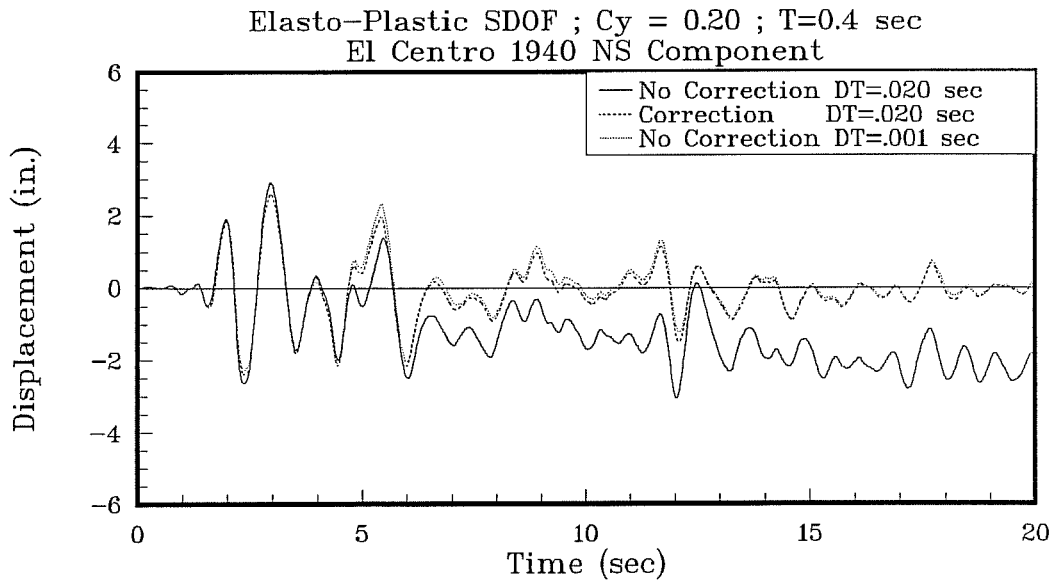
Figure 3.2 Effect of Equilibrium Imbalance

3.5 Damping

One of the most influential parameters controlling the dynamic response of structural systems is the amount of equivalent viscous damping considered in the calculations.

In this study the damping matrix [C] (Eq. 3.1) was considered to be a linear combination of the initial stiffness and mass matrices:

$$[C] = \alpha[M] + \beta[K_o]$$

(3.10)

This formulation allows specifying values of damping for two vibrational modes of the structure. If ω_1 and ω_2 are the natural frequencies of those two modes, then

$$\alpha = 2\omega_1\omega_2\frac{\xi_2\omega_1 - \xi_1\omega_2}{\omega_1^2 - \omega_2^2}$$

$$\beta = 2\frac{\xi_1\omega_1 - \xi_2\omega_2}{\omega_1^2 - \omega_2^2}$$

(3.11)

where ξ_1 and ξ_2 are the fraction of critical damping to be considered for the two modes.

Newmark et al.[2] suggest values of viscous damping for reinforced concrete structures ranging from 2 to 10% depending on the level of deformation or strain in the structure. However, if energy dissipation by means of cracking and yielding of the structural components is considered in the analytical model, it seems reasonable to consider reduced values of damping. In this study 2% damping, as suggested by Lopez [3], was used in all the calculations.

3.6 Joint Element Stiffness Matrix

It is common practice to model beam-column connections as being infinitely rigid. However, experimental studies have demonstrated that joint shear distortions contribute

significantly to lateral deflections [4,5,6].

In this study it was decided to include a joint element to take into account the joint flexibility and to consider the cyclic deterioration of beam-column connections subjected to cyclic loads.

The joint was modeled by means of a compression strut (which for modeling purposes can act in tension too) bounded by rigid links as shown in Fig 3.3. This representation allows shear-type deformations of the joint to be represented by means of axial deformations of the strut. The load-deflection response of the strut was assumed to be bilinear to account for pre-cracking and post-cracking behavior of the joint (in shear) and will be discussed later in Chapter 4.

Figure 3.4 shows a joint element subjected to a shear distortion γ. If L is the length of the undeformed concrete strut, the axial deformation δ, is given by

$$\delta = \frac{1}{2}L\gamma \qquad (3.12)$$

Assuming the equivalent area A_{eq} of the concrete strut to be known, the internal force S in the strut is

$$S = \frac{A_{eq}E}{L}\delta \qquad (3.13)$$

Equation 3.13 represents the stiffness equation in the local coordinate δ. Using Eq. (3.12), the stiffness matrix (1x1) of the joint element in global coordinates can be computed as

$$K_j = \frac{A_{eq}EL}{4} \qquad (3.14)$$

The equivalent concrete strut area, A_{eq}, before shear cracking of the joint, can be
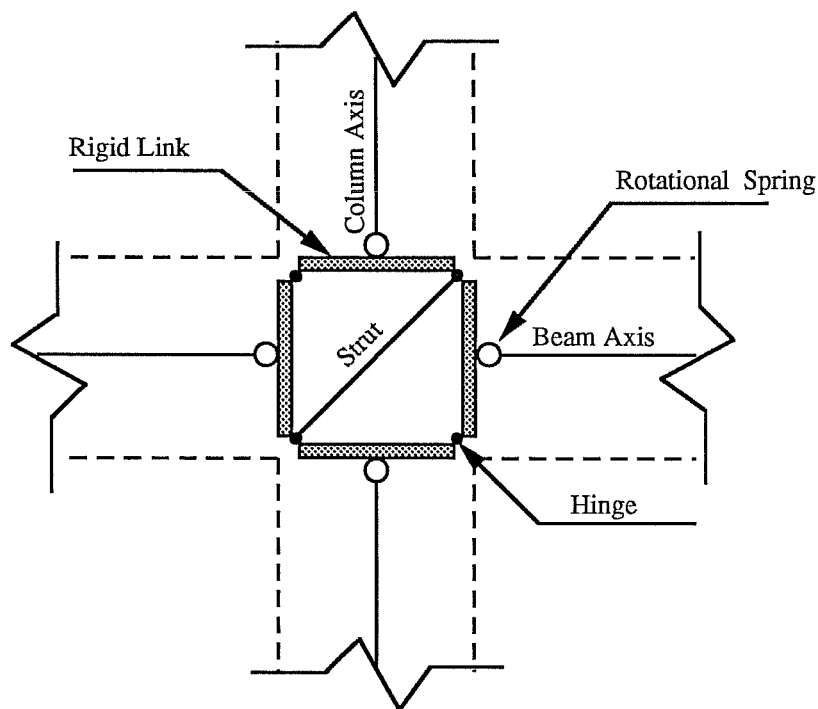
Figure 3.3 Structural Idealization of a Beam-Column Connection

$$L = \sqrt{h_b^2 + h_c^2}$$

$$\delta = \frac{\gamma}{2} L$$

$$S = K\delta = \frac{A_{eq} E}{L} \delta$$

$$K_j = \frac{A_{eq} E L}{4}$$
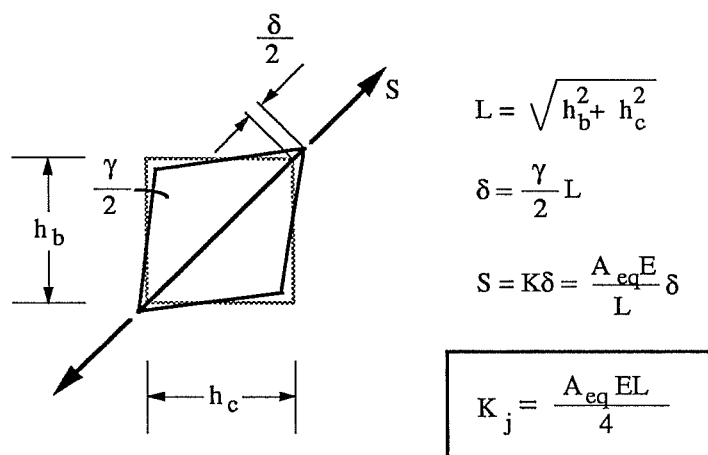
Figure 3.4 Joint Stiffness

computed by considering the shear panel of Fig. 3.5a subjected to a shear stress τ. From this figure

$$\gamma = \frac{\tau}{G} = \frac{V}{A_j G}$$ (3.15)

where:

V = Shear force in the joint,

A_j = Area of the joint = $h_c \cdot b_j$,

h_c = horizontal dimension of the joint,

b_j = width of the joint, perpendicular to the plane of Fig. 3.5a

G = Shear modulus of the concrete

Figure 3.5b shows the idealization of the shear panel of Fig. 3.5a by means of the equivalent compression strut. If S is the force in the strut due to the shear distortion γ, the shear force can be expressed as

$$V = S\cos\alpha$$ (3.16)

Using Eq. 3.13 and 3.16 gives

$$\gamma = \frac{2V}{A_{eq} E \cos\alpha}$$ (3.17)

Finally equating Eq. 3.17 and 3.15 gives

$$A_{eq} = \frac{2A_j G}{E\cos\alpha} = \frac{2G}{E} b_j L$$ (3.18)

Equation 3.18 gives the equivalent strut area to be used in Eq. 3.14 prior to shear cracking of the joint. For the post cracking stage, the equivalent area of the strut was assumed to be given by

$$A_{eq} = \beta b_j L \tag{3.19}$$

The factor β was calibrated from experimental results [4,6] and values of 1/4 and 1/8 were adopted for joints with and without lateral beams, respectively.

3.7 Beam and Column Stiffness Matrices

Beams and columns were modeled using the one-component model proposed by Giberson [7]. In this model the element is considered to be composed of an elastic portion and two rotational springs at the member ends connected in series to the elastic part. The model assumes the element is deformed in double curvature with its inflection point at mid-length.

Figure 3.6b shows a beam element subjected to equal moments M_a and M_b. Assuming the moment-curvature relationship (Fig. 3.6a) to be known, the distribution of curvatures along the member can be computed as well as the end rotations θ_a and θ_b. By computing these rotations at moments associated with cracking, yielding and ultimate, an approximate trilinear moment-rotation curve can be obtained as shown in Fig. 3.6c. This moment-rotation curve can be reproduced by selecting proper values of the rotational spring stiffness of the one-component model shown in Fig. 3.7. It can be seen that the stiffnesses of the rotational springs must be set equal to infinity for end moments below the cracking level, and to finite values for end moments above the cracking level.

The stiffness equation for a one-component model element subjected to end moments M_a and M_b is

$$A_{eq} = \frac{2G}{E} b_j L \quad \text{(pre-cracking)}$$

$$A_{eq} = \beta b_j L \quad \text{(post-cracking)}$$
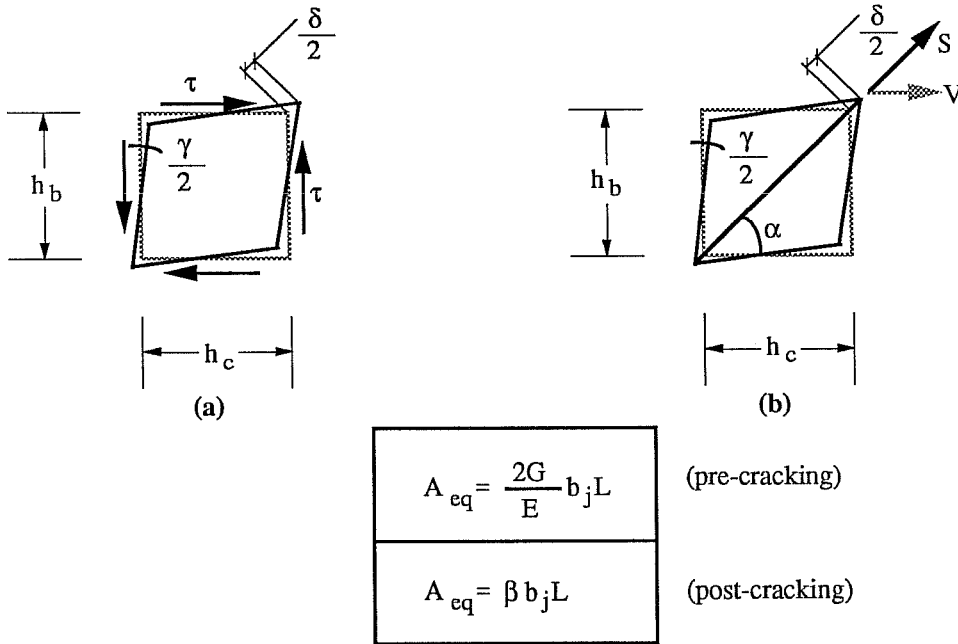
Figure 3.5   Equivalent Strut Area
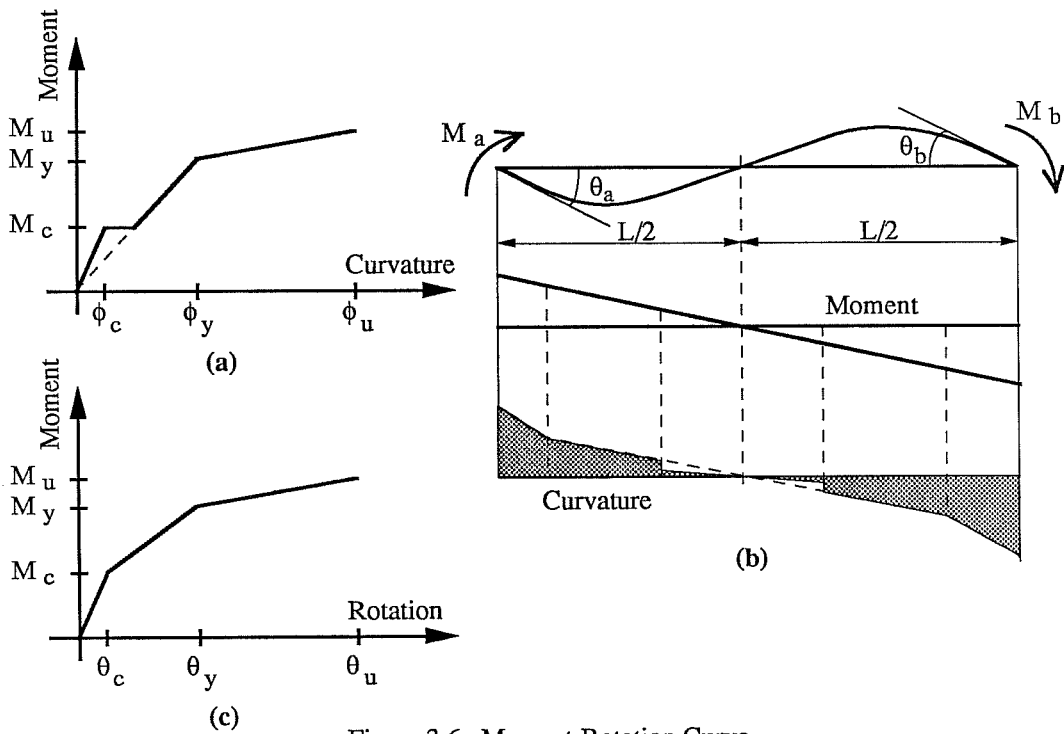
Figure 3.6   Moment-Rotation Curve

$$\left\{ \begin{matrix} M_a \\ M_b \end{matrix} \right\} = \frac{1}{D} \begin{bmatrix} k_1 & k_2 \\ k_2 & k_3 \end{bmatrix} \left\{ \begin{matrix} \theta_a \\ \theta_b \end{matrix} \right\} = [K_L]\{\theta\} \qquad (3.20)$$

$$D = \frac{1}{12}(\frac{L}{EI})^2 + (f_a + f_b)\frac{L}{3EI} + \frac{1}{AGL}(\frac{L}{3EI} + f_a + f_b) + f_a f_b$$

$$k_1 = \frac{L}{3EI} + \frac{1}{AGL} + f_b$$

$$k_2 = \frac{L}{6EI} - \frac{1}{AGL}$$

$$k_3 = \frac{L}{3EI} + \frac{1}{AGL} + f_a$$

with:

E = modulus of elasticity

G = shear modulus

I = moment of inertia

L = clear length of the member

A = shear area

f_a = rotational spring flexibility for end a

f_b = rotational spring flexibility for end b

The stiffness matrix of a beam element in global coordinates can be obtained by transformation of the local stiffness matrix $[K_L]$. Referring to Fig. 3.8a, if v, ϕ, and γ are the global DOF's representing the vertical displacement, joint rotation, and joint distortion of the nodes, the relationship between these global DOF's and the local DOF's is given by:

$$\left\{ \begin{array}{c} \theta_a \\ \theta_b \end{array} \right\} = \left[\begin{array}{cccccc} -\dfrac{1}{L} & 1+\lambda_a & \dfrac{1}{2}(1-\lambda_a) & \dfrac{1}{L} & \lambda_b & -\dfrac{1}{2}\lambda_b \\[2ex] -\dfrac{1}{L} & \lambda_a & -\dfrac{1}{2}\lambda_a & \dfrac{1}{L} & 1+\lambda_b & \dfrac{1}{2}(1-\lambda_b) \end{array} \right] \left\{ \begin{array}{c} v_a \\ \phi_a \\ \gamma_a \\ v_b \\ \phi_b \\ \gamma_b \end{array} \right\} \qquad (3.22)$$

$$\{\theta\} = [T_b]\{u\}$$

where:

$$\lambda_a = a/L$$

$$\lambda_b = b/L$$

The stiffness matrix of a beam element in global coordinates is then:

$$[K_b] = [T_b]^t[K_L][T_b] \qquad (3.23)$$

The same procedure can be used for columns. In this case the relation between the local displacements and the global DOF's is given by (see Fig. 3.8b):

$$\left\{ \begin{array}{c} \theta_a \\ \theta_b \end{array} \right\} = \left[\begin{array}{cccccc} -\dfrac{1}{L} & 1+\lambda_a & -\dfrac{1}{2}(1-\lambda_a) & \dfrac{1}{L} & \lambda_b & \dfrac{1}{2}\lambda_b \\[2ex] -\dfrac{1}{L} & \lambda_a & \dfrac{1}{2}\lambda_a & \dfrac{1}{L} & 1+\lambda_b & -\dfrac{1}{2}(1-\lambda_b) \end{array} \right] \left\{ \begin{array}{c} u_a \\ \phi_a \\ \gamma_a \\ u_b \\ \phi_b \\ \gamma_b \end{array} \right\} \qquad (3.24)$$

$$\{\theta\} = [T_c]\{u\}$$

and therefore, the column stiffness matrix is:

$$[K_c] = [T_c]^t[K_L][T_c]$$

(3.25)

3.8 Wall Stiffness Matrix

Walls, unless coupled by very strong beams, are not expected to deform in double curvature. For this reason, the stiffness matrix for wall elements was computed using the following procedure. Each wall element was divided into several subelements between each story level (Fig 3.9). By assuming a linear variation of moments along the height of the wall, the moment at the center of each subelement was computed, and its flexural rigidity, EI, was obtained from the moment-curvature relationship for the wall. The stiffness matrix for each subelement was computed and assembled into the stiffness matrix of the wall. By static condensation, the interior degrees of freedom were eliminated to obtain the stiffness matrix related to the nodal DOF's.

3.9 Bond-Slip Deformations

Bond-slip rotations, often referred to in the literature as fixed-end rotations, occur at beam column interfaces when the applied moment exceeds the cracking moment of the section. The formation of these cracks gives rise to concentrated rotations between the column and the girder. Fixed-end rotations grow in magnitude primarily due to two effects: the increase in magnitude of the tensile stress that the longitudinal bars must develop, and bond deterioration along the anchorage length due to cyclic loading.

An analytical model to consider this latter effect has been proposed by researchers at the University of California at Berkeley [8,9,10]. Good agreement with experimental results has been demonstrated. The model requires the definition of the hysteretic bond stress-slip

Inelastic Spring

EI

Elastic Member

M_a θ_a θ_b M_b

L/2   L/2
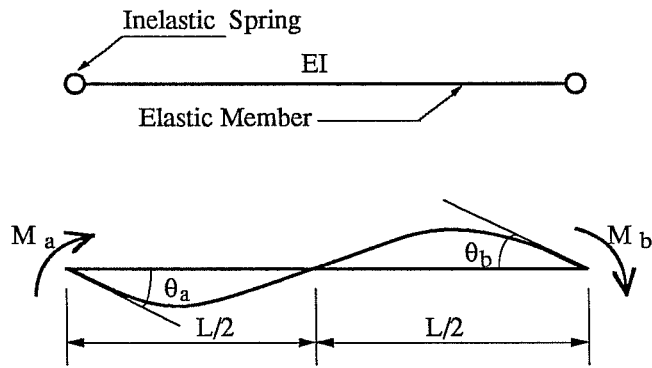
Figure 3.7 One-Component Model

(a) Beam Element

V_a u_a
ϕ_a γ_a ψ θ_a θ_b $\bar{\psi}$ V_b u_b
ϕ_b γ_b

2a   L   2b

(b) Column Element

V_a u_a
ϕ_a γ_a ψ θ_a 2a

L

θ_b ψ V_b u_b
ϕ_b γ_b 2b
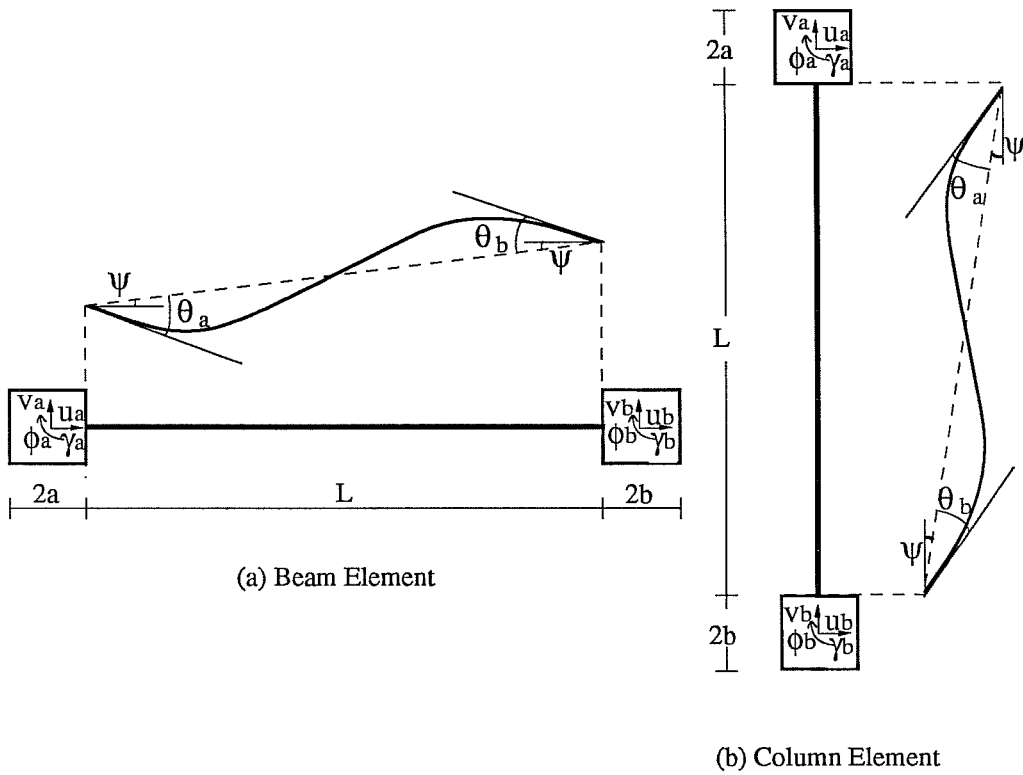
Figure 3.8 Relation Between Local and Global DOF's

relation, the subdivision of the longitudinal reinforcing bars within the anchorage zone into several segments, and finally, the integration of the bond equation. In a multistory reinforced concrete frame this procedure must be implemented in all the beam-to-column connections.

Beam-column connection tests showed that bond deterioration due to load reversals was significant at drift levels above 2% [4]. Because it was desirable to keep the analytical model as simple as possible, it was decided to include in the present analytical model for fixed-end rotations only the effect of the elongation of the longitudinal bars within the anchorage zone.

The approach followed in this study to include bond-slip deformations is very similar to that proposed by Saiidi [12] and Lopez [3], but instead of specifying an average bond stress and computing the development length, the development length was specified and the corresponding bond stress was obtained.

Assuming that the fixed end rotation θ_b, takes place about the compression reinforcement as shown in Fig. 3.10, and that the steel stress varies linearly along the development length L_b, the fixed end deformation and rotation at yielding of the longitudinal bar are:

$$\delta_{by} = \frac{1}{2}\epsilon_y L_b \qquad \theta_{by} = \frac{\delta_{by}}{d-d'} \qquad (3.26)$$

By assuming that the tensile force in the longitudinal reinforcement is proportional to the applied moment, the fixed-end rotation associated with the cracking moment is given by θ_{bc} where f_{sc} is the tensile stress in the steel immediately after cracking. Finally, the fixed-end rotation at ultimate moment conditions is given by:

$$\theta_{bc} = \frac{f_{sc}}{f_y} \theta_{by}$$ (3.27)

$$\theta_{bu} = \frac{e_y L_y + (L_b - L_y)(e_y + e_{su})}{2}$$ (3.28)

where:

$$\theta_{bu} = \frac{\delta_{bu}}{d - d'}$$

L_y = length at which $f_s = f_y$

ϵ_{su} = steel strain at $M = M_u$

The moment-rotation curve including the bond-slip effect is then obtained by adding the fixed-end rotations associated with cracking, yielding, and ultimate to the moment-rotation curve computed for a member without fixed-end rotations, as shown in Fig. 3.11.

3.10 Hysteresis Model

The SINA hysteresis model [11] was adopted in this study to model the non linear behavior of the rotational springs in beams and columns and the moment-curvature hysteretic relations for wall elements.

Because it was desirable to model the behavior of beams with non-continuous bottom reinforcement and columns that fail prematurely due to splice failures, two additional rules were added to the nine original rules of the SINA model. The effect of strength reduction due to repeated cycles at the same deformation level was also included. The main characteristics of the model are summarized below, and a detailed description of all the rules can be found in Ref. 11.

The model operates on a primary curve consisting of four linear segments for positive and negative bending as shown in Fig. 3.12. For elements in which a premature failure is expected, the primary curve was assumed to be as shown in Fig. 3.13.

The primary curve need not be symmetric about the origin, but a single straight line must be specified for moments below the cracking moment in both directions (line C'OC in Fig 3.12) due to the nature of the one component model. Points Y and U (and Y' and U') correspond to moments associated with yielding and ultimate. An horizontal line following the ultimate moment was adopted.

For moments below the cracking level, loading and unloading follow the primary curve. For moments above the cracking moment, unloading follows a line connecting the unloading point with the cracking point in the other direction (line PC' in Fig 3.12). If the yield moment is exceeded and unloading takes place at point P_1, the slope of the unloading branch P_1P_2 is computed [12] as

$$K_{un} = K_{yc'} \left(\frac{\theta_y}{\theta_{max}} \right)^\alpha \tag{3.29}$$

where θ_{max} is the maximum rotation attained in the loading direction and $K_{yc'}$ is the slope of the line connecting the yield point in the loading direction with the cracking point in the opposite direction. The exponent α controls the slope of the unloading branch and will be discussed in Chapter 4.

Pinching of hysteresis loops in reinforced concrete members can be caused by, but is not limited to, opening and closing of flexural cracks in zones of maximum moments, slipping of longitudinal reinforcement due to bond deterioration, and shearing of the connection region. In the present model, pinching is considered by specifying a "crack-closing moment" indicated
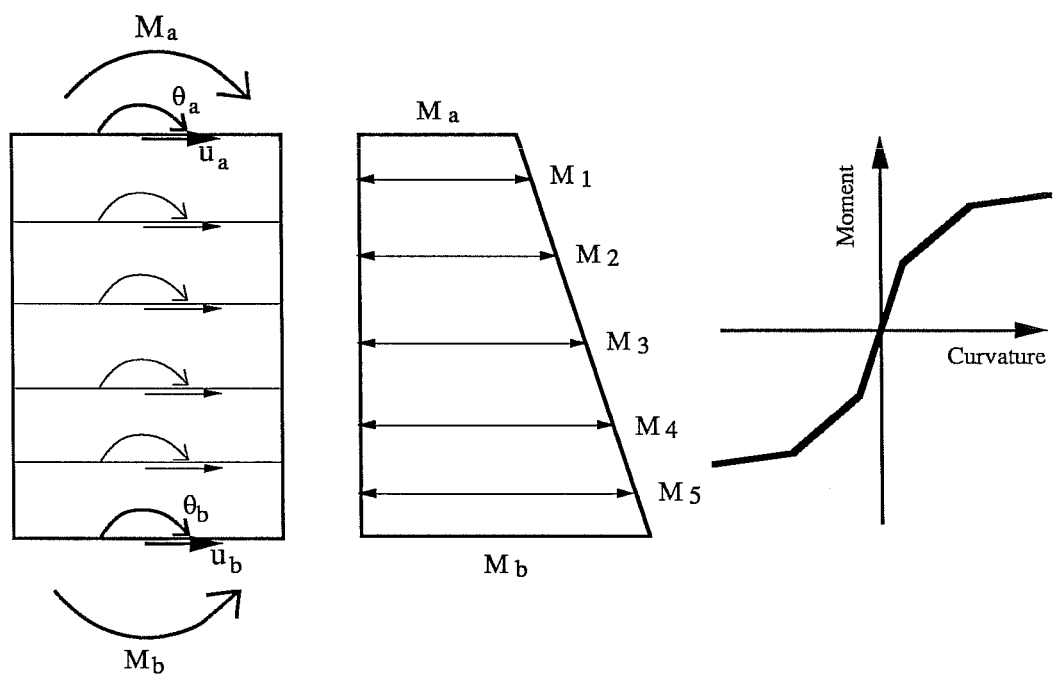
Figure 3.9 Wall Element Representation
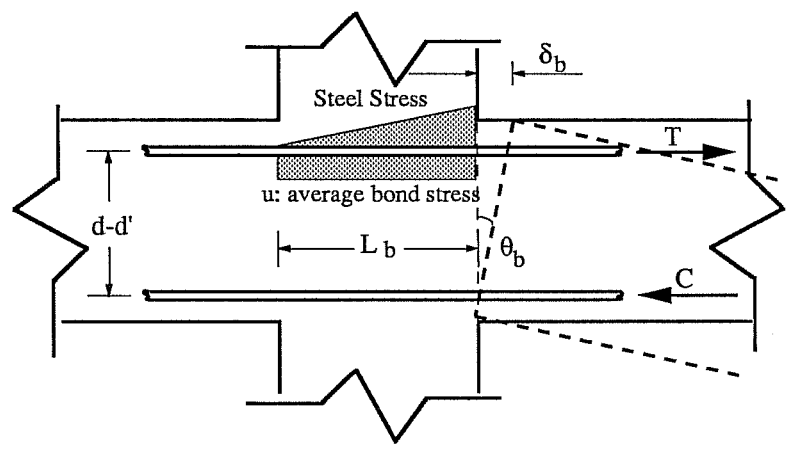
Figure 3.10 Bond Slip Rotations

with the horizontal broken line in Fig 3.12. Reloading in the negative direction after reaching point P_2 follows the line P_2P_3, where the rotation associated with P_3 is a fraction of the unloading rotation θ_o reached in previous cycles. After reaching point P_3, a stiffening effect takes place. If strength reduction due to cyclic loading is neglected, loading should follow the line P_3P_4, where P_4 represents the previous unloading point. In order to consider the effect of strength reduction, the target point is set at P'_4 by multiplying the rotation associated with P_4 by a strength reduction factor, R, greater than one.

The calibration of the R factor and the parameters necessary to define the pinching effect are discussed in Chapter 4.
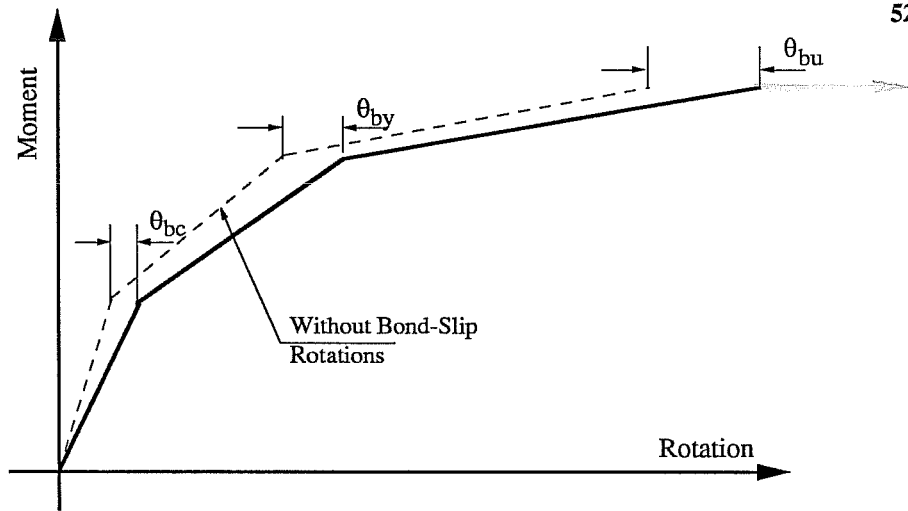
Fig 3.11 Moment Rotation Curve Inluding Bond-Slip Rotations
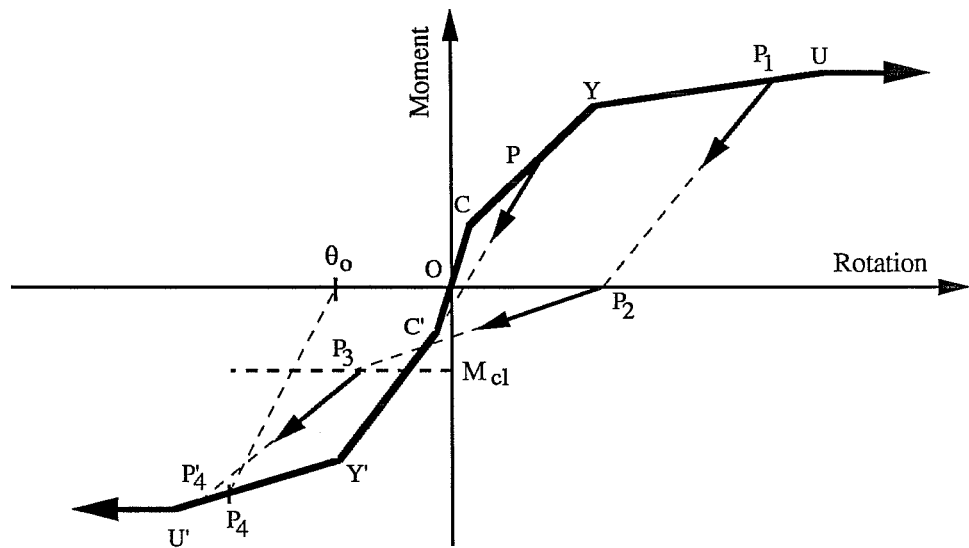
Figure 3.12 SINA Hysteresis Model (from Ref. 11)
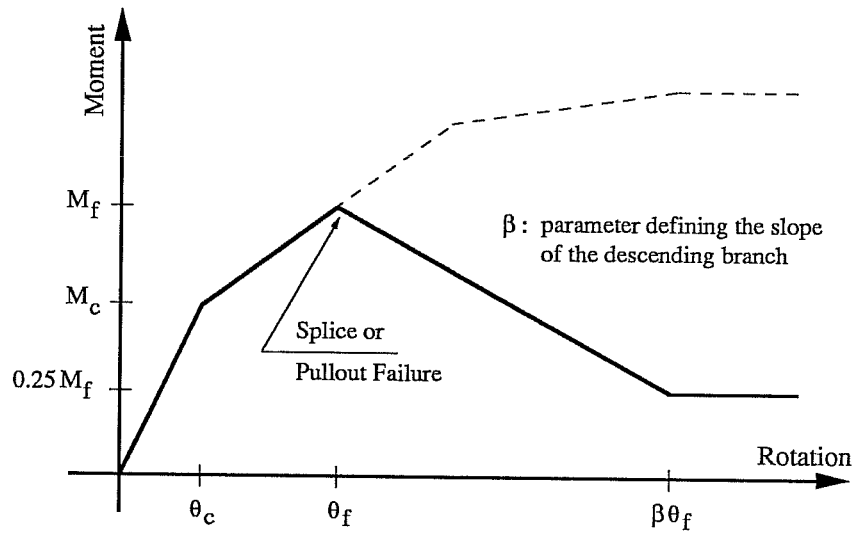
Fig 3.13 Moment Rotation Curve for Elements with Splice or Pullout Failure

CHAPTER 4

CALIBRATION OF THE ANALYTICAL MODEL

4.1 Introduction

The analytical model outlined in the previous chapter contains built-in empirical relations related primarily to the hysteretic behavior of the structural elements. Although the hysteresis model incorporated operates on a primary curve that can be derived from basic principles (material properties, equilibrium, and compatibility), the rules governing stiffness, strength deterioration, and pinching of the hysteresis loops are highly empirical. Because these parameters control the energy dissipation characteristics of the structural members, and therefore affect the dynamic response of the structure being modeled, it was believed necessary to evaluate the ability of the analytical model to predict the response of reinforced concrete subassemblage test specimens.

The experimental results obtained by Guimaraes [4] for beam-column connections and by Alcocer [6] for jacketed beam-column connections were used in this study to calibrate the parameters controlling the hysteresis rules of the SINA model [11], bond-slip deformations, and modeling of joint cores.

4.2 Test Specimens

Five reinforced concrete beam-column subassemblages were used to calibrate the analytical model. Four of the specimens (J-Series) that were tested by Guimaraes [4] are illustrated in Fig. 4.1. All specimens were large-scale models with a 5-in. thick slab. Specimen J1 had beams in one direction only, specimens J2 and J4 represented interior joints with beams

54

in both directions, and specimen J3 represented an exterior joint. Beam dimensions were 16x20" and columns were 20x20". Specimen J1 was subjected to unidirectional reversed cyclic loads up to a 4% drift level. Specimens J2, J3 and J4 were loaded cyclically to 2% drift levels, primarily with unidirectional loading, and then to 4% drift using a bidirectional loading history. The test setup is shown in Fig. 4.2. Load histories are shown in Fig. 4.3. Normal weight concrete with a design strength of 4000 psi and Grade 60 bars were used in all specimens except in specimen J4 where Grade 75 steel was used. Concrete compressive strengths and tensile properties of the reinforcing steel are summarized in Table 4.1 and 4.2 respectively. Specimen details are presented in Table 4.3.

TABLE 4.1 Concrete Compressive Strength (psi) at 28 days, J-Series

POSITION	SPECIMEN			
	J1	J2	J3	J4
Slab, Beams and Lower Column	3,240 (3,500)	3,700 (4,010)	4,700	4,800 (4,590)
Upper Column	3,520	3,780	3,250	4,420

( ): At testing

56

(Side View)

92"

20"

(Top View)

9'-4"

(c) Specimen J3

(Side View)

92"

20"

92"

(Top View)

17'-0"

(b) Specimens J2 & J4

(Side View)

92"

20"

92"

(Top View)

17'-0"

(a) Specimen J1

75.8"

20"

71"
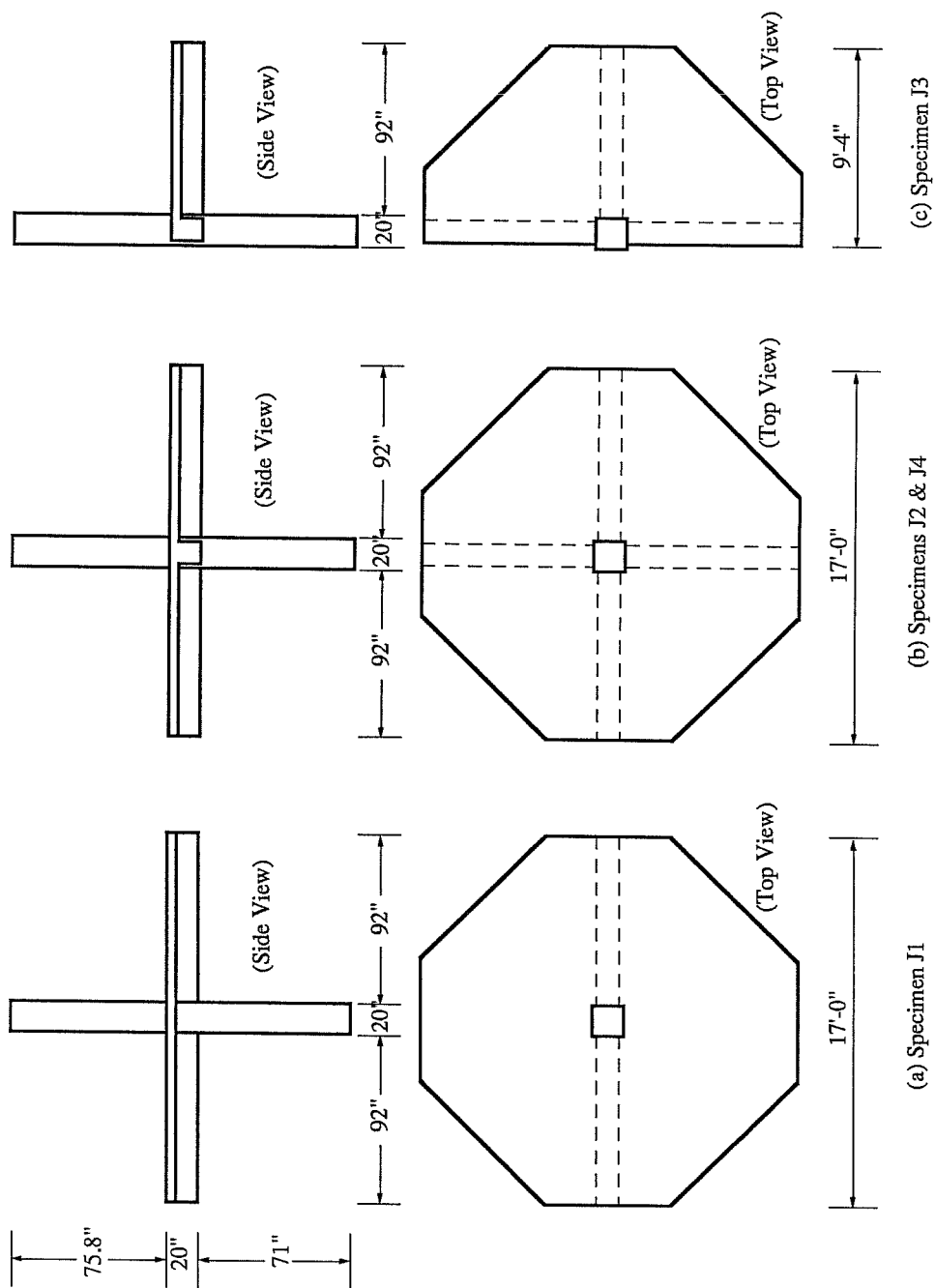
Figure 4.1 Specimen Configurations (from Ref. 4)
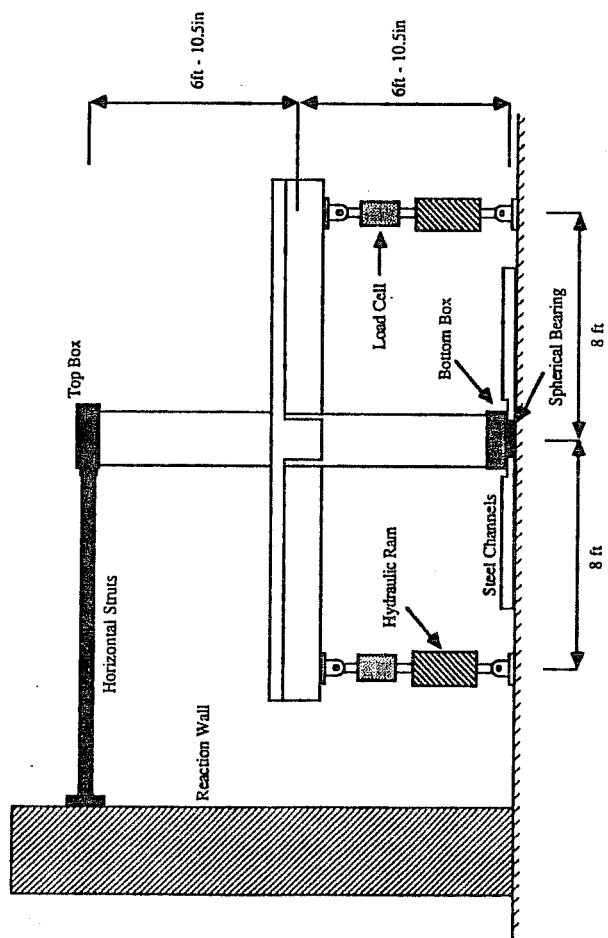
Figure 4.2 Test Setup for Specimen J2 (from Ref. 4)
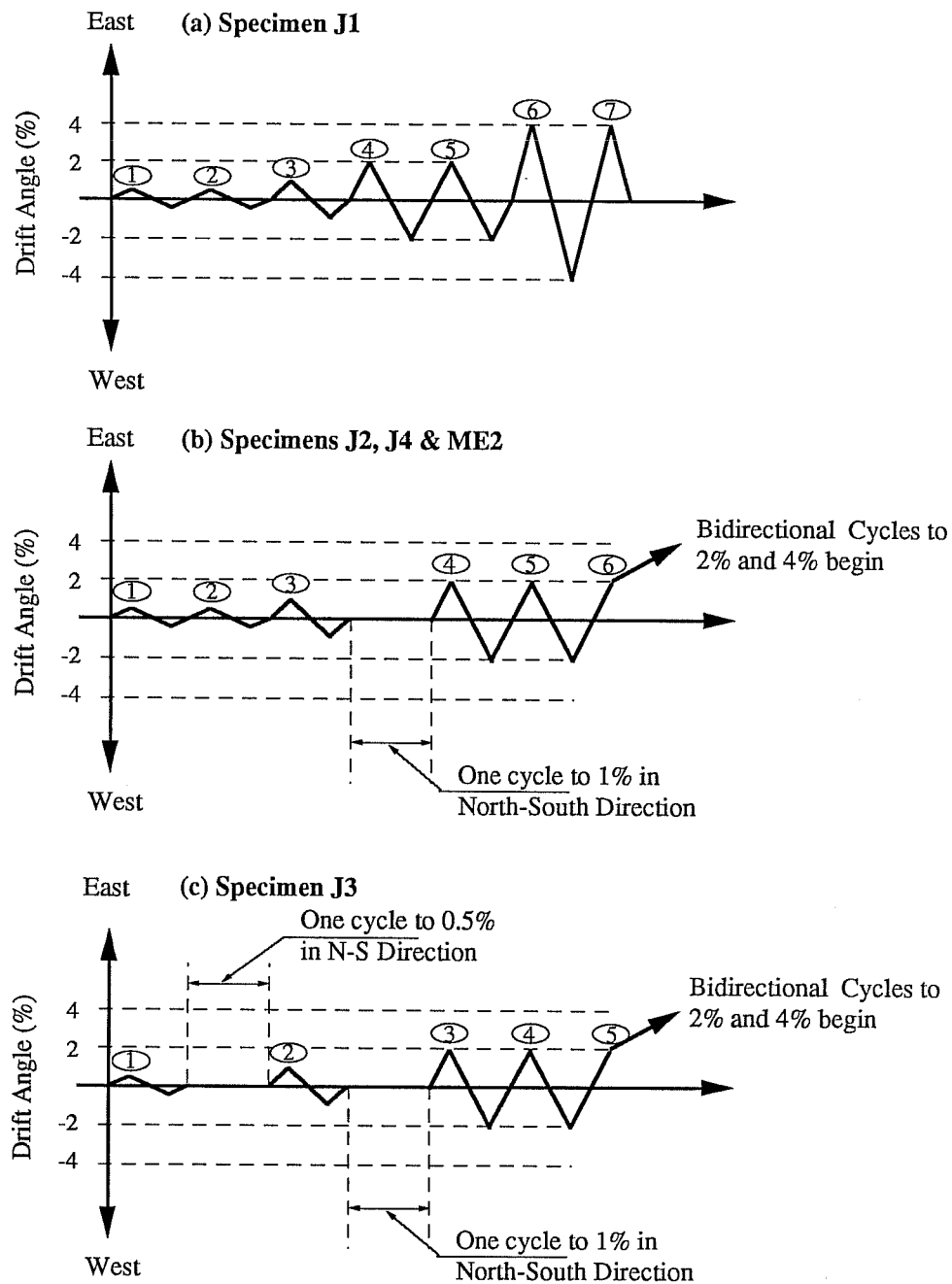
Figure 4.3 Loading Histories (from Ref. 4)

TABLE 4.2 Tensile Reinforcement Properties - J Series

	BAR SIZE								
	GRADE 60					GRADE 75			
	#4	#6	#7	#8	#9	#3	#4	#7	#8
f_y (ksi)	79.7	74.2	65.6	67.2	66.6	84.8	82.6	79.5	80.0
E (ksi)	28500	27600	27600	27900	27000	25000	25000	27000	26000
ϵ_{sh}	0.010	0.013	0.013	0.009	0.0095	0.02	0.02	0.008	0.012
f_{ult} (ksi)	111.9	108.9	101.4	106.0	106.1	90.0	99.0	120.0	108.0
ϵ_{ult}	0.08	0.08	0.08	0.08	0.08	0.04	0.04	0.08	0.08

TABLE 4.3 Specimen Details - J Series

SPECIMEN	Design Strength		Beam Reinforcement			Column Reinforc.	
	f_c' (psi)	f_y (ksi)	Longitudinal		Trans.	Long.	Trans.
			Top	Bottom			
J1	4,000	60	4#8	4#7	2#4@4"	12#8	3#4@4"
J2	4,000	60	6#8	6#6	2#4@4"	16#9	3#4@4"
J3	4,000	60	5#9	4#8	2#4@3.5"	12#9	3#4@4"
J4	4,000	75	4#8	4#7	3#3@4"	16#9	3#3@3"

One additional interior beam-to-column connection (ME2 Specimen) tested by Alcocer [6] was also analyzed. The specimen had a 5 in. thick slab, 8x20" beams and 12x12" columns. A reinforced concrete jacket was later cast around the original column, making the final cross section 20x20". The test setup and load history was virtually the same as that used for the J specimens. Concrete compressive strengths and steel properties are indicated in Table 4.4 and 4.5 respectively. Specimen details are summarized in Table 4.6.

TABLE 4.4 Concrete Strength at Testing (psi) - ME2 Specimen

POSITION	Concrete Strength (psi)
Slab, Beams and Lower Column	3,960
Upper Column	3,300
Lower Col. Jacket	5,750
Upper Col. Jacket	5,870
Beam Jacket	-

Because the analytical model developed in this study is a planar model, no attempt was made to reproduce the bidirectional loading response of the specimens considered.

TABLE 4.5 Tensile Reinforcement Properties - ME2 Specimen

	BAR SIZE (GRADE 60)			
	#3	#6	#7	#9
f_y (ksi)	67.4	62.2	64.4	63.5
E (ksi)	25,380	27,460	28,150	26,980
ϵ_{sh}	N.A.	0.0065	N.A.	N.A.
f_{ult} (ksi)	110.3	107.0	91.4	108.8
ϵ_{ult}	N.A.	N.A.	N.A.	N.A.

N.A. : Not available

TABLE 4.6 Specimen Details - ME2 Specimen

SPECIMEN	Beam Reinforcement			Column Reinforc.	
	Longitudinal		Trans.	Long.	Trans.
	Top	Bottom			
ME2	4#7	4#7	2#3@5"	8#6	4#3@6"
	(-)	(-)	(-)	(12#9)	(2#4@3")

( ): Additional Jacketed Section Reinforcement

4.3 Energy Dissipation Parameters

Hysteretic energy dissipation is accounted for in the SINA model for both low-amplitude and high-amplitude cycles.

The inclusion of a breakpoint at the cracking level makes it possible to account for hysteretic energy dissipation in low-amplitude cycles as shown in Fig. 4.4. Energy dissipated during low-amplitude cycles is important because in an actual structure many elements will behave essentially in the elastic range (below yielding) even when the structure is subjected to a severe ground motion. This may be the case for columns designed following the strong column-weak beam concept. Hysteresis models that fail to include the cracking effect of reinforced concrete members will generally overestimate the response of the structure being modeled.

Energy dissipation during high-amplitude cycles is controlled in the model used in this study by the following parameters (refer to Fig. 4.5):

a) The exponent α in Eq. 3.29 defines the unloading stiffness after yielding. A value of $\alpha = 0$ means no unloading stiffness degradation (unloading is parallel to C'Y), while values of α greater than zero reduces the unloading slope and therefore the area enclosed in the hysteresis loops (which is directly related to the energy dissipated). A value of $\alpha = 0.5$ produced the best fit of the measured unloading slopes for the test structures. Other researchers have proposed values of α ranging from 0.4 to 0.5 [3,12].

b) The coordinates of the "crack closing point", defined by M_{cl} and θ_{cl}, control the pinching of the hysteresis loops near the origin. The crack closing moment for a section is computed as:

$$M_{cl} = \alpha_1 A_s f_y (d-d')$$ (4.1)

where A_s is the tensile reinforcement area, f_y its yield stress, and (d-d') the distance between the tensile and compressive longitudinal reinforcement. Saiidi [11] proposed a value of $\alpha_1 = 0.5$ based on experimental observations on reduced-scale reinforced concrete models [13]. Based on experimental results from the large-scale specimens analyzed in this study, a value of $\alpha_1 = 0.25$ best approximated the energy dissipated during large-amplitude cycles. The abscissa θ_{cl} was computed as:

$$\theta_{cl} = \alpha_2 \theta_0$$ (4.2)

where θ_0 is the rotation defined by the intercept of the unloading branch with the horizontal axis of the moment rotation curve. The parameter α_2 was set equal to 0.75 as proposed by Saiidi.

c) The strength reduction factor R_f defines the coordinate of the target point on the primary curve for subsequent loading cycles. If the cycle shown in Fig 4.5 is repeated, the stiffening branch would be softened by displacing the target point abscissa, θ_{max}, on the primary curve to $\theta_{target} = R_f \theta_{max}$. A value of $R_f = 1.05$ best reproduced the strength reduction effect of the tested subassemblages.

4.4 Joint Element Hysteresis Parameters

The joint element developed in this study operates on a bilinear primary curve, symmetric about the origin, that accounts for the precracking and post-cracking stages of the joint in shear as shown in Fig. 4.6. The equations developed in Chapter 3 define the stiffness of the two branches of the primary curve. The breakpoint between the two branches is defined
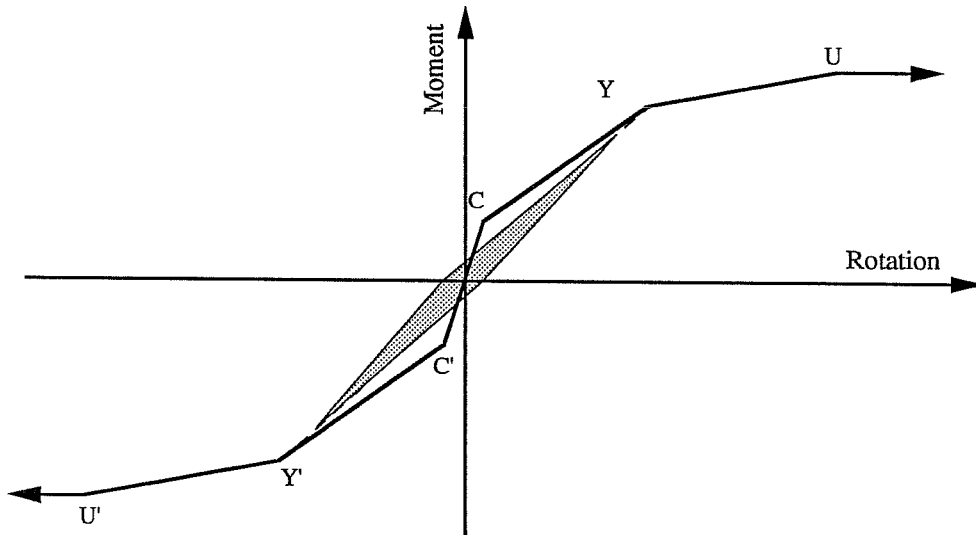
Figure 4.4 Energy Dissipation at Low-Amplitude Cycles
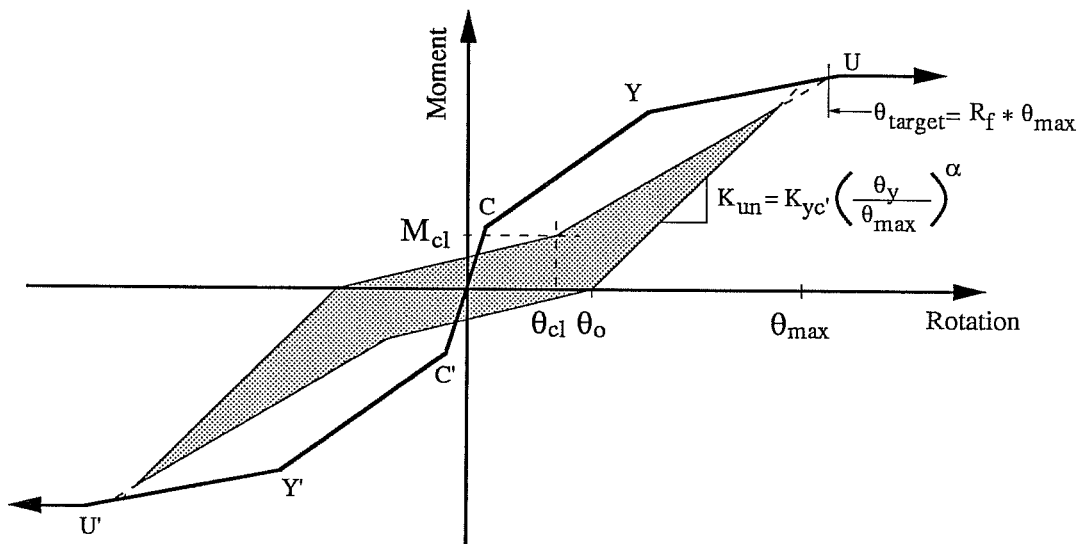
Figure 4.5 Energy Dissipation at Large-Amplitude Cycles

by the shear force in the joint that produces first cracking, after which the compression strut is properly developed. The compression strut is assumed to be bounded by the beam and column longitudinal bars passing through the joint.

The shear stress that produces first cracking of the joint was computed using the formula proposed by Meinheit [14]:

$$v_{cr} = 3.04\sqrt{f_c'} + 0.242\frac{P}{A_g} + 318Mask \qquad (4.3)$$

where:

f'_c = compressive strength of the concrete (psi)

P = axial load on the column (lb)

A_g = cross section area of the column (in^2)

Mask = ratio of cross sectional area of lateral beams to joint area

Table 4.7 shows a comparison between the measured and predicted cracking strengths of 14 beam-column connections tested by Meinheit and four of the beam-column joints tested by Guimaraes. Measured joint shear stress at cracking was determined as the point when the strain in the joint hoops first began to increase, as shown in Fig. 4.7.

Hysteresis rules for the joint element are similar to the ones implemented in the SINA model. For joint shear forces below the cracking level, loading and unloading is elastic following the line C'OC (Fig. 4.6). Once the cracking force is exceeded, loading proceeds along the branch CP. Unloading from a point P_1 after cracking follows a line with a slope given by:

$$K_{un} = K_{cc'}\left(\frac{\gamma_{cr}}{\gamma_{max}}\right)^{\alpha_j} \qquad (4.4)$$
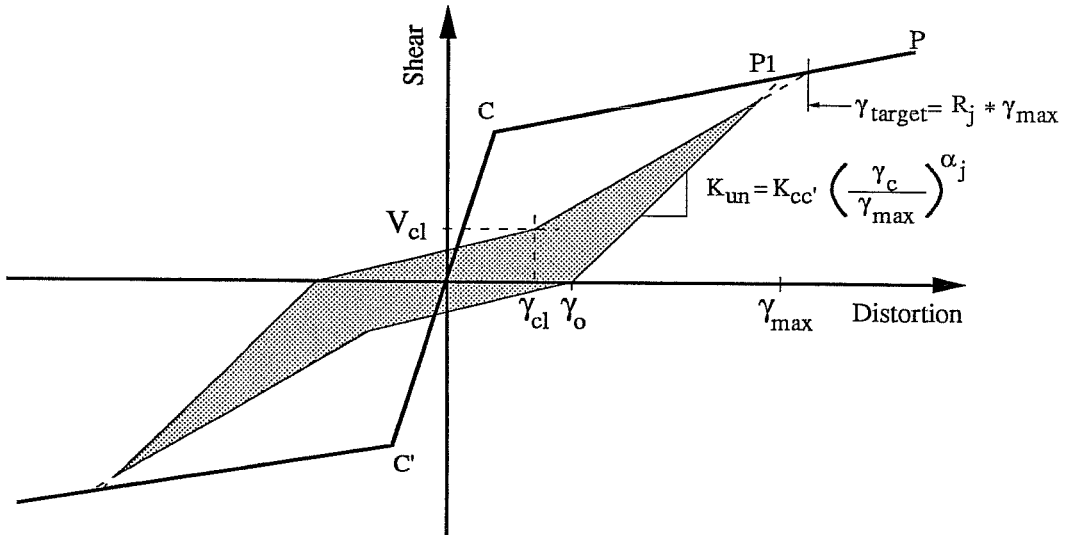
Figure 4.6 Hysteresis Rules - Joint Element
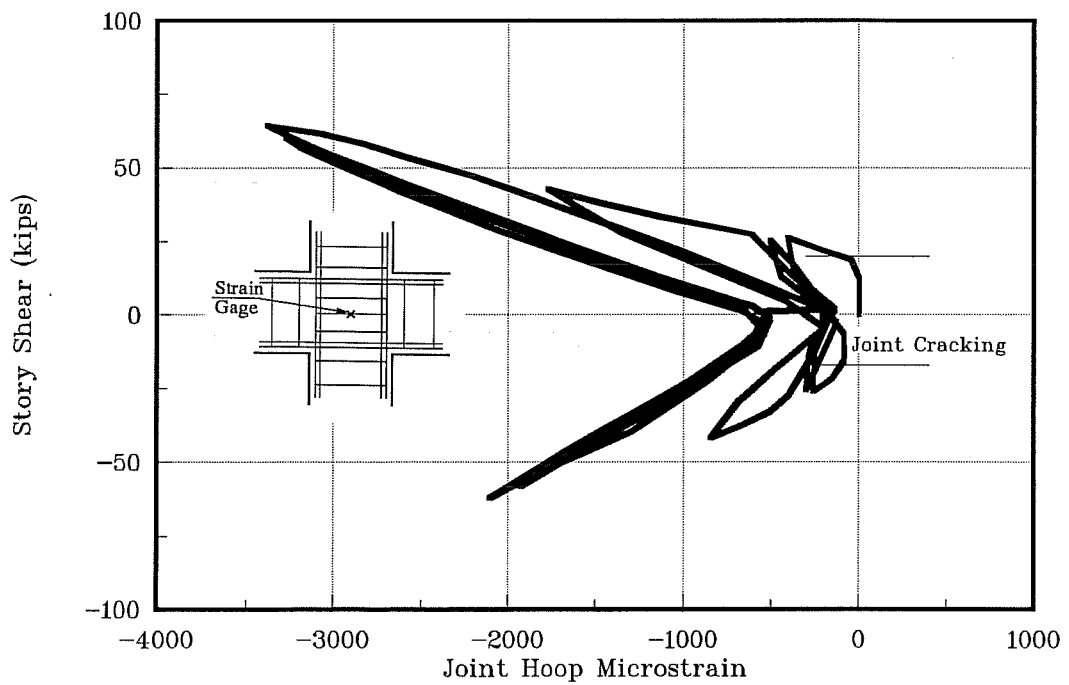
Figure 4.7 Joint Shear vs. Strain in Joint Hoop
Specimen J2

where K_{cc}, is the slope of the elastic branch of the primary curve, γ_{cr} is the joint distortion at cracking and γ_{max} is the maximum distortion attained in the loading direction. The exponent α_j was calibrated from measured joint shear-distortion curves, and a value of $\alpha_j = 0.40$ was adopted.

Table 4.7 Predicted vs. Measured Cracking Strength of Joint Cores

Specimen	f'_c (psi)	P/A_g (psi)	Mask	$(v_{cr})_{calc}$ (psi)	$(v_{cr})_{meas}$ (psi)	$\dfrac{(v_{cr})_{meas}}{(v_{cr})_{calc}}$
I	3,800	1,527	0	557	451	0.81
II	6,060	1,538	0	609	577	0.95
III	3,860	1,526	0	558	513	0.92
IV	5,230	1,551	0	596	680	1.14
V	5,200	205	0	269	242	0.90
VI	5,330	2,577	0	846	791	0.93
VII	5,400	2,551	0	842	952	1.13
VIII	4,800	1,524	0.69	799	982	1.23
IX	4,500	1,567	0.37	701	552	0.79
X	4,290	1,538	0.37	689	620	0.90
XI	3,720	1,527	0.38	676	566	0.84
XII	5,100	1,553	0	593	610	1.03
XIII	5,990	1,511	0	601	692	1.15
XIV	4,810	1,554	0	587	674	1.15
J1	3,500	0	0.80	180	252	0.71
J2	4,010	0	0.80	447	475	1.06
J3	4,700	0	0.80	463	465	1.00
J4	4,590	0	0.80	460	449	0.98
					Average:	0.98
					St. Dev:	0.14

Pinching of the joint shear-distortion hysteresis loops was simulated as in the SINA model by specifying a crack-closing shear force equal to 25% of the cracking strength of the joint and a crack-closing distortion equal to 75% of the unloading distortion intercept with the horizontal axis.

Strength deterioration due to cyclic loading was observed to be more severe in joint cores than in flexural elements. A strength reduction factor R_j = 1.10 was adopted for the analysis of the joints (instead of R_f=1.05 used for flexural elements).

4.5 Computed vs. Experimental Response

In this section a comparison between the measured response of the beam-column connections described in Section 4.2 and the computed response is presented. The computed response is evaluated in terms of the predicted displacement history of the beams, the energy dissipated per cycle, and the joint contribution to the total deflection or drift angle of the specimens.

Moment-curvature relationships for beams and columns were obtained with the computer program RCCOLA [15] using the material properties shown in Tables 4.1 through 4.6. A portion of the slab, as defined by ACI 318-89 [16], was considered when computing the moment-curvature relationships for the beams. For specimen ME2, full compatibility between the original and the jacketed concrete sections was assumed when computing moment-curvature relationships. Moment-rotation curves were obtained by integration of the moment-curvature relationships, and were later modified to consider bond-slip rotations as described in Chapter 3. For computing bond-slip rotations it was assumed that longitudinal bars passing through the joint were developed over a length (L_b in Equations 3.26 to 3.28) equal to the

beam (or column) height.

All specimens were idealized with the column pinned at the base and top connection. The load history measured with the load cells located at the beam tips was used as the input force to compute the structural response of each subassemblage.

4.5.1 Beam Displacement Histories

Figures 4.8 to 4.12 show a comparison between the measured and computed beam tip deflection histories through the 2% cycles. As can be seen, the agreement between computed and measured displacements is generally very good. The predicted responses of the jacketed beam-column connection agree with the measured response as well as the non-jacketed specimens, supporting the assumption made of full compatibility between the original concrete section and the concrete jacket.

4.5.2 Energy Dissipation

A comparison between the measured and computed energy dissipation per cycle is shown in Figs. 4.13 to 4.17. In cycles up to 1.0% drift no yielding of the longitudinal bars was measured in any of the tested subassemblages [4,6], therefore the only source of energy dissipation was cracking of the concrete. Computed energy dissipation agrees reasonably well with measured energy dissipation, although in general it is underestimated by the analytical model. This may be attributed to the rather simple hysteresis rules implemented in the SINA model for low-amplitude cycles.

Good agreement is also observed at large-amplitude cycles (2% drift), with a general trend of overestimating the energy dissipation in the first of the 2% drift cycles. It must be
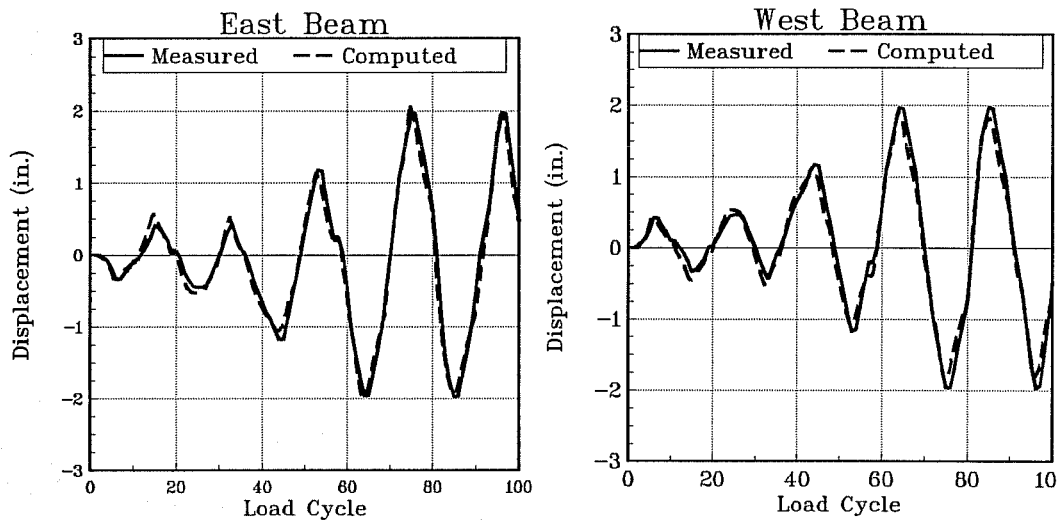
Figure 4.8 Beam Tip Displacement Histories - Specimen J1
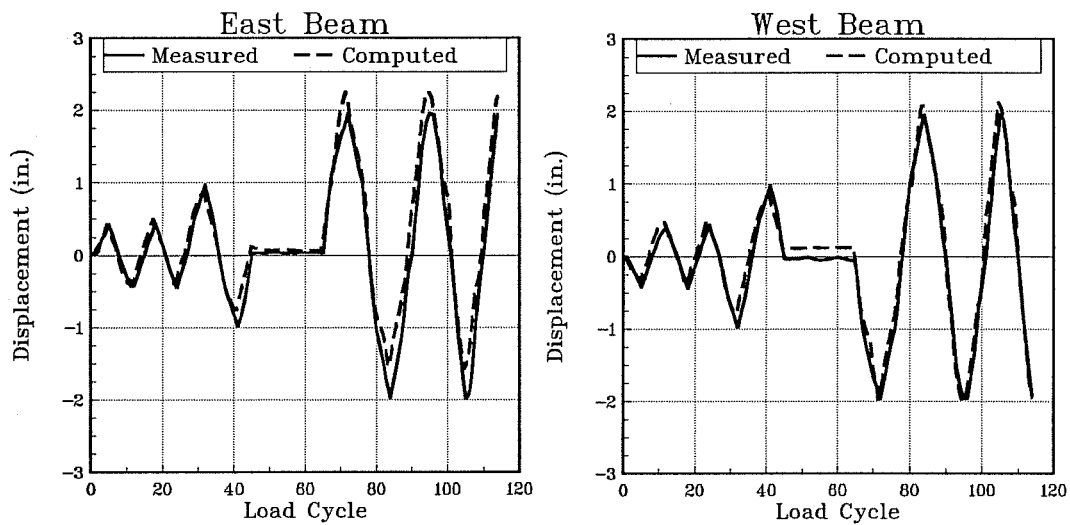
Figure 4.9 Beam Tip Displacement Histories - Specimen J2
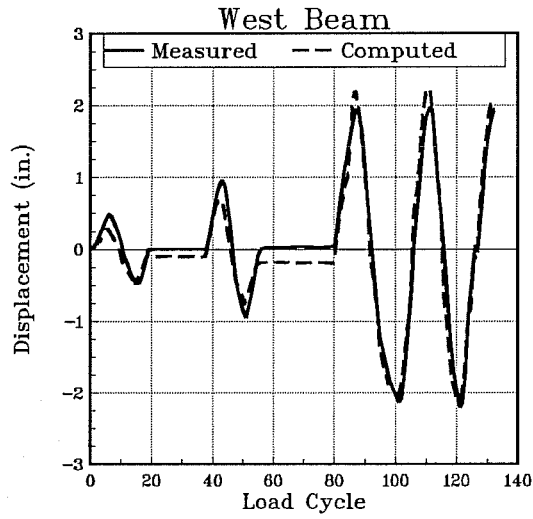
Figure 4.10 Beam Tip Displacement History - Specimen J3
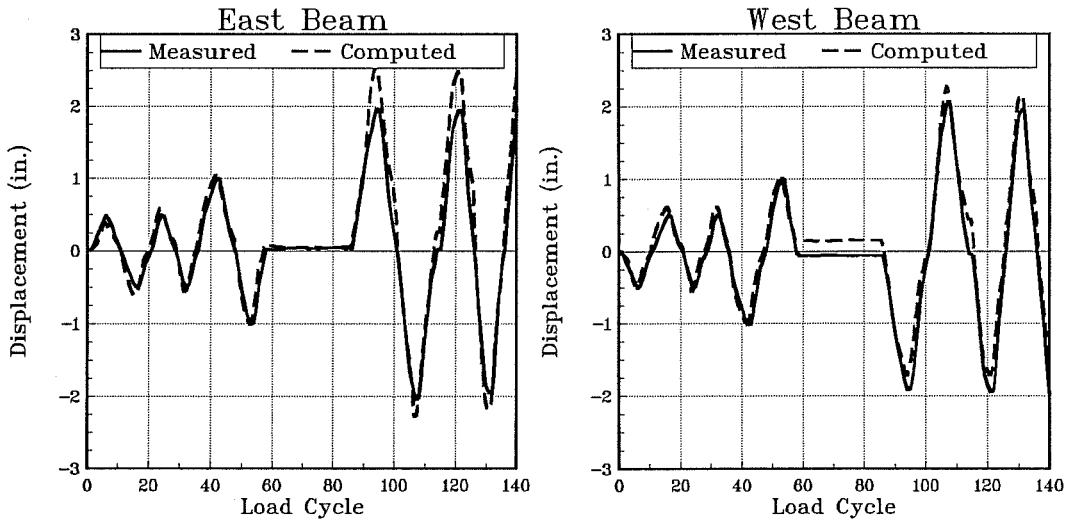
Figure 4.11 Beam Tip Displacement Histories - Specimen J4
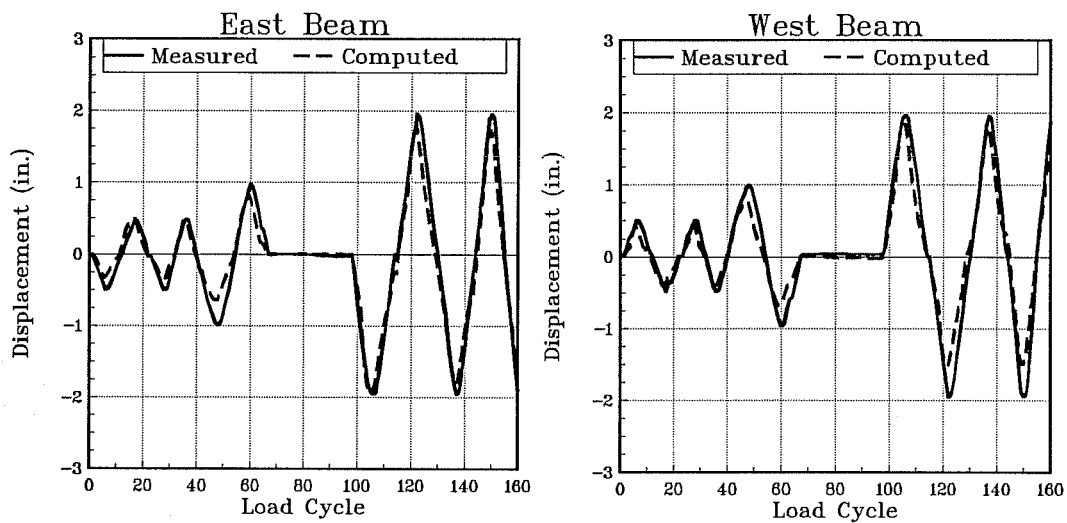
Figure 4.12 Beam Tip Displacement Histories - Specimen ME2
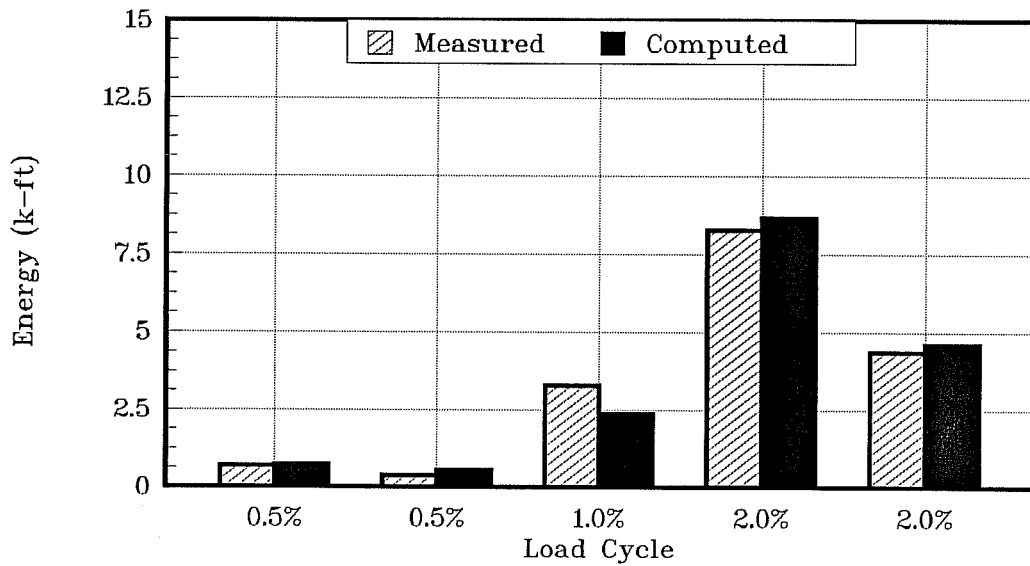
Figure 4.13 Energy Dissipated per Cycle – J1 Specimen
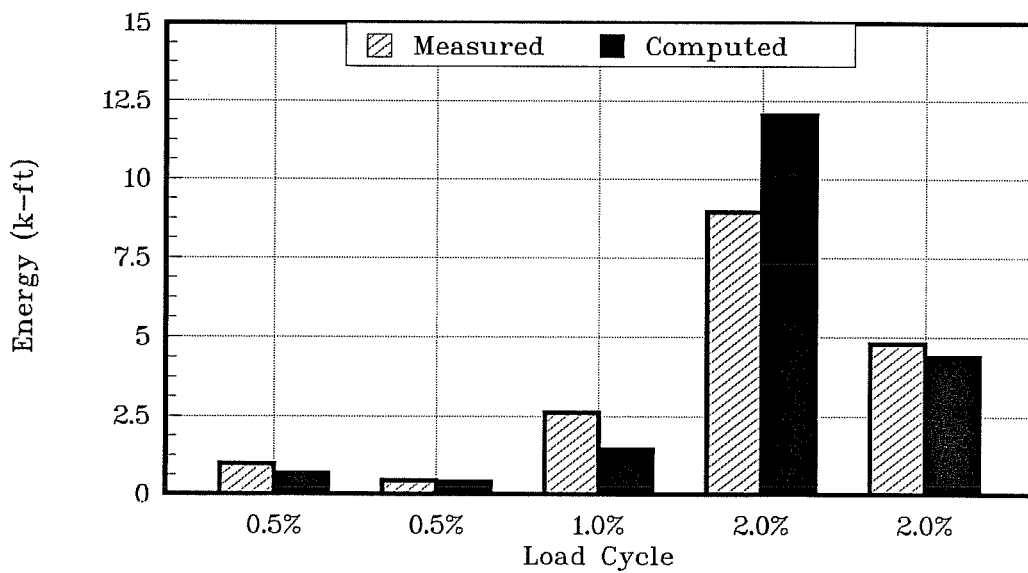
Figure 4.14 Energy Dissipated per Cycle – J2 Specimen
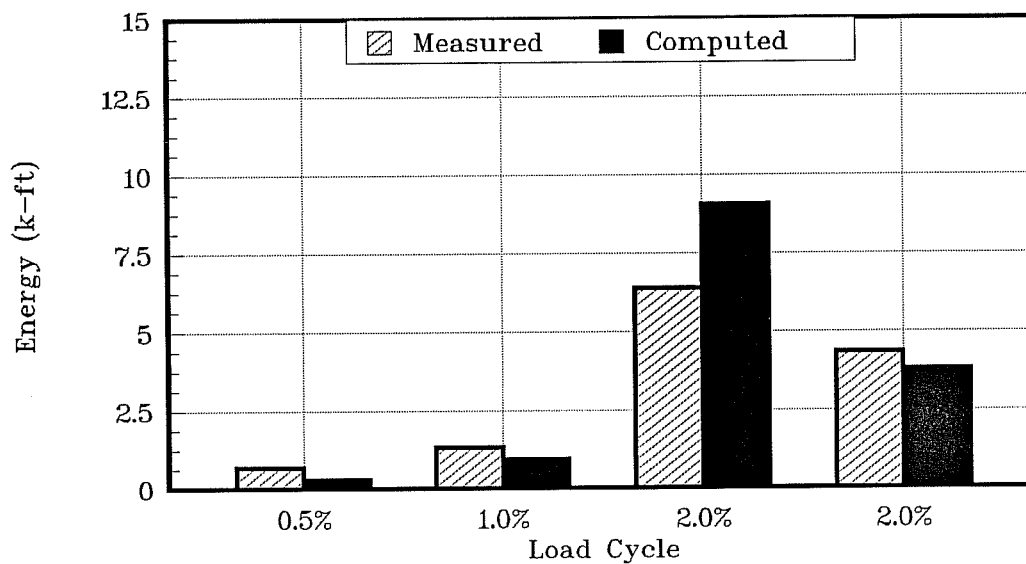
Figure 4.15 Energy Dissipated per Cycle — J3 Specimen
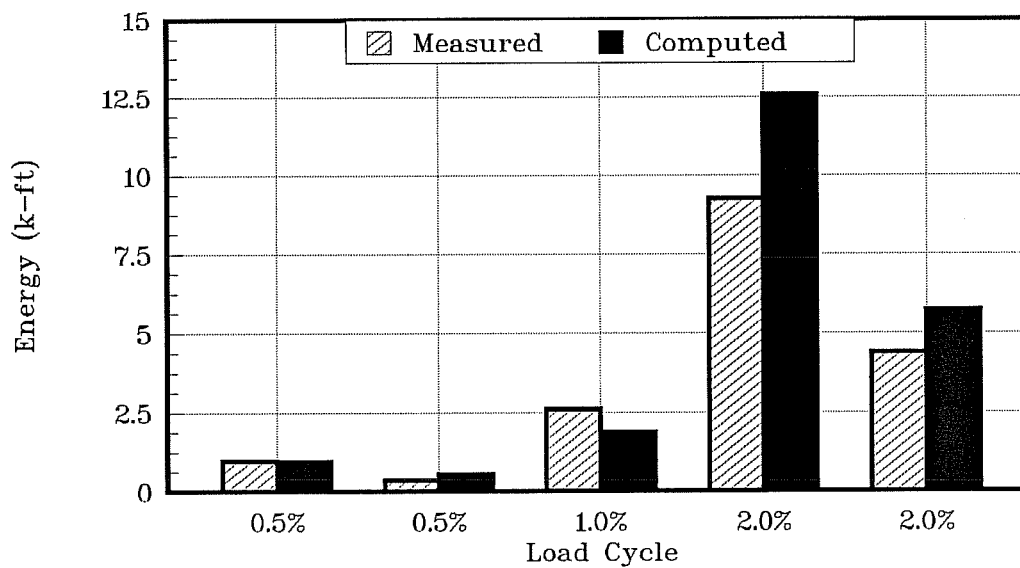
Figure 4.16 Energy Dissipated per Cycle — J4 Specimen
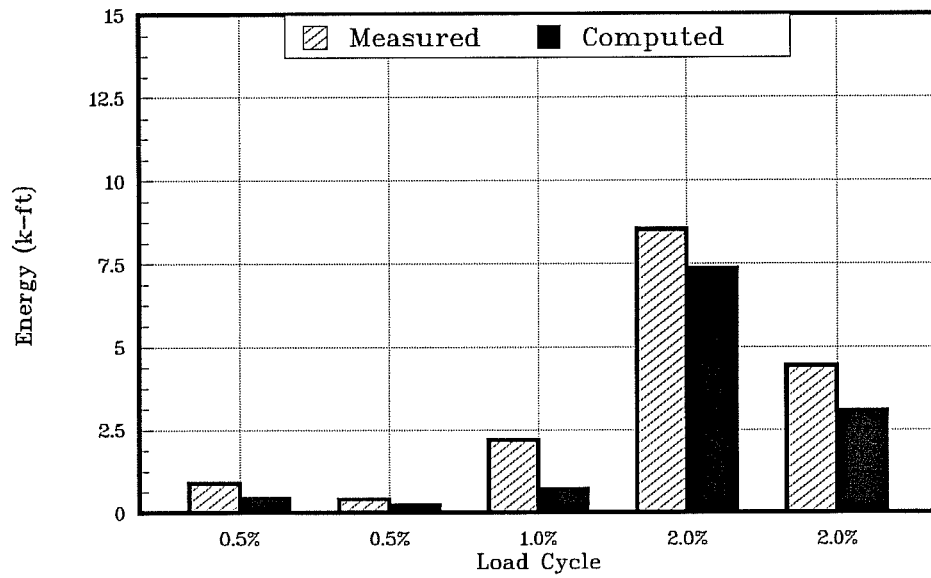
Figure 4.17 Energy Dissipated per Cycle — ME2 Specimen

pointed out that since the test specimens were all statically determinate, and because the load history was used to predict the displacements, the computed response is very sensitive to the post-yielding stiffness of the computed moment-rotation curves, which is usually very low. Much better agreement is observed for the second cycle to 2% drift, where the parameters controlling the energy dissipation are the unloading stiffness and the pinching of the hysteresis loops.

4.5.3 Joint Contribution to Drift Angle

Drift angle is defined as the sum of the beam tip deflections divided by the total length of the beam (beam tip to beam tip). A comparison between the contribution of the flexural elements (beams and columns) and the joint core to the drift angle is presented in Figs. 4.18 to 4.22.

Specimen J1, which did not have lateral beams and was cycled up to 4% drift, showed the largest joint contribution to the drift angle (approximately 35% before the joint began to fail during the 2% drift cycles). The computed joint contribution agrees very well with the measured contribution up to this point. For drift angles larger than 2%, joint deterioration is evident, and since the joint element developed in this study does not have a descending branch after maximum strength is reached, predicted vs. measured response is very poor.

For all the other specimens, which were confined in the transverse direction by lateral beams on both sides of the joint, the contribution of the joint to the drift angle was approximately 20%, and good agreement between the measured and computed joint contribution was obtained.
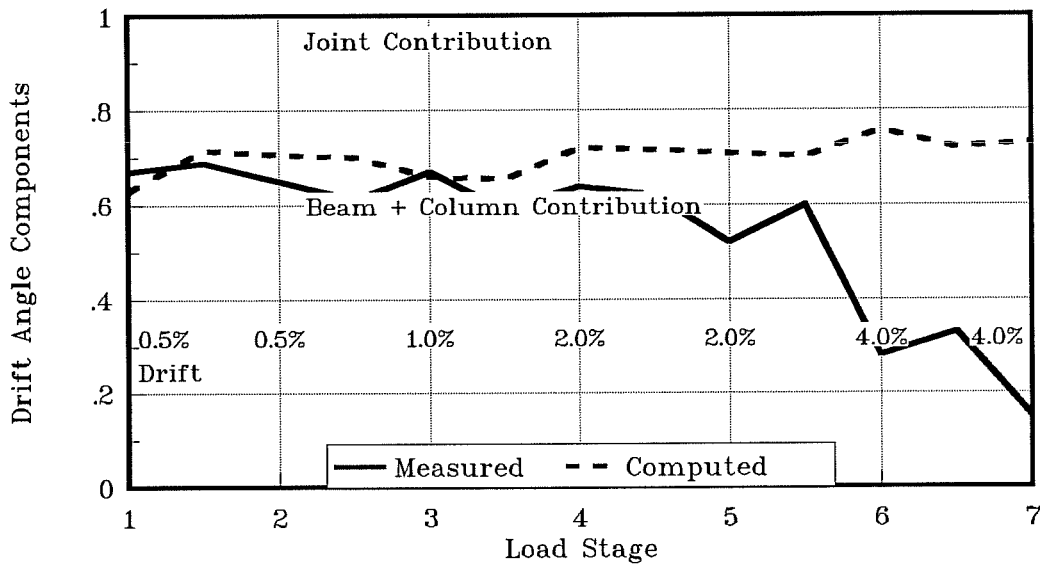
Figure 4.18 Drift Angle Components — J1 Specimen
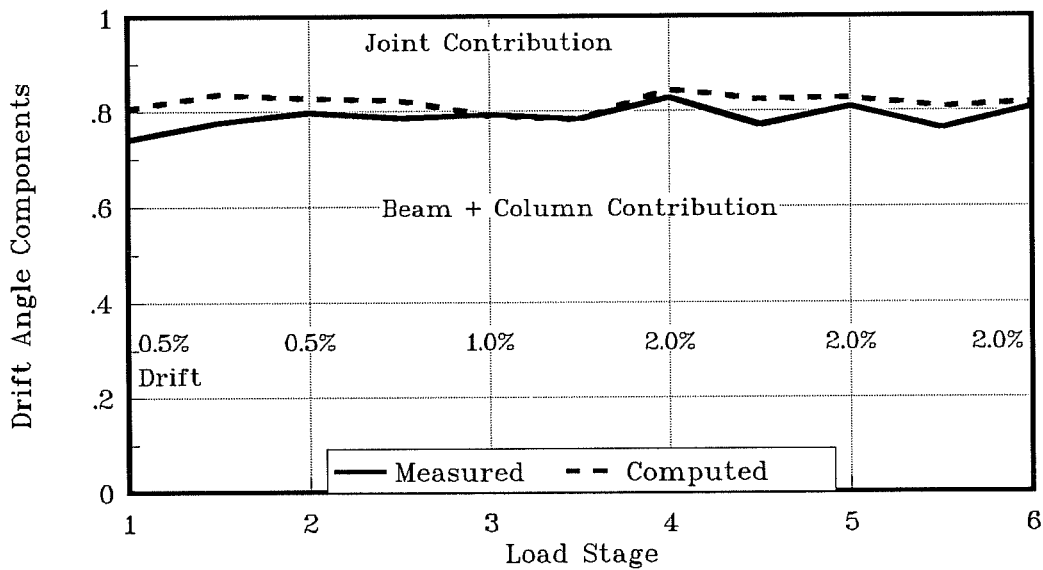
Figure 4.19 Drift Angle Components — J2 Specimen
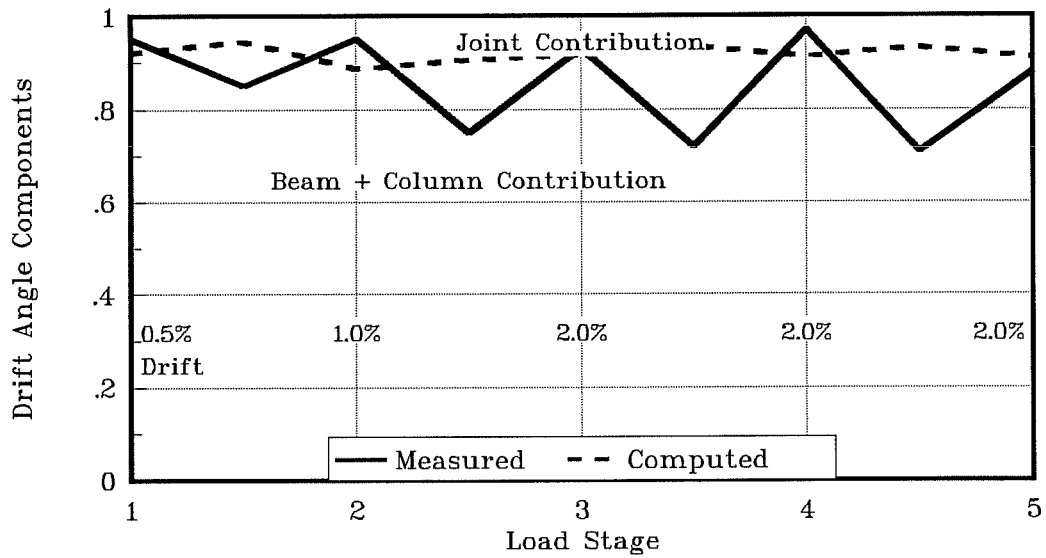
Figure 4.20 Drift Angle Components – J3 Specimen
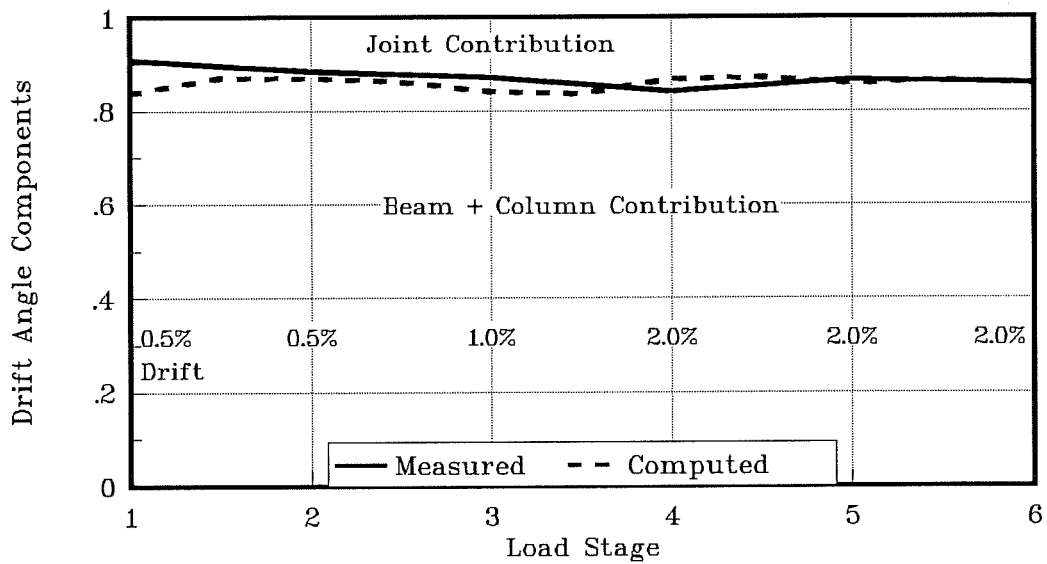
Figure 4.21 Drift Angle Components – J4 Specimen
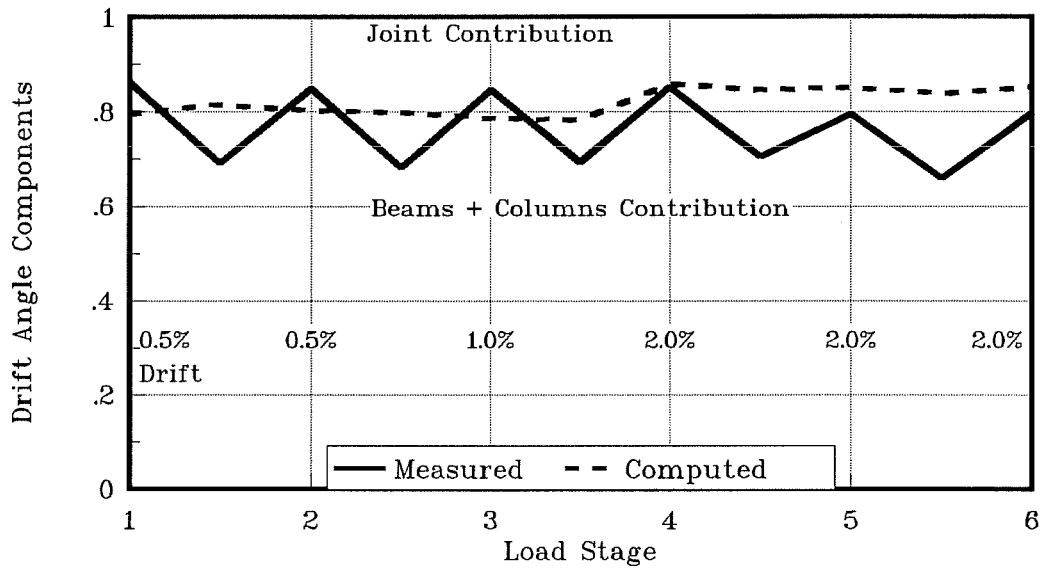
Figure 4.22 Drift Angle Components — ME2 Specimen

CHAPTER 5

CASE STUDIES

5.1 Introduction

Non-ductile reinforced concrete moment-resisting frames constructed twenty five or more years ago have been identified as one of the most serious problems associated with mitigating hazards in the existing building inventory. During the past decade a variety of strengthening techniques for reinforced concrete frames has been investigated [6,24,25,26]. During the same period, however, little analysis has been performed to extrapolate the behavior of complete structural systems from tests conducted on frame connections and subassemblages.

Two reinforced concrete frame buildings designed with outdated codes are studied in this chapter. An evaluation of their main weaknesses is presented first. Several strengthening schemes that consider frame jacketing or addition of reinforced concrete infill walls are then proposed to improve the seismic performance of the original buildings. The effectiveness of these strengthening schemes is evaluated by comparing the dynamic response of the original and the strengthened buildings to selected ground motions using the analytical model described in the previous chapters. Finally, the effect of the main parameters defining the analytical model on the dynamic response of the buildings is discussed in the last section of this chapter.

5.2 Original Buildings

Two reinforced concrete moment-resisting frame buildings, representative of low and medium-rise buildings designed for the west coast of the U.S. in the 1950's or 1960's, are presented in this section.

The low-rise building is characterized by a three-story moment-resisting frame shown in Figure 5.1. The ten-story moment-resisting frame, shown in Fig. 5.2, represents the typical medium-rise building considered in this study.

5.2.1 Design

The three-story building was designed for the lateral force levels specified in the 1964 edition of the Uniform Building Code [19]. Proportioning and detailing of the structural elements was performed following the provisions of the ACI 318-63 [17] ultimate strength design. The specified compressive strength of the concrete was 3000 psi. All reinforcement was assumed to be Grade 60 steel.

Structural drawings of a ten-story building were provided by Dr. Thomas Sabol of Englekirk, Hart, and Associates. Some modifications to the original drawings were made to simplify the structural layout used in this study, while maintaining the basic characteristics of the original design.

Dead loads were computed on the basis of 145 lb/ft^3 normal weight concrete. Live loads for the three-story building were taken from Table 23-A of UBC-64 assuming office occupancy, and from the structural drawings for the medium-rise building. Table 5.1 summarizes the gravity loads considered for the two buildings.

The seismic base shear, as specified by UBC-64 was computed using the following equations

18x18"

18x18" ———14x20"

Slab t=7"

24'

24'

24'

5 @ 24' = 120'

Typical Floor Plan

3@12' = 36'

3@24' = 72'
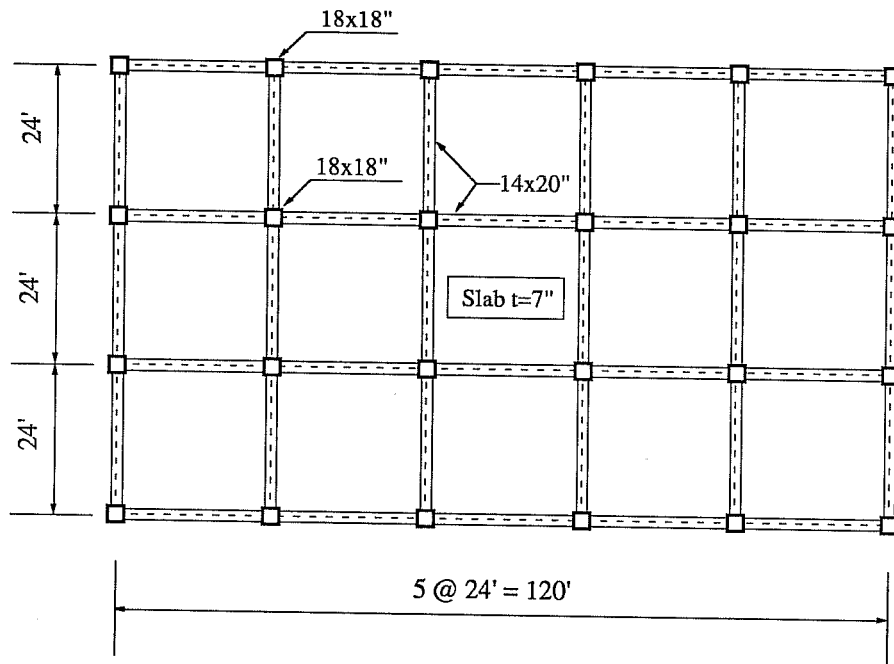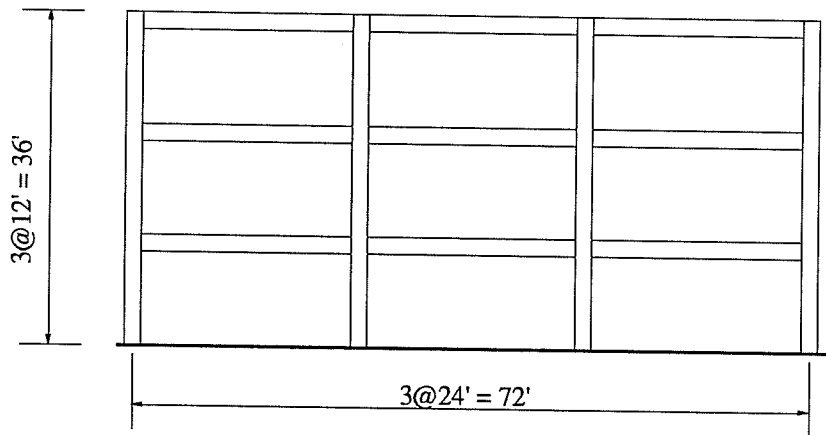
Typical Frame Elevation

Figure 5.1 Three-Story Building
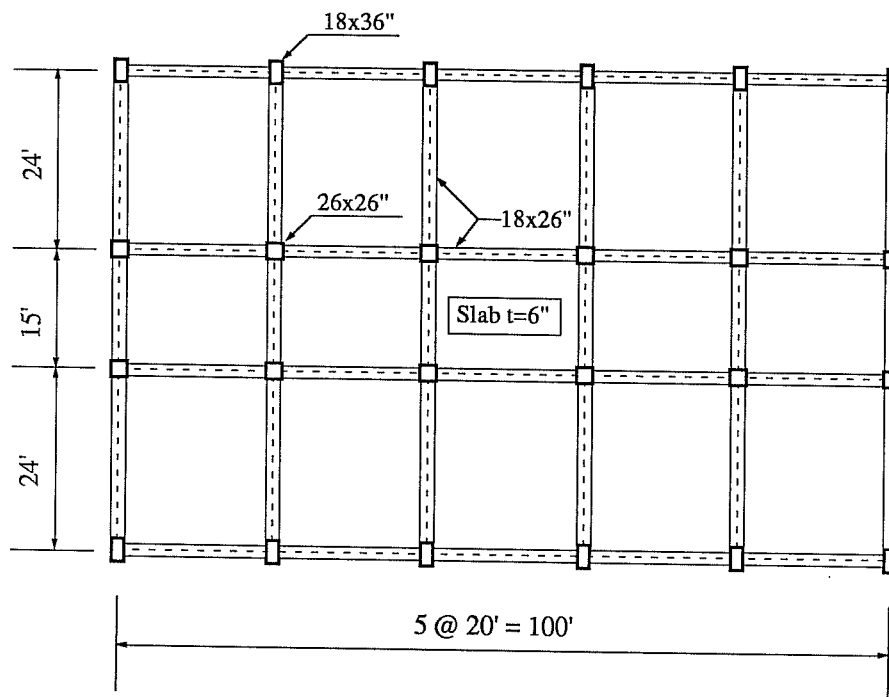
a) Typical Floor Plan

Figure 5.2   Ten-Story Building

10 @ 12' = 120'

18x36"

26x26"

26x26"

18x36"

18x26"

18x26"

18x26"

24'   15'   24'
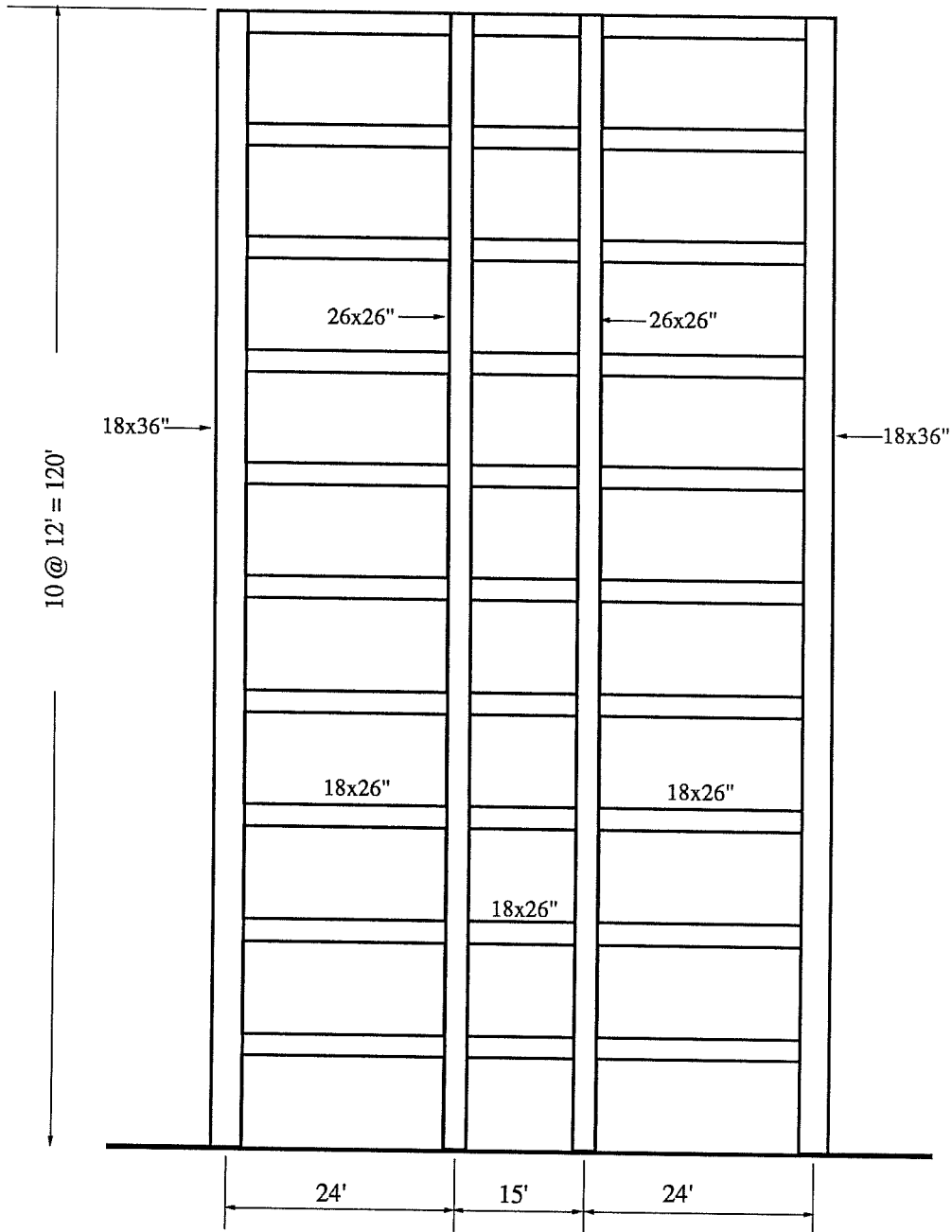
b) Typical Frame Elevation

Figure 5.2 (cont.) Ten-Story Building

$$V = ZKCW$$

$$C = \frac{0.05}{\sqrt[3]{T}} \leq 0.10 \tag{5.1}$$

where Z is a zone coefficient which takes a value of one for buildings located in active seismic zones, K is the horizontal force factor taken as 0.67 for moment-resisting frames, T is the fundamental period of the building in the direction being analyzed, and W represents the total seismic weight of the building, which was taken as the dead load plus 25% of the live load in this study.

Table 5.1 Gravity Loads (psf)

3 Story Building			10 Story Building		
Story Level	Dead	Live	Story Level	Dead	Live
1st & 2nd	160	50	1st thru 9th	180	100
Roof	140	16	Roof	140	20

Application of Eq. 5.1 resulted in design base shears of 212 kips (5% of W) and 414 kips (3.4% of W) for the three-story building and ten-story building, respectively. Wind load was computed to be smaller than seismic load. Gravity and lateral loads were combined as required by ACI 318-63 using the following equations

$$U = \begin{cases} 1.5D + 1.8L \\ 1.25(D + L + E) \\ 0.9D + 1.1E \end{cases} \tag{5.2}$$

Figures 5.3 and 5.4 summarize cross-section dimensions and reinforcement details for beams and columns of the three-story building and ten story-building, respectively. In both cases the

Ast =8#6
#3 ties @12"

18"

18"

Columns

7"

13"

2#8+1#7

#3@9"

2#6

|←14"→|

1st & 2nd Story Beams

7"

13"

2#7

#3@9"

2#6

|←14"→|

3rd Story Beams

a) Exterior Frames

Ast =8#7
#3 ties @14"

18"

18"

Columns

7"

13"

4#9

#3@5"

2#8

|←14"→|

1st & 2nd Story Beams

7"

13"

2#8+1#9

#3@9"

2#8

|←14"→|
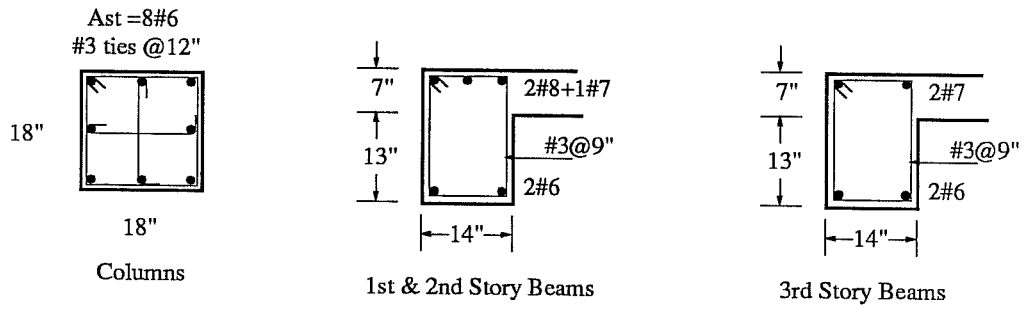
3rd Story Beams
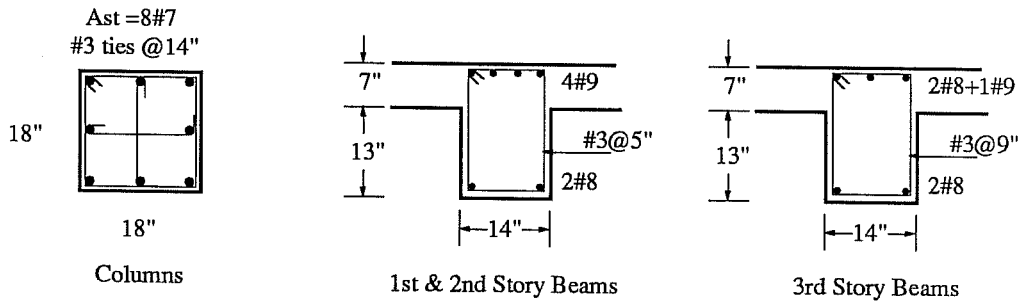
b) Interior Frames

Figure 5.3   Three-Story Building Cross Section Details

Ast =8#10
#3 ties @ 18"

Ast = 8#9
#3 ties @ 18"

36"

18"

18"

1st thru 4th floor

5th thru 10th floor

a) Exterior Column Cross Sections

6"

20"

4#9

#3@9"

2#8

|—18"—|

b) Beam Cross Section

Ast = 8#11
#3 ties @ 18"

Ast = 8#10
#3 ties @ 18"

Ast = 8#9
#3 ties @ 18"

26"

26"

26"

26"

26"

26"

1st thru 4th floor

5th thru 7th floor

8th thru10th floor

c) Interior Column Cross Sections
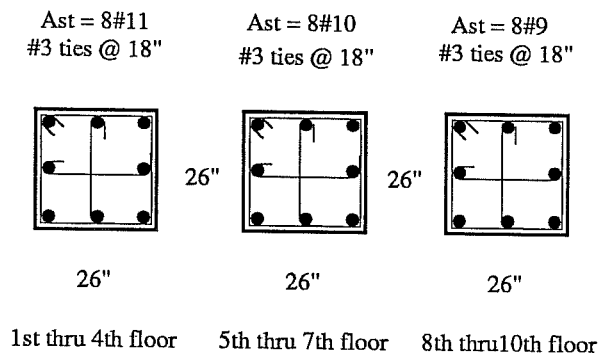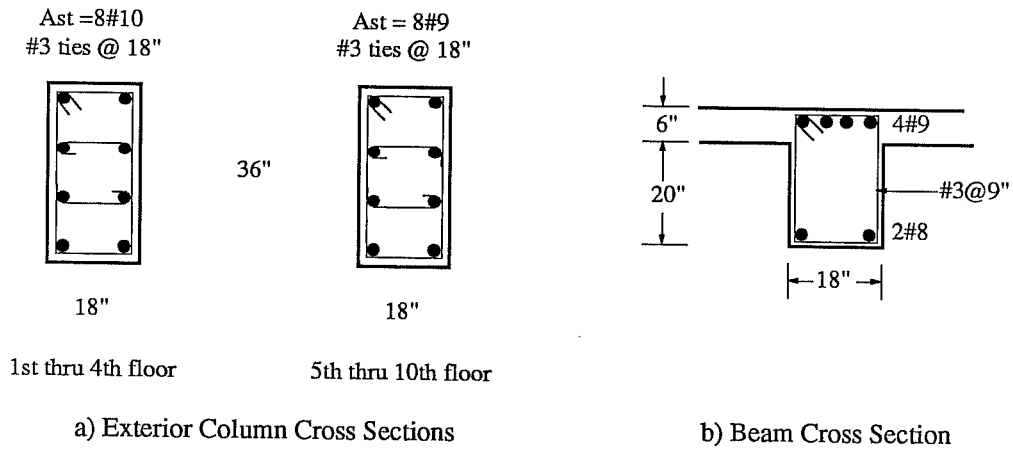
Figure 5.4 Ten-Story Building Cross Section Details

design was controlled by the load combination that includes gravity loads only. The following observations, regarding the resulting design, can be made:

a) Compression Splice in Columns

Because of very small shear demands imposed by the specified lateral loads, columns were designed strictly as compression members. Longitudinal bars were spliced above the slab at each story level, and a splice length of 24 bar diameters was provided [17]. Table 5.2 compares splice length requirements of ACI 318-89 with those actually provided.

Table 5.2 Provided vs. Required Splice Length by ACI 318-89

Bar Size	Provided	Required	Observations
#6	$24d_b$	$33d_b$	3 Story Bldg.
#7	$24d_b$	$33d_b$	3 Story Bldg.
#8	$24d_b$	$48d_b$	10 Story Bldg.
#10	$24d_b$	$61d_b$	10 Story Bldg.
#11	$24d_b$	$68d_b$	10 Story Bldg.

As indicated above, splice lengths are well below current requirements, especially for #8 or larger bars. A splice failure would suddenly reduce the moment capacity of the section and may also reduce the axial load carrying capacity of the columns due to spalling of the cover.

b) Non-continuous beam bottom reinforcement

As stated earlier, beam design was controlled by gravity loads. Computed seismic moments were much smaller than negative gravity moments at column faces. Because moment reversals due to lateral loads were not anticipated, beam bottom reinforcement would need to be anchored only six inches into the joints. Pullout of bottom reinforcement would likely occur in the early stages of a severe ground motion.

c) Confinement Reinforcement

Confinement reinforcement was not required at potential plastic hinge locations by ACI 318-63, and was not provided. The ability of the structural elements to sustain several cycles of load reversals is dubious given the transverse reinforcement actually provided in critical zones of beams and columns of the original buildings. Table 5.3 compares current confinement reinforcement requirements for columns with that actually provided in the original buildings.

Table 5.3 Provided vs. Required Column Confinement Reinforcement by ACI 318-89

Building	Element	Provided	Required
3 Story Building	Ext. Frame Columns	3#3@12"	3#3@3.5"
	Int. Frame Columns	3#3@14"	3#3@3.5"
10 Story Building	26x26" Columns	3#3@18"	3#3@3.0"
	18x36" Columns	2#3@18"	2#3@3.0"

d) Shear Capacity of Beams and Columns

Provisions to ensure the development of the flexural capacity of beams and columns

prior to a shear failure were first incorporated in Appendix A of the 1971 edition of the ACI

318 Building Code [18]. Shear reinforcement in beams and columns of the original buildings

was provided to satisfy shear demands due to specified gravity load and lateral load

combinations, resulting in lightly reinforced elements. Table 5.4 compares the shear capacity

of the first-story columns with that required to develop their flexural strength.

Table 5.4 Shear Capacity vs. Required Shear Strength for Flexural Strength Development of 1st Story Columns (kips)

Building	Element	Shear Strength ϕV_n	Shear Strength for Development $(M_{top}+M_{bot})_{max}/L$
3 Story Building	Ext. Columns	48	30
	Int. Columns	45	42
10 Story Building	26x26" Columns	77	180
	18x36" Columns	79	171

It can be seen that while a column shear failure is not likely to occur in the three-story

building, the shear strength of columns in the ten-story building is clearly inadequate.

e) Joint Reinforcement

Joint reinforcement was not required by ACI 318-63, and was not provided in any of

the beam-column connections of the buildings considered.

5.2.2 Lateral Strength Estimation

An estimation of the lateral strength of the buildings using the analytical model described in Chapter 3 is presented in this section.

Moment-curvature relationships were computed for critical sections of each structural element using the computer program RCCOLA [15]. The concrete stress-strain relation proposed by Scott, Park and Priestley [20] was adopted, and the steel stress-strain curve was idealized as shown in Fig. 5.5.

For modeling of columns that featured a short compression splice at each floor level, an estimate of the mean maximum tensile stress (and moment) that the spliced bars could develop was obtained using Eq. 5.3 proposed by Orangun [21]

$$ f_s = \left\{ \left(1.2 + 3\frac{C}{d_b} + \frac{A_{tr} f_y}{500 s d_b} \right) \frac{l_d}{d_b} + 50 \right\} 4 \sqrt{f_c'} \qquad (5.3) $$

where

C   =   smaller of bottom cover of main reinforcement and half clear spacing between bars being spliced (in.),

d_b =   diameter of main reinforcement (in.),

A_{tr} =   area of transverse reinforcement normal to the plane of splitting through the anchored bars (in^2),

f_y =   yield strength of transverse reinforcement (psi),

l_d =   development length (in.),

f_c' =   concrete cylinder strength (psi).

Table 5.5 shows the maximum tensile stresses, computed using Eq. 5.3, that column
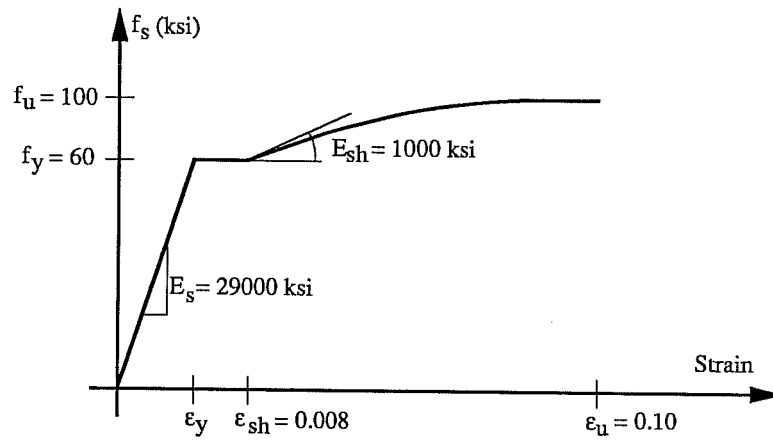
Figure 5.5 Idealized Steel Stress -Strain Relationship

and beam bars would be able to develop given the splice length and anchorage conditions discussed previously in Section 5.2.1. Although column bars of the three-story building would be expected to develop yielding prior to a splice failure, a maximum tensile stress equal to the yield stress was conservatively assumed in this study.

There is very little information in the literature about the behavior of columns with short splices subjected to load reversals [22,27]. In this study it was assumed that the moment-rotation curve is described by a typical ascending branch and a descending branch that connects the maximum moment that the section can resist before a splice failure occurs, with a point defined by a moment equal to 25% of the maximum moment and a rotation equal to ten times the rotation associated with the peak moment (Fig. 3.13). The effect of this assumption on the computed response of the buildings will be discussed later.

After preliminary dynamic analyses showed that maximum inertial forces associated with inelastic behavior of the buildings were better approximated by a uniform lateral load rather than by an inverted triangular lateral load distribution, an estimate of the lateral strength of the buildings was made by subjecting them to a uniform lateral load distribution that was increased until each structure became unstable.

Figure 5.6 illustrates the applied base shear, expressed as a percentage of the building weight, versus the overall drift, defined as the roof displacement divided by the building height, for the three-story building. The solid curve represents the response of the building assuming all structural elements to be uncracked before load was applied (uncracked model). The curve clearly shows three different stages in the response of the building. In the first stage the response is linear elastic. A sharp reduction in stiffness takes place at a drift level of about 0.10%, primarily due to cracking of beams and columns. Stiffness continues to decrease for

drift levels above 0.10% as beams yield in negative moment and bottom reinforcement pulls

out of the joints. Finally, after the splice capacity of all first-story columns is exceeded at an

overall drift of 0.65%, the load-deflection curve becomes very flat. The load-deflection

response assuming beams and columns to be cracked before load is applied is shown by the

broken line in Fig. 5.6 (cracked model). In this case the response is elastic up to a drift level

of about 0.30%, after which beam bars begin to pull out of the joints, gradually reducing the

building stiffness. The splice capacity of all first-story columns is exceeded at a drift level of

0.90%.

Table 5.5 Maximum Tensile Stress in Spliced Column Bars and Non-Continuous Beam Bottom Reinforcement

Building	Element	Bar size	l_d (in.)	f_s (ksi)
3 Story Building	Exterior Frame Columns	#6	18	69.8
	Interior Frame Columns	#7	21	64.2
	Exterior Frame Beams	#6	6	30.6
	Interior Frame Beams	#8	6	23.2
10 Story Building	18x36" Columns (1st-4th floor)	#10	30	46.7
	18x36" Columns (5th-10th floor)	#9	27	50.3
	26x26" Columns (1st-4th floor)	#11	34	46.4
	26x26" Columns (5th-7th floor)	#10	30	49.7
	26x26" Columns (8th-10th floor)	#9	27	53.7
	Beams	#8	6	23.2

The response of the ten-story building under monotonic lateral load is shown in Fig. 5.7, and can be characterized in the same way as was done for the three-story building. For the uncracked model, cracking takes place at a drift level of about 0.05%, and the maximum strength of the building is reached shortly after splice capacities of all first-story columns have been exceeded at 0.45% drift. For the cracked model, pullout of the beam bottom reinforcement begins at 0.15% drift, and splice failure of all first-story columns takes place at 0.51% drift. It should be noted that although the shear capacity of the columns was inadequate, as shown in Table 5.4, shear forces at maximum drift were computed to be below the shear capacity of the columns.

Because the behavior of the buildings is very uncertain after all first-story column splice capacities have been reached, and also considering that the load-deflection curves become very flat after this event, the building lateral strength was defined as the base shear that first produces a generalized splice failure of the first-story columns. Using the previous definition, lateral strengths of 15% and 11% of the building weight were estimated for the low-rise and medium-rise buildings.

One recommendation for the minimum lateral strength that the original buildings should possess can be obtained from ATC-22 [23], which is intended for use in evaluating the seismic resistance of existing buildings. According to this document an existing building should have a minimum lateral strength given by

$$C_s = 0.80 \, \frac{A_v \, S}{R \, T^{2/3}} \leq 2.12 \, \frac{A_a}{R} \tag{5.4}$$

where T is the fundamental period of the building, A_v and A_a are the velocity-related acceleration and acceleration coefficients, S is a coefficient that considers the soil properties,
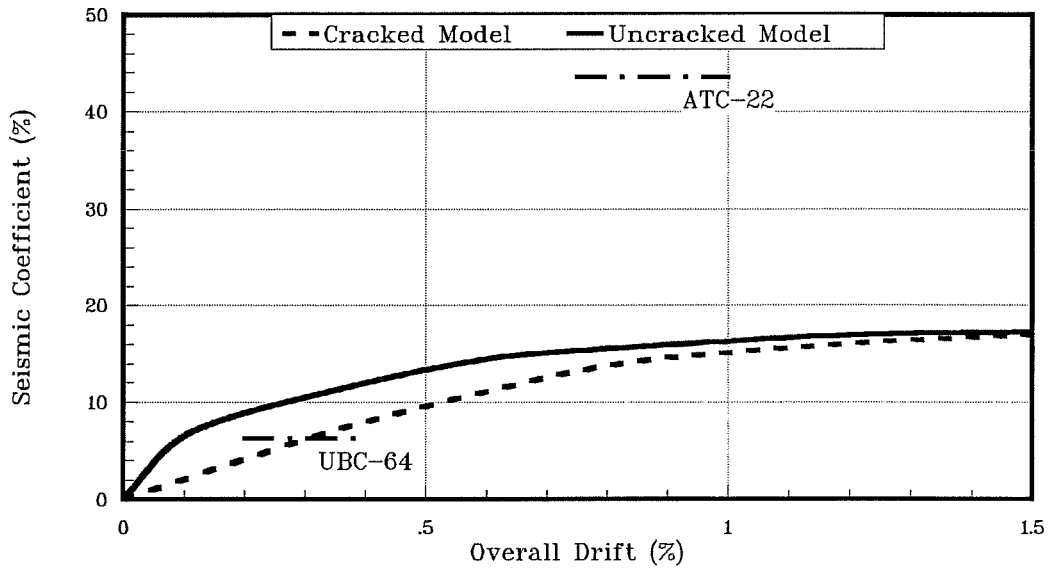
Figure 5.6 Load—Deflection Response — 3 Story Building
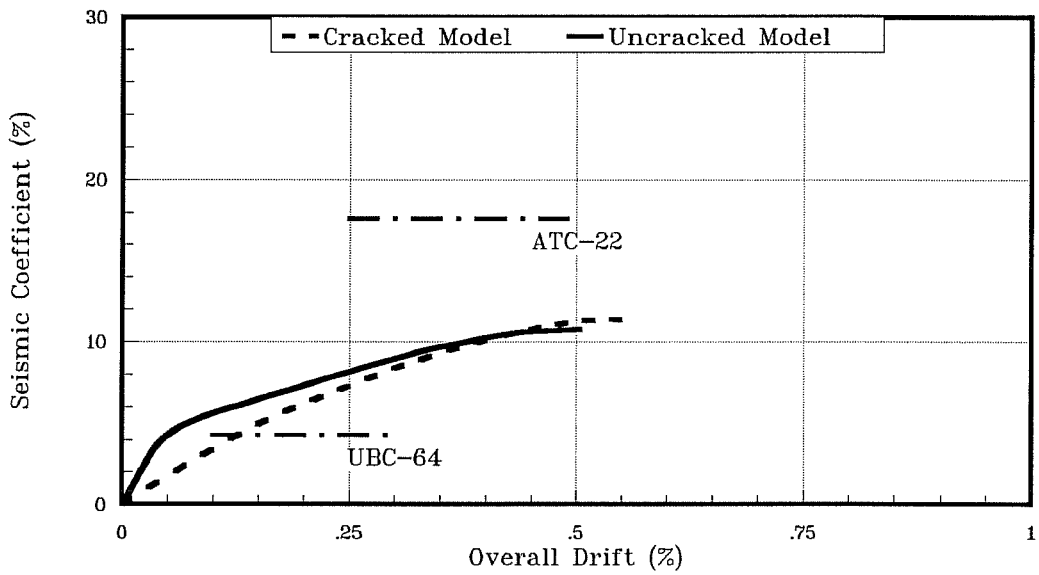
Figure 5.7 Load—Deflection Response — 10 Story Building

and R is a response modification factor. Assuming $A_v = A_a = 0.4$ (high-risk seismic zone), $S = 1.2$ (stiff soil conditions), and $R = 2$ (ordinary moment resisting frame) a comparison between the seismic coefficient computed using Eq. 5.4 and the lateral strength of the buildings is also presented in Figs. 5.6 and 5.7.

5.2.3 Summary

From the discussion of the previous sections it can be concluded that the hypothetical buildings considered in this study would have been deficient in both strength and ductility. Others buildings designed with the same [17,19] or similar codes are very likely to exhibit similar deficiencies.

5.3 Strengthening Schemes

From a practical point of view it is desirable to concentrate the construction process on the exterior of buildings undergoing seismic retrofit. As a result, strengthening schemes that considered modifications to only the exterior frames of the existing buildings were analyzed. One must keep in mind that, although it is possible to design the strengthened portions of the structure to meet current detailing requirements for ductility, the retrofitted building as a whole will not conform to current standards because of the presence of unstrengthened elements that still have the potential for undesirable behavior. The basic question that arises is,"What lateral load level should a retrofitted building be designed for?" As was noted in Chapter 2, there is no explicit answer to this question in currently accepted codes of practice. Due to this fact, several strengthening schemes that provide different levels of lateral strength were considered, rather than designing for a given fixed base shear. Detailing of reinforcement for the

strengthened elements was done following the provisions of ACI 318-89. Concrete compressive

strength was assumed to be 4.0 ksi, and Grade 60 steel was used in all calculations.

Strengthening schemes that considered frame jacketing or the addition of reinforced

concrete infill walls were designed to improve the lateral strength and ductility of the original

buildings. A brief description of their basic characteristics is given next.

5.3.1 Three-Story Building

Four retrofitting options were designed for the three-story building. Strengthening

schemes J3A, J3B and J3C involved jacketing of the perimeter frames. A four-inch jacket was

provided around all existing 18x18" exterior columns resulting in 26x26" jacketed columns.

Practical considerations for placement of the longitudinal reinforcement in jacketed beams led

to 24x24" beams in all the exterior frames for jacketing schemes J3A and J3B, and to 24x30"

beams for scheme J3C. The difference between scheme J3A and J3B resides in the amount

of longitudinal reinforcement in beams and columns. Scheme J3C has the same column

reinforcement as scheme J3B but jacketed beams are stronger and stiffer in the former case.

Table 5.6 summarizes reinforcement details for the three cases. Figures 5.8 and 5.9 give

further details of jacketing schemes J3A, J3B, and J3C.

A fourth strengthening scheme (W3) consisting of the addition of a 10" thick

reinforced concrete infill wall placed in the interior bay of the exterior frames was also

considered. A concrete jacket cast around the adjacent columns was provided to preclude a

splice failure of the original column longitudinal reinforcement and to allow the columns to act

as boundary elements for the infill wall. Reinforcement details are given in Table 5.6 and in

Figs. 5.10 and 5.11.

26x26"

18x18"

14x20"

Slab t=7"

26x26"

24x24" (J3A-B)
24x30" (J3C)

24'

24'

24'

5 @ 24' = 120'
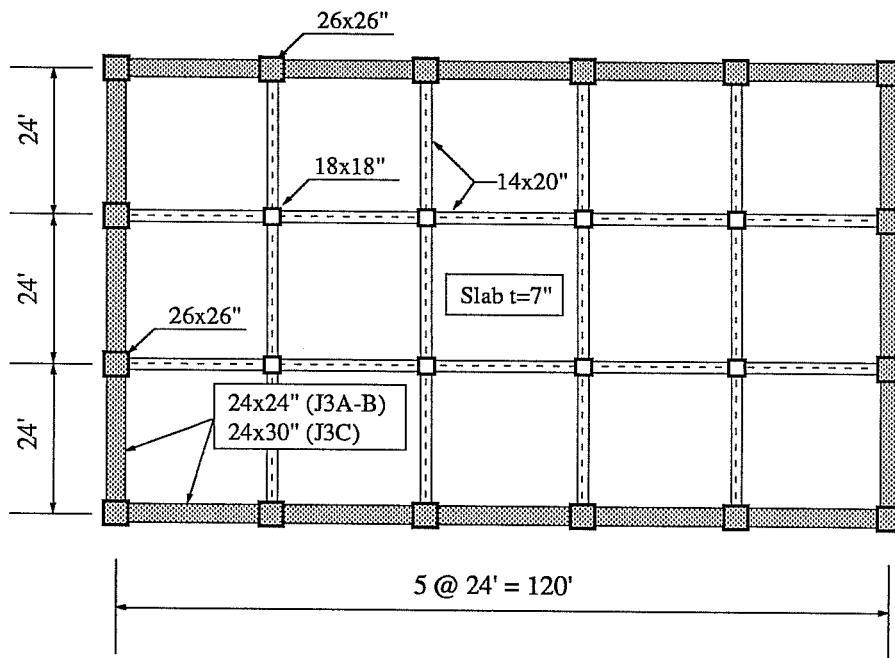
Typical Jacketed Building Floor Plan

26x26"(typ.)

24x24" (J3A-B)

24x30" (J3C)

3@12' = 36'

3@24' = 72'
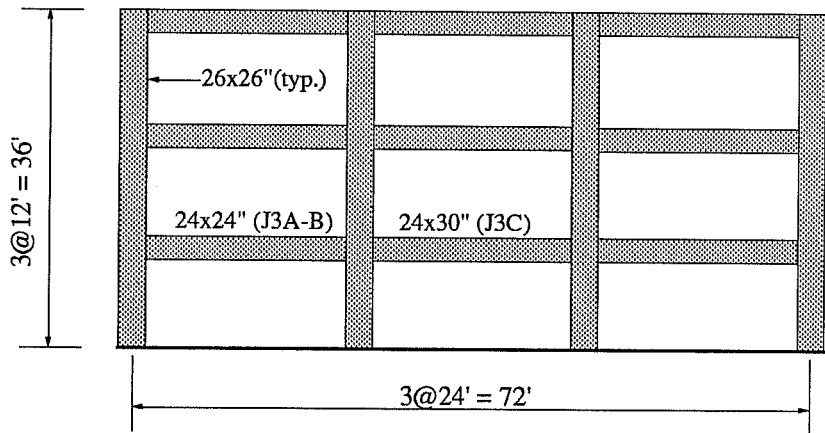
Typical Jacketed Frame Elevation

Figure 5.8 Strengthening Schemes J3A, J3B and J3C

Ast =12#6
#3 ties @4"

26"

26"

Columns

7"

17"

4#8

#3@4"

2#8+2#6

24"

1st Story Beams

4#7 (2#8 3rd Floor)

2#7+2#6
(2#8 3rd Floor)

24"

2nd and 3rd Story Beams

a) Strengthening Scheme J3A

Ast =12#10
#4 ties @4"

26"

26"

Columns

7"

17"

4#9

#4@4"

4#9

24"

Beams (all Stories)

b) Strengthening Scheme J3B

Ast =12#10
#4 ties @4"

26"

26"

Columns

7"

23"

4#9

#4@4"

4#9

24"

Beams (all Stories)
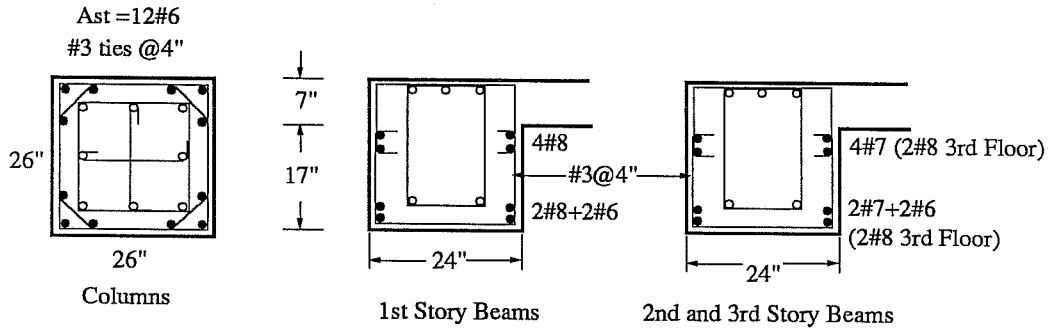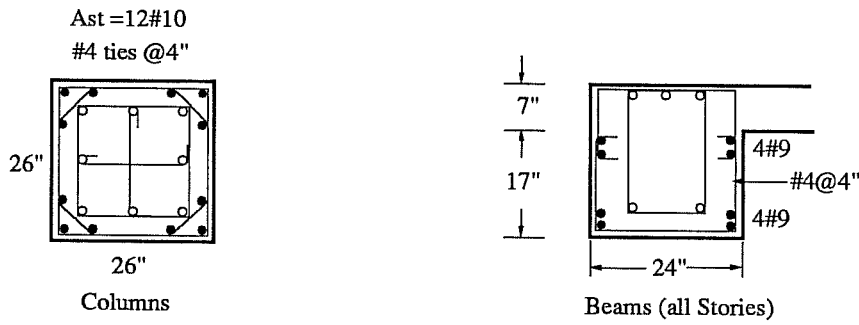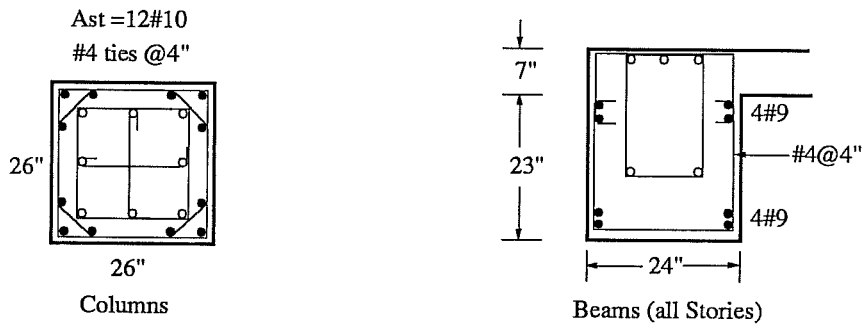
c) Strengthening Scheme J3C

Figure 5.9   Strengthening Schemes J3A, J3B, andJ3C - Cross Section Details

18x18"

24'

26x26"   18x18"   —14x20"   26x26"

24'

Wall t=10"   Slab t=7"   Wall t=10"

24'

5 @ 24' = 120'

Typical Floor Plan

3@12' = 36'

3@24' = 72'

Typical Exterior Frame Elevation
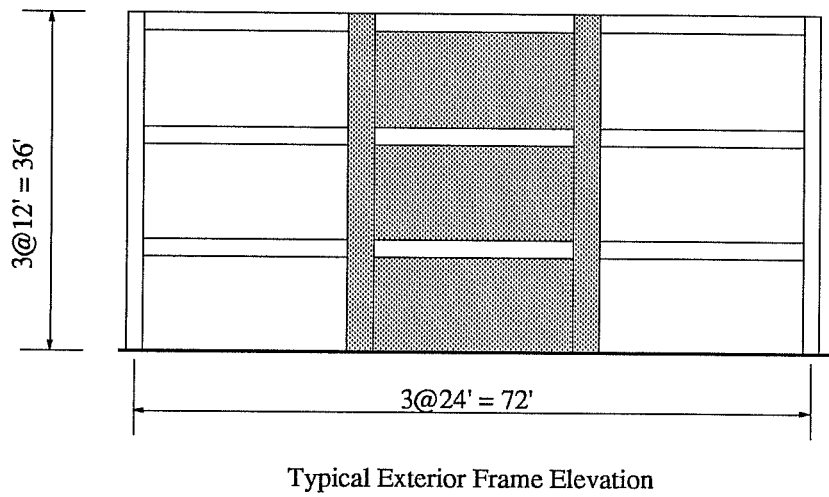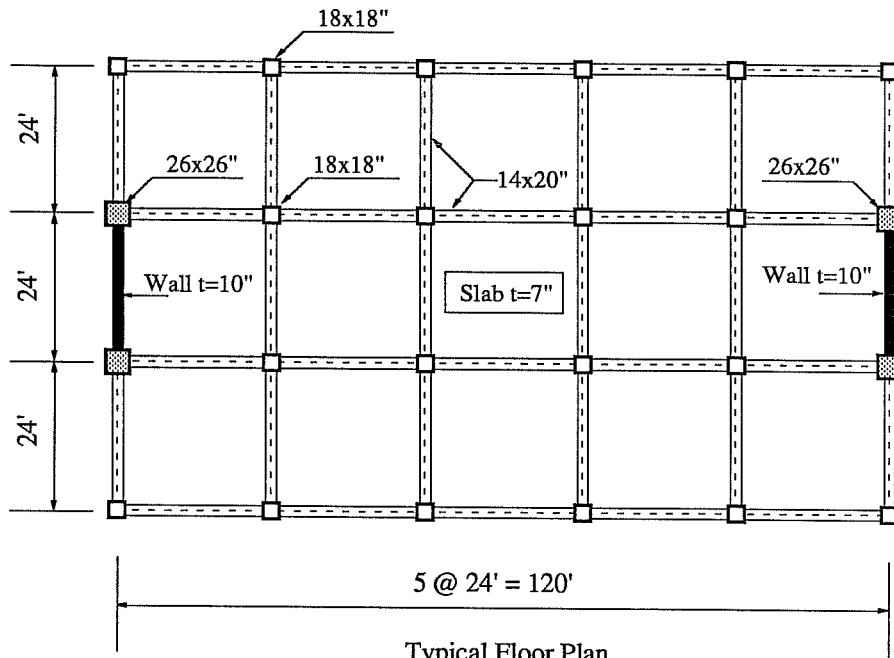
Figure 5.10 Strengthening Scheme W3
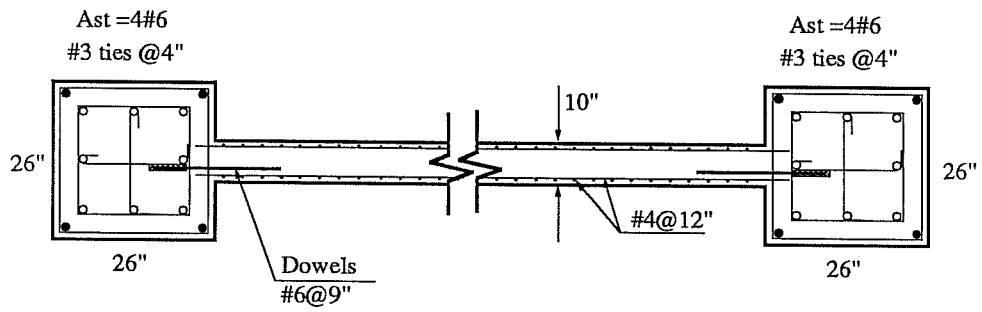
Figure 5.11 Strengthening Scheme W3 - Cross Section Details

Table 5.6 Reinforcement Details of Strengthened Three-Story Buildings

Element	Reinforcement Position	Strengthening Scheme			
		J3A	J3B	J3C	W3
Jacketed Columns	Longitudinal	12#6	12#10	12#10	4#6
	Ties	#3@4"	#4@4"	#4@4"	#3@4"
Jacketed Beams	Top	4#8[1]	4#9	4#9	-
	Bottom	2#8+2#6[1]	4#9	4#9	-
	Stirrups	#3@4"	#4@4"	#4@4"	-
Infill Wall	Web	-	-	-	2#4@12"

(1) First-story beams

5.3.1.1 Lateral Strength

Non-linear lateral load analyses were performed to compare the stiffness and strength of the retrofitted buildings with that of the original building.

Figure 5.12a compares non-dimensional base shear vs. roof displacement curves for the different strengthening schemes subjected to a uniform lateral load distribution applied in the transverse direction (Y-DIR). Similar plots for loading in the longitudinal direction (X-DIR) are presented in Figure 5.12b.

Regarding the shapes of the curves, all jacketing schemes demonstrate a load-deflection response similar to the original building. Behavior is nearly elastic up to a drift level of approximately 0.70%, leaving little room for inelastic behavior, and therefore, little energy dissipation under reversed cyclic loading before splice failures in unstrengthened columns occur.

Strengthening schemes J3A, J3B and J3C can therefore be classified as strength reliant schemes.

The load deflection response for strengthening scheme W3 demonstrates a very stiff structure with a well defined "yield" point at approximately 0.10% drift. Fracture of the longitudinal bars in the boundary columns was predicted at 0.90% drift, which was before the unstrengthened columns reached the moment associated with splice failure.

Two characteristic points have been marked in the load-deflection curves: the point at which splice failure of the unstrengthened columns occurs, and the point at which a sidesway mechanism is formed in the jacketed frames or hinging at the base of the wall is predicted by the analytical model. From an energy dissipation point of view, it is desirable for the strengthened portions of the building to be able to form a complete mechanism before failure of the unstrengthened elements. As illustrated in Fig. 5.12a, strengthening scheme W3 is the only one that satisfies this condition.

The lateral strength of the low-rise buildings, defined as the seismic coefficient (base shear divided by the building weight) that produces a generalized splice failure of the first-story columns in the jacketed buildings or fracture of the longitudinal reinforcement in the boundary columns of strengthening scheme W3, is compared in Fig. 5.13 with the seismic coefficient given by Eq. 5.4.

5.3.1.2 Stiffness

The additional stiffness provided by the strengthening schemes can be easily appreciated from the load-deflection curves previously discussed (Fig. 5.12).

A comparison of the relative stiffness between the strengthened frames and interior
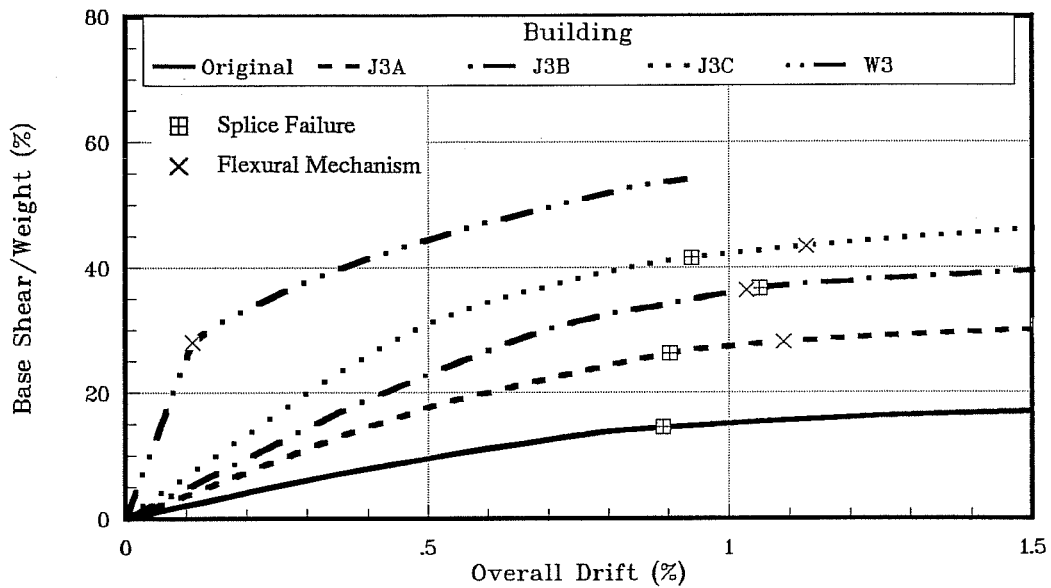
a) Load—Deflection Response Y—DIR
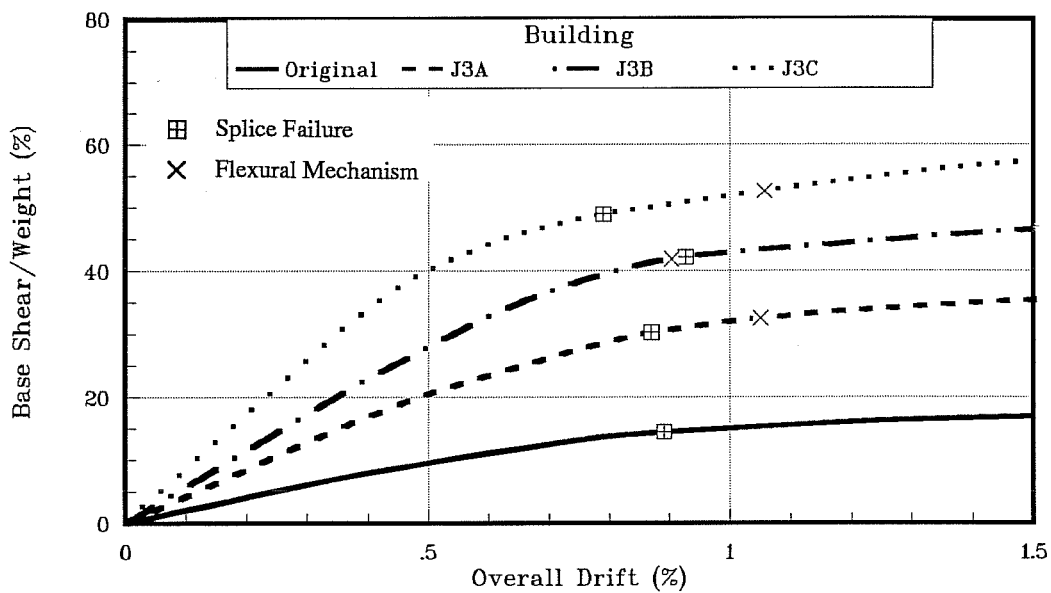
b) Load—Deflection Response X—DIR

Figure 5.12 Load-Deflection Curves, Three-Story Buildings
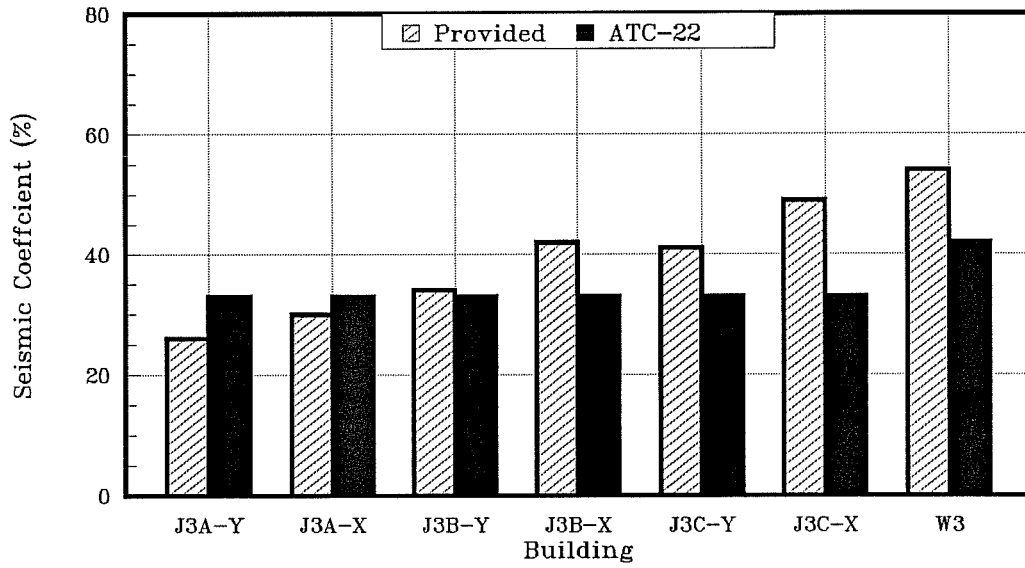
Figure 5.13 Provided vs. Required Strength — 3 Story Buildings
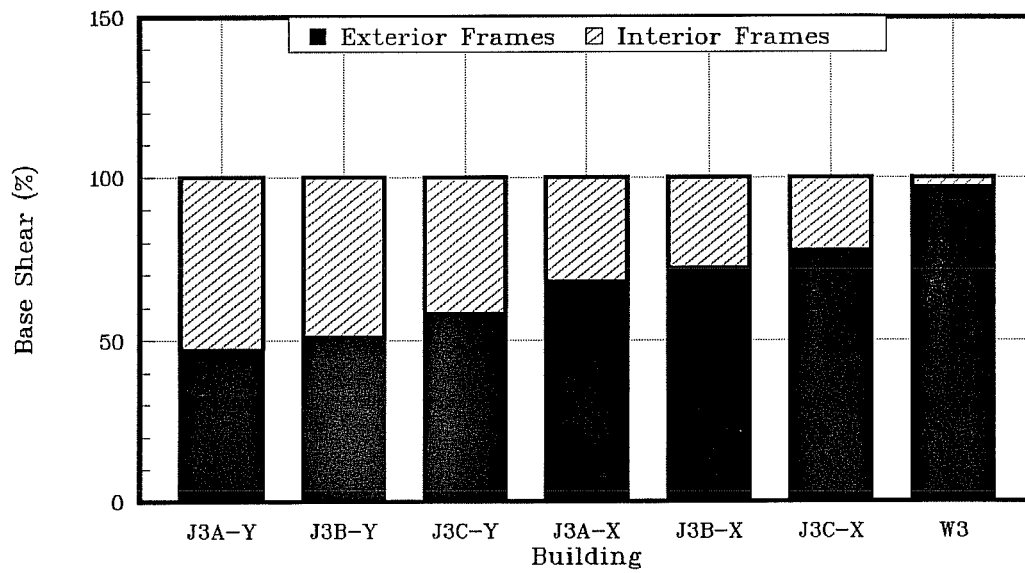
Figure 5.14 Elastic Base Shear Distribution — 3 Story Buildings

frames is of interest because it gives an idea of how the lateral forces distributed to the frames. Figure 5.14 shows how the base shear is distributed among exterior and interior frames of the buildings, assuming elastic behavior. Small variations in the base shear distribution, of the order of ±4%, were computed as buildings J3A, J3B and J3C were loaded to failure, confirming the fact that jacketed and original frames tend to exhibit inelastic behavior at similar drift levels. In contrast, the contribution of the infill walls of strengthening scheme W3 to the base shear was reduced from 96% in the elastic range to 84% when the walls were about to fail.

5.3.2 Ten-Story Building

Five strengthening schemes were designed for the ten-story building. Two considered jacketing of the exterior frames, two involved addition of concrete infill walls, and a fifth considered a combination of frame jacketing and addition of infill walls.

Jacketing scheme J10A considered jacketing of both exterior frames. A five inch jacket was provided around the interior columns resulting in 36x36" columns. In order to make passing the additional longitudinal reinforcement through the joints possible without interfering with the existing columns, jacketed beam cross sections were 31x32". Jacketed exterior columns were 31x48" to match the width of the beams.

Strengthening scheme J10B also considered jacketing of the exterior frames, but in this case only the exterior columns and beams at every other level, starting from the second floor, were strengthened. It is assumed that this structural layout would be more attractive, from a construction point of view, and less expensive than J10A. Cross-section dimensions and reinforcement for the strengthened elements were selected to obtain a strengthened building

with about the same lateral strength of building J10A.

Table 5.7 summarizes reinforcement details for both jacketing schemes previously described. Further details are given in Figs. 5.15 and 5.16 for J10A and J10B, respectively.

Strengthening scheme W10A considered the addition of a concrete infill wall to the interior bays of the exterior frames. To facilitate comparisons with the jacketed buildings, cross-section dimensions and reinforcement of the wall were chosen to approximately match the lateral strength of buildings J10A and J10B.

Strengthening scheme W10B considered two reinforced concrete infill walls in each exterior frame. Table 5.7 and Figs. 5.17 and 5.18 present reinforcement details and structural layouts for W10A and W10B.

Finally, strengthening scheme WJ10 combines the infill wall of scheme W10A with beam and column jacketing of scheme J10A. Reinforcement details are summarized in Table 5.7 and Fig. 5.19.

5.3.2.1 Lateral Strength

In the same manner as for the low-rise buildings, non-linear lateral load analyses were performed to compare the stiffness and strength of the retrofitted medium-rise buildings with that of the original building.

Figure 5.20a shows computed load-deflection curves for all strengthening schemes but J10B. The coordinates associated with splice failure of all first-story unstrengthened columns and with formation of a flexural mechanism in the strengthened frames are also indicated. Strengthening schemes that make use of infill walls show early yielding and tend to delay splice failure to higher drift levels. Frame jacketing scheme J10A shows generalized splice failure

31x46" 18x36" 31x46"

24'

36x36" 26x26" 18x26"

15'

31x32"

24'

5 @ 20' = 100'

Typical Floor Plan

Ast = 12#9
#4 ties @ 4"

Ast = 12#8
#4 ties @ 4"

Ast = 12#9
#4ties @ 4"

Ast = 12#8
#4ties @ 4"

46"

36"

31"

31"

36"

36"

1st thru 6th floor

7th thru 10th floor

1st thru 6th floor

7th thru10th floor

Column Cross Sections

Figure 5.15 Strengthening Scheme J10A

Exterior Frame Elevation

Figure 5.15 (cont.) Strengthening Scheme J10A

31x60"   18x36"   31x60"

24'

26x26"   26x26"   18x26"

15'

31x60"

24'

5 @ 20' = 100'

Typical Floor Plan

Ast = 16#9   Ast = 16#8
#4 ties @ 4"   #4 ties @ 4"

60"

31"   31"
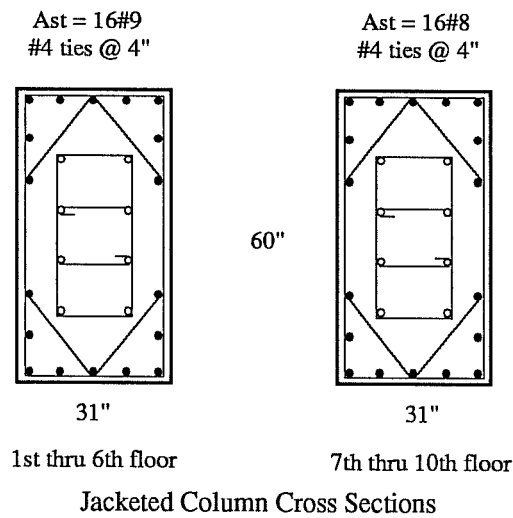
1st thru 6th floor   7th thru 10th floor

Jacketed Column Cross Sections

Figure 5.16 Strengthening Scheme J10B

Exterior Frame Elevation

Figure 5.16 (cont.) Strengthening Scheme J10B

18x36"   18x36"

24'

36x36"   26x26"   18x26"

Wall, t =12"   Wall, t =12"

15'

18x26"

24'

5 @ 20' = 100'

Typical Floor Plan

36"   36"

t = 12"   #4@12" (V)

36"   36"

Dowels   #5@10" (H)
#6@6"

Ast = 12#5   Ast = 12#5
#4 ties @ 4"   #4 ties @ 4"

Wall Cross Section

Figure 5.17 Strengthening Scheme W10A
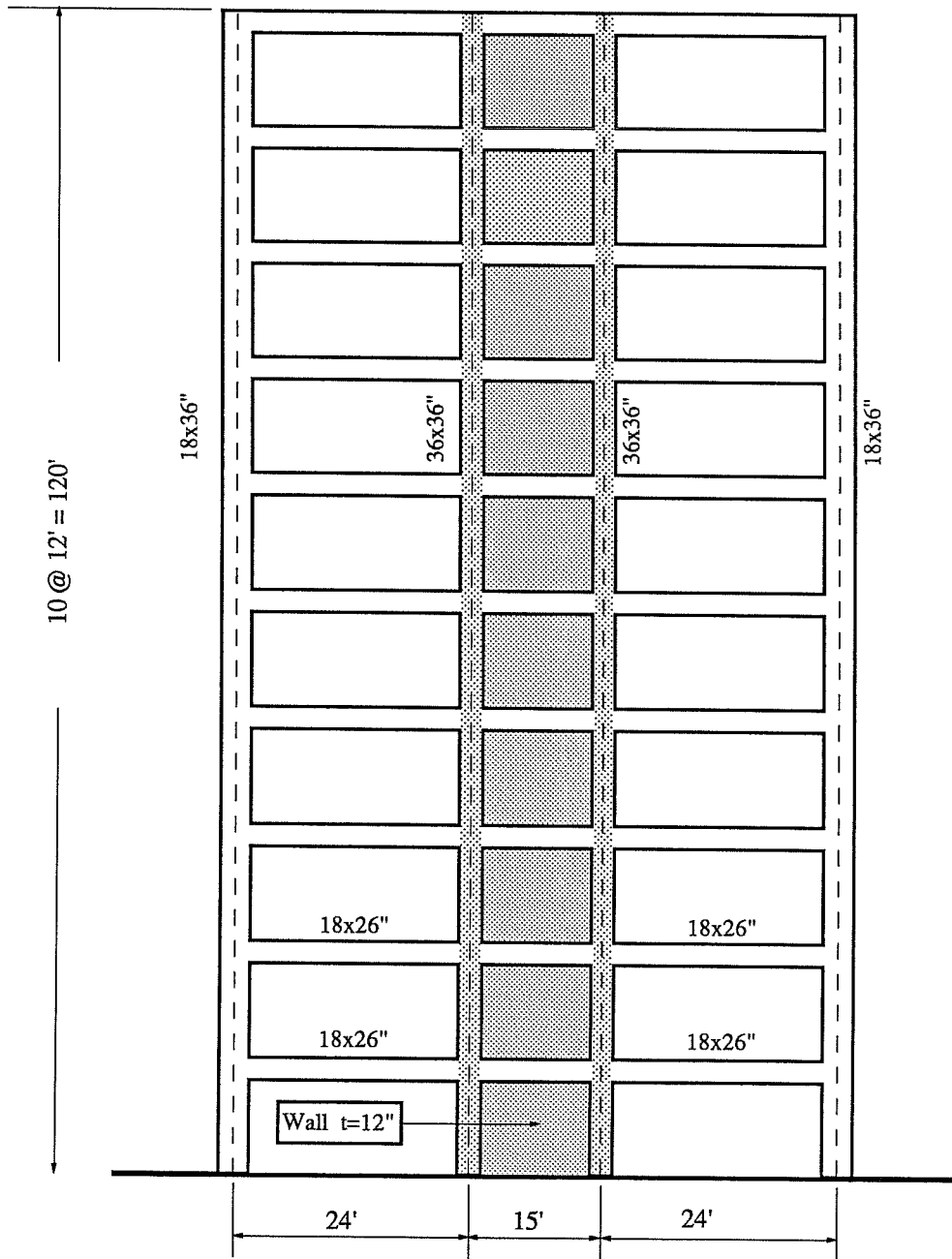
Exterior Frames Elevation

Figure 5.17 (cont.) Strengthening Scheme W10A
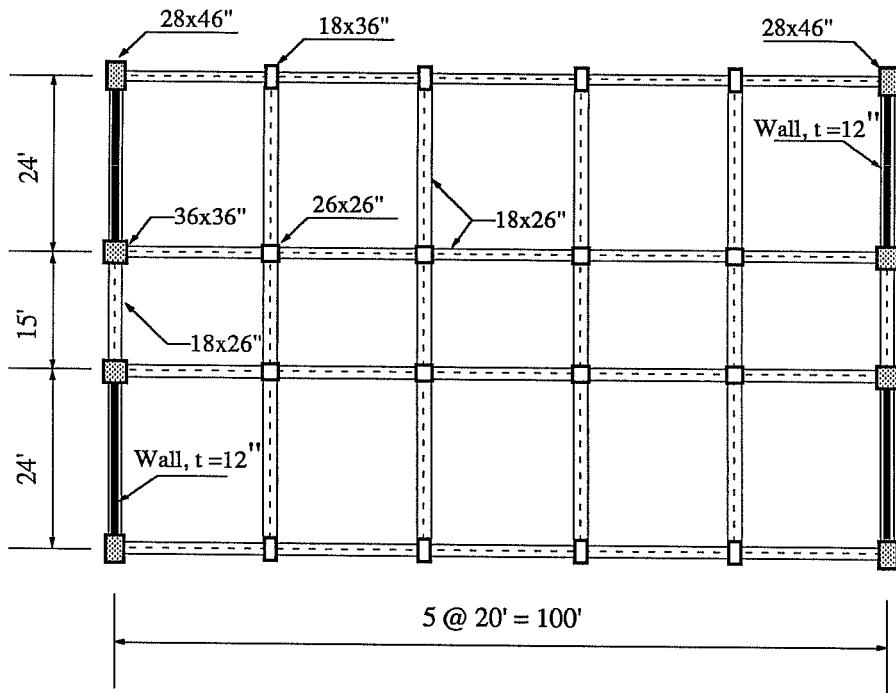
Typical Floor Plan

Wall Cross Section
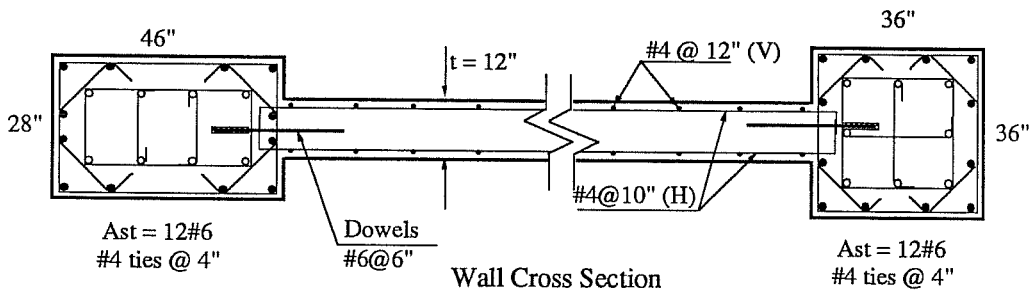
Figure 5.18 Strengthening Scheme W10B
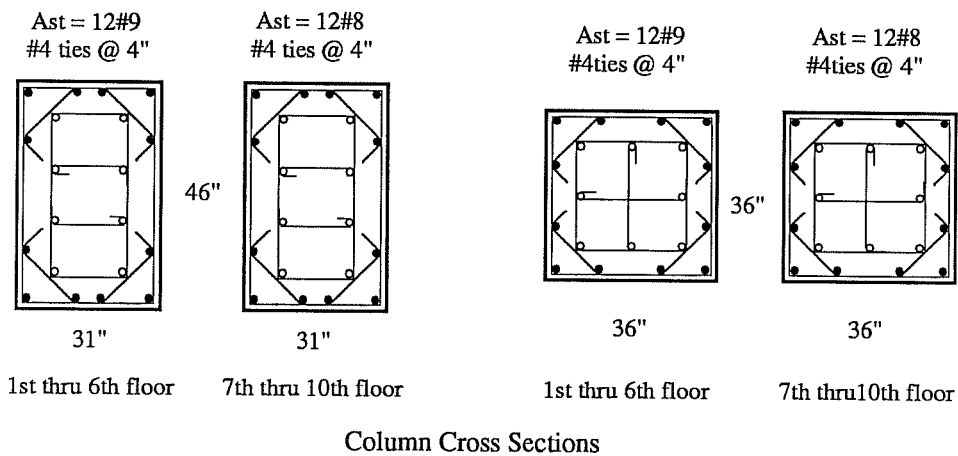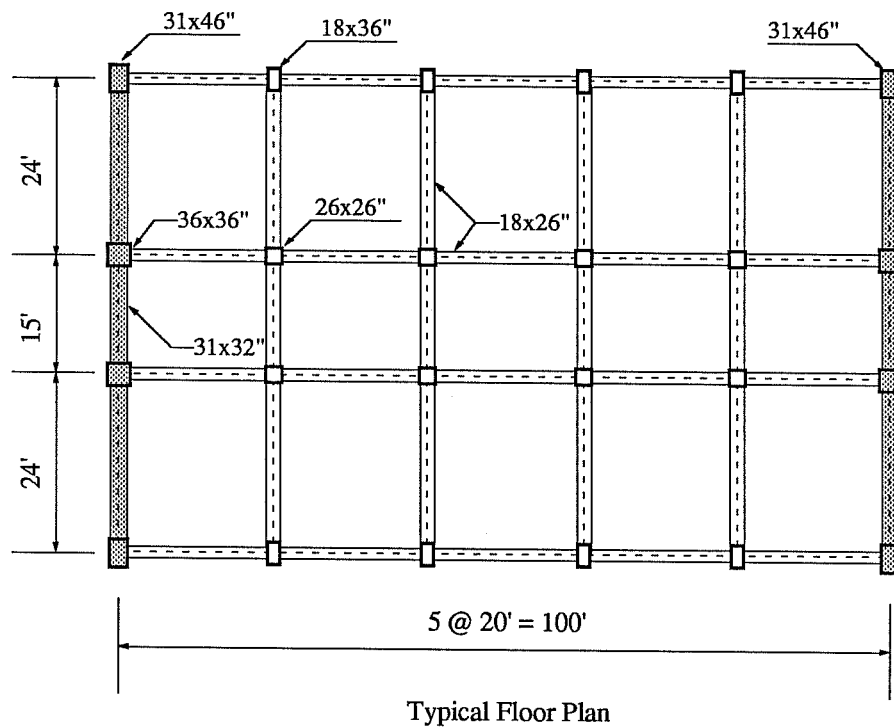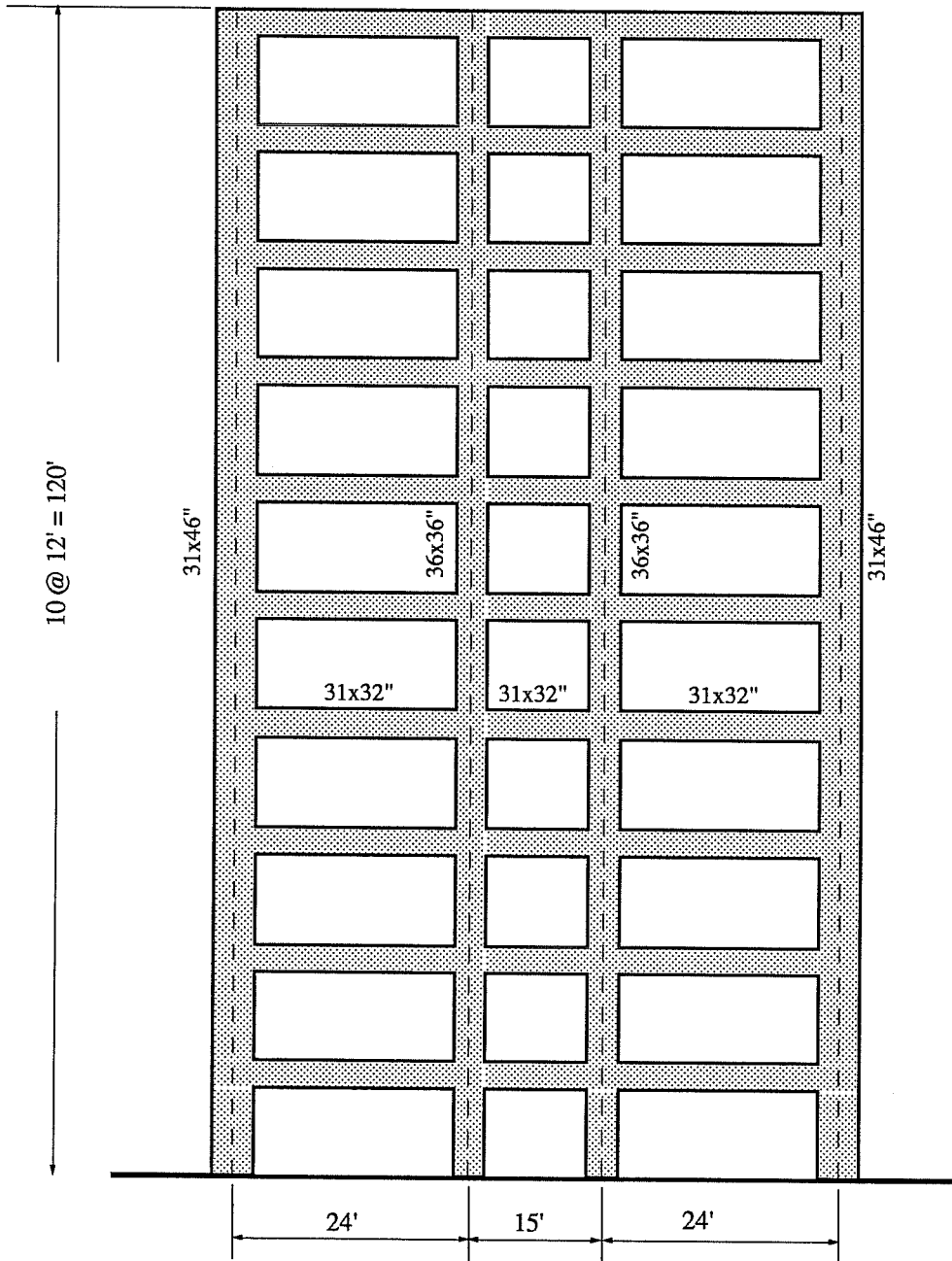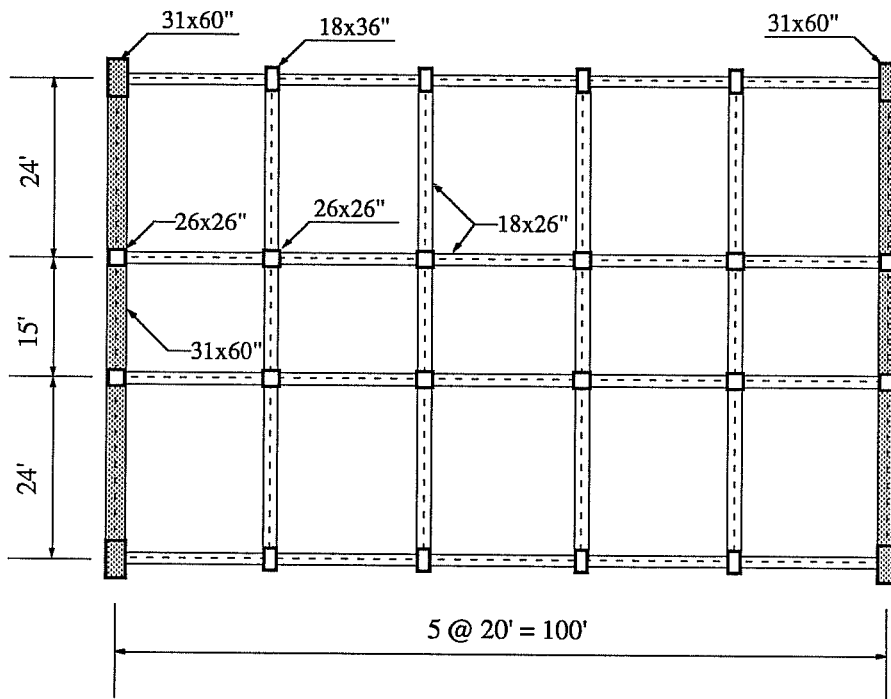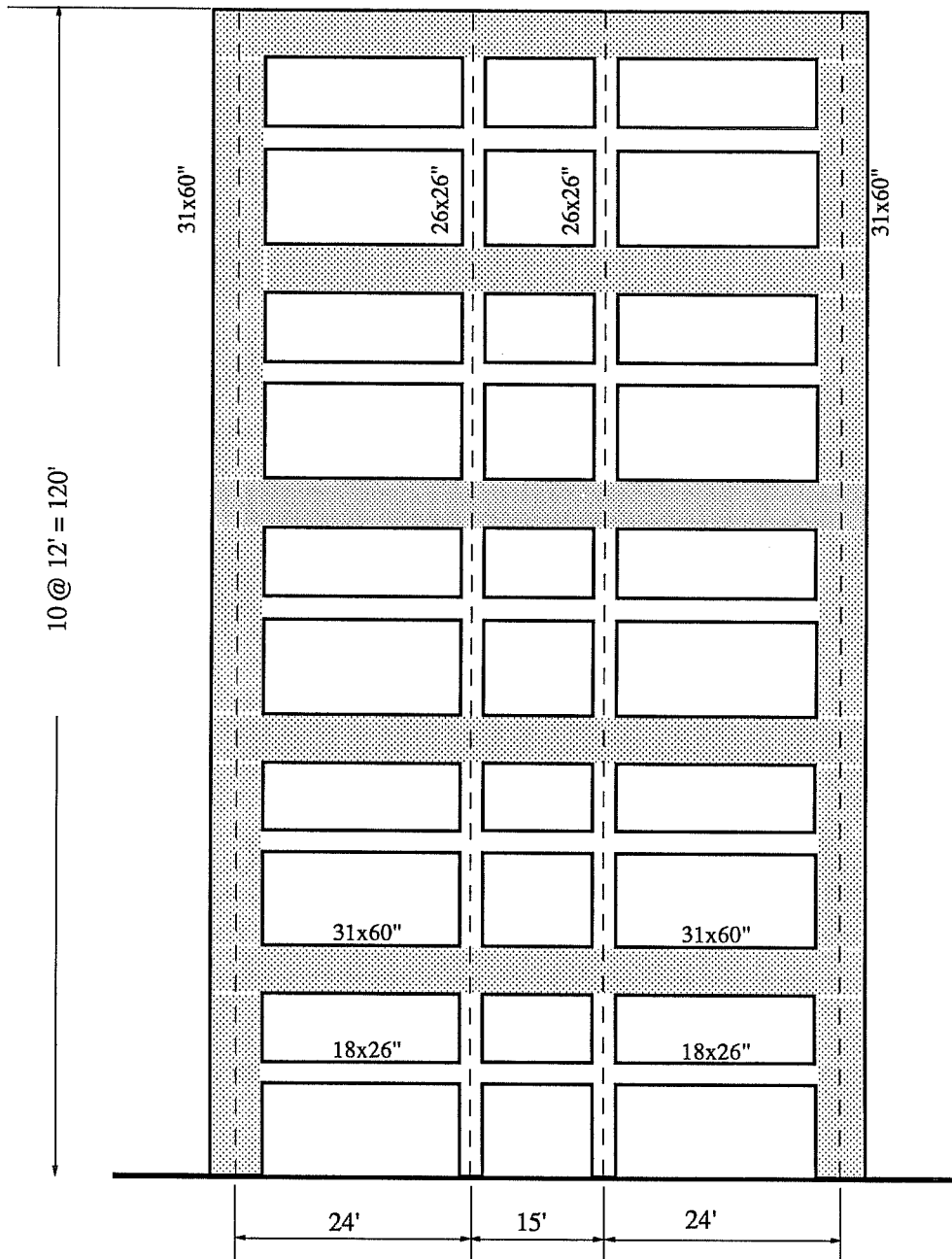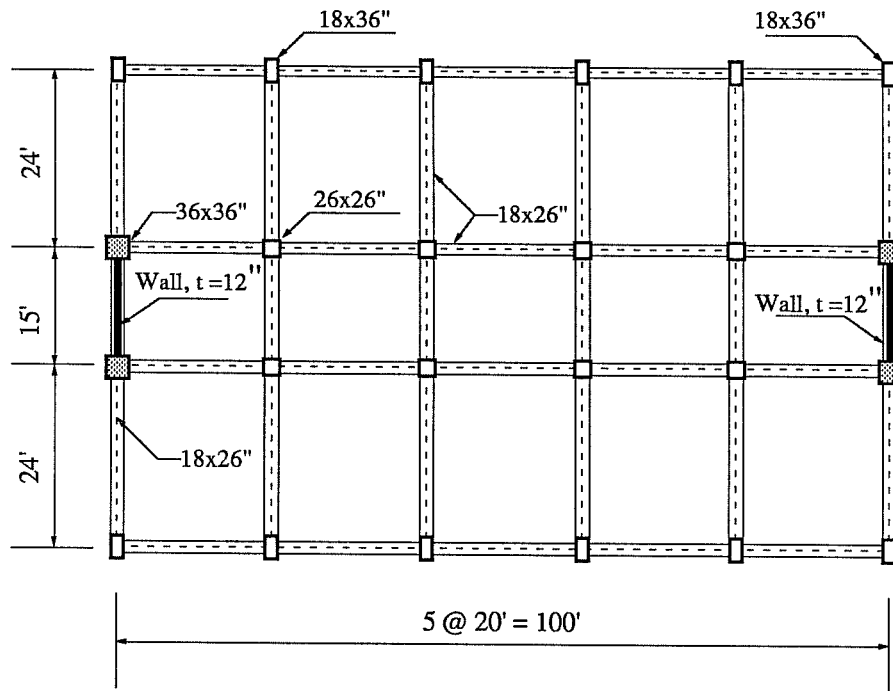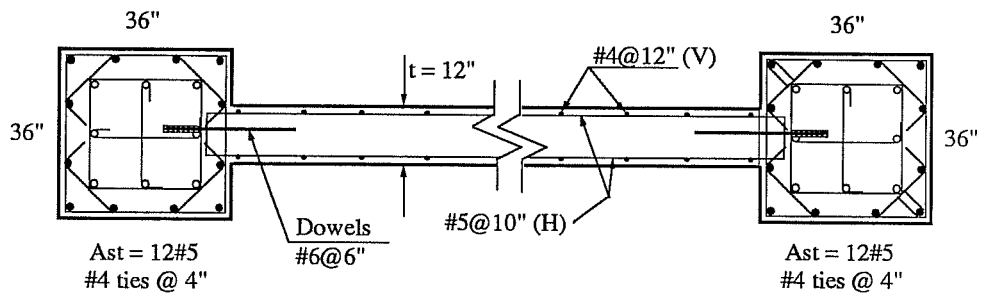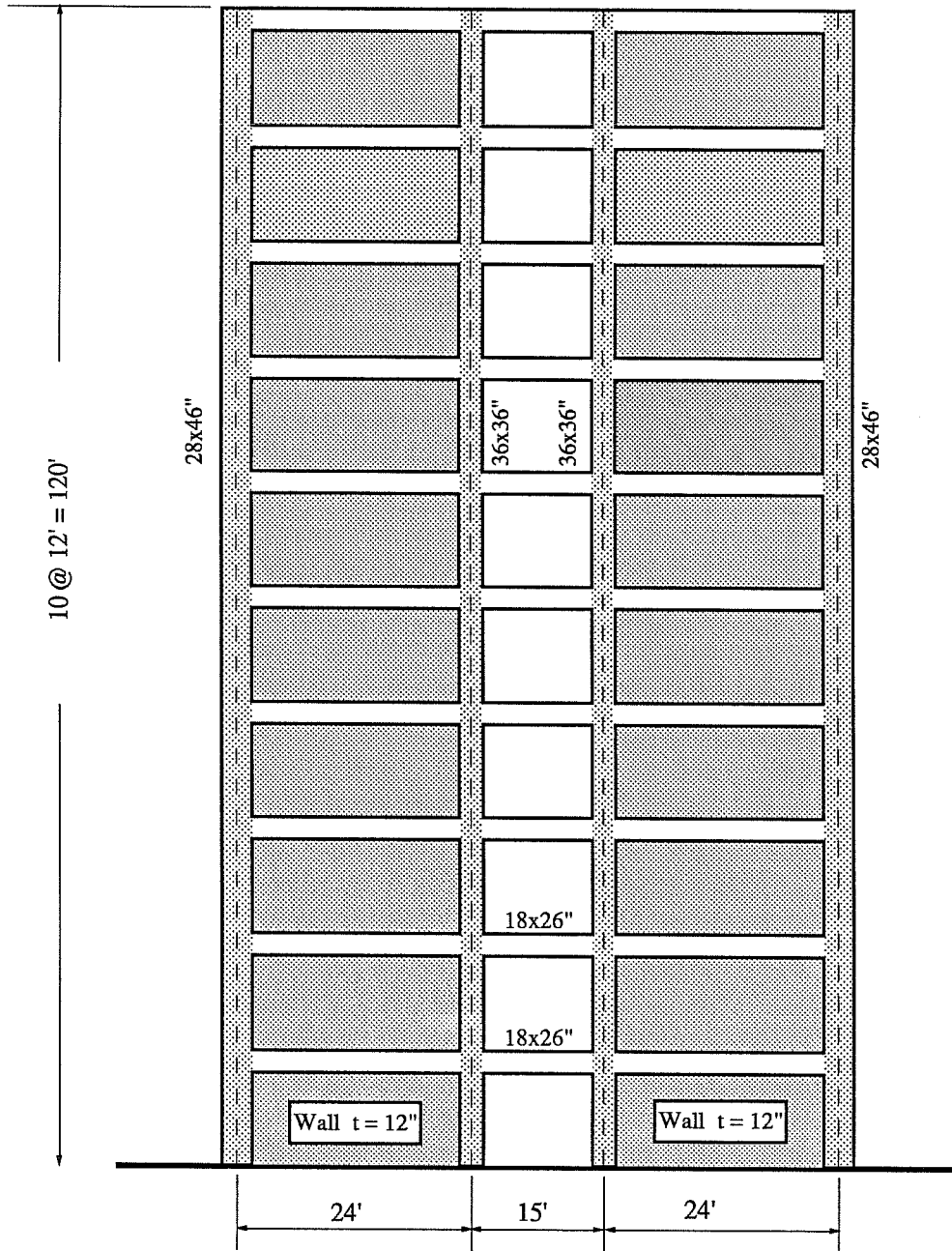
Exterior Frames Elevation

Figure 5.18 (cont.) Strengthening Scheme W10B
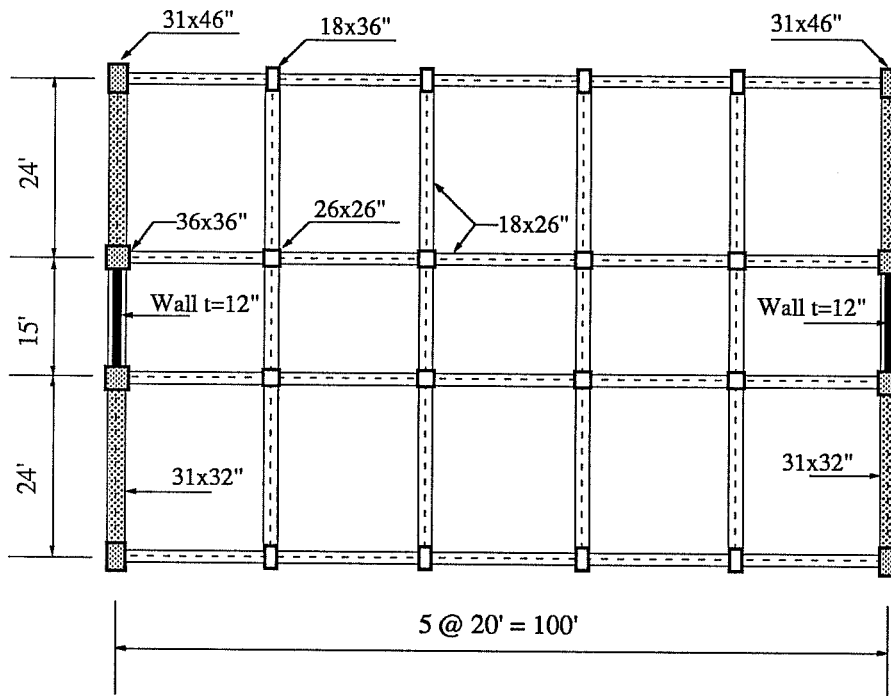
Figure 5.19 Strengthening Scheme WJ10

prior to mobilization of the deformation capacity of the jacketed elements.

Table 5.7 Reinforcement Details for Strengthened 10 Story Buildings

Story Level	Element	Reinforc. Position	Strengthening Scheme				
			J10A	J10B	W10A	W10B	WJ10
1-6	Exterior Columns	Long.	12#9	16#9	-	12#6	12#9
		Ties	#4@4"	#4@4"	-	#4@4"	#4@4"
7-10	Exterior Columns	Long.	12#8	16#8	-	12#6	12#8
		Ties	#4@4"	#4@4"	-	#4@4"	#4@4"
1-6	Interior Columns	Long.	12#9	-	12#5	12#6	12#5
		Ties	#4@4"	-	#4@4"	#4@4"	#4@4"
7-10	Interior Columns	Long.	12#8	-	12#6	12#6	12#6
		Ties	#4@4"	-	#4@4"	#4@4"	#4@4"
1-10	Beams	Top	2#8	4#8	-	-	2#8
		Bottom	4#10	6#10	-	-	4#10
		Stirrups	#4@4"	#4@4"	-	-	#4@4"
1-10	Walls	Web (V) (H)	-	-	2#4@12" 2#5@10"	2#4@12" 2#4@10"	2#4@12" 2#5@8"

Strengthening scheme J10B which featured an alternate jacketing scheme, and was promising from a construction point of view, revealed the creation of a weak link associated with shear failure of the unstrengthened columns of the exterior frames (Fig. 5.16). High shear stresses were computed in these columns primarily due to the boundary conditions imposed by the very stiff jacketed beams, and secondarily due to a reduction in the column clear height caused by the deep jacketed beams. A premature shear failure of these columns was predicted by the analytical model at 0.10% drift. The solid line in Figure 5.20b shows the computed load-deflection curve up to shear failure of the columns. The broken line assumes no shear failure of the unstrengthened columns of the exterior frames.

The lateral strength of the retrofitted buildings is compared in Fig. 5.21 to that required by the ATC-22 document, using the computed natural period of the buildings
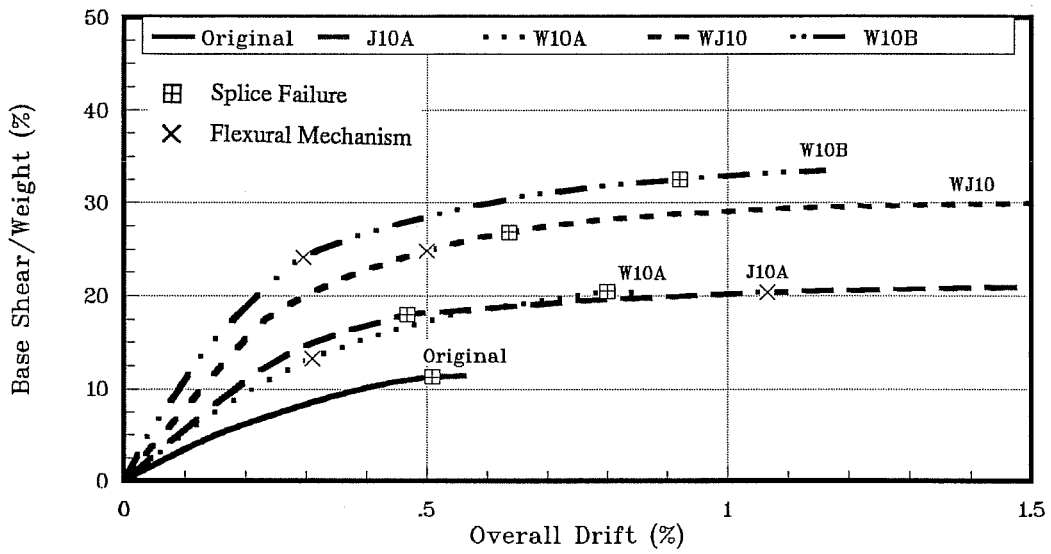
(a)
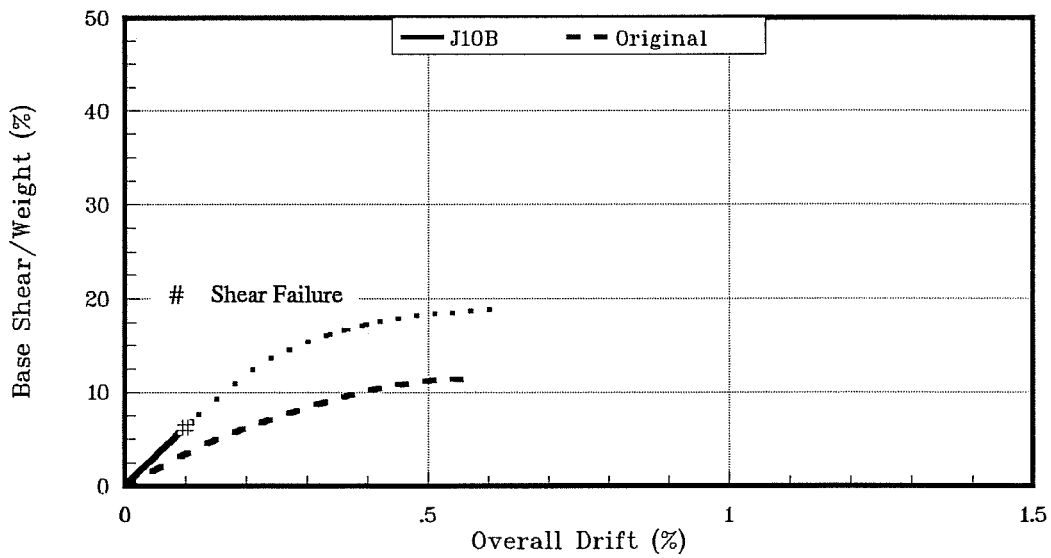
(b)

Figure 5.20 Load-Deflection Curves, Ten-Story Buildings

assuming gross section properties and a response modification factor, R, equal to 2. It can be seen that all of the buildings have lateral strength comparable to that required by ATC-22, with the exception of J10B.

5.3.2.2 Stiffness

Story shear distribution among exterior and interior frames, assuming elastic behavior, is presented in Fig. 5.22. Frame jacketing schemes showed almost constant distribution of story shears with along the height of the building, while for strengthening schemes that make use of shear walls, a major proportion of the story shear was taken by the walls in the lower floors followed by a gradual reduction in the story shear contribution along the height of the building.

5.4 Selected Ground Motions

Four ground motions recorded at three different locations were considered in this study for evaluating the dynamic response of the buildings: (1) El Centro 1940, California, (2) El Centro 1940 amplified by 1.5, (3) Viña del Mar 1985, Chile, (4) Secretaria de Caminos y Transportes (SCT) 1985, Mexico City, Mexico. The El Centro record has been widely used in several analytical studies and can be classified as a medium-size earthquake. It has the advantage of having a wide frequency content for a record obtained in stiff soil conditions. The 1985 Chilean earthquake and the "scaled" El Centro record were selected to represent a severe ground motion that might be expected along the western coast of the U.S. Finally, the record obtained after the 1985 Mexico earthquake is of interest because it represents an extreme event in soft soil conditions, and because most of the retrofitting operations in real buildings have been implemented in Mexico City after the 1985 earthquake. Table 5.8 contains basic
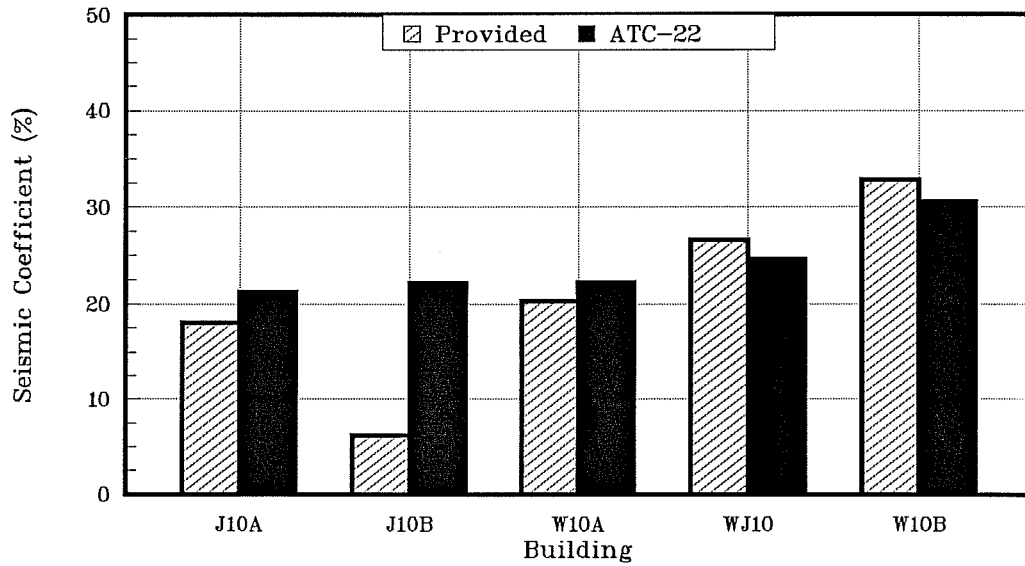
Figure 5.21   Provided vs. Required Strength — 10 Story Buildings
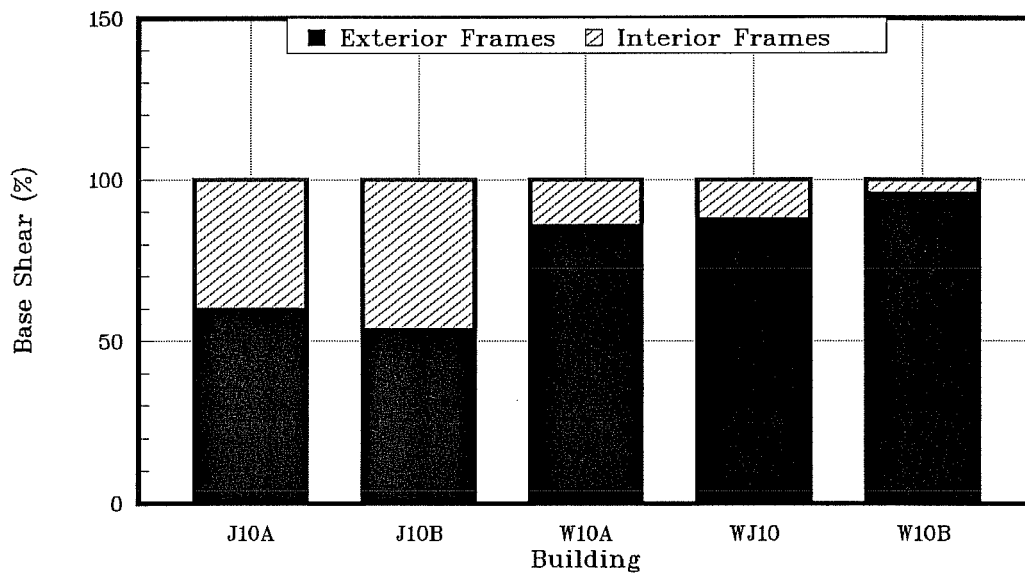
Figure 5.22   Elastic Base Shear Distribution — 10 Story Buildings

information about the records.

Table 5.8 Ground Motions Considered

Location	Direction	Soil Type	Maximum Acceleration	Magnitude, M_s
El Centro, California, 1940	NS	alluvial deposits	0.35g	7.1
El Centro, California, 1940[1]	NS	alluvial deposits	0.52g[1]	-
Viña del Mar, Chile, 1985	S20W	alluvial deposits	0.36g	7.8
SCT, Mexico City,Mexico, 1985	NS	deep silty clay deposits	0.16g	8.1

(1) Ground accelerations scaled by 1.5

Figure 5.23a-c show the acceleration records of El Centro, Viña del Mar, and SCT plotted to the same scale. Elastic pseudo-acceleration spectra for the three records are shown in Fig. 5.24. The difference in frequency content of the El Centro and Viña del Mar records compared with the SCT record is evident. Peak spectral ordinates are 1.26g, 1.91g and 1.71g for El Centro, Viña del Mar and SCT, respectively. Viña del Mar shows higher spectral ordinates than El Centro for periods up to 1.7 sec. The SCT record dominates the other two for periods larger than 1.40 sec.

Figure 5.25 compares elastic displacement spectra. As can be seen spectral displacement ordinates for SCT are much bigger than El Centro and Viña del Mar for periods beyond 1.5 sec.

Displacement ductility requirements shown in Fig. 5.26a-d were computed for the four ground motions listed in Table 5.8 for yield strength levels of 10, 20, 30, and 50% of the single degree of freedom oscillator. Viscous damping was assumed to be 2% of critical. A bilinear stiffness degrading model with 20% strain hardening was used in all the calculations to simulate

123
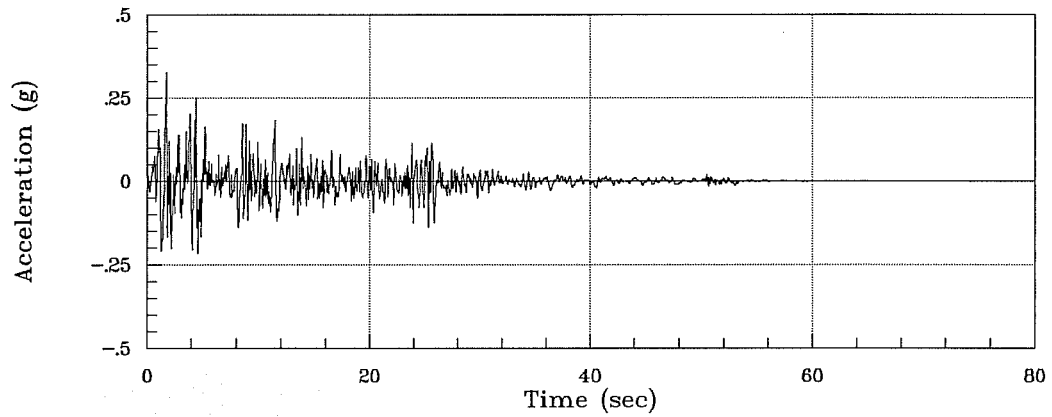
(a) El Centro 1940, California
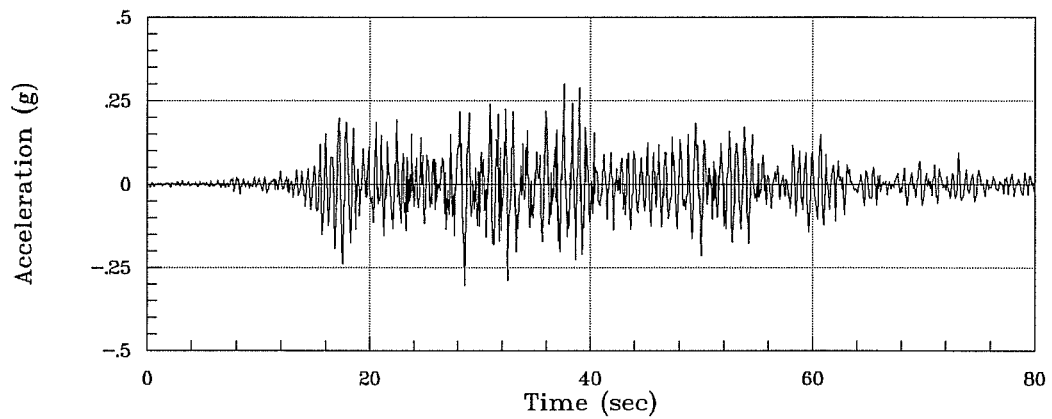
(b) Vina del Mar 1985, Chile
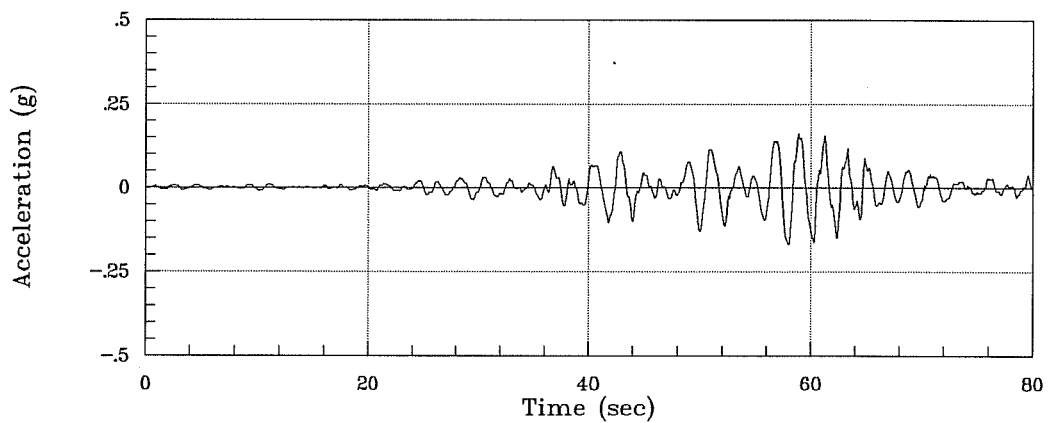
(c) SCT Mexico City 1985, Mexico

Figure 5.23 Acceleration Records

a) Response to El Centro

b) Response to Scaled El Centro
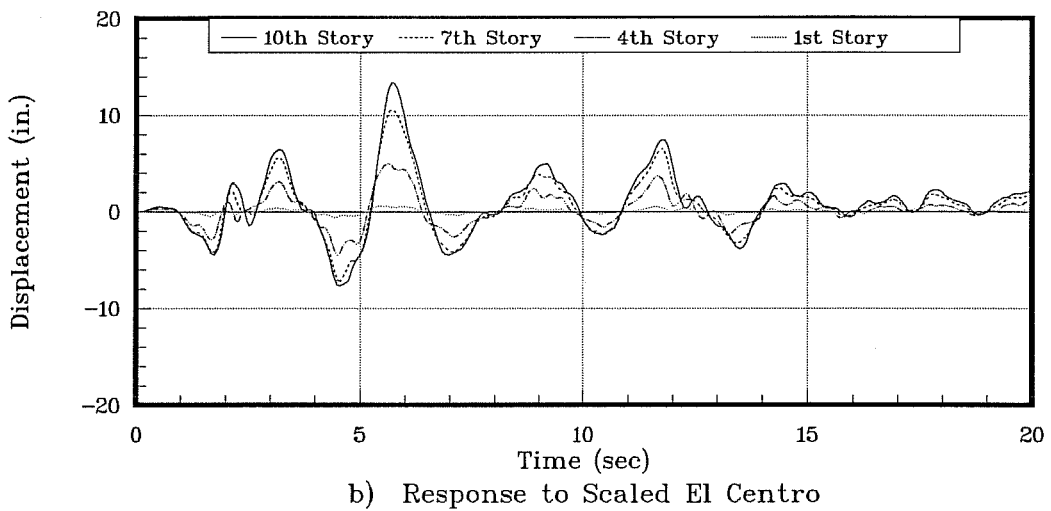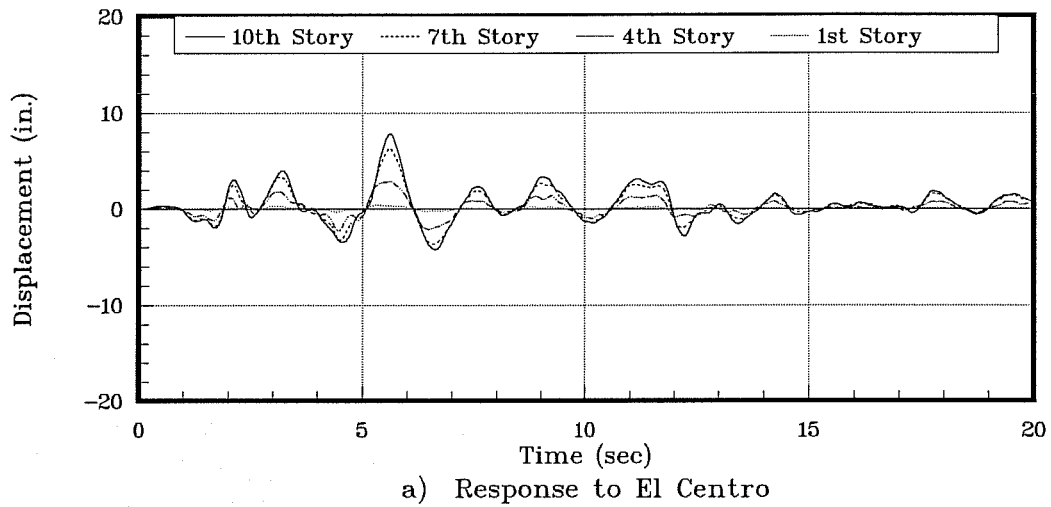
Figure 5.38 Displacement Histories, Original Ten-Story Building

gradual yielding of the structural components of a building system. Ductility requirements for the Scaled El Centro record are similar to those obtained for Viña del Mar but are higher for periods above 1.5 sec. Ductility requirements for the SCT record are extremely high for structures with low yield levels, and a shift of peak response toward shorter periods can be observed as lateral strength decreases.

5.5 Dynamic Analyses

This section presents the computed dynamic response of the original and strengthened buildings described in Sections 5.2 and 5.3.

The method of analysis was described in Chapter 3. The buildings were idealized as a series of planar frames having a common lateral degree of freedom at each story level. Axial deformations of the columns were neglected in the three-story buildings, and joint flexibility was taken into account by considering a joint element in all the beam-to-column connections of the buildings. Time history analyses were performed using an integration time step of 0.01 sec for most of the cases after preliminary runs showed that smaller integration time steps were not required to achieve convergence of the computed response of the buildings.

Rayleigh damping was used to specify 2% critical equivalent viscous damping for the two first modes in all calculations. Pinching of the hysteresis loops was controlled by the parameters α_1 and α_2 of Eqs. 4.1 and 4.2. A value of 0.25 was selected for α_1, and α_2 was set equal to 0.75. The slope of the descending branch of the moment-rotation curve for elements exhibiting a splice or pullout failure was defined as shown in Fig 3.13 using a value of $\beta = 10$. Joints were assumed to be flexible and to follow the hysteresis rules discussed in Chapter 4, Section 4.4.
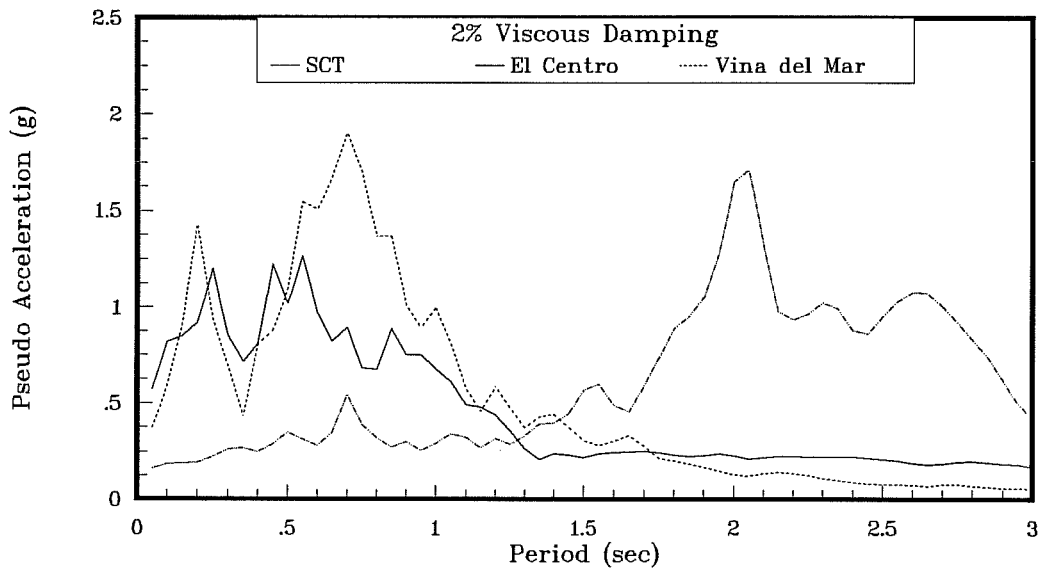
Figure 5.24   Ground Motion Pseudo Acceleration Spectra
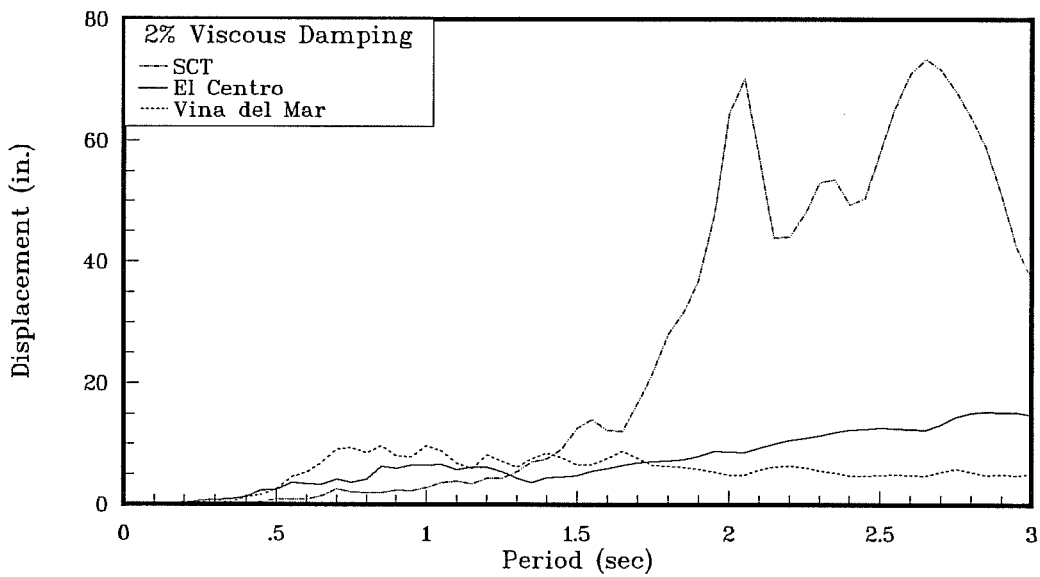
Figure 5.25   Ground Motion Displacement Spectra
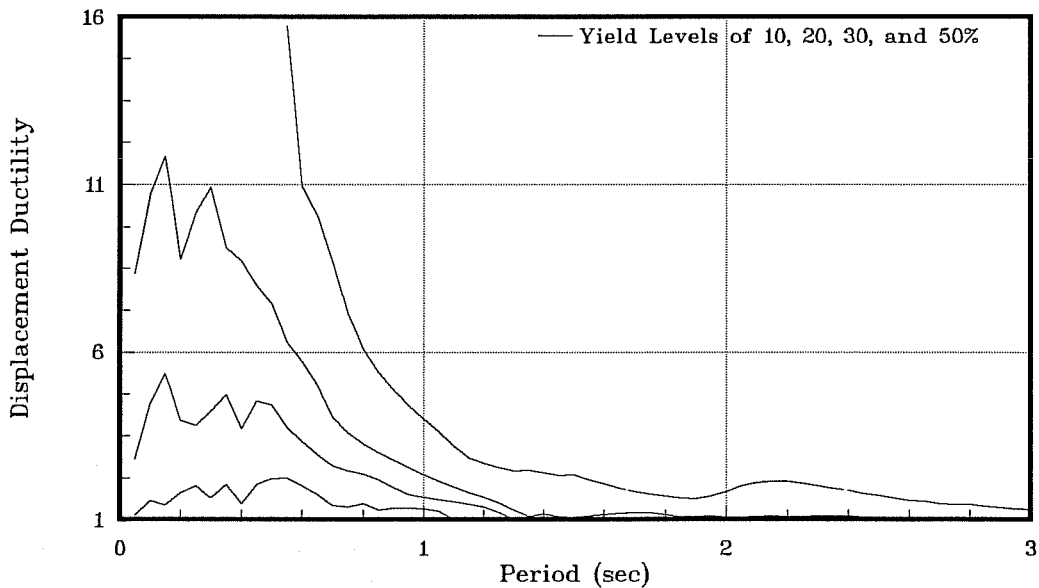
(a) El Centro 1940
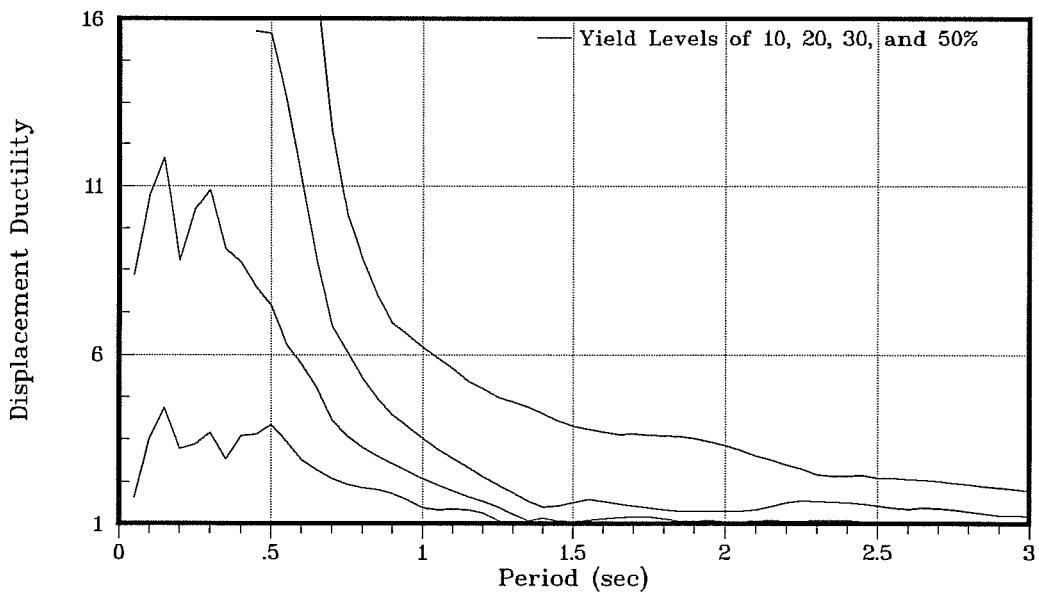
(b) El Centro 1940 Scaled by 1.5

Figure 5.26 Displacement Ductility Requirements
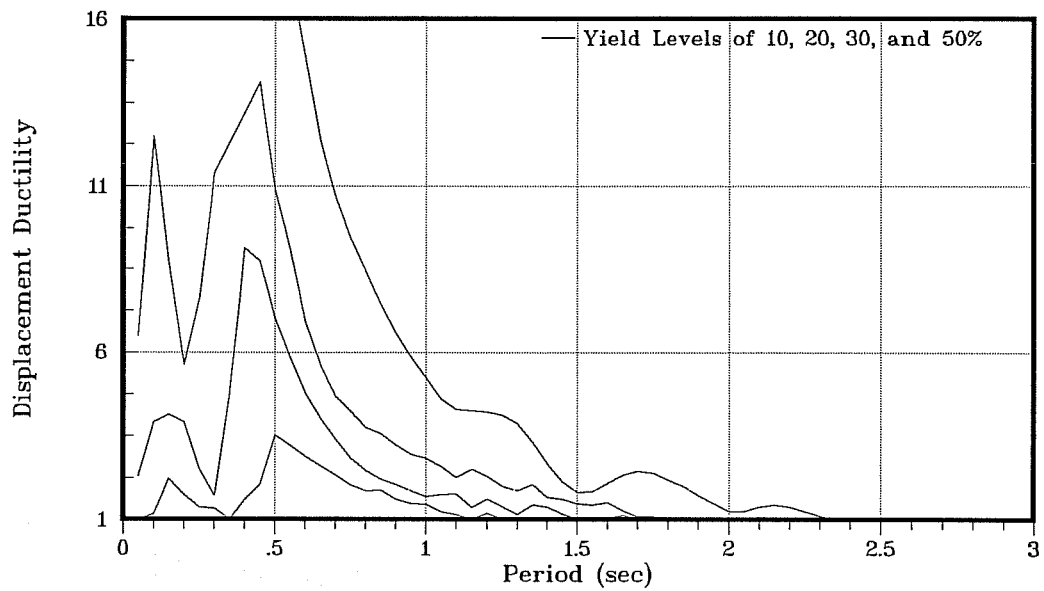
(c) Vina del Mar 1985
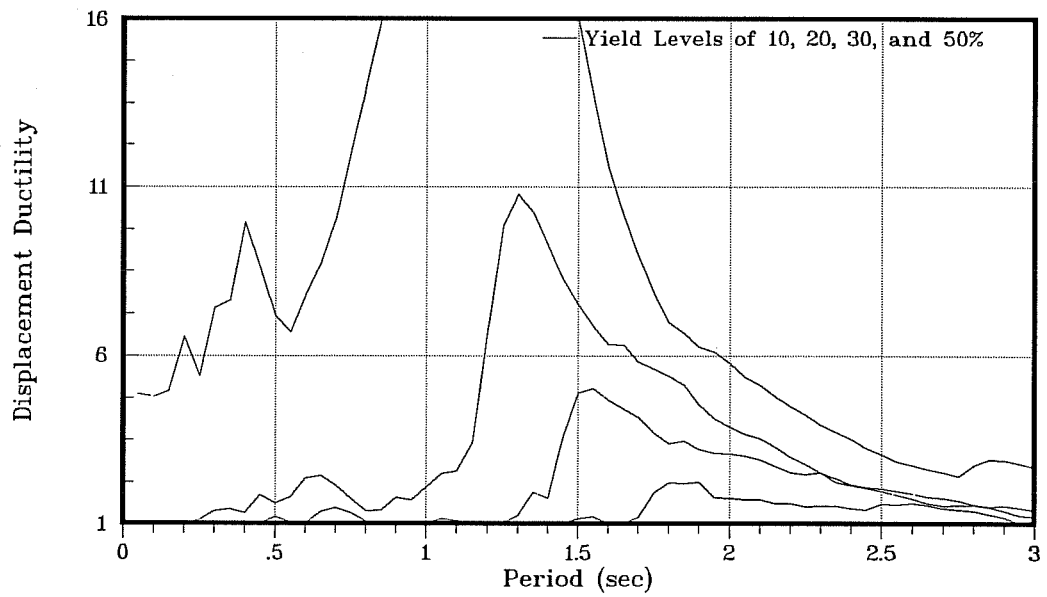
(d) SCT Mexico City 1985

Figure 5.26 (Cont.) Displacement Ductility Requirements

Elastic dynamic properties such as periods and mode shapes were computed for all the buildings. Tables 5.9 and 5.10 show computed seismic weights and natural periods for the three-story and ten-story buildings, respectively. Because cracking of the structural elements takes place very early in the response of a building to severe ground motion, computations of the natural periods were performed assuming all the elements to be cracked. Modal mass ratios associated with the first three vibrational modes are also indicated. Significant reduction in the fundamental period of the strengthened buildings with respect to the original building is observed, while the increment in building weight is not significant.

5.5.1 Three-Story Buildings

a) Original Building

Computed maximum base shears, top-level displacements, interstory drifts, and rotational ductility demands for the first-story columns are presented in Table 5.11. A rotational ductility greater than one for a column indicates that a splice failure was predicted at its base. Computed base shears indicate that the building was pushed to, or close to, its lateral strength. A splice failure in all first-story columns and pullout of the beam bottom reinforcement was predicted for all four cases. Maximum shear stresses in beam-column joints varied from 13.2 to $17.7\sqrt{f_c'}$ for the El Centro and SCT record, respectively. These values were considered to be high given the fact that no transverse reinforcement was provided within the joint region [22]. Drift levels computed for the Scaled El Centro and SCT records show inadequate behavior of the building. Although drift levels for the El Centro and Viña del Mar records seem to be within reasonable limits, the fact that all the first-story columns failed in the splice region at the base raises serious questions about the integrity of the building.

Table 5.9 Dynamic Properties, Three-Story Buildings

Building	Weight (kips)	Elastic Period (sec)			Modal Mass Ratio		
		1st Mode	2nd Mode	3rd Mode	1st Mode	2nd Mode	3rd Mode
Original	4220	1.18	0.36	0.20	0.85	0.12	0.03
J3A-Y	4650	0.93	0.25	0.12	0.81	0.14	0.05
J3B-Y	4650	0.82	0.20	0.10	0.81	0.14	0.05
J3C-Y	4810	0.72	0.21	0.10	0.83	0.13	0.04
J3A-X	4650	0.89	0.24	0.12	0.82	0.13	0.05
J3B-X	4650	0.76	0.19	0.09	0.82	0.13	0.05
J3C-X	4810	0.63	0.19	0.10	0.85	0.12	0.03
W3	4490	0.35	0.08	0.04	0.74	0.22	0.04

Table 5.10 Dynamic Properties, Ten-Story Buildings

Building	Weight (kips)	Elastic Period (sec)			Modal Mass Ratio		
		1st Mode	2nd Mode	3rd Mode	1st Mode	2nd Mode	3rd Mode
Original	12340	1.71	0.55	0.31	0.80	0.10	0.04
J10A	13400	1.37	0.44	0.25	0.80	0.10	0.04
J10B	13530	1.30	0.42	0.24	0.80	0.10	0.04
W10A	12900	1.35	0.37	0.17	0.72	0.14	0.06
WJ10	13540	1.14	0.33	0.16	0.74	0.13	0.06
W10B	13710	0.83	0.21	0.09	0.69	0.16	0.07

Table 5.11 Response Maxima - Original Three-Story Building

Earthquake	Base Shear[1] (%)	Overall Drift (%)	Interstory Drift (%)			Rotational Ductility Demand 1st Story Columns
			1st Story	2nd Story	3rd Story	
El Centro	14.8	0.94	1.2	1.2	0.9	1.99
Viña del Mar	17.3	1.56	1.4	1.8	1.6	2.35
Scaled El Centro	17.2	1.88	2.7	2.0	1.4	4.56
SCT	17.8	5.00	7.4	6.4	2.2	12.04

(1) Base Shear Strength = 15%

Computed displacement histories are shown in Fig. 5.27. All plots are drawn to the same vertical scale, except for the response of the building to the SCT record which contained extremely high displacements. Lengthening of the natural period can be observed after maximum response was reached, and is directly related to the stiffness degradation incorporated in the hysteresis model. Figure 5.28 shows a typical moment-rotation curve for a first-story column obtained for the Scaled El Centro record. A similar plot for a first-level beam is presented in Fig. 5.29.

b) Frame Jacketing Schemes

Analyses of jacketed buildings J3A, J3B, and J3C in both directions (X and Y) showed similar global responses for the same ground motion record, with the exception being the response to the SCT record. Table 5.12 compares maximum computed overall drifts (roof displacement divided by the building height).

Table 5.12 Computed Overall Drift (%)
Three-Story Building Frame Jacketing Schemes

Building	El Centro	Viña del Mar	Scaled El Centro	SCT
J3A-Y	0.98	1.33	1.44	0.47
J3B-Y	0.97	1.32	1.44	0.46
J3C-Y	0.96	1.27	1.39	0.31
J3A-X	0.94	1.23	1.43	0.46
J3B-X	0.99	1.31	1.33	0.30
J3C-X	0.78	1.20	1.31	0.23

Frame jacketing schemes proved to be a very efficient retrofitting alternative when the buildings were subjected to the SCT record. Strengthening scheme J3A-Y, which is the weakest of all frame jacketing schemes, was able to reduce a computed drift of 5.0% for the original building to 0.47%. A rotational ductility demand of 1.2 was computed at the base of the first-story jacketed columns of building J3A-Y, showing incipient inelastic behavior. No yielding of the jacketed beams was detected. The behavior of the unstrengthened elements was also very good; columns remained elastic, and although pullout of beam bottom reinforcement was predicted, yielding of the original beams in negative bending was not observed.

The response of the jacketed buildings to the other records showed that inelastic demands in the unstrengthened elements could be reduced with respect to those computed for the original building. However, failure of the splice region of all first-story unstrengthened columns was still predicted. Table 5.13 shows computed rotational ductility demands for the first-story interior columns. It is of interest to note that strengthening scheme J3B, which had
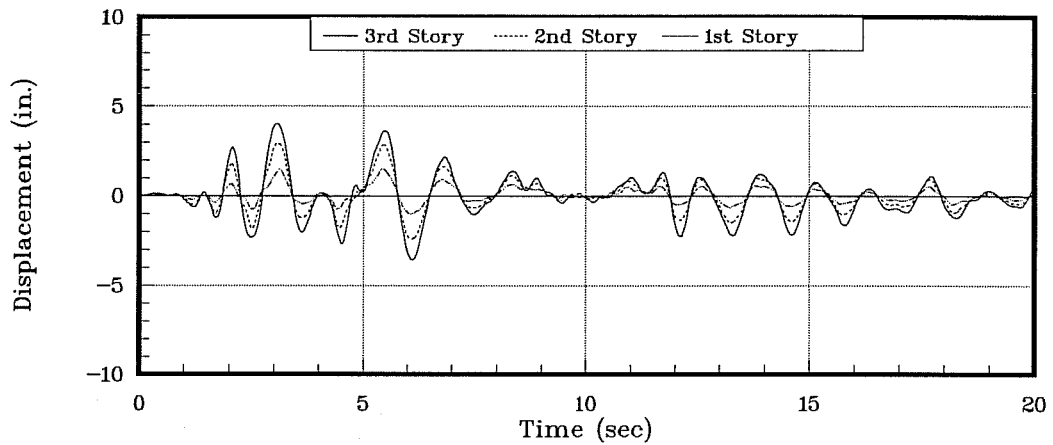
a) Response to El Centro
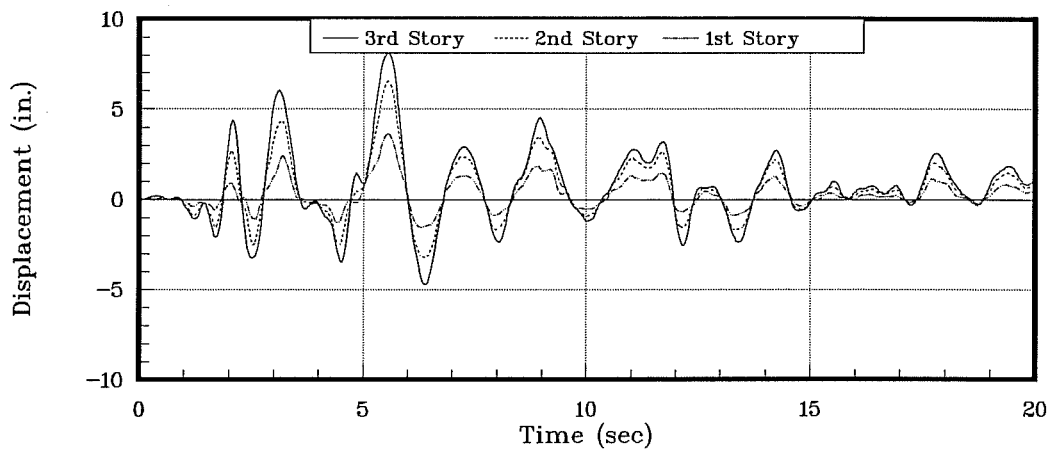
b) Response to Scaled El Centro

Figure 5.27 Displacement Histories, Original Three-Story Building
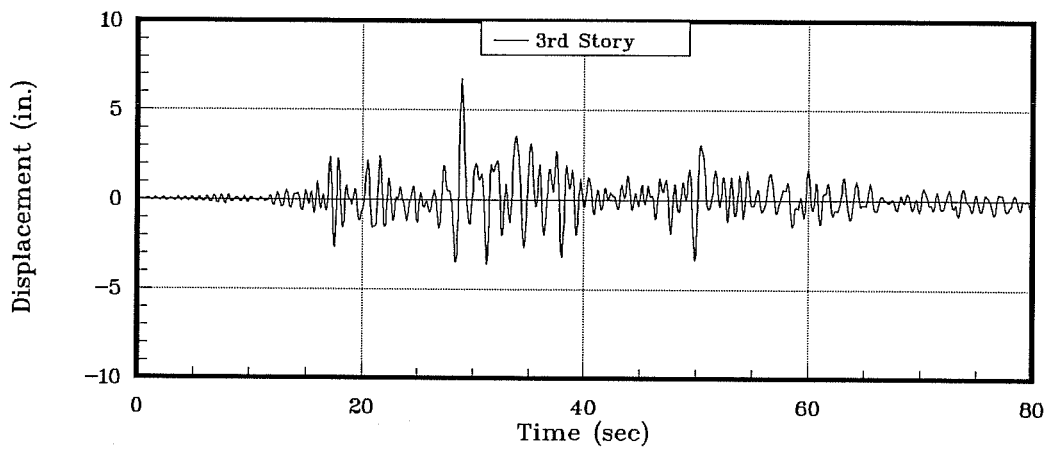
c) Response to Vina del Mar
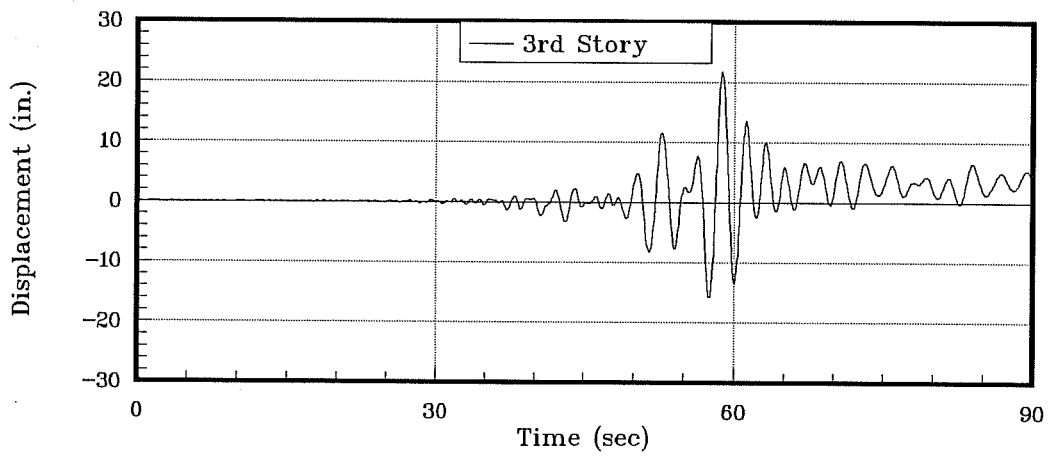
d) Response to SCT

Figure 5.27 (Cont.) Displacement Histories, Original Three-Story Building
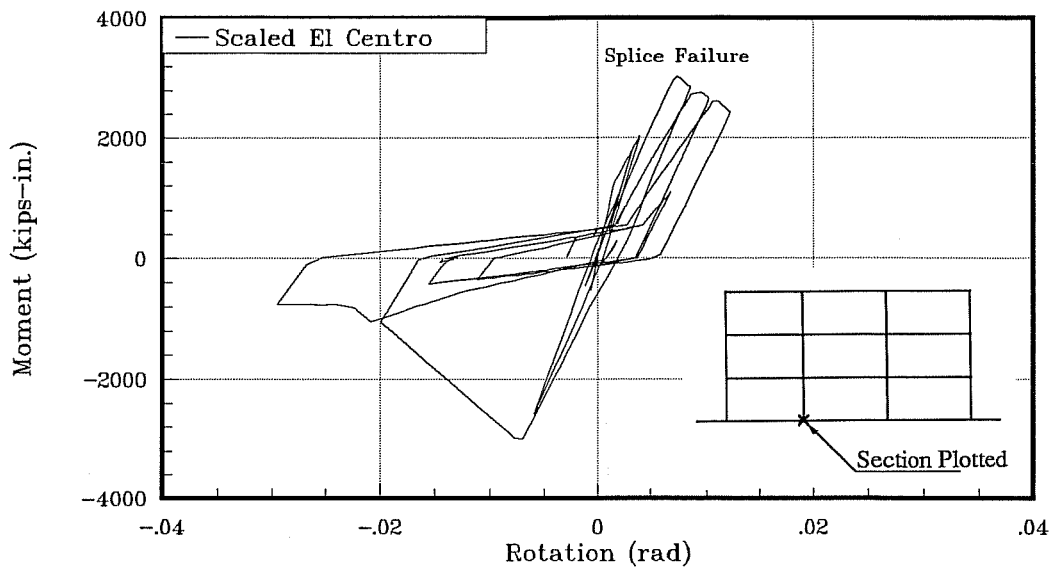
Figure 5.28 Typical 1st Story Column Moment–Rotation Curve
Three–Story Original Building
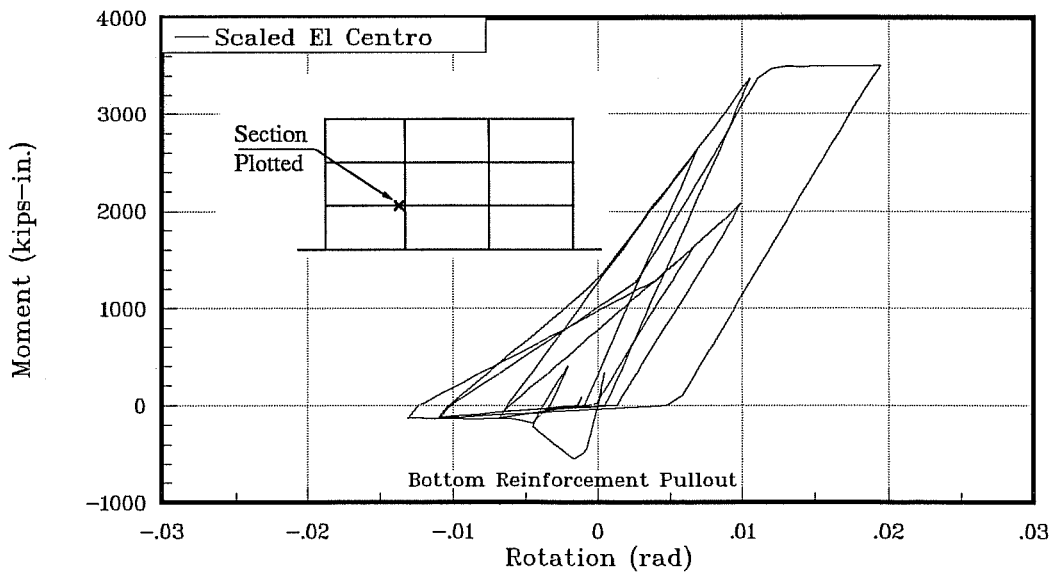
Figure 5.29 Typical Beam Moment–Rotation Curve
Three–Story Original Building

a lateral strength between the strengths associated with jacketing schemes J3A and J3C, and which had a flexural mechanism in the jacketed frames that can be developed at smaller drift levels (see Fig. 5.12), is the one that demonstrated the smallest ductility demands in the unstrengthened columns for all ground motions considered.

**Table 5.13 Rotational Ductility Demands in Interior First-Story Columns
Three-Story Building Frame Jacketing Schemes**

Building	El Centro	Viña del Mar	Scaled El Centro	SCT
J3A-Y	1.24	1.61	2.05	(0.61)
J3B-Y	1.15	1.44	1.56	(0.52)
J3C-Y	1.20	1.63	1.80	(0.41)
J3A-X	1.39	1.67	2.30	(0.60)
J3B-X	1.02	1.54	1.81	(0.39)
J3C-X	1.11	1.93	1.91	(0.35)

() Elastic behavior

High shear stresses were still developed in the unconfined joints of the unstrengthened frames. Maximum values of 13.3 and $16.6 \sqrt{f_c'}$ were computed for strengthening scheme J3B for the El Centro and Scaled El Centro records.

The behavior of the jacketed frames can be classified as acceptable given the fact that reinforcement details for the structural elements meet current standards for moment-resisting frames subjected to seismic forces. Computed inelastic behavior was in general confined to formation of plastic hinges at the base of first-story columns and in beams. Maximum joint shear stresses did not exceed $13.5 \sqrt{f_c'}$ in any strengthening scheme for any of the records

considered. Figure 5.30 shows distribution of plastic hinges and rotational ductility demands in the jacketed frames of building J3B computed for the Scaled El Centro record.

Displacement histories for strengthening scheme J3B (Y-Direction) are shown in Fig. 5.31 for the four records. The plots were made to the same scale as those shown in Fig. 5.27 (original building) for ease of comparison. Figures 5.32 and 5.33 show computed moment-rotation curves for the same column and beam plotted in Figs. 5.28 and 5.29, respectively.

c) Infill Wall Scheme

Strengthening scheme W3 proved to be the best for protecting the unstrengthened elements from inelastic action. No splice failures of interior columns were detected for any of the records considered. Maximum response was computed for the Scaled El Centro record, which showed maximum joint shear stress in the unreinforced beam-column connections below the cracking stress given by Eq. 4.3. Pullout of the beam bottom reinforcement could not be prevented for the El Centro and Scaled El Centro records. Table 5.14 summarizes response maxima computed for the four records.

Computed response of the building was elastic for the SCT record. Response to the other records showed concentration of inelastic demand in the reinforced concrete infill walls. Maximum curvature ductilities of 13 were computed at the base of the walls for the Scaled El Centro record requiring the longitudinal reinforcement of the boundary elements to develop strains of 2.0%. Concrete compressive strains were computed to be below 0.003 at maximum response. Displacement history plots for the four records considered are shown in Fig. 5.34.

Because the behavior of the building is dominated by the performance of the infill walls, and failure of one of them would clearly endanger the stability of the building, careful
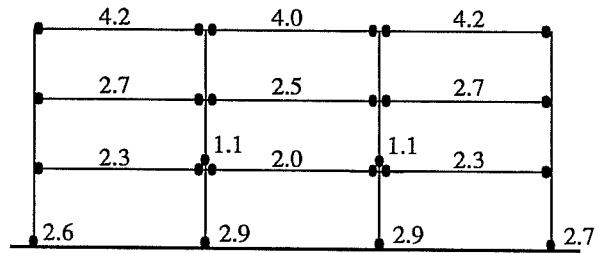
a) Jacketing Scheme J3B-Y
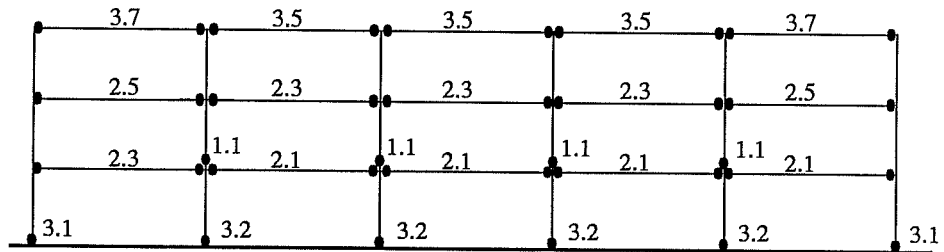
b) Jacketing Scheme J3B-X

Figure 5.30 Rotational Ductility Demands on Jacketed Frames
Strengthening Scheme J3B - Scaled El Centro Record
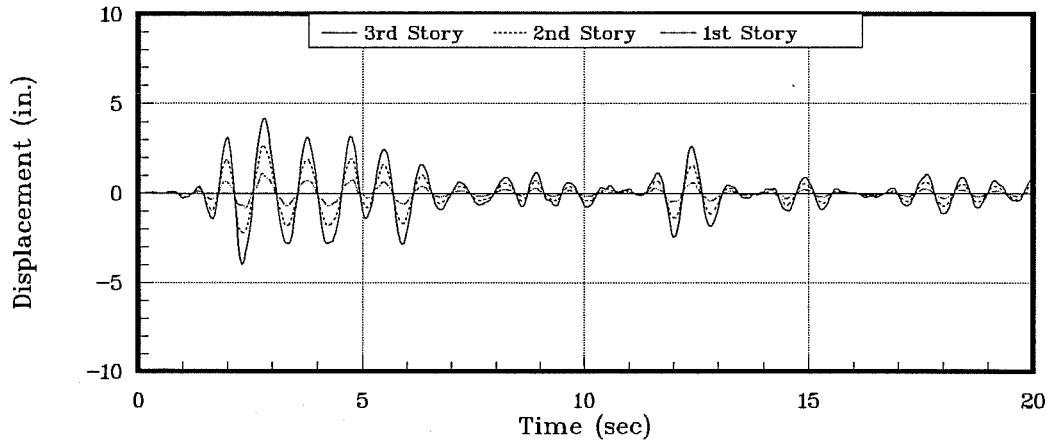
a) Response to El Centro
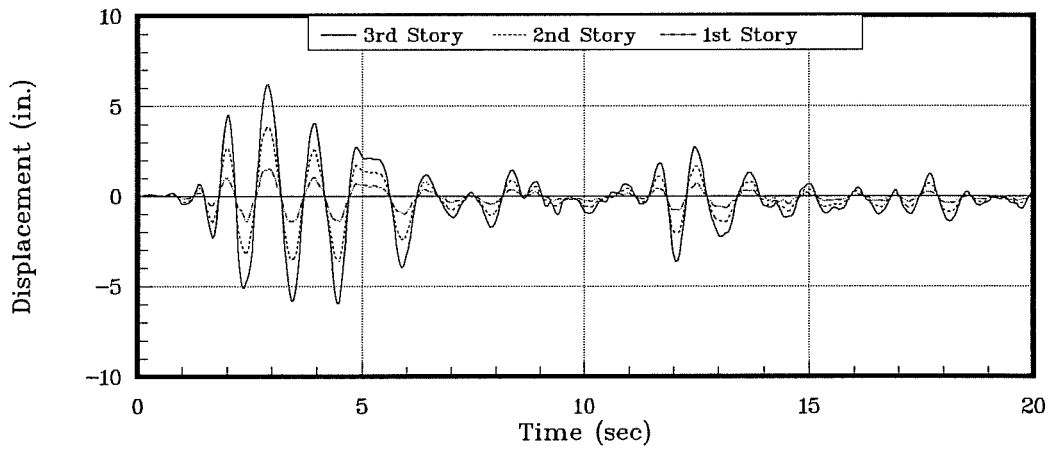
b) Response to Scaled El Centro

Figure 5.31 Displacement Histories, Strengthening Scheme J3B
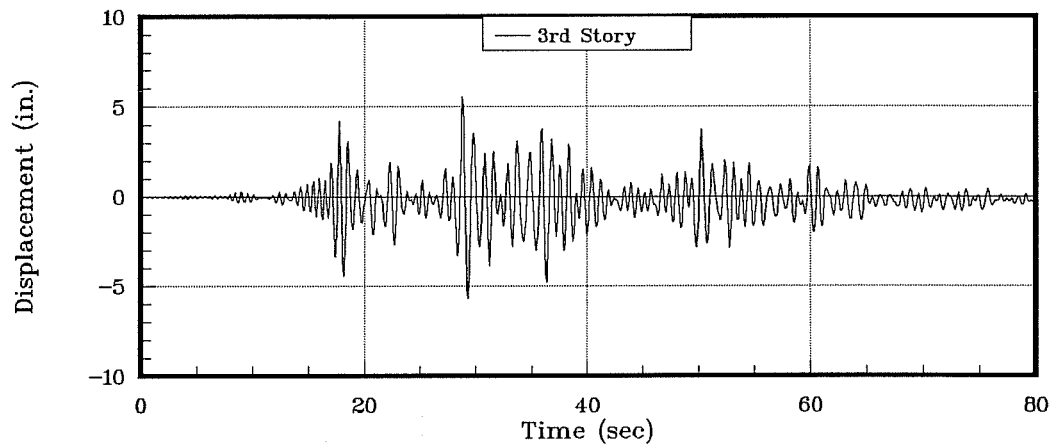
c) Response to Vina del Mar
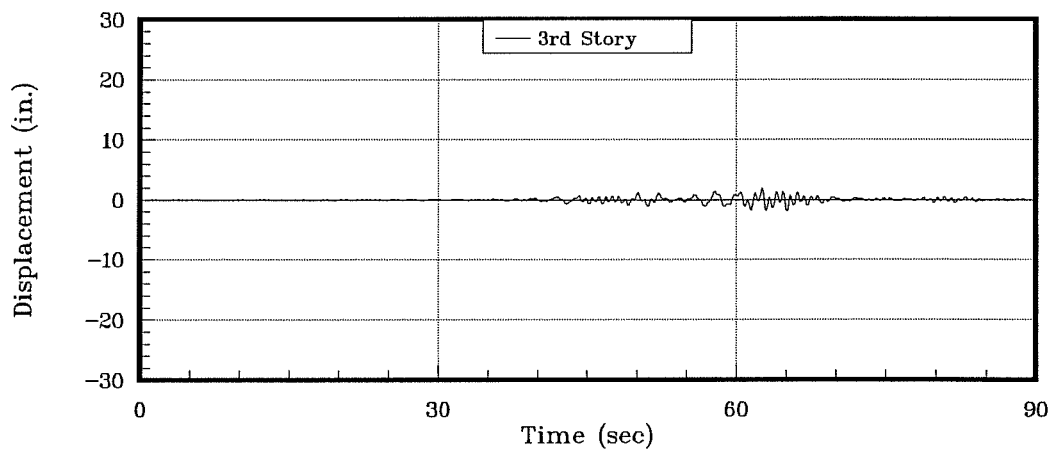
d) Response to SCT

Figure 5.31 (Cont.) Displacement Histories, Strengthening Scheme J3B
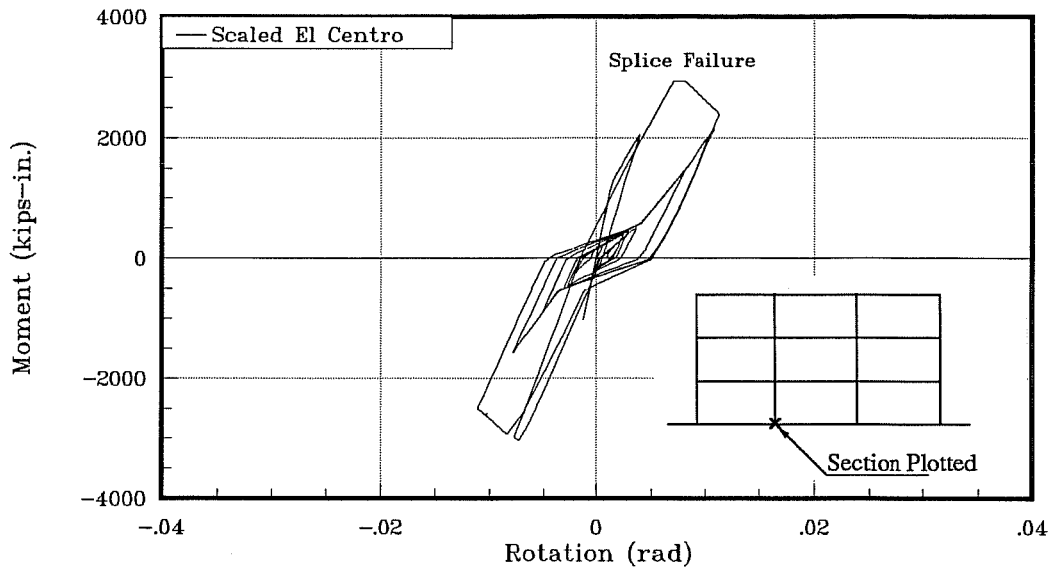
Figure 5.32 1st Story Unstrengthend Interior Column
Moment–Rotation Curve, Frame Jacketing Scheme J3B
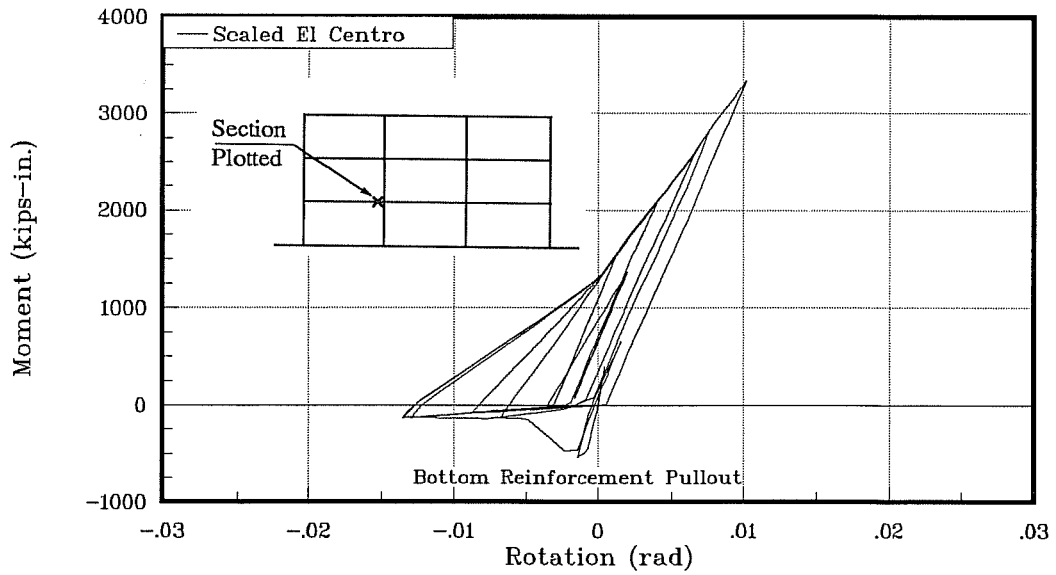
Figure 5.33 Unstrengthened Beam Moment–Rotation Curve
Frame Jacketing Scheme J3B

detailing of the infill walls and adequate proportioning of the foundations is imperative.

Table 5.14 Response Maxima - Strengthening Scheme W3

Earthquake	Base Shear[1] (%)	Overall Drift (%)	Wall Shear Stress $(\tau_{max}/\sqrt{f_c'})$
El Centro	39.6	0.30	4.2
Viña del Mar	31.5	0.14	3.8
Scaled El Centro	50.7	0.57	5.1
SCT	18.9	0.02	2.0

(1) Base Shear Strength = 55%

d) Summary

The findings from the behavior of the original and strengthened buildings to the selected ground motions may be summarized as follows:

- The original building exhibited inadequate behavior when subjected to moderate to severe ground motions. For all the records considered, splice failure of all first-story columns was predicted. High joint shear stresses were developed in the unreinforced beam-column connections and pullout of the beam bottom reinforcement was also predicted.

- Frame jacketing schemes showed that inelastic demands in the unstrengthened elements could be reduced, but failure of the splice region of unstrengthened columns could not be avoided for the El Centro, Viña del Mar and Scaled El Centro records. The maximum computed response for these records was shown to be insensitive to the lateral strength provided by the different retrofit schemes. Frame jacketing proved to be a very efficient retrofitting alternative when the building was subjected to the SCT record. The additional
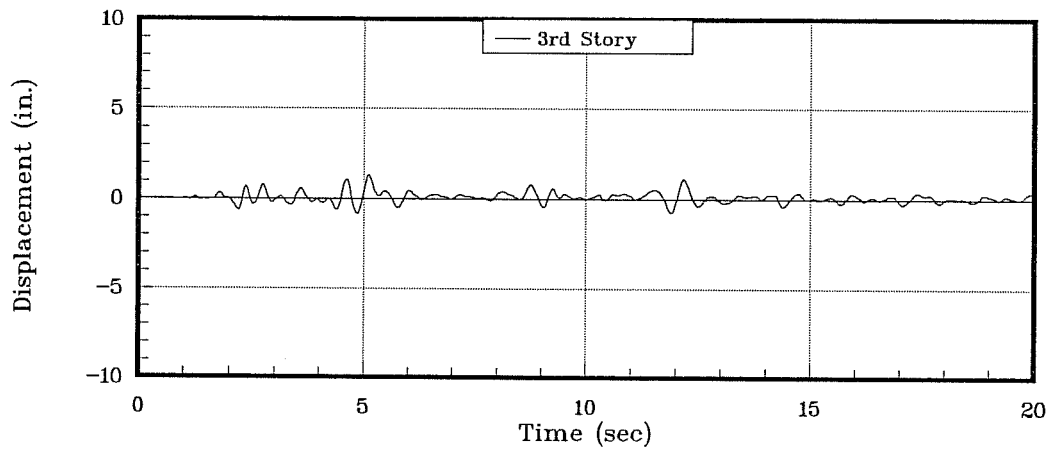
a) Response to El Centro
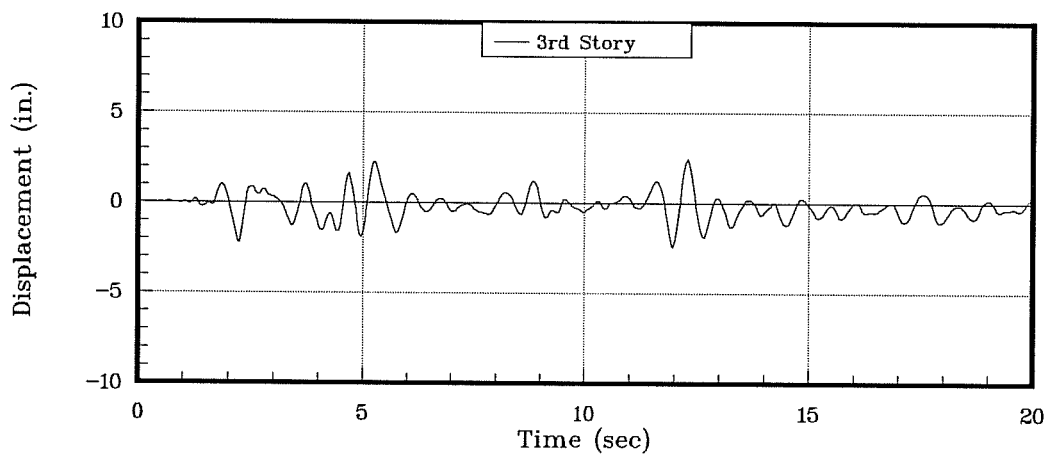
b) Response to Scaled El Centro

Figure 5.34 Displacement Histories, Strengthening Scheme W3
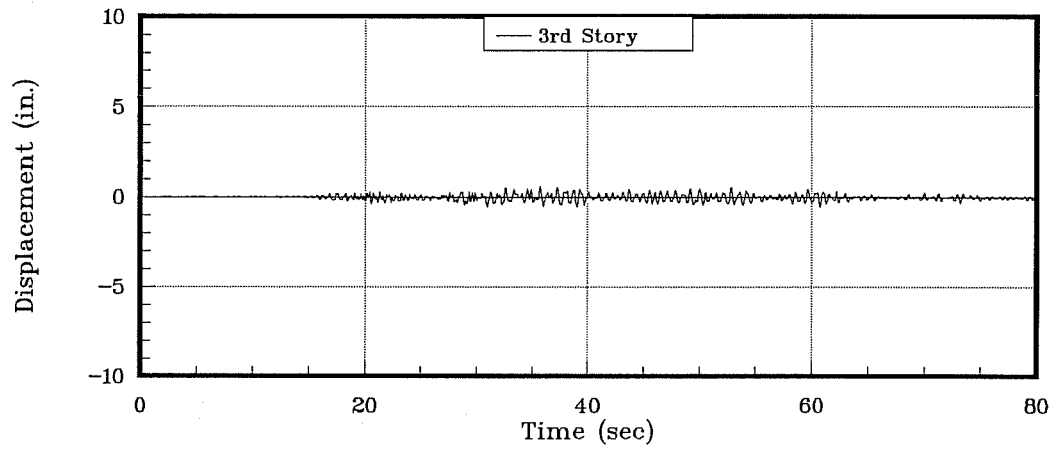
c) Response to Vina del Mar
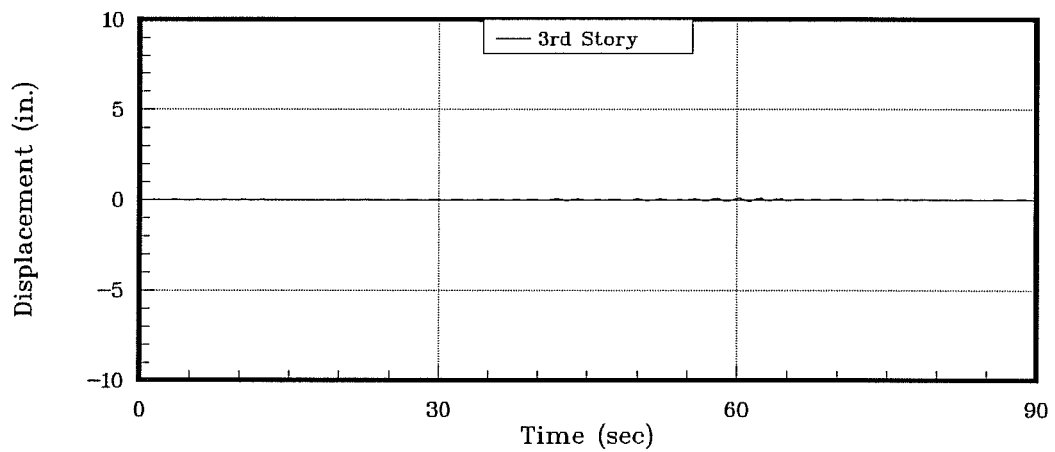
d) Response to SCT

Figure 5.34 (Cont.) Displacement Histories, Strengthening Scheme W3

stiffness provided by frame jacketing produced the necessary shift in the building period to move the building response to lower levels in the response spectra.

- Strengthening scheme W3 was the only one that was able to prevent inelastic action in unstrengthened first-story columns for all the records considered. Good design of the infill walls is of paramount importance for the success of the retrofitting operation since the seismic performance of the building is dependent upon the very stiff shear walls.

Figures 5.35 and 5.36 summarize computed maximum drifts and rotational ductility demands in the first-story unstrengthened columns, respectively, for the original and strengthened buildings.

5.5.2 Ten-Story Buildings

a) Original Building

Dynamic analyses showed that, in general, the performance of the ten-story building was better than that exhibited by the three-story building for the same ground motion. The following aspects were found to be common to the dynamic response of the building to the four ground motions:

- Pullout of the beam bottom reinforcement was predicted in all the beam column joints of the structure.

- Joint shear stresses were computed to be below the shear-cracking stress specified by Eq. 4.3.

- The shear capacity of the columns was never exceeded, although, as was seen in Section 5.2 (Table 5.4), shear strength was not enough to allow development of flexural capacity.
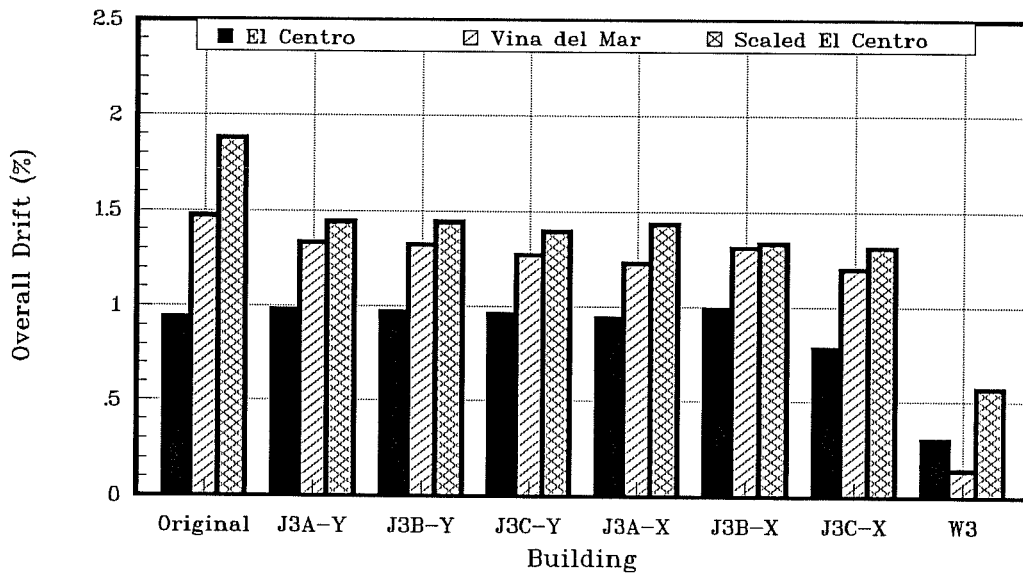
Figure 5.35 Maximum Overall Drift
3 Story Buildings
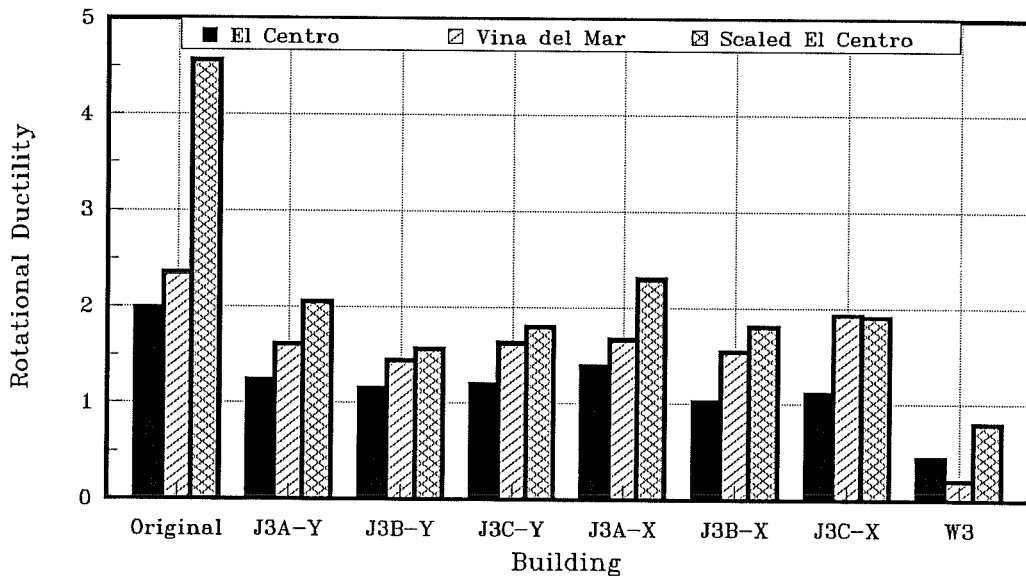
Figure 5.36 Average Rotational Ductility Demands
Unstrengthened Columns − 3 Story Buildings

- When splice failure in columns was predicted, it occurred only at the base of the first-story columns.

The behavior of the building to the Viña del Mar record was nearly elastic. All columns remained elastic, and yielding in negative bending was only detected in the 2nd through 6th floor beams of the interior bays. Computed rotational ductility demands for these beams varied from 1.2 to 1.4, with associated maximum compressive strains in the concrete below 0.003.

Similar response of the building was computed when it was subjected to the El Centro record, with the main difference being that a splice failure was predicted for all the first-story exterior columns. The pattern of beam yielding was the same as for the Viña del Mar record.

Inadequate response of the building was computed for the Scaled El Centro and SCT records given the fact that a splice failure was predicted for all first-story columns.

Maximum base shear, overall drift, and ductility demands in the first-story columns computed for the four records are presented in Table 5.15.

Maximum computed interstory drifts are shown in Fig. 5.37. Concentration of lateral displacements in the first three levels (Fig. 5.37d) computed for the SCT record can be explained in terms of excessive rotational ductility demands in the beams and first-story columns that made the columns behave as if they were cantilevered at the base.

Displacement histories for the four records are presented in Fig. 5.38. Lengthening of the fundamental period of the building to approximately 3.0 sec can be observed in the computed response for the Scaled El Centro and SCT records. Displacement histories for the El Centro and Viña del Mar records show no lengthening in period beyond 2.0 sec confirming the fact that the building exhibited little inelastic behavior.
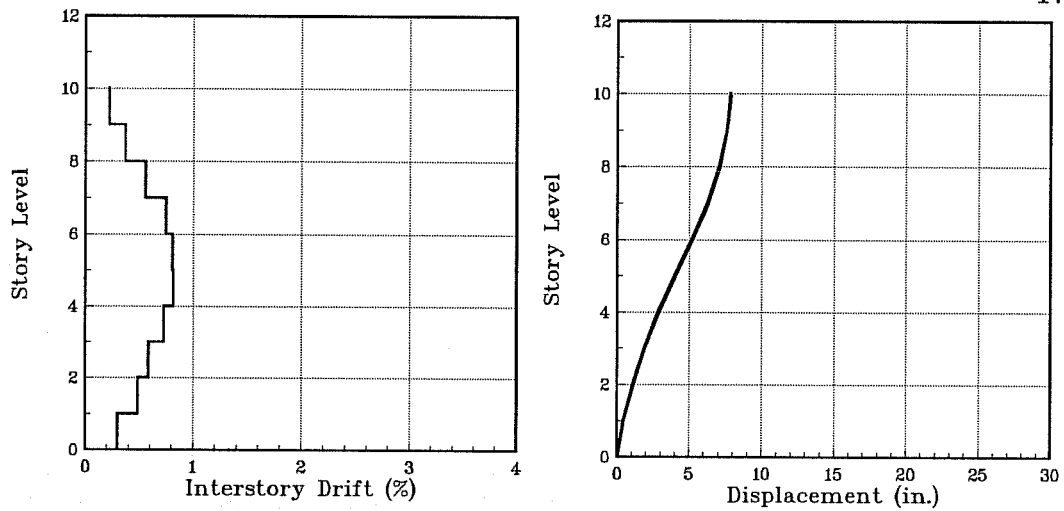
a) El Centro
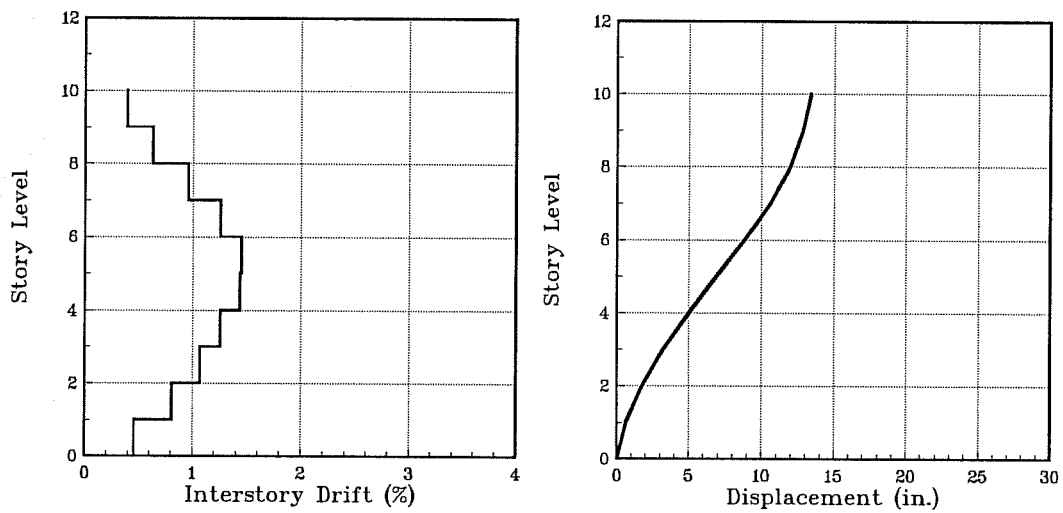
b) Scaled El Centro

Figure 5.37 Drift and Displacement Envelopes, Original Ten-Story Building

148
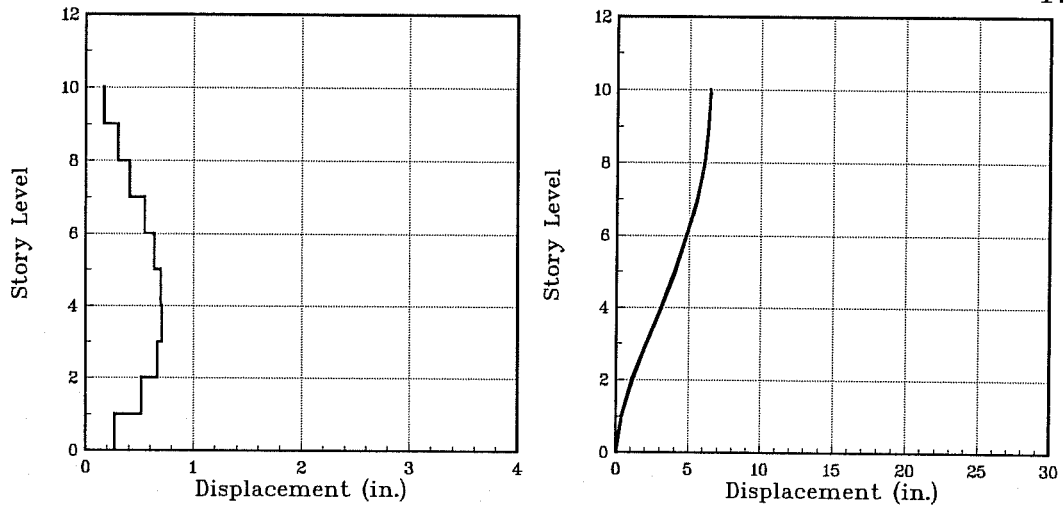
c) Viña del Mar
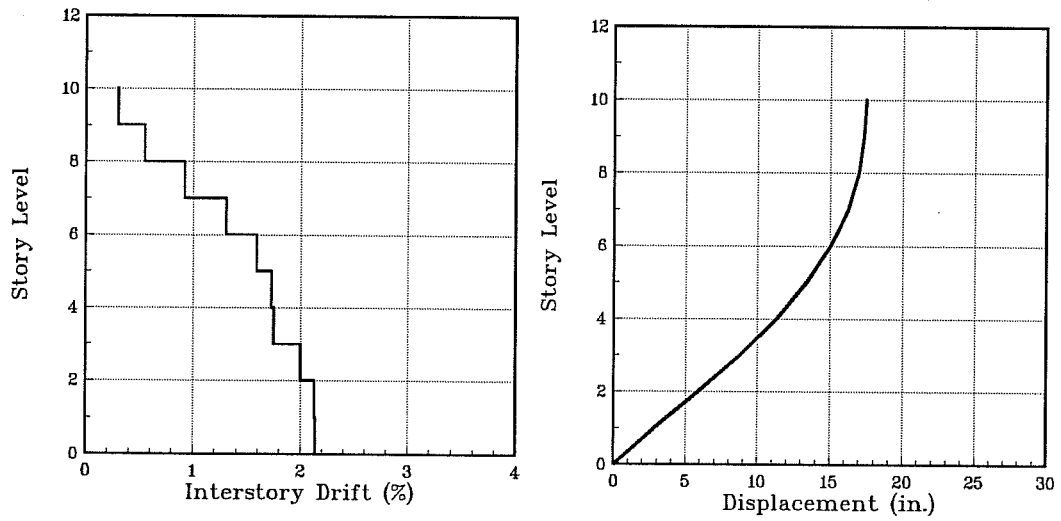
d) SCT

Figure 5.37 (Cont.) Drift and Displacement Envelopes, Original Ten-Story Building

c) Response to Vina del Mar

d) Response to SCT
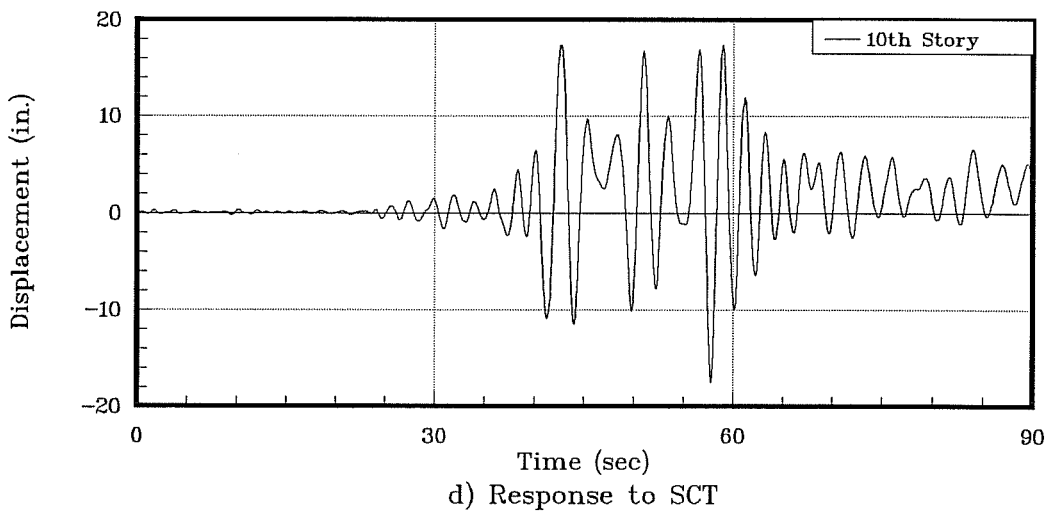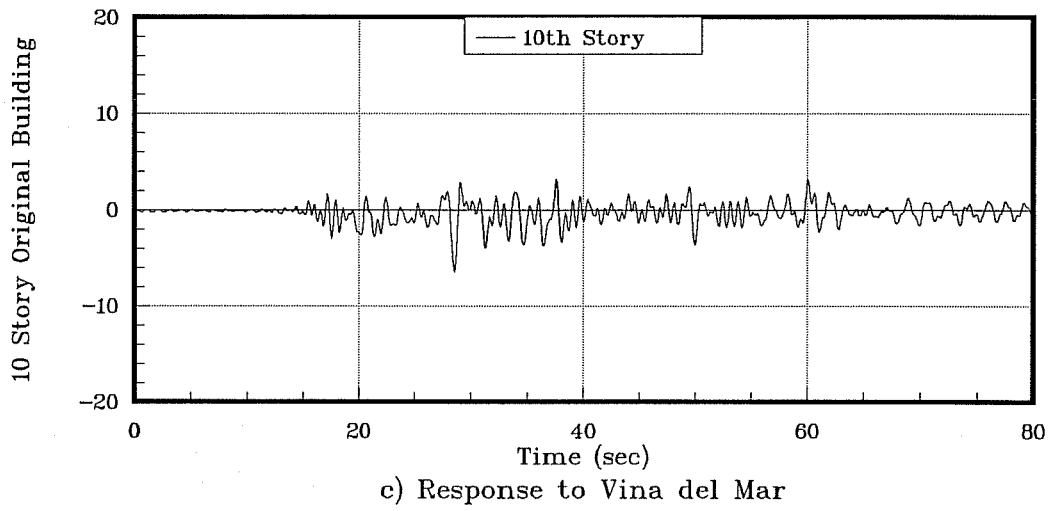
Figure 5.38 (Cont.) Displacement Histories, Original Ten-Story Building

Table 5.15 Response Maxima - Original Ten-Story Building

Earthquake	Base Shear[1] (%)	Overall Drift (%)	Rotational Ductility Demands 1st Story Columns
El Centro	10.6	0.54	1.1[*]
Viña del Mar	7.6	0.45	(0.76)
Scaled El Centro	13.0	0.93	1.56
SCT	11.9	1.22	10.3

* Only Exterior Columns
() Columns remained elastic
(1) Base shear capacity = 11%

b) Strengthening Scheme J10A

The dynamic response of strengthening scheme J10A to the El Centro and Viña del mar records showed, as could be expected, good performance of the building. Regarding the behavior of the unstrengthened elements, columns still remained elastic and joint shear stresses were still computed to be below the cracking level. In the jacketed frames, inelastic actions were observed in the 1st through 6th floor beams, and incipient yielding of the corner columns was predicted. Maximum joint shear stresses were computed to be $8.2\sqrt{f_c'}$ at the fourth floor level.

The response of the building to the Scaled El Centro record showed that drift levels and inelastic demands in the unstrengthened elements were reduced with respect to those computed for the original building, but still splice failure of first-story interior columns was predicted. The displacement history computed for this case is shown in Fig 5.39a.

For the SCT record, the behavior of the building was worse than that exhibited by the

a) Response to Scaled El Centro

b) Response to SCT
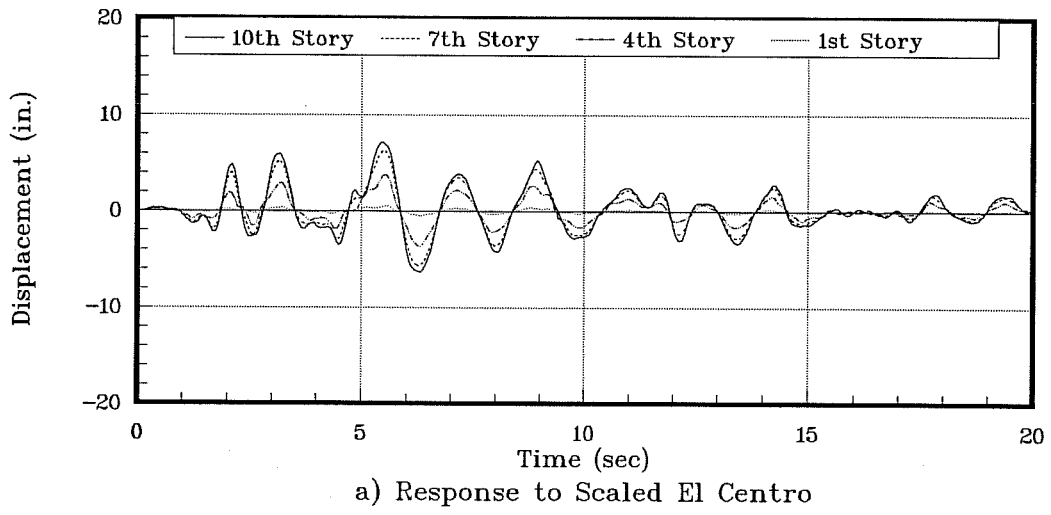
Figure 5.39 Displacement Histories, Strengthening Scheme J10A
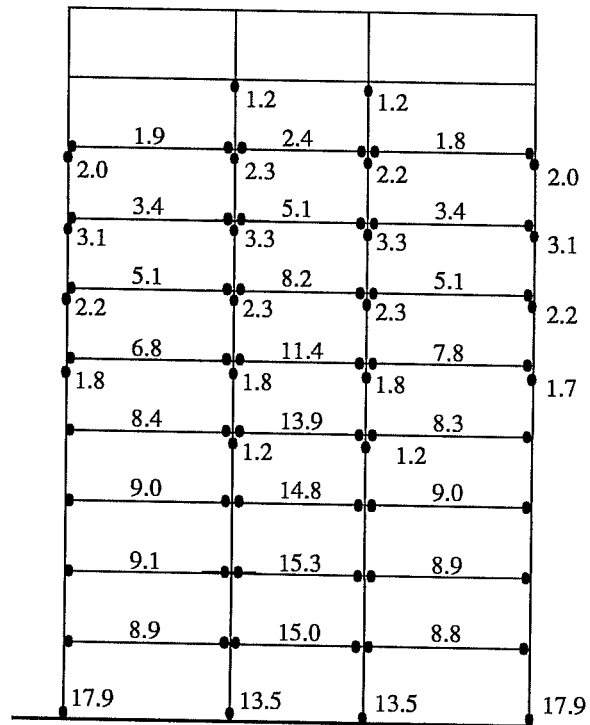
Figure 5.40   Rotational Ductility Demands in Jacketed Frames
Strengthening Scheme J10A - SCT Record
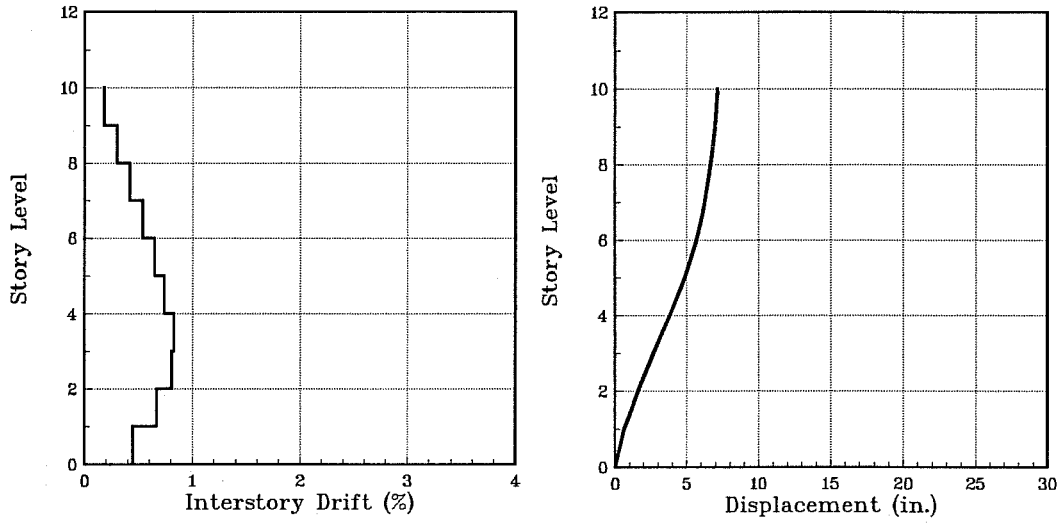
a) Scaled El Centro

b) SCT

Figure 5.41 Drift and Displacement Envelopes, Strengthening Scheme J10A

original building. The maximum computed roof displacement increased by 50%. Splice

failures in the interior columns, which occurred only in the first-story in the original building,

were also predicted from the 5th to 8th floors. The behavior of the jacketed frame was also

unacceptable because of high rotational ductility requirements (shown in Fig. 5.40). The

worsening of the global response of the building can be explained in terms of the displacement

history shown in Fig. 5.39b. It can be appreciated that during maximum response the

fundamental period has lengthened to approximately 2.0 sec, which coincides with the zone of

maximum response in the spectra shown in Figs. 5.24 and 5.25.

Table 5.16 summarizes global response quantities computed for the four records.

Interstory drifts and displacement envelopes for the scaled El Centro and SCT records are

shown in Fig. 5.41.

Table 5.16 Response Maxima - Strengthening Scheme J10A

Earthquake	Base Shear[1] (%)	Overall Drift (%)	Rotational Ductility Demands Unstrengthened 1st Story Columns
El Centro	13.7	0.29	(0.73)
Viña del Mar	13.8	0.43	(0.77)
Scaled El Centro	17.7	0.50	1.51
SCT	21.0	1.85	13.10

() Elastic Response
(1) Base Shear Strength = 18%

c) Strengthening Scheme J10B

The behavior of strengthening scheme J10B to the selected ground motions is

considered unacceptable because of shear failures predicted in the original columns that frame

into the very stiff jacketed beams of the exterior frames (Fig 5.16). An attempt was made to avoid the shear failure of these columns by reducing the moment capacity of the original beams to a minimum value (just enough to carry gravity moments), however, computed shear demands were reduced very little, showing that high shear stresses induced in these columns were due to the irregular stiffness distribution of the jacketed frames rather than to the reduction in the shear span caused by the deep jacketed beams. Figure 5.42 shows the ratio of shear demand to shear capacity computed for the original columns when the building was subjected to the El Centro record.

d) Strengthening Scheme W10A

A behavior similar to that computed for strengthening scheme J10A (that has about the same lateral strength and stiffness of W10A) was observed when the building was subjected to the El Centro and Viña del Mar records. No inelastic action was observed in the unstrengthened elements other than pullout of the beam bottom longitudinal reinforcement. Curvature ductility demands at the base of the infill walls were small, with a maximum value of 1.3 computed for the response to the El Centro record.

The building also exhibited good behavior when subjected to the Scaled El Centro record. In contrast to what was observed for strengthening scheme J10A in which a generalized splice failure of first-story columns was predicted, a splice failure was observed for only one unstrengthened column. Although inelastic behavior of the original beams in negative bending was observed from the 2nd to the 9th floor, rotational ductility demands were computed to be below the rotational ductility capacity of the beams.

The response of the building to the SCT record also showed inadequate behavior and
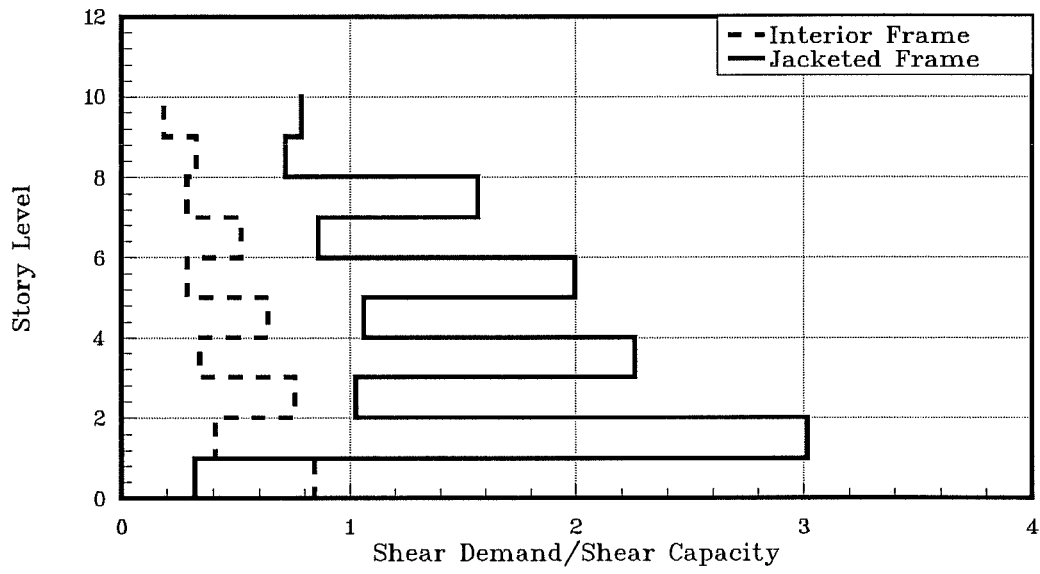
Fig 5.42 Shear Demand in Unstrengthened Columns
Frame Jacketing Scheme J10B

larger displacements than those computed for the original building. Splice failures in the unstrengthened columns were predicted in the first and second stories, and the rotational ductility capacity of the original beams was exceeded throughout the height of the building. Failure of the infill walls was also predicted due to excessive ductility demands that led to fracture of the longitudinal reinforcement in the boundary columns.

Table 5.17 summarizes global response maxima computed for the four records. Displacement histories for the Scaled El Centro and SCT records are shown in Fig. 5.43. Interstory drifts and displacement envelopes for the same records are presented in Fig. 5.44.

Table 5.17 Response Maxima - Strengthening Scheme W10A

Earthquake	Base Shear[1] (%)	Overall Drift (%)	Rotational Ductility Demands Unstrengthened 1st Story Columns
El Centro	14.7	0.39	(0.30)
Viña del Mar	14.5	0.49	(0.34)
Scaled El Centro	18.2	0.61	1.04[*]
SCT	19.5	2.22	6.67

( ) Elastic behavior
* One exterior column
(1) Base Shear Strength = 20%

e) Strengthening Schemes W10B and WJ10

Dynamic analyses showed that, in general, the performance of the retrofitted buildings W10B and WJ10 was good for all the records considered. The following aspects of the dynamic response of the buildings were found to be common to both strengthening schemes:

-   No splice failures were detected in any of the unstrengthened elements

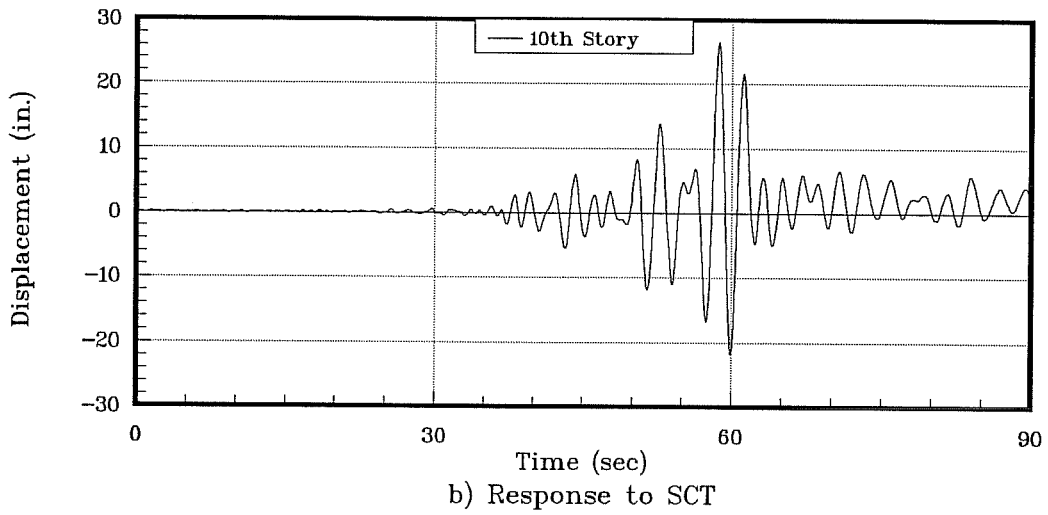   of the buildings, and

a) Response to Scaled El Centro

b) Response to SCT

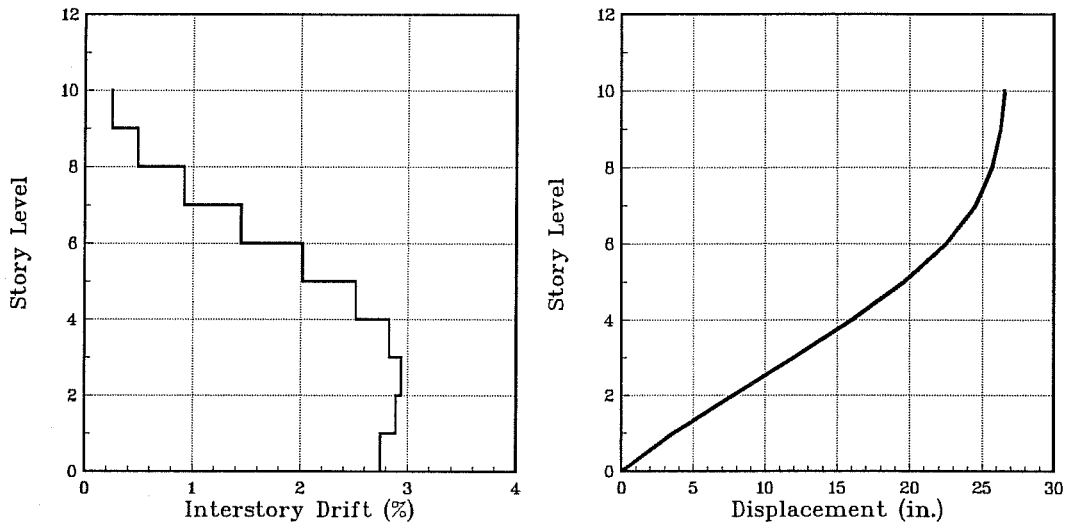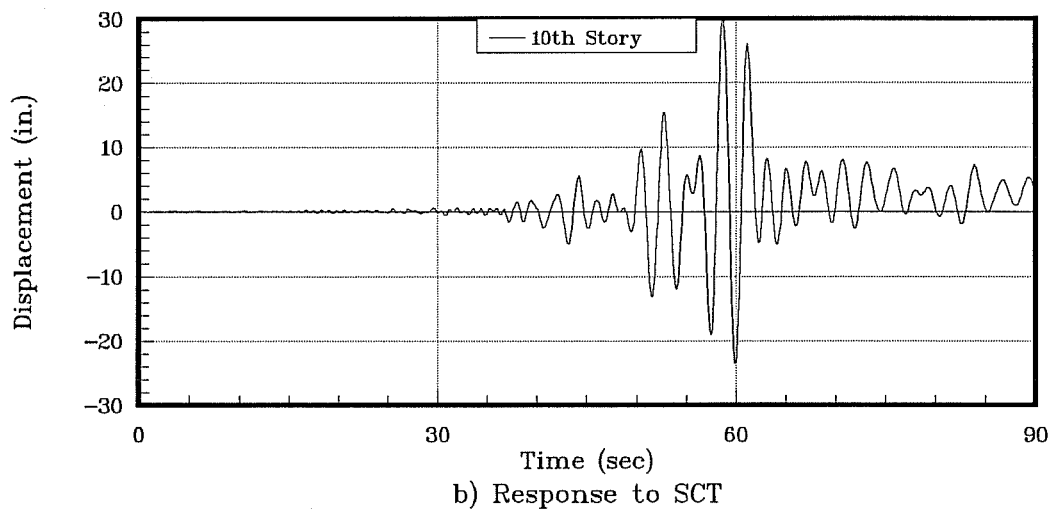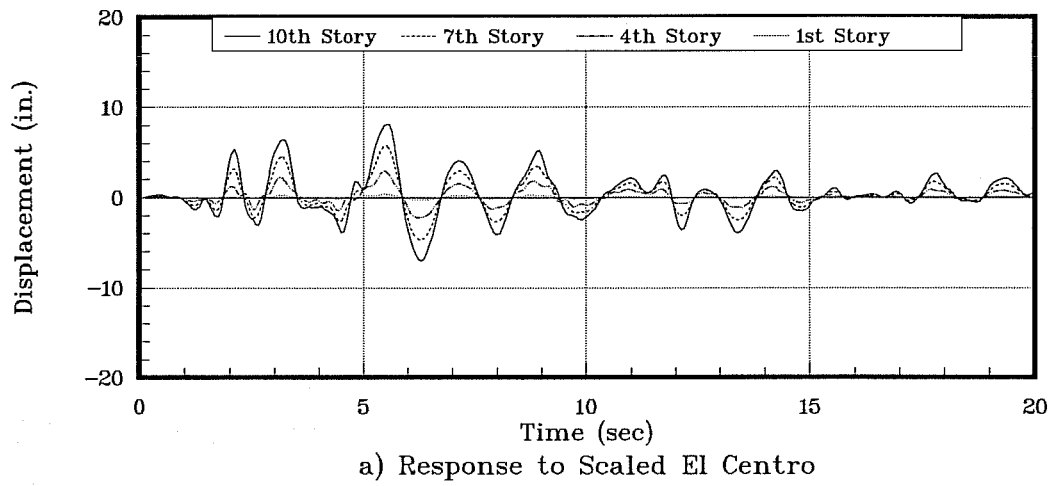Figure 5.43 Displacement Histories, Strengthening Scheme W10A
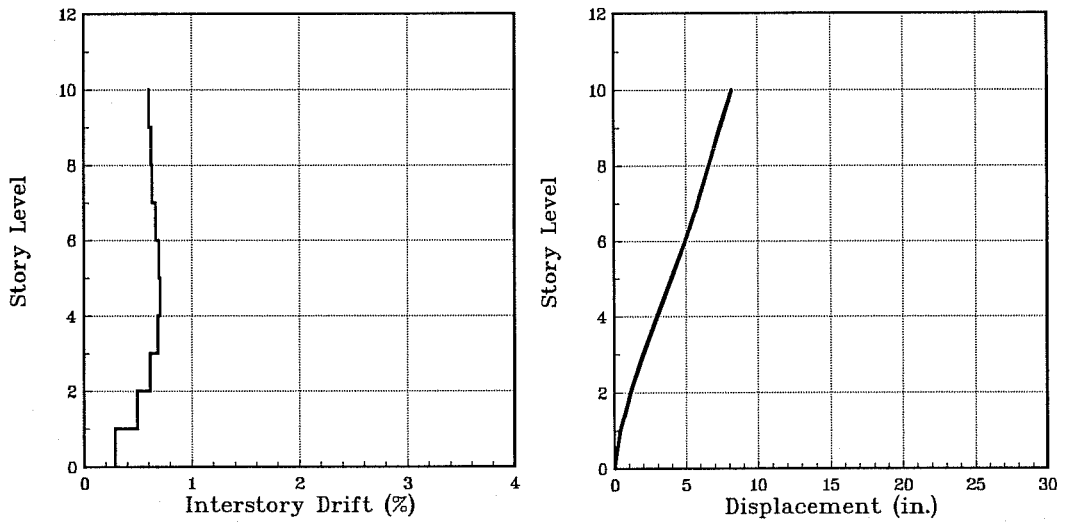
a) Scaled El Centro
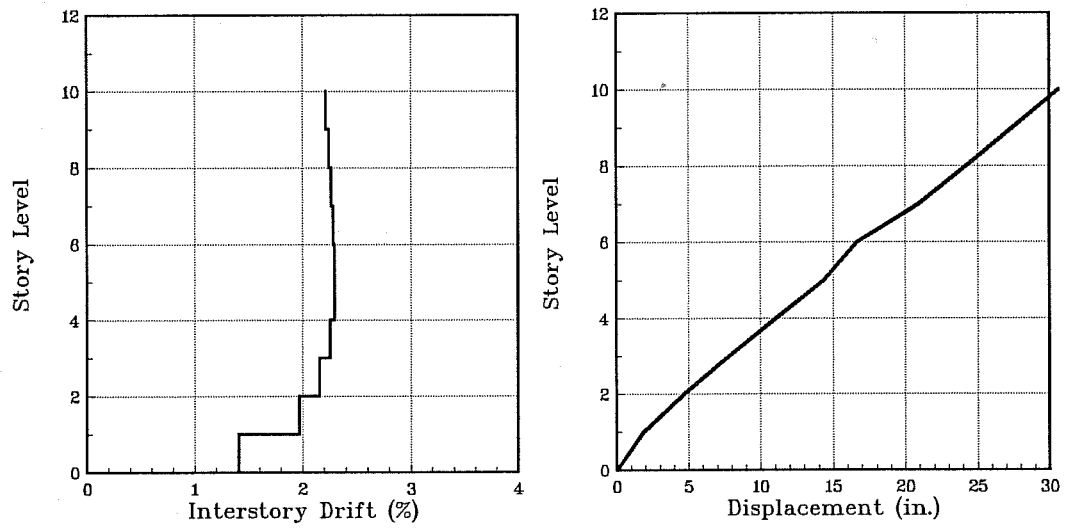
b) SCT

Figure 5.44 Drift and Displacement Envelopes, Strengthening Scheme W10A

- Pullout of the original beam bottom reinforcement was predicted in all

the beam-column connections.

Strengthening scheme W10B showed that the rotational ductility capacity of the coupling beams (that were not strengthened) was exceeded by about 25% at every story level. Shear demands in these beams were computed to be below their capacity, which can be explained because the early loss of their positive moment capacity helped to reduce the shear demand.

Table 5.18 summarizes global response maxima computed for the four records for both strengthening schemes. Displacement histories for the Scaled El Centro and SCT are shown in Fig. 5.45 for strengthening scheme W10B, and in Fig 5.46 for strengthening scheme WJ10. Interstory drifts and displacement envelopes for the same records are presented in Figs. 5.47 and 5.48.

f) Summary

The results obtained from the dynamic analyses of the ten-story buildings can be summarized as follows:

- The original ten-story building was less vulnerable than the three-story building to the four records considered in this study. No splice failures in columns were predicted for the El Centro and Viña del Mar records. Shear stresses in the joints were computed to be below the cracking level, and shear forces developed in the columns were smaller than their shear capacity for all the records considered.

- A generalized splice failure of first-story unstrengthened columns could not be prevented in building J10A when subjected to the Scaled El Centro record. In fact, ductility

a) Response to Scaled El Centro

b) Response to SCT
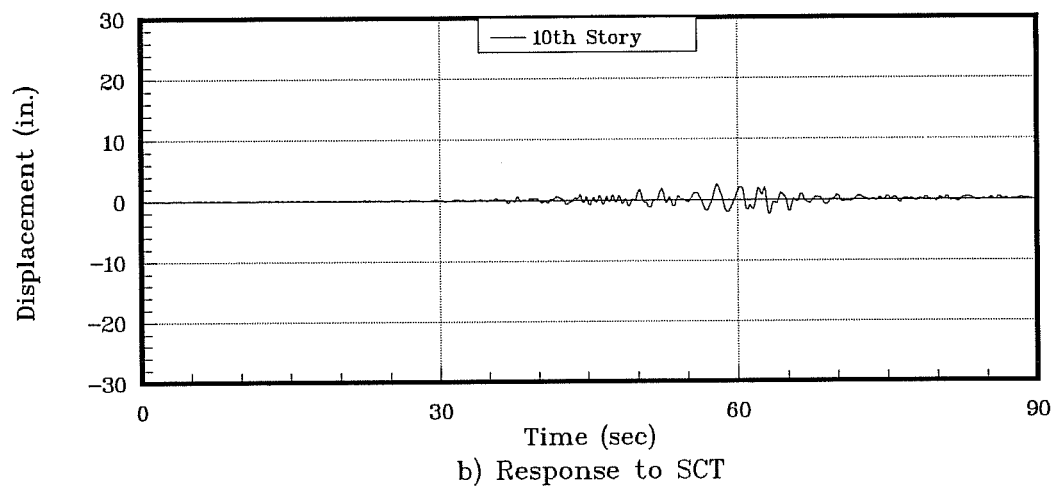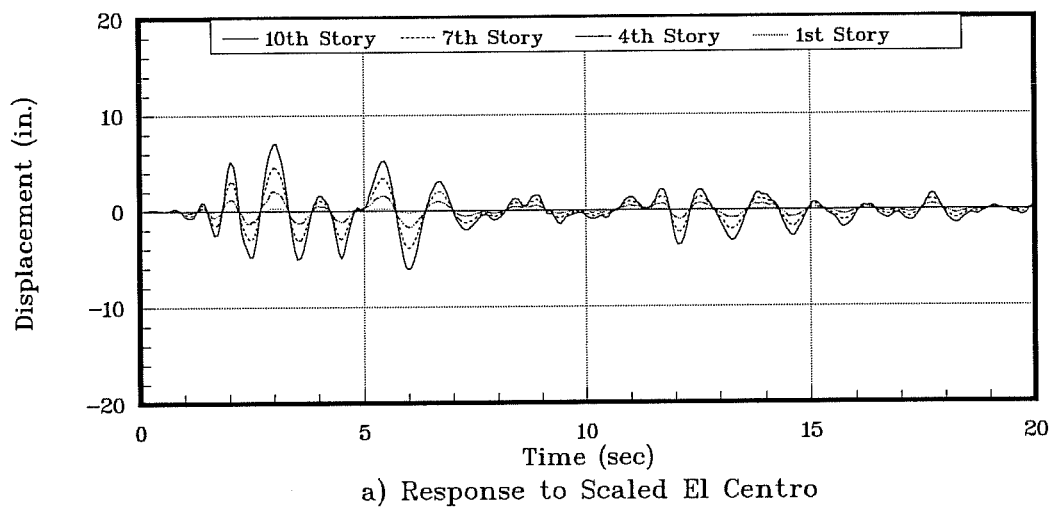
Figure 5.45 Displacement Histories, Strengthening Scheme W10B

a) Response to Scaled El Centro

b) Response to SCT
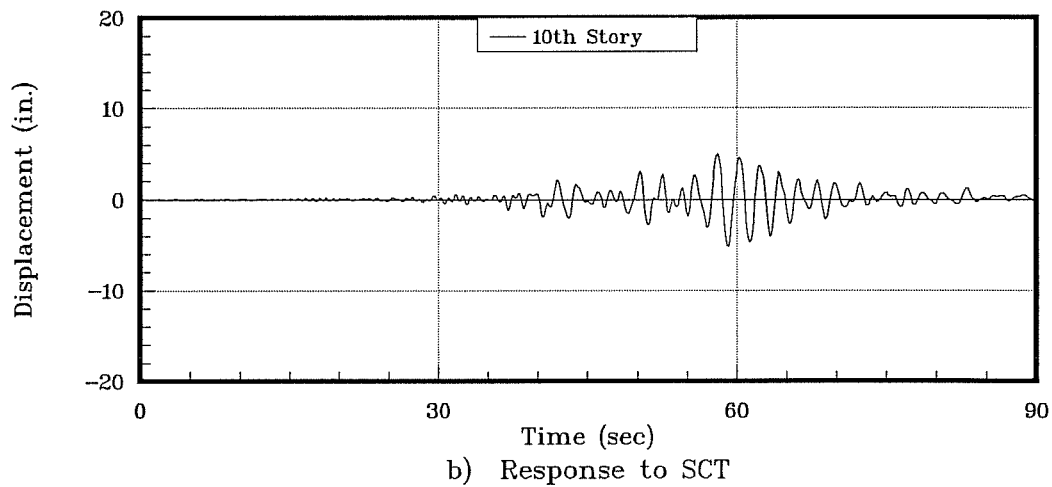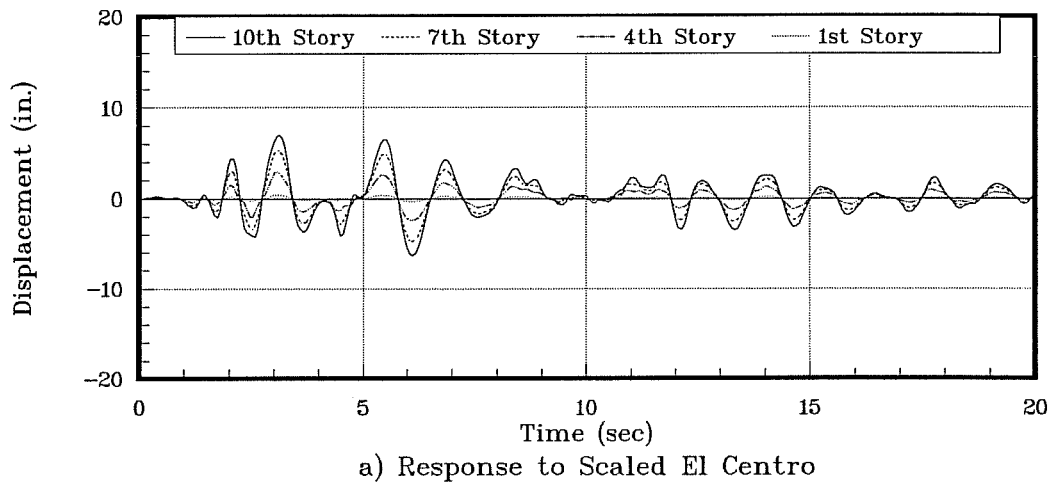
Figure 5.46 Displacement Histories, Strengthening Scheme WJ10
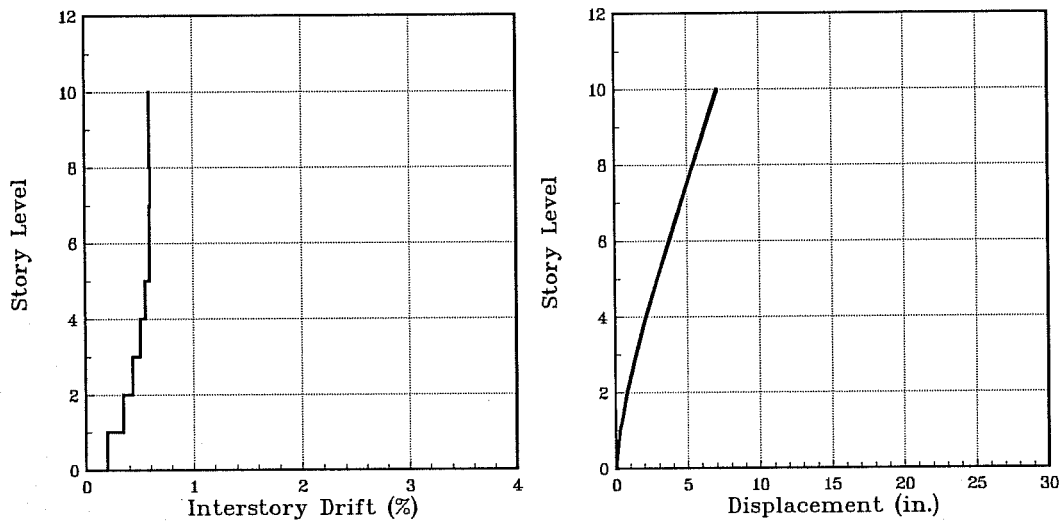
a) Scaled El Centro
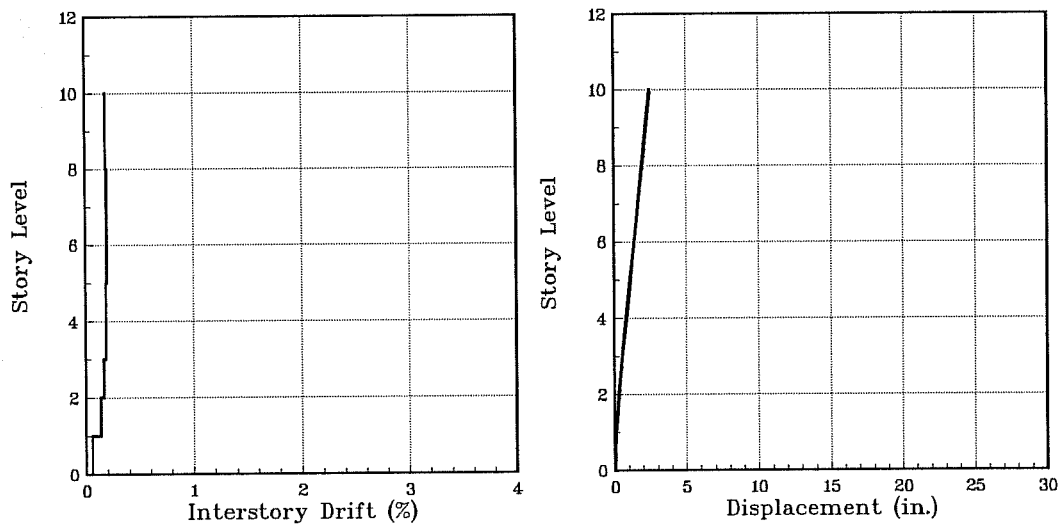
b) SCT

Figure 5.47 Drift and Displacement Envelopes, Strengthening Scheme W10B
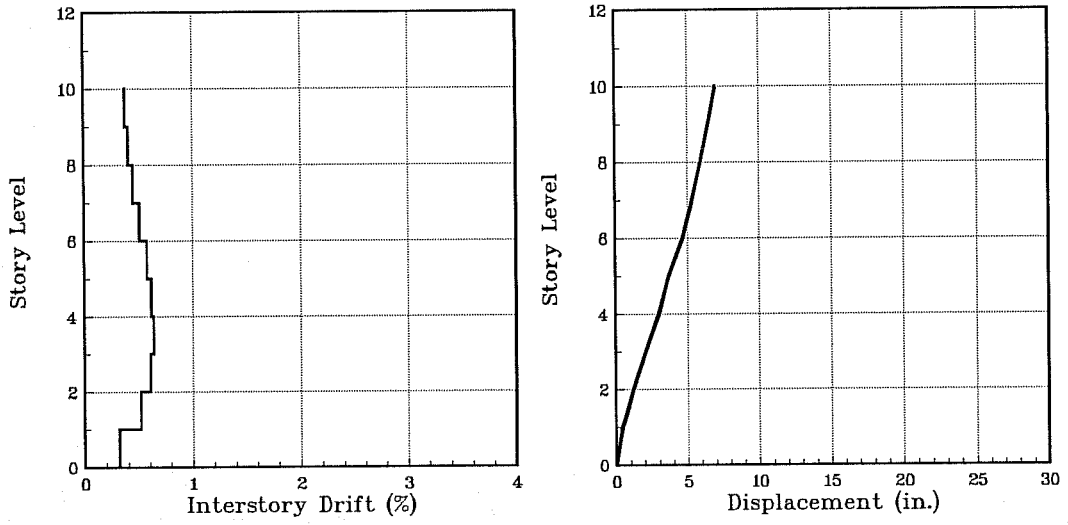
a) Scaled El Centro
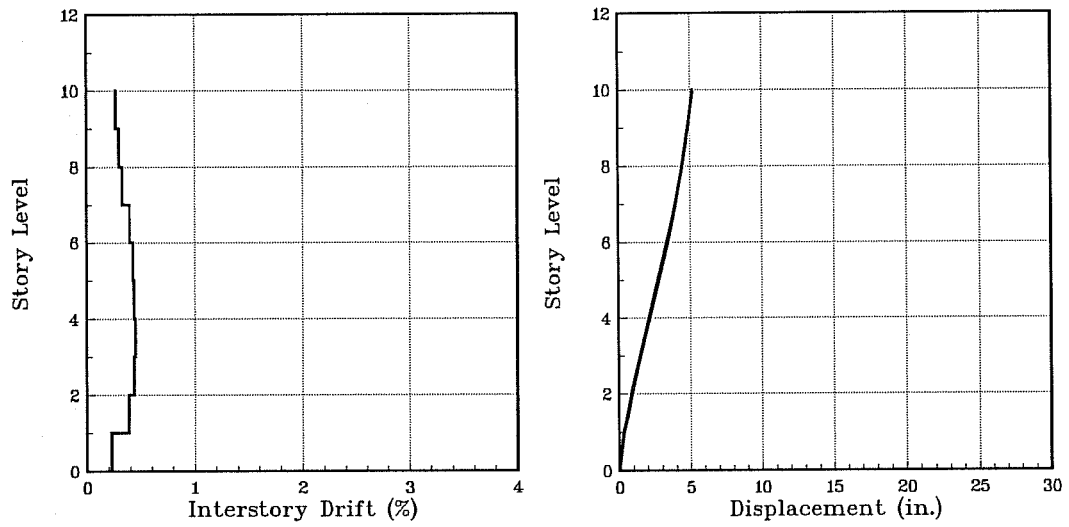
b) SCT

Figure 5.48 Drift and Displacement Envelopes, Strengthening Scheme WJ10

requirements for these elements were computed to be very similar to those obtained for the

original building.

Table 5.18 Response Maxima - Strengthening Schemes W10B and WJ10

Building	Earthquake	Base Shear (%)	Overall Drift (%)	Rotational Ductility Demands, Unstrengthened 1st Story Columns
W10B	El Centro	25.5	0.36	(0.30)
	Viña del Mar	25.1	0.44	(0.40)
	Scaled El Centro	32.8	0.49	(0.53)
	SCT	20.3	0.17	(0.13)
WJ10	El Centro	23.3	0.34	(0.51)
	Viña del Mar	19.6	0.51	(0.43)
	Scaled El Centro	23.4	0.48	(0.80)
	SCT	22.2	0.36	(0.65)

( ) Elastic behavior

- Strengthening scheme W10A, which has a lateral strength similar to J10A, proved

to be very effective in limiting inelastic action in the unstrengthened elements. The capacity of

the spliced bars was slightly exceeded in one exterior column for the Scaled El Centro record.

It is of interest to note that although maximum drifts computed for building W10A were always

larger than those computed for building J10A, rotational ductility demands were always smaller

for the building W10A.

- Strengthening schemes W10A and J10A exhibited inadequate behavior for the SCT

record. Large ductility demands computed in most of the structural elements can be attributed to a lengthening in the building period to approximately 2.0 sec, which coincides with the zone of maximum response for the SCT spectra.

 - Strengthening schemes that have an irregular distribution in stiffness are very likely to activate weak links that are potentially present in the original structure. This was the case for strengthening scheme J10B, which featured an alternate story beam jacketing, and for which shear failure of the original columns that framed into the jacketed beams was predicted for all the records considered.

 - Schemes that considered the addition of infill walls proved to be more effective for avoiding splice failures in the original columns. However, high shear stresses that were computed for these walls (indicated in Table 5.19), show that a good design of the infill walls is of vital importance for the success of the retrofitting operation. The use of thicker walls in the lower stories would be advisable to reduce shear demand in these elements.

Table 5.19 Maximum Computed Shear Stress in Infill Walls
$(\tau_{max} / \sqrt{f_c'})$

Building	El Centro	Viña del Mar	Scaled El Centro	SCT
W10A	4.4	4.1	5.7	5.9
WJ10	6.9	5.1	6.8	5.5
W10B	3.2	3.2	4.1	2.7

A comparison of maximum overall drift computed for the buildings subjected to the records considered is shown in Fig. 5.49. Average rotational ductility demands computed for
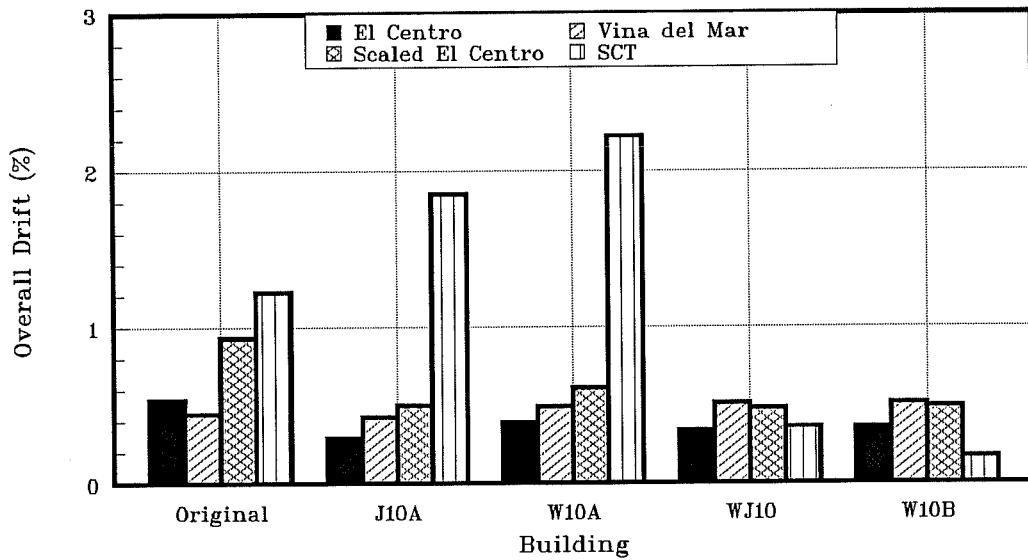
Figure 5.49   Maximum Overall Drift
Ten–Story Buildings
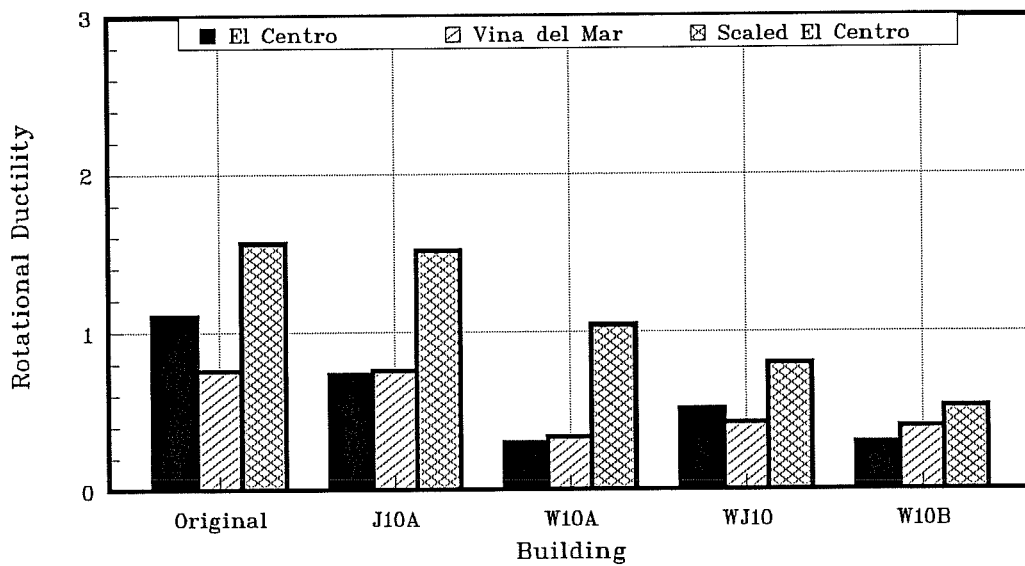
Figure 5.50   Average Rotational Ductility Demands
Unstrengthened Columns, Ten–Story Buildings

the first-story original columns are compared in Fig 5.50 for all but the SCT record.

5.6 Effect of Initial Assumptions

The effect of the assumptions made regarding the amount of viscous damping, pinching of the hysteresis loops, slope of the descending branch of elements exhibiting splice or pullout failure, and the effect of joint flexibility in the dynamic response of the buildings is discussed next.

Table 5.20 compares maximum overall drifts computed for the original ten-story building, strengthening scheme J10A, and strengthening scheme W10A. The second column reproduces the results presented in Section 5.5. Drift levels indicated in the third column were obtained assuming 5% viscous damping. The fourth column shows drifts computed assuming no pinching of the hysteresis loops. Drift levels computed assuming a steeper descending branch of the moment-rotation curves, characterized by a value of $\beta = 3$ (Fig 3.13), are presented in the fifth column, and finally, the results obtained assuming the joints of the buildings to be infinitely rigid are presented in the sixth column.

Similar comparisons in terms of inelastic requirements in the first-story unstrengthened columns are presented in Table 5.21.

From the results indicated in the previous tables, the following observations can be made:

- The amount of equivalent viscous damping seems to be the most influential parameter affecting the dynamic response of the building. Reductions of about 20% in maximum displacements and even larger reductions in inelastic demands were obtained assuming 5% damping. A 2% viscous damping, as considered in this study, seems to be more

appropriate if hysteretic damping at low amplitude cycles (due to cracking of the concrete) is

considered in the analytical model.

Table 5.20 Effect of Parameters Defining the Analytical Model
on Maximum Computed Overall Drift for
Scaled El Centro Record

Building	Overall Drift (%)				
	Initial Assumptions[1]	5% Damping	No Pinching	Descending Branch ($\beta = 3$)	Rigid Joints
Original (10 Story)	0.93	0.74	0.82	0.87	0.90
J10A	0.50	0.43	0.48	0.50	0.51
W10A	0.61	0.48	0.53	0.57	0.57

(1) 2% viscous damping, pinching, $\beta = 10$, flexible joints

Table 5.21 Effect of Parameters Defining the Analytical Model
on Ductility Requirements in Original Columns for
Scaled El Centro Record

Building	Average Rotational Ductility Demands				
	Initial Assumptions[1]	5% Damping	No Pinching	Descending Branch ($\beta = 3$)	Rigid Joints
Original (10 Story)	1.56	1.31	1.35	4.38	1.49
J10A	1.51	1.06	1.35	1.58	1.41
W10A	1.04	(0.63)	(0.78)	1.04	1.04

(1) 2% viscous damping, pinching, $\beta = 10$, flexible joints

- The effect of neglecting pinching of the hysteresis loops reduced the computed response of the buildings by about 10%. Since some degree of pinching of the hysteresis loops is always present in reinforced concrete members subjected to cyclic loads, variations in the amount of pinching with respect that considered in this study are not likely to affect significantly the results obtained previously (Section 5.5).

- The effect of the rate of deterioration of the splice region after its capacity has been reached had an effect on the predicted response of the original building. However, in the strengthened buildings, where the response is controlled by the strengthened portions of the structure, the slope of the descending branch did not appear to be important.

- The effect of considering the joint flexibility in the analytical model proved to be the least important of the parameters studied. This can be attributed to small changes in the fundamental period of the building (with respect to the flexible joint assumption) that resulted when the joints were considered rigid.

CHAPTER 6

GENERALIZATION OF THE RESULTS

6.1 Introduction

A generalization of the results obtained from the dynamic analyses of the buildings is presented in this chapter. Basic building characteristics, such as strength and available ductility, are presented in the following section and are derived from the base shear-roof displacement computed for the buildings analyzed. A simplified model is used in Section 6.3 to investigate the strength, stiffness, and ductility characteristics that must be given to a retrofitted building to lead to acceptable behavior of the retrofitted structure. Finally, design implications inferred from the simplified model are discussed in the last section of this chapter.

6.2 Basic Building Characteristics

An attempt to explain the global behavior of the buildings analyzed in the previous chapter is presented next. The discussion that follows is based on the following assumptions and definitions:

- Basic building characteristic such as strength and available ductility can be obtained from the seismic coefficient-overall drift curves obtained assuming all elements of the structure to be initially cracked (C-Δ curves, see Figs. 5.12 and 5.20).

- Lateral strength of a building is defined as the seismic coefficient (base shear divided by building weight) that produces failure of the strengthened portions of the building or splices in all the unstrengthened first-story columns of the building, whichever occurs first.

172

- The C-Δ curves can be idealized as bilinear curves in which the initial branch is tangent at the origin to the computed C-Δ curve. The slope of the second branch, or "yield branch", of the idealized curve is assumed to be 20% of the elastic stiffness.

- The "yield strength" of a building, C_y, is determined from the bilinear C-Δ curve by locating the intersection of the elastic branch and the yield branch that passes through the point of maximum strength (splice failure coordinates).

- The available ductility of the building, μ_a, is obtained from the idealized C-Δ curve, and is defined as the ratio between the maximum overall drift (splice failure coordinates) and the drift at yield, Δ_y.

- In order to make comparisons between available ductility, as defined above, and ductility requirements for a given earthquake record (Fig. 5.26) a possibility, an "effective strength", C_{eff}, of the building is defined as its yield strength divided by the modal mass ratio associated with the first mode of vibration.

Figure 6.1 shows idealized C-Δ curves for some of the three-story buildings, computed using the procedure explained above. Similar curves for the ten-story buildings are presented in Fig. 6.2.

Table 6.1 indicates for each building the yield drift, yield strength, effective strength, and available ductility. Note that for strengthening schemes which make use of frame jacketing, little additional ductility, if any, could be achieved with respect to that computed for the original building. Success of the retrofitting operation for these cases relies mainly on the additional strength provided to the building. On the other hand, for strengthening schemes that make use of reinforced concrete infill walls, an increase in available ductility and strength with respect to the original buildings can be realized.
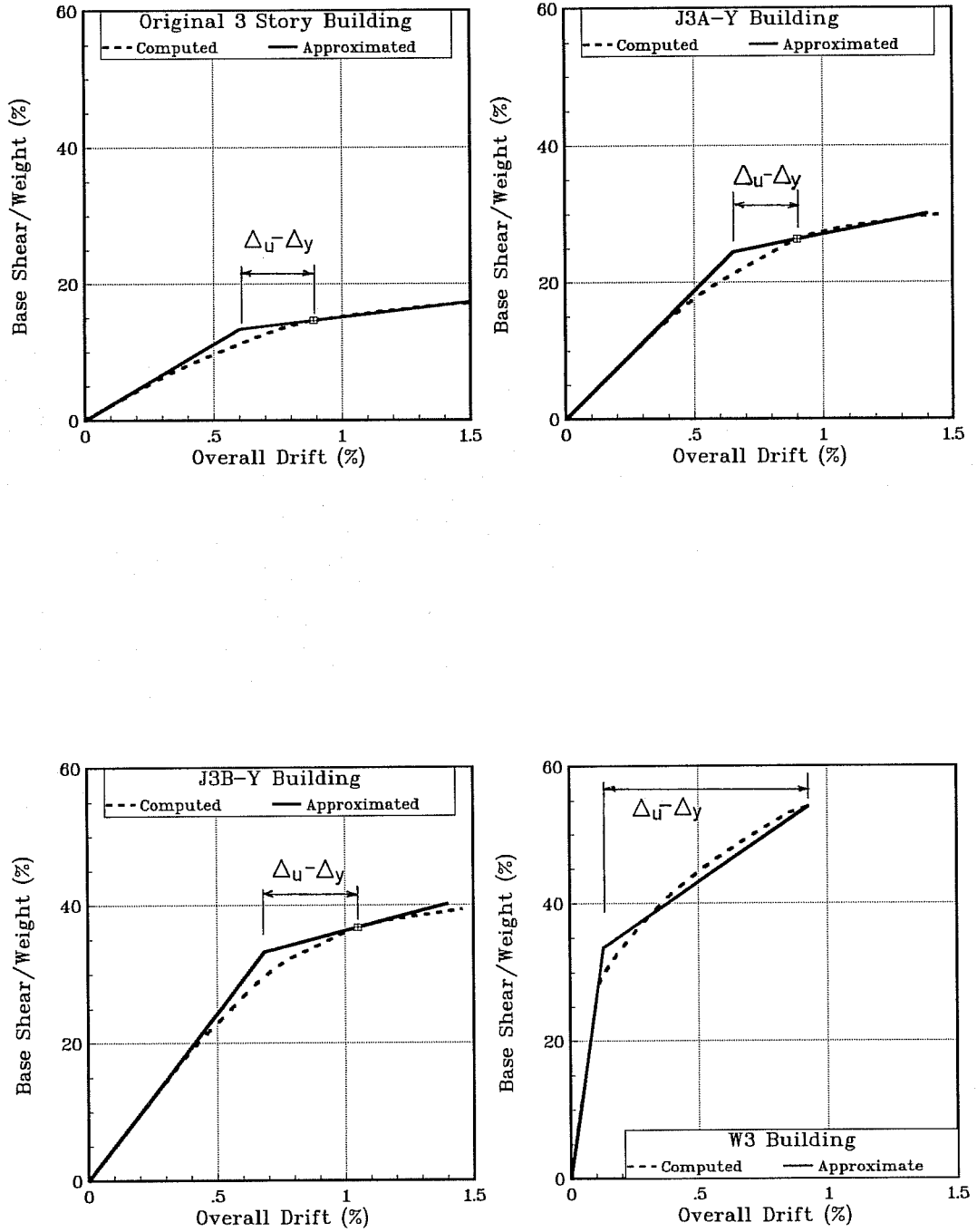
Figure 6.1 Approximate C-Δ Curves - Three-Story Buildings
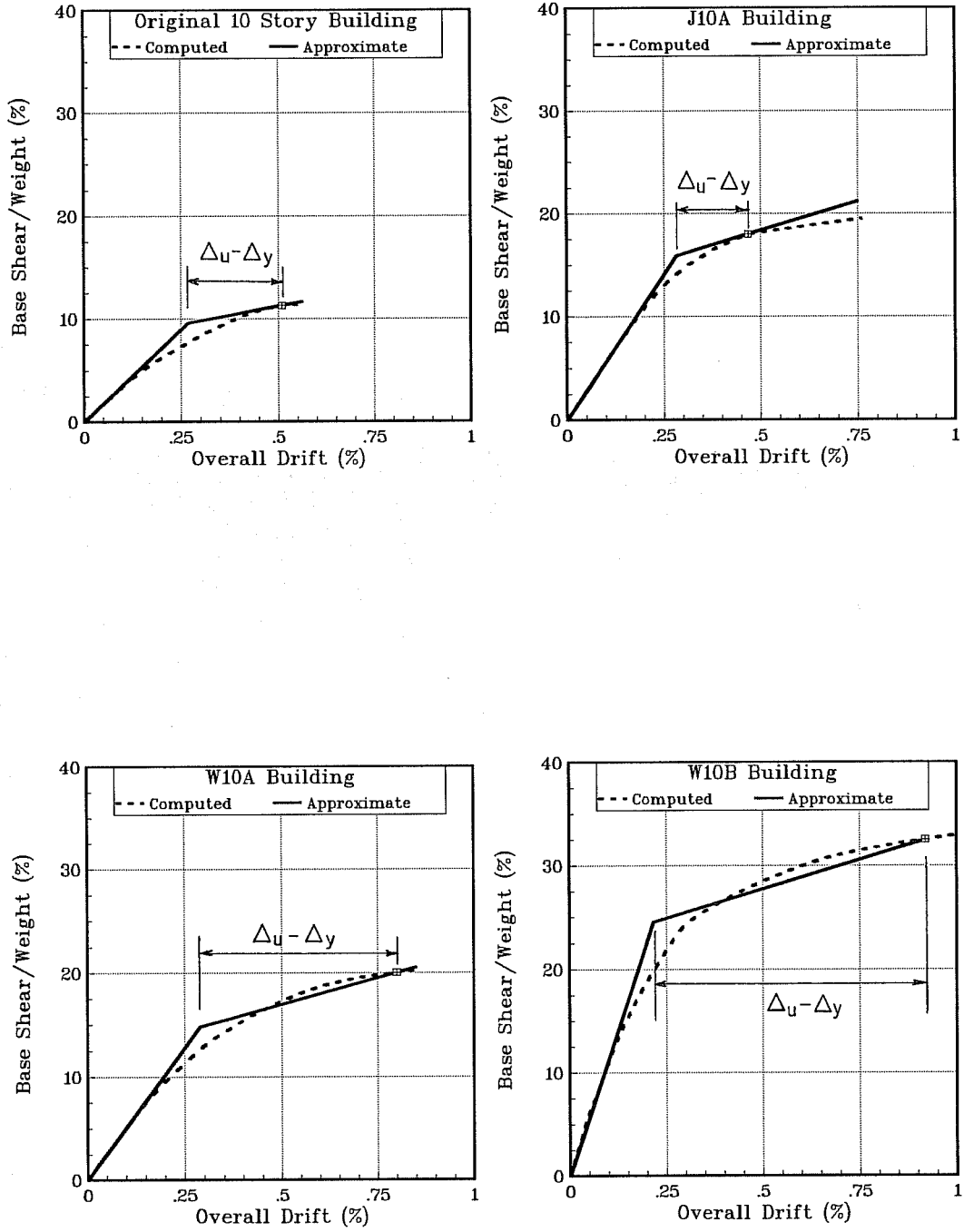
Figure 6.2 Approximate C-Δ Curves - Ten-Story Buildings

Table 6.1 Idealized Building Properties

Building	Δ_y (%)	C_y (%)	C_{eff} (%)	μ_a
3 Story Original	0.60	13.4	15.7	1.48
J3A-Y	0.65	24.4	30.1	1.38
J3B-Y	0.68	33.2	41.0	1.54
J3C-Y	0.53	36.0	43.0	1.78
J3A-X	0.65	28.4	34.6	1.33
J3B-X	0.67	39.2	47.8	1.39
J3C-X	0.48	43.4	51.0	1.64
W3*	0.13	33.6	45.0	7.11
10 Story Original	0.27	9.6	12.0	1.90
J10A	0.28	15.9	19.9	1.66
W10A	0.29	14.8	20.6	2.76
WJ10	0.25	20.5	27.7	2.53
W10B*	0.22	24.5	35.5	4.25

* The slope of the yield branch was assumed to be 10% of the elastic stiffness

The displacement ductility spectra shown in Fig. 5.26 were used to obtain ductility requirements (μ_r) for each buildings using its fundamental period (Tables 5.9 and 5.10) and effective yield strength (Table 6.1). A comparison between available and required displacement ductility ratios for the buildings, for the four records considered in this study, is presented in Table 6.2. Ductility ratios, μ_a/μ_r, smaller than one indicate that a splice failure of all first-story unstrengthened columns should occur. Cases in which splice failures were predicted for the unstrengthened columns $(\mu_a/\mu_r < 1)$ but were not observed in the dynamic analysis of the building are indicated by a pound symbol (#). Similarly, cases indicated with a star symbol (*) correspond to situations in which no splice failures were predicted $(\mu_a/\mu_r > 1)$ but splice

failures were detected in the dynamic analysis.

Table 6.2 Available Ductility vs. Required Ductility Ratios

Building	μ_a	Available Ductility/Required Ductility (μ_a/μ_r)			
		El Centro	Viña del Mar	Scaled El Centro	SCT
3 Story Original	1.48	0.91	0.53	0.49	0.10
J3A-Y	1.38	0.76	0.72	0.52	1.17
J3B-Y	1.54	0.96	0.72	0.63	1.66
J3C-Y	1.78	1.03*	0.72	0.65	1.40
J3A-X	1.33	0.72	0.68	0.54	1.25
J3B-X	1.39	0.94	0.67	0.61	1.38
J3C-X	1.64	0.90	0.61	0.61	2.19
W3	7.11	3.13	6.08	1.67	8.78
10 Story Original	1.90	1.16	0.88[#]	0.59	0.23
J10A	1.66	1.50	0.88[#]	1.11*	0.17
W10A	2.76	2.56	1.35	1.86	0.27
WJ10	2.53	1.66	1.43	1.28	2.30
W10B	4.25	2.23	1.91	1.55	3.54

The results presented in the previous table indicate that, in general, the global behavior of the strengthened and original buildings can be predicted using the procedure outlined previously. Ductility ratios presented in Table 6.2 are indicators of the potential behavior of the buildings, and therefore, it is the author's opinion that buildings where $0.80 < \mu_a/\mu_r < 1.25$ should be regarded as borderline cases where no conclusive evidence of good or bad behavior can be inferred without a more refined analysis.

A usual concern when strengthening an existing building located in a seismic zone in which the pseudo acceleration spectrum shows increasing lateral force demands as the period

of the building decreases, is that shortening of the building period due to the retrofitting operation may lead to excessive ductility demands. The results indicated in Table 6.2 show that the gain in strength tends to compensate for the additional lateral force demands that result from stiffening the building. However, it should be pointed out that additional lateral force demands in the retrofitted building may lead to major modification of the foundation system, which is a problem that is outside the scope of this study, and is likely to be particular for a given building.

6.3 Simplified Model

A simplified model to explain the behavior of the buildings analyzed is presented in this section. First, the case of a single degree of freedom structure is discussed, followed by an extension to multiple degree of freedom systems.

6.3.1. Single Degree of Freedom System

In the discussion that follows, the subscript "o" will be used to identify properties of the original building or structure to be strengthened. Properties of the strengthened structure will be identified by the subscript "s".

Figure 6.3a shows a simplified model of a building to be strengthened, composed of two columns, A and B, which represent exterior and interior frames of the building. Lets assume that the load deflection curve for the building, when laterally loaded, has been previously determined and approximated with a bilinear curve, as shown in Fig. 6.4. Let K_o, R_{yo} and δ_{yo}, be the stiffness, strength, and lateral displacement at yield, and δ_{mo} be the maximum lateral displacement that the structure can be subjected to without endangering its overall stability (splice failure coordinates for the buildings analyzed). If the original structure

is going to be retrofitted by strengthening its exterior frames (column A), as shown in Fig. 6.3b, what characteristics of strength, stiffness, and ductility, represented by the load-deflection curve shown in Fig 6.4, should the strengthened structure be given to withstand a major earthquake without exceeding the capacity of the strengthened frames and the displacement level that will produce unacceptable behavior in its unstrengthened portions (column B in Fig 6.3b)?

The ability of a structure to survive a major earthquake depends primarily on three factors:

- Strength (R),

- Available ductility (μ_a), and

- Dynamic characteristics of the structure (natural period and damping)

As was shown in the previous section, the available ductility of the strengthened buildings was limited by the drift at which a splice failure occurred in all first-story unstrengthened columns of the buildings. In strengthening schemes that made use of frame jacketing this event occurred at about the same drift level computed for the original structure, while the generalized splice failure was delayed to higher drifts for strengthening schemes that made use of concrete infill walls. To keep the following discussion simple (and on the conservative side), it will be assumed from here on that the maximum displacement (drift) the strengthened structure can be subjected to is the same as that computed for the original structure.

The available ductility of the strengthened structure can then be expressed as:

$$\mu_a = \frac{\delta_{mo}}{\delta_{ys}}$$ (6.1)

and,

a) Original Structure   b) Strengthened Structure
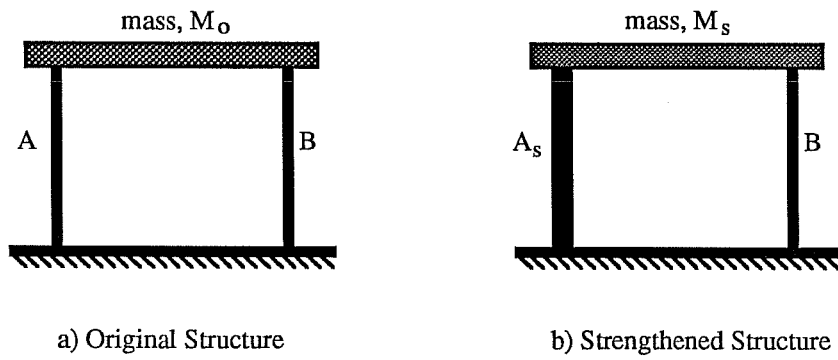
Figure 6.3 Idealized Single Degree of Freedom Structures
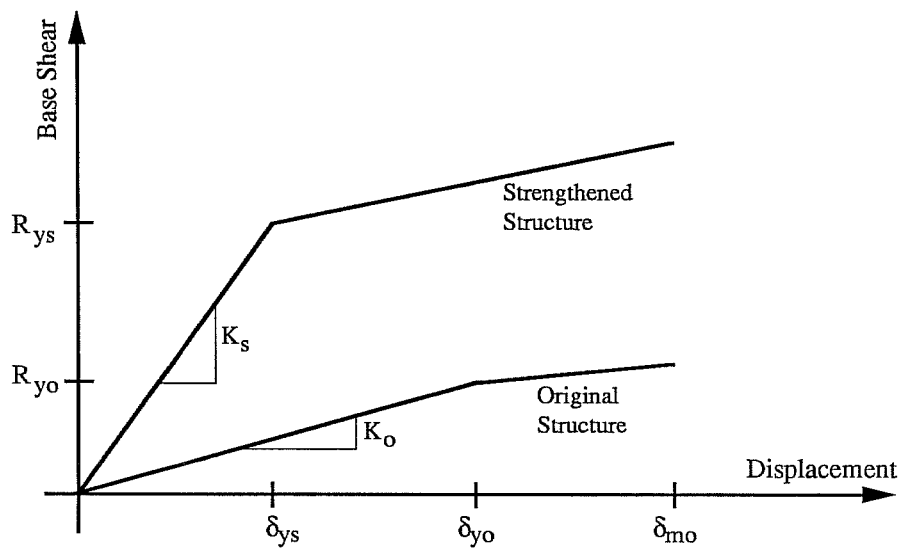
Figure 6.4 Load-Deflection Curves for Idealized SDOF System

$$\delta_{mo} = \mu_o \delta_{yo} = \mu_o \frac{R_{yo}}{K_o}$$

$$\delta_{ys} = \frac{R_{ys}}{K_s} \tag{6.2}$$

Expressing the stiffness in terms of the mass and natural frequency of the building gives,

$$K_o = M_o \omega_o^2 = 4\pi^2 \frac{W_o}{gT_o^2}$$

$$K_s = M_s \omega_s^2 = 4\pi^2 \frac{W_s}{gT_s^2} \tag{6.3}$$

Finally, introducing Eq. 6.3 and 6.2 into Eq. 6.1 leads to

$$\mu_a = \mu_o \frac{C_{yo}T_o^2}{C_{ys}T_s^2} \tag{6.4}$$

Equation 6.4 shows that the maximum ductility which can be achieved in the strengthened building can be expressed as a function of yield strength and natural period of both, the original and strengthened structures, and the ductility of the original structure. It should be noted that it was assumed that the strengthened portions of the structure would be able to develop the ductility given by Eq. 6.4, and the mode of failure of the unstrengthened frames of the structure will not be changed due to the retrofitting operation.

An example of the application of Eq. 6.4 is presented next. Let's assume that the original structure to be strengthened (Fig 6.3a) has a natural period of 1.28 sec, a yield strength, $C_{yo} = 0.14$, and a ductility, $\mu_o = 1.5$. Several strengthening schemes having a yield strength, $C_{ys} = 0.40$, but with different periods are proposed, and it is desired to know which ones would be able to survive the Scaled El Centro earthquake. The dotted line in Fig. 6.5

indicates ductility requirements for the Scaled El Centro record for a single degree of freedom system that has a yield strength equal to 40% of its weight. Equation 6.4 has been plotted in the same figure and is indicated by the solid line. It can be concluded that any strengthening scheme having a period smaller than approximately 0.40 sec would be able to survive the Scaled El Centro earthquake, provided that the structure can develop the ductility required by the earthquake (dotted line), while failure of the unstrengthened portions of the structure is predicted for strengthening schemes with periods longer than 0.40 sec.

Curves similar to those shown in Fig. 6.5 can be obtained for different yield levels of the strengthened structure. For each set of curves a critical period, T_{cr}, beyond which μ_a is smaller than μ_r, can be identified. The curve connecting the points (T_{cr}, μ_{cr}) defines an upper limit for the period of the strengthened structure in order to prevent undesirable behavior in its unstrengthened portions. A plot of such a curve is presented in Fig. 6.6. A strengthened structure having a natural period to the right of the thick solid line in Fig. 6.6 will not be successful because of failure of unstrengthened portions of the structure, regardless of how much strength is added to the structure. On the other hand, structures located to the left of the solid line can be successful if the ductility provided is greater than that required by the earthquake.

From the previous discussion it can be concluded that the most important parameter controlling success of the retrofitting operation is the natural period of the strengthened structure, and therefore the additional stiffness provided. Equation 6.4 can be regarded as a stiffness requirement that the strengthened structure must meet in order to prevent the unstrengthened portions of the retrofitted structure from experiencing undesired and uncertain inelastic behavior. Once that this stiffness requirement has been met, factors such as required
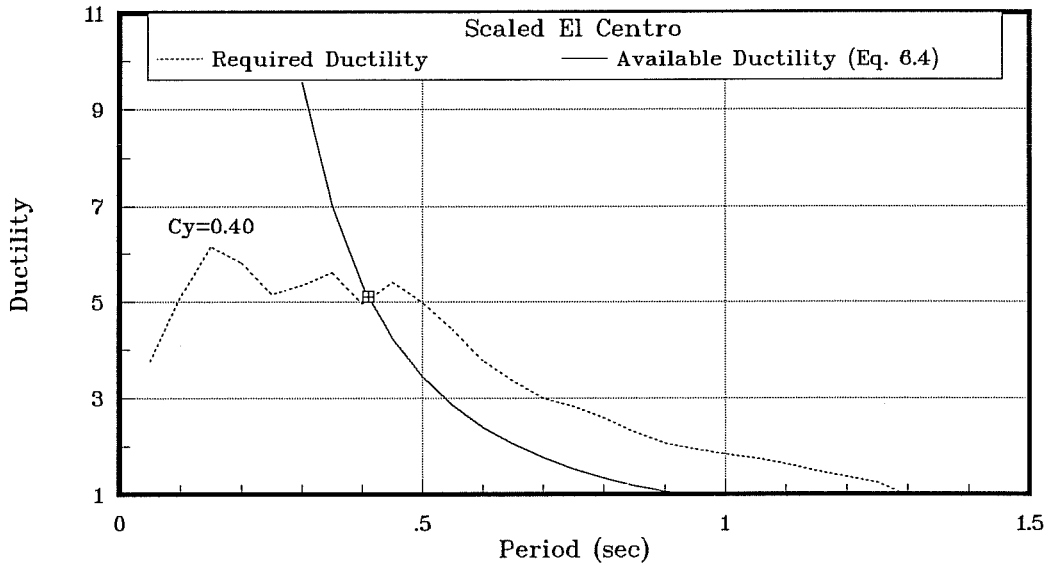
Figure 6.5   Required vs Available Ductility
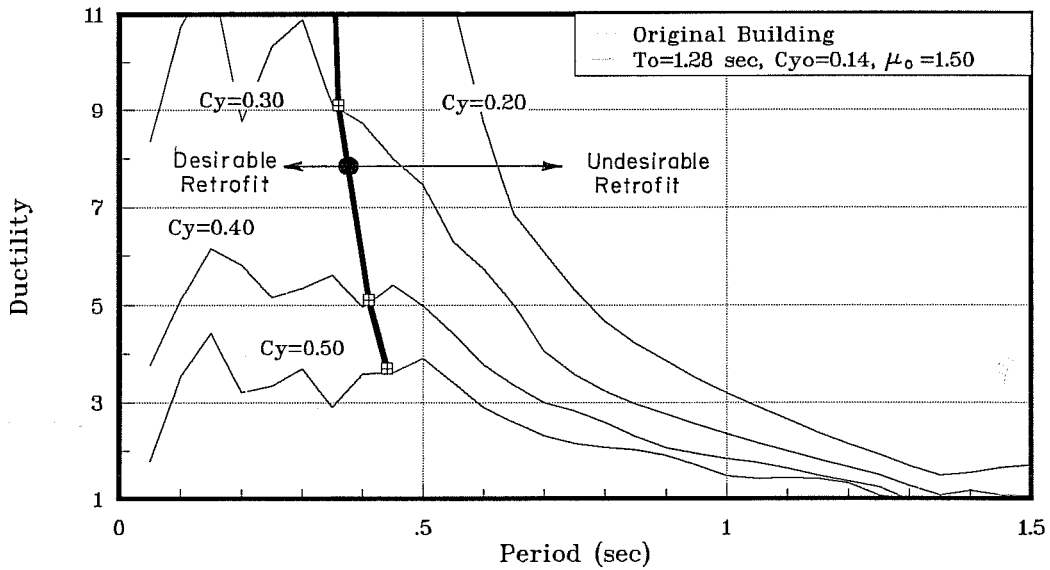
Figure 6.6   Limiting Periods — Scaled El Centro

strength and ductility should be addressed.

6.3.2 Extension to Multiple Degree of Freedom Systems

Figure 6.7 shows idealized models of the original building and the strengthened building. Again, the retrofitting operation considers modifications to some of the frames of the original building. The strengthened frames of the retrofitted building are represented by column A_s in Fig. 6.7b, while column B, in the same figure, represents the frames that have not been modified. The base shear-roof displacement curves for both structures are assumed to be like those shown in Figure 6.4, and have been obtained by applying a uniform lateral load distribution to the buildings. The deflected shape of the buildings under this load is represented by the vectors $\{\phi_o\}$ and $\{\phi_s\}$, normalized with respect to the roof displacement.

An estimate of the natural frequency of the original building can be obtained using the Rayleigh quotient,

$$\omega_o^2 = \frac{\sum f_{io} \delta_{io}}{\sum m_{io} \delta_{io}^2} \tag{6.5}$$

Assuming a regular mass distribution along the height of the building, and remembering that f_i was assumed to be constant, multiplying the numerator and denominator of Eq. 6.5 by the number of stories in the building, and normalizing the displacements with respect to the roof displacement leads to,

$$\omega_o^2 = \frac{V_{yo}}{M_o \delta_{yo}} \frac{\sum \phi_{io}}{\sum \phi_{io}^2} \tag{6.6}$$

where M_o is the total mass of the building, V_{yo} the base shear at yield, and δ_{yo} the roof
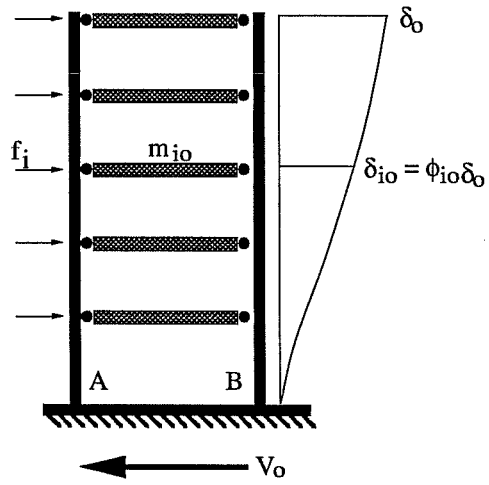
a) Original Structure
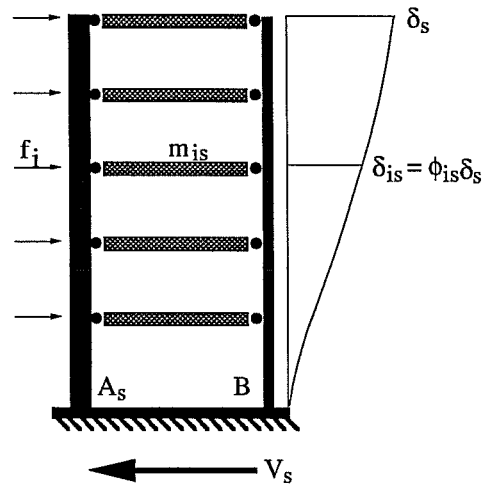
b) Strengthened Structure

Figure 6.7 Idealized Multiple Degree of Freedom Structures

displacement at yield. If μ_o is the ductility ratio for the original structure, the maximum roof displacement will again be given by Eq. 6.2. Combining Eq 6.2 with Eq. 6.6, and introducing as before the seismic coefficient at yield, C_{yo}, gives

$$\delta_{mo} = \mu_o C_{yo} T_o^2 \frac{g}{4\pi^2} \frac{\sum \phi_{io}}{\sum \phi_{io}^2} \tag{6.7}$$

In a similar manner, the displacement at yield of the strengthened structure is

$$\delta_{ys} = C_{ys} T_s^2 \frac{g}{4\pi^2} \frac{\sum \phi_{is}}{\sum \phi_{is}^2} \tag{6.8}$$

and, therefore, the maximum available ductility in the strengthened structure is

$$\mu_a = \mu_o \frac{C_{yo} T_o^2 \sum \phi_{io} \sum \phi_{is}^2}{C_{ys} T_s^2 \sum \phi_{io}^2 \sum \phi_{is}} \tag{6.9}$$

The terms involving the summation of the deflected shapes of the original and strengthened structures were computed to be very similar when frame jacketing schemes were considered, and therefore they may be omitted from Eq. 6.9. For strengthening schemes that considered infill walls, neglecting this term overestimated the available ductility given by Eq. 6.9 by approximately 10%. However, since failure of the unstrengthened frames of the buildings was delayed to higher drift levels, the summations in Eq. 6.9 can be safely neglected. It may also be noted that the use of the first mode shape of the buildings in Eq. 6.9 will lead to very similar results.

It is important to emphasize again the assumptions made for deriving Eq. 6.9, which are:

- The mode of failure of the unstrengthened frames of the original structure will not be altered due to the retrofitting operation.

- The drift level at which failure of the unstrengthened frames occurs is the same for the retrofitted and original structure.

- The strengthened frames of the retrofitted structure can develop the ductility given by Eq. 6.9. If this is not the case, the available ductility of the retrofitted structure will be controlled by the strengthened frames.

6.3.3 Application to the Buildings Analyzed

The results obtained in Chapter 5 indicated that, in general, frame jacketing schemes were not successful in limiting inelastic demands in the unstrengthened portions of the buildings. In the previous section, it was shown that the retrofitted building must satisfy a stiffness requirement when the building to be strengthened has limited ductility. An explanation of the success or failure of the strengthening schemes considered in this study, in terms of this stiffness requirement, is presented next.

6.3.3.1 Three-Story Buildings

Figures 6.8 and 6.9 show displacement ductility spectra for the Viña del Mar and Scaled El Centro record, respectively. These spectra were computed considering a mass modal ratio of 0.83 (average value of frame jacketing schemes) in order to allow direct access of information from the figures by entering into the plot with the yield strength, C_y, of a MDOF system. Maximum allowable periods for the retrofitted structure, considering original building ductilities, μ_o, of 1.0, 1.5, and 2.0, are indicated in the same figures by thick solid lines.
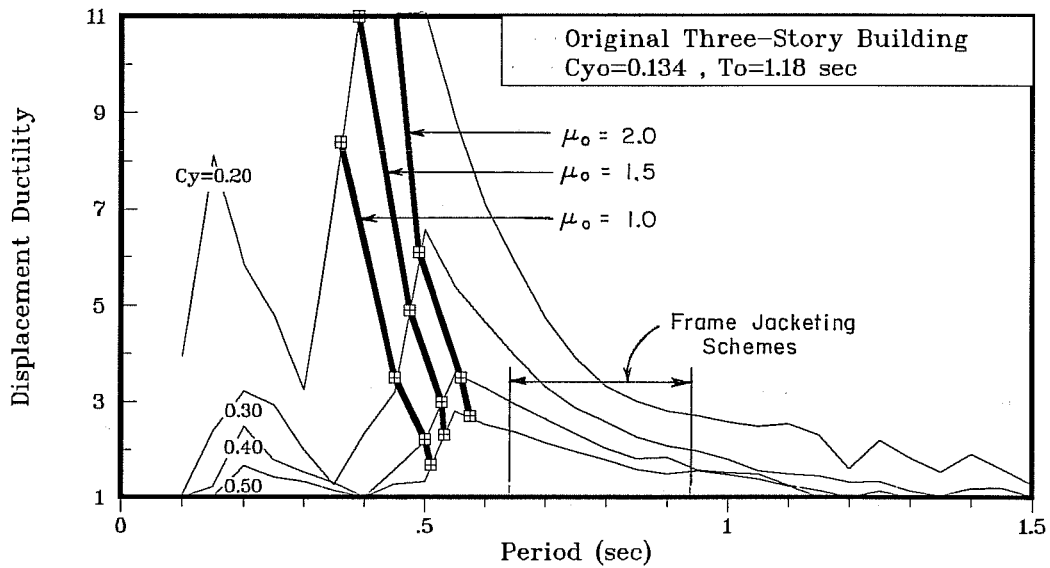
Figure 6.8   Limiting Periods for the Three–Story Buildings
Vina del Mar Record
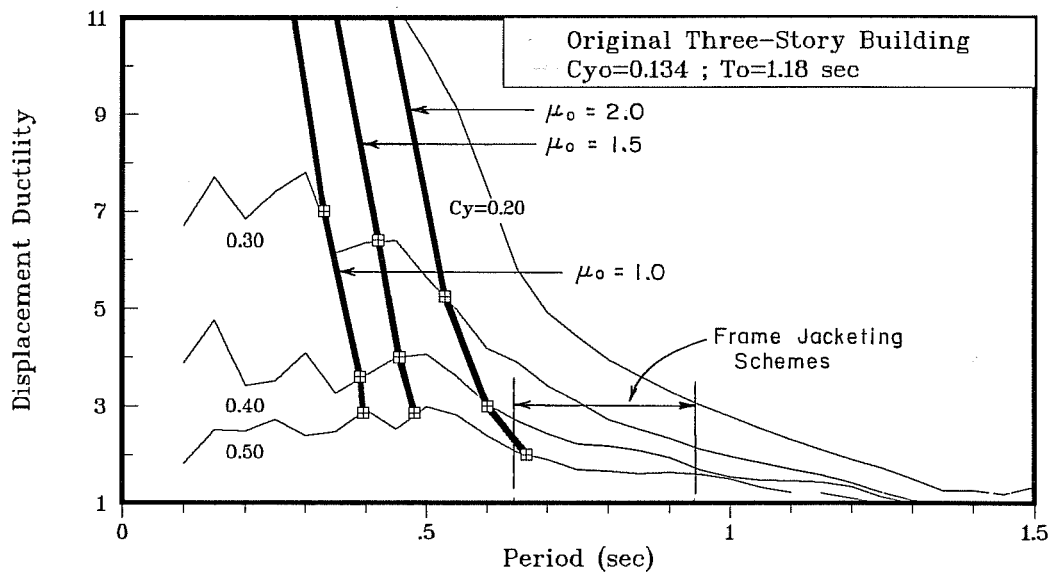
Figure 6.9   Limiting Periods for the Three–Story Buildings
Scaled El Centro Record

Considering that the fundamental period of strengthening schemes that contemplated frame jacketing ranged from 0.63 to 0.93 sec (Table 5.9), and that the displacement ductility of the original building was estimated to be about 1.5, none of the jacketing schemes meets the maximum period requirements indicated in Figs. 6.8 and 6.9, and therefore, general splice failure of all first-story unstrengthened columns can be predicted, as was observed in the dynamic analysis of the buildings.

Success of the retrofitting operation could have been achieved in two ways: by designing a strengthened structure with a period smaller than approximately 0.50 sec, or by increasing the ductility of the unstrengthened frames of the building. The success of the first alternative was demonstrated by strengthening scheme W3, which has a fundamental period of 0.35 sec, and in which no splice failures were detected for any of the records considered. Increasing the ductility of the unstrengthened frames, although possible, may be less cost-efficient and less practical from a construction point of view, because the retrofitting operation would need to be extended to include at least all the first-story columns of the building.

6.3.3.2 Ten-Story Buildings

Maximum allowable periods for original building ductilities, μ_o, of 1.0, 1.5 and 2.0 for the Scaled El Centro and SCT records are presented in Figs. 6.10 and 6.11, respectively. For a ductility factor $\mu_o = 2.0$, no intercepts were found for the Scaled El Centro record for yield levels of 0.10 to 0.40, meaning that the available ductility computed using Eq. 6.4 was always greater than that required. Displacement ductility requirements in these figures were computed assuming a mass modal ratio for the first mode of 0.71, which was an average value for strengthening schemes that considered addition of reinforced concrete infill walls. Because
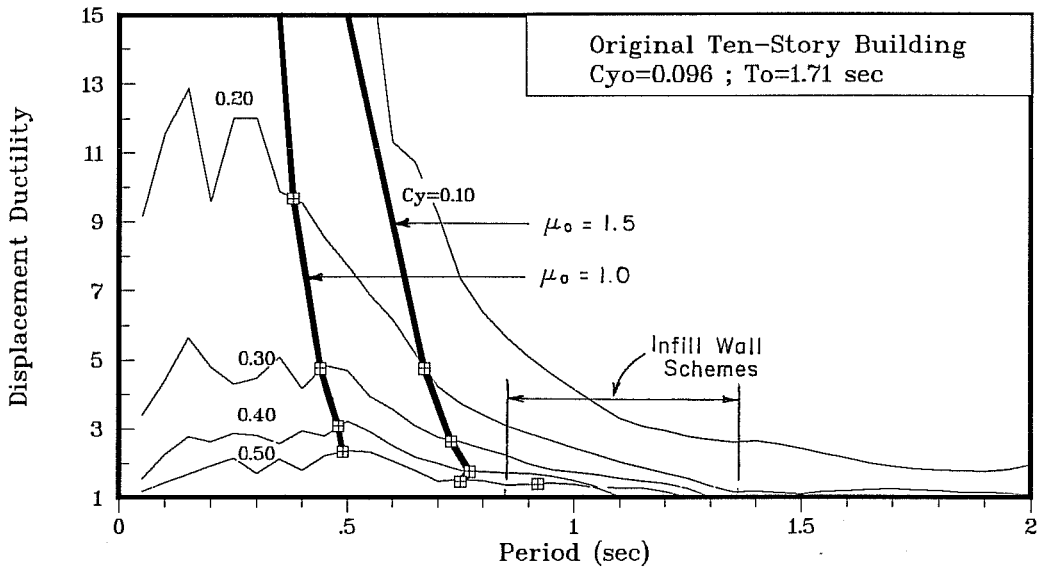
Figure 6.10 Limiting Periods for the Ten–Story Buildings
Scaled El Centro Record
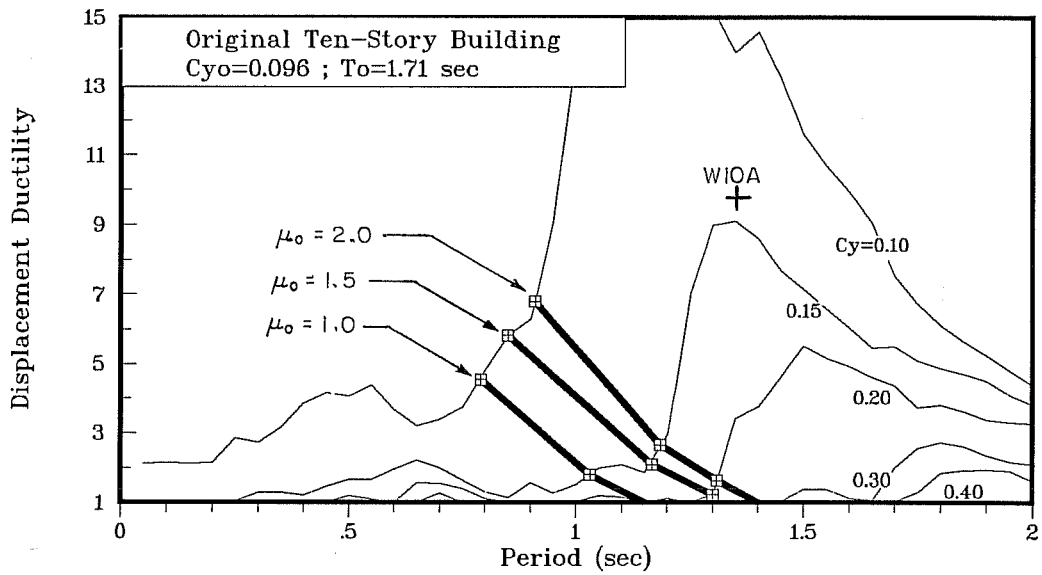
Figure 6.11 Limiting Periods for the Ten–Story Buildings
SCT Record

the ductility of the original ten-story building was estimated to be approximately 1.90, and considering that the period of the strengthened buildings W10B, WJ10, and W10A ranged from 0.83 to 1.35 sec, all these schemes meet the stiffness requirement specified by Eq. 6.4, and therefore, they should be successful in limiting inelastic demands in the unstrengthened frames for a ground motion like the Scaled El Centro record, as was observed in the dynamic analysis. Figure 6.11 indicates that if the buildings are subjected to the SCT record, only strengthening schemes W10B and WJ10 would prevent a splice failure of all first-story columns of the unstrengthened frames, while strengthening scheme W10A would not. High ductility requirements predicted for W10A indicate that not only the capacity of the unstrengthened frames will be exceeded, but collapse of the whole building is very likely.

6.4 Design Implications

The discussion presented in the previous sections showed that, for the buildings considered in this study, non-linear dynamic analysis of the buildings could have been obviated, and enough information can be obtained from a non-linear analysis under static lateral loads. From the later type of analysis, a good estimate of the strength, available ductility, and maximum lateral displacement that the building (original or strengthened) can be subjected to without endangering its overall stability can easily be obtained. The use of these data in combination with Eq. 6.4 and the inelastic response spectra for a given earthquake motion will provide a good estimation of the performance of the retrofitted building when subjected to the earthquake being investigated. For design purposes however, development of simpler procedures is advised.

Ductility of the original buildings was estimated to be 1.5 and 1.9 for the low and

medium-rise buildings, respectively. These approximately coincide with the response modification factor (R=2) proposed in the ATC 22 and ATC 3-06 documents for ordinary moment-resisting frame buildings. Several elastic analysis computer programs (ETABS, SAP, etc.) are available to estimate the natural period and lateral strength of the building. Finally, an inelastic design response spectrum can be used, instead of a series of earthquake records, to evaluate the performance of the building.

Current documents for evaluating the seismic performance of existing buildings recommend the use of a median response spectra, based on the 50th percentile amplification factors of the ground motion parameters (peak ground acceleration, velocity and displacement) proposed by Newmark et al. [2]. For this reason the response spectra included in ATC-14 [28] and ATC-22 were reduced with respect to the ATC 3-06 [29] design spectra for new buildings. Although this procedure may be justified when evaluating the seismic performance of an existing building, it is the author's opinion that if, as a result of the evaluation process, a decision is made to strengthen the building, it is advisable to add a measure of conservatism to the design of the retrofitted building at little extra cost by performing the design using the response spectra proposed for new buildings. For this reason, in the discussion that follows, the response spectrum proposed in ATC 3-06 is used.

Figure 6.12 shows the pseudo acceleration response spectra proposed by ATC 3-06 considering stiff soil conditions (S=1.2), 2% viscous damping, and ductility factors of 1, 2, 3, and 4. The original three-story building, which has a period of 1.18 sec and a yield strength of 13.4%, would be required to develop a ductility of about 3.9, which is greater than the available ductility of the structure. The spectral displacement predicted for this building is indicated in Fig. 6.13 by the boxcross symbol. Spectral displacements associated with ductility

factors, μ_o, of 1.0, 1.5, and 2.0 are indicated in the same figure, and were obtained by simply dividing the displacement corresponding to 1.18 sec by the ductility factor obtained from Fig 6.12 (μ_r=3.9) and multiplying this value by the appropriate ductility factor (1, 1.5 and 2). The intercepts of these spectral displacements with the displacement spectrum defines the maximum period that the strengthened structure can have in order to limit inelastic action in the unstrengthened frames of the building to an acceptable level (reflected by the original building ductility, μ_o). The vertical lines in Fig 6.12 represent the minimum stiffness (or maximum period) that should be provided in the retrofitted structure. Once this requirement has been met, a decision regarding the strength and ductility to be provided to the retrofitted building can be made. It is of interest to note how well the maximum periods computed using the procedure explained previously compare with those shown Fig. 6.9.

Maximum periods for the retrofitted ten-story buildings computed using the procedure outlined previously, are presented in Figs. 6.14 and 6.15. For original building ductilities of 1.0 and 1.5, they compare very well with those obtained in Fig. 6.10. For an original building ductility of 2.0, the maximum period obtained from Fig. 6.15 is a very conservative estimate. This can be attributed to the fact that the response spectra proposed by ATC 3-06 has an extra factor of safety built in for long period structures (the ordinate of design response spectra at 2.0 sec is amplified by a factor of 1.5 [29]).

Other design implications follow from the previous discussion:

- Designing the strengthened frames of a structure to be able to carry all design seismic forces does not guarantee success of the retrofitting operation.

- The success of the retrofitting operation is not directly related to the lateral force capacity of the strengthened structure, but to the ability of the retrofitted structure

to limit displacements that the building will experience when subjected to a severe ground motion.

- Stiffness requirements for a stiff building of limited ductility are likely to be very difficult to meet, therefore, the retrofitting operation in this case needs to be focused on improving the ductility rather than the strength of most of the existing structural elements.
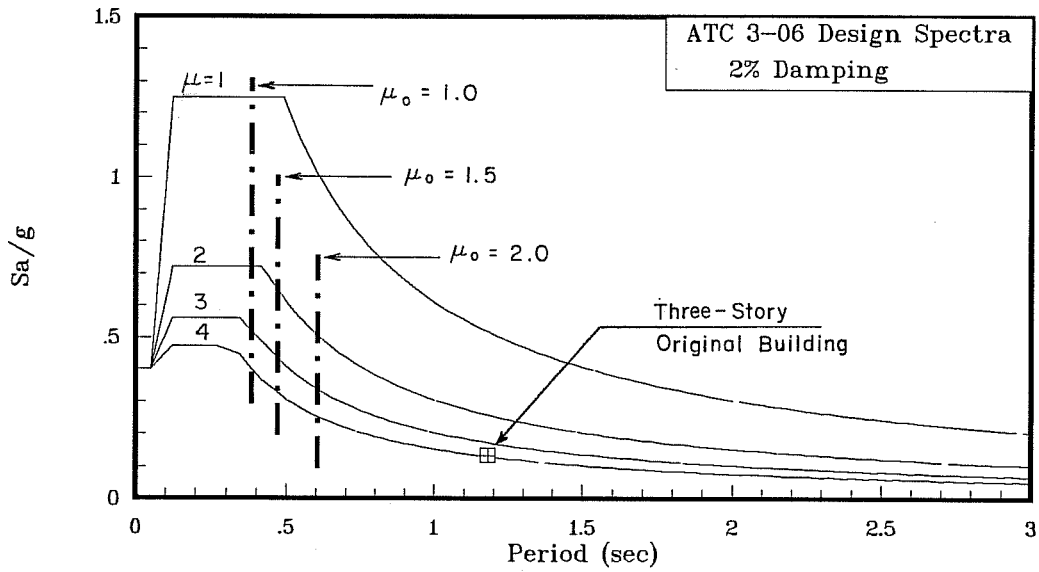
Figure 6.12   Limiting Periods for the Three-Story Buildings
Acceleration Design Spectra
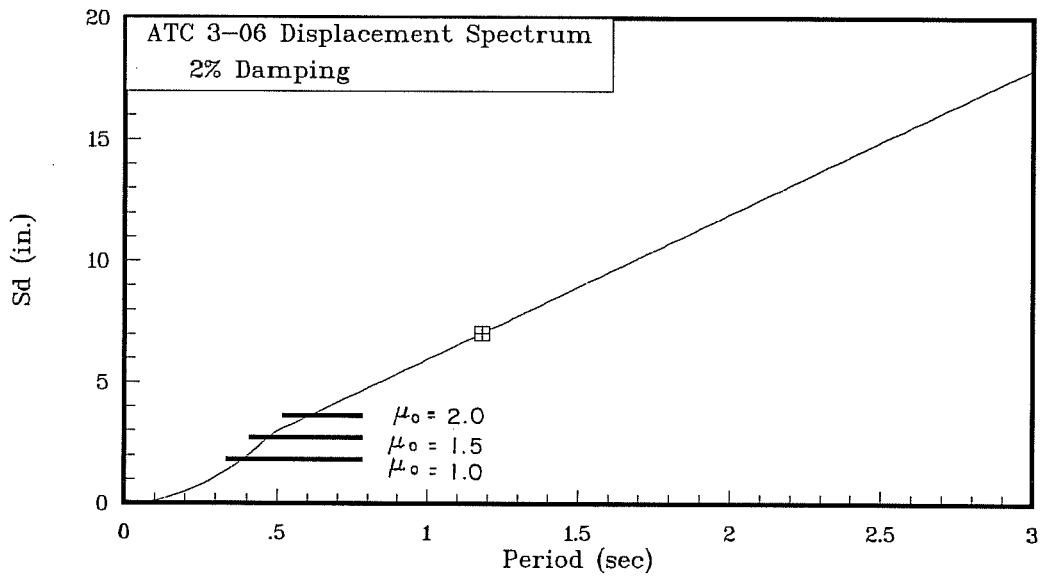
Figure 6.13   Limiting Periods for the Three-Story Buildings
Displacement Design Spectrum
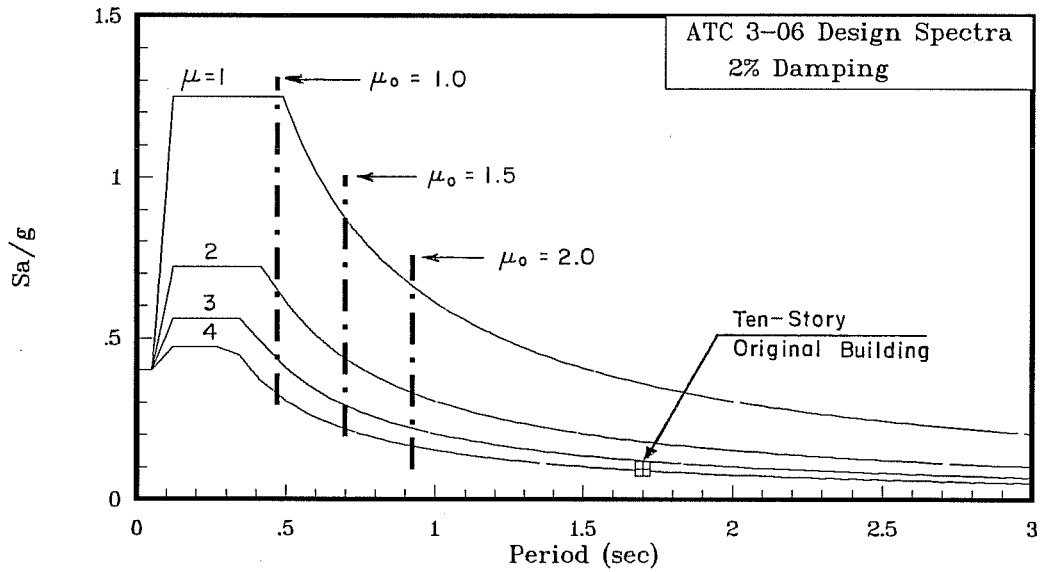
Figure 6.14   Limiting Periods for the Ten–Story Buildings
Acceleration Design Spectra
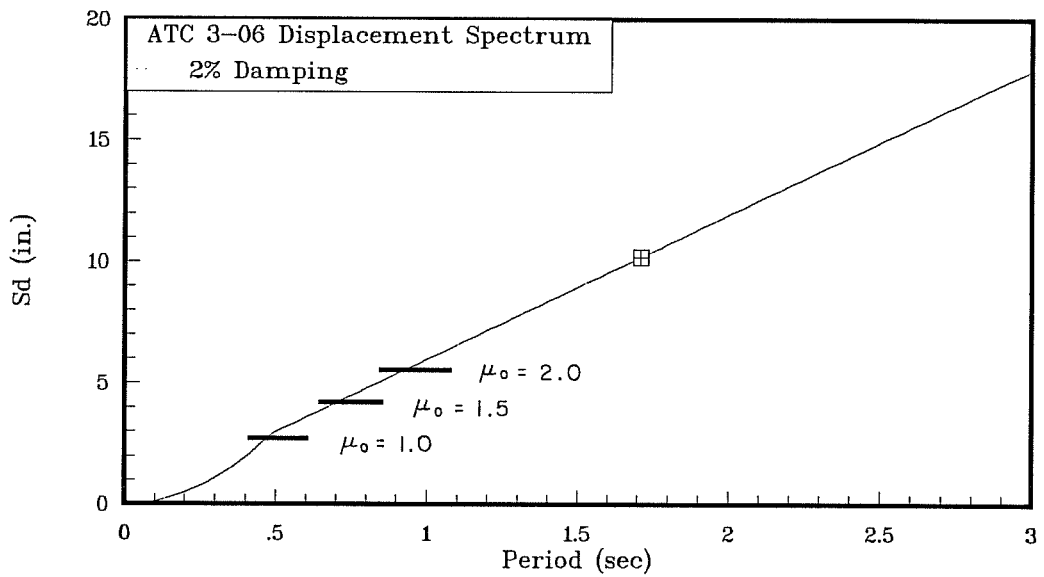
Figure 6.15   Limiting Periods for the Ten–Story Buildings
Displacement Design Spectrum

CHAPTER 7

SUMMARY AND CONCLUSIONS

7.1 Summary

An analytical investigation was performed to evaluate the effectiveness of different strengthening schemes for existing reinforced concrete moment-resisting frame buildings.

A low-rise and a medium-rise building representative of typical American construction and design practice in the 1950's or 60's were analyzed. Evaluation of their main structural properties revealed that the buildings had inadequate lateral strength and lack of ductile detailing. Wide tie spacing in columns and beams, non-continuous beam bottom reinforcement through the joints, lack of confinement reinforcement in potential plastic hinge zones, absence of ties in the beam-column connections, and short compression splices unable to develop yielding of column longitudinal reinforcement were identified as the primary problems in the buildings.

Strengthening schemes that considered reinforced concrete frame jacketing (jacketing of beams and columns) of exterior frames of the buildings, or addition of reinforced concrete infill walls were considered to improve the lateral strength and/or ductility of the original buildings.

An analytical model was used to simulate the non-linear response of reinforced concrete structures subjected to arbitrary ground motions or static lateral loads. Special features considered in the analytical model included a joint element to consider the flexibility and stiffness degradation of beam-column connections subjected to reversed cyclic loads, and an hysteresis model to account for pinching of the hysteresis loops of reinforced concrete

197

members. For columns that featured a short compression splice, or beams with embedded reinforcement, special hysteresis rules were implemented to model the reduction in flexural capacity of the section after the peak moment was reached. The parameters controlling energy dissipation during each hysteresis cycle, as well as the joint element properties, were calibrated using experimental results from tests on beam-column connections at the University of Texas at Austin.

Static analyses for monotonic lateral loads were performed to estimate the lateral strength and ductility of the original and strengthened buildings. In order to evaluate the response of the buildings to severe ground motions, four earthquake records were considered. Three of the records were recorded at sites with stiff soil conditions; the fourth one represented an extreme earthquake recorded on soft soil. The dynamic response of the buildings was evaluated in terms of drift levels, ductility demands in the strengthened frames of the buildings, and damage to the unstrengthened frames of the retrofitted structures.

The effect of the main parameters defining the analytical model on the dynamic response of the structure was evaluated. These main parameters included the amount of viscous damping, pinching of the hysteresis loops, rate of deterioration of the splice region in columns after peak resistance is reached, and the effect of joint flexibility.

7.2 Conclusions

The main objective of this study was to extrapolate test results of different strengthening techniques, conducted on subassemblages representing critical zones of a building to complete structural systems. The following are the most important conclusions obtained from this study.

a) A methodology for retrofitting existing buildings with low lateral strength and/or ductility was developed. Although the mode of failure for the existing hypothetical buildings and the retrofitting schemes considered in this study represent a limited sample, the proposed methodology can be applied to retrofit a wide variety of existing buildings with different structural deficiencies than those examined here.

b) Test results conducted on subassemblages, that typically show considerable gain in strength and ductility of the test specimen, may not be necessarily extrapolated to the case of strengthening existing buildings with limited ductility. The available ductility of the retrofitted structure is likely to be limited by the deformation capacity of the unstrengthened frames, rather than by the ductility provided in the strengthened frames.

c) The most important parameter for guaranteeing success of the strengthening operation on an existing reinforced concrete moment-resisting frame building with limited ductility, in which only some of the frames are going to be strengthened, is the additional stiffness provided to the strengthened structure. Therefore, the design process should be oriented toward limiting displacements of the retrofitted structure rather than providing strength.

d) For the hypothetical buildings analyzed, an estimate of the maximum ductility (or maximum displacement) that could be achieved in the strengthened building could be obtained as a function of the lateral strength, fundamental period and ductility

of the building to be strengthened, and the strength and fundamental period of the retrofitted structure.

e) Strengthening with reinforced concrete infill walls proved to be a very effective retrofitting alternative for all the ground motions considered in this study. This can be attributed to two observed facts:

- The use of infill walls delayed splice failure of the unstrengthened columns to higher drift levels, and

- Early yielding of the walls at the base allowed for energy dissipation at drift levels associated with nearly elastic behavior of the unstrengthened frames.

High shear stresses computed at the base of the walls pointed out the need for careful detailing of elements to guarantee the success of the retrofitting operation.

f) Because energy dissipation in the strengthened frames takes place at drift levels similar to those producing undesired inelastic action in the unstrengthened frames, frame jacketing can be classified as a strength-reliant technique when used to strengthen an existing moment-resisting frame building with limited ductility. Frame jacketing schemes proved to be very effective for the low-rise building when subjected to a severe ground motion in soft soil conditions. However, for all the other records considered and for the medium rise building, the capacity of the spliced bars of all unstrengthened columns was exceeded. Consideration of soil/foundation flexibility will likely alter the demand on column splices at the base of the structure.

g) Strengthening schemes that consider an irregular distribution of stiffness along the height of the building can activate potential weak links in the structure that will not be activated when a regular distribution of stiffness is provided.

h) Reduction of the fundamental period for buildings located in seismic zones where the acceleration spectrum shows increasing lateral force demands as the period of the building decreases, did not lead to excessive ductility demands. This observation can be explained because the gain in lateral strength was offset by the additional lateral force demands that resulted from stiffening of the building.

Regarding the influence of the primary parameters defining the analytical model, the following was observed:

a) The amount of equivalent viscous damping, for a given building strength, proved to be the most influential parameter affecting the dynamic response of the buildings.

b) The effect of neglecting pinching of the hysteresis loops reduced the computed response of the buildings by approximately 10%.

c) The effect of considering joint flexibility did not change the computed response significantly with respect to the computed response for the usual rigid joint assumption. However, it provided valuable information regarding the maximum shear stress that the beam-column connections experienced.

7.3 Suggestions for Future Research

The study reported here satisfactorily met the proposed objectives within the scope of this research. However, further analytical and experimental research is recommended to complement the findings of this study.

- The buildings analyzed in this study had the potential to exhibit a brittle flexural failure mode associated with splice failure of the short compression splice in the unstrengthened columns. Ductility factors between 1.5 and 2.0 were estimated for the original buildings. Even smaller ductility factors can be anticipated for buildings failing in shear. This may pose even stricter stiffness requirements for the retrofit to be successful.

- Further analytical studies are needed to extrapolate test results of other strengthening techniques, such as the addition of braces or prestressed cables, to complete structural systems, and to validate the results obtained in this research.

- Torsional effects may be important to consider when strengthening only the exterior frames of a building. Unexpected eccentricities due to uneven mass distributions or construction errors may overload one of the exterior frames (or walls) resulting in excessive displacements due to torsion in plan. An analytical model that considers at least three degrees of freedom per floor plan is recommended to be developed.

- More experimental research is needed to assess the behavior of lightly-reinforced concrete elements. In particular, the effect of a splice failure on the axial load carrying capacity of the column after the splice has failed should be investigated. The behavior of beams with bottom reinforcement anchored in the joint region

also needs further research. The severity of the damage induced to the joint region

by pullout of the beam bottom reinforcement needs to be examined.

- Simple techniques to enhance the splice capacity of column bars are advisable to

be experimentally investigated.

REFERENCES

1   Newmark, N.M.,"A Method of Computation for Structural Dynamics," Transactions, ASCE, Vol. 127, pp. 1406-1435, 1962

2   Newmark, N.M. and W.J. Hall, "Earthquake Spectra and Design," Engineering Monographs on Earthquake Criteria, Structural Design, and Strong Motion Records, Earthquake Engineering Research Institute, 1982.

3   Lopez, R.R., "A Numerical Model for Non Linear Response of Reinforced Concrete Frame-Wall Structures," Ph.D. Dissertation, University of Illinois, Urbana, 1988.

4   Guimaraes, G.N., "Reinforced Concrete Frames Connections Constructed Using High Strength Materials," Ph.D. Dissertation, The University of Texas at Austin, December 1988.

5   Leon, R.T., "Shear Strength and Hysteretic Behavior of Interior Beam-Column Joints," ACI Structural Journal, Vol. 87, No.1, pp. 3-11, January-February 1990.

6   Alcocer, S.M., "Rehabilitation of Reinforced Concrete Frame Connections Redesigned by Jacketing," Unpublished Ph.D. Dissertation, The University of Texas at Austin.

7   Giberson, M.F., "Two Nonlinear Beams with Definition of Ductility," Journal of the Structural Division, ASCE, ST2, pp. 137-157, Feb 1969.

8   Filippou, F.C., E.P. Popov, and V.V. Bertero, "Effects of Bond Deterioration on Hysteretic Behavior of Reinforced Concrete Joints," Report No. UCB/EERC 83-19, Earthquake Research Center, University of California, Berkeley, Aug. 1983.

9   Eligenhausen, R., E.P. Popov, and V.V. Bertero, "Local Bond Stress-Slip Relationships of Deformed Bars Under Generalized Excitations," Report No. UCB/EERC 83-23, Earthquake Research Center, University of California, Berkeley, Oct. 1983.

10   Filippou, F.C., "A Simple Model for Reinforced Concrete Bar Anchorages Under Cyclic Excitations," Report No. UCB/EERC 85-05, Earthquake Research Center, University of California, Berkeley, March 1985.

11   Saiidi, M., and M.A. Sozen, "Simple and Complex Models for Nonlinear Seismic Response of Reinforced Concrete Structures", Civil Engineering Studies, Structural Research Series, University of Illinois, Urbana, August 1979.

12   Takeda, T., M.A. Sozen, and N.N. Nielsen, "Reinforced Concrete Response to Simulated Earthquakes," Journal of the Structural Division, ASCE, Vol. 96, No. ST12, December 1970, pp. 2557-2573.

13   Kreger, M.E. and D.P. Abrams, "Measured Hysteresis Relationships for Small Scale Beam-Column Joints," Civil Engineering Studies, Structural Research Series No. 453, University of Illinois, Urbana, August 1978.

14   Meinheit, D.F., "The Shear Strength of Reinforced Concrete Beam-Column Joints," Ph.D. Dissertation, The University of Texas at Austin, May 1977.

15   Farahany, M.M., "Computer Analysis of Reinforced Concrete Cross Sections," Master's Thesis, The University of Texas at Austin, December 1983.

16   American Concrete Institute, "Committee 318, Building Code Requirements for Reinforced Concrete," American Concrete Institute, Detroit, 1989.

17   American Concrete Institute, "Committee 318, Building Code Requirements for Reinforced Concrete," American Concrete Institute, Detroit, 1963.

18   American Concrete Institute, "Committee 318, Building Code Requirements for Reinforced Concrete," American Concrete Institute, Detroit, 1971.

19   International Conference of Building Officials, Uniform Building Code, 1964 Edition, Whittier, CA., 1964.

20   Scott, B.D., R. Park, and M.J.N. Priestley, "Strain-Stress Behavior of Concrete Confined by Overlapping Hoops at Low and High Strain Rates," ACI Journal, January-February 1982, pp. 13-25.

21   Orangun, C.O., J.O. Jirsa, and J.E. Breen, "A Reevaluation of Test Data on Development Length and Splices," ACI Journal, March 1977, pp.114-122.

22   Pessiki, S.T., C. Conley, R.M. White, and P. Gergely, "Seismic Behavior of the Beam-Column Connection Region in Lightly-Reinforced Concrete Frame Structures," Proceedings of Fourth U.S. National Conference on Earthquake Engineering, Vol. 2, pp. 707-716, May 20-24, 1990, Palm Springs, California.

23   Applied Technology Council, "A Handbook for Seismic Evaluation of Existing Buildings (Preliminary)," ATC-22, Redwood City, California, 1989.

24   Shah, S.N., "Evaluation of Infill Wall Strengthening Schemes for Non-Ductile Reinforced Concrete Buildings," Master's Thesis, The University of Texas at Austin, May 1989.

25   Jimenez, L.R., "Strengthening of a Reinforced Concrete Frame Using an Eccentric Wall," Master's Thesis, The University of Texas at Austin, May 1989.

26   Bush, T.D., "Seismic Strengthening of a Reinforced Concrete Frame," Ph.D. Dissertation, The University of Texas at Austin, May 1987.

27   El-Attar, A., R.N. White, P. Gergely, and C. Conley, "Shake Table Test of a 1/6 Scale 2-Story Lightly Reinforced Concrete Building," Proceedings of Fourth U.S. National Conference on Earthquake Engineering, Vol. 2, pp. 767-776, May 20-24, 1990, Palm Springs, California.

28   Applied Technology Council, "Evaluating the Seismic Resistance of Existing Buildings," ATC-14, Redwood City, California, 1987.

29   Applied Technology Council, "Tentative Provisions for the Development of Seismic Regulations for Buildings," ATC Publication ATC 3-06, Palo Alto, California, 1978.

30   International Conference of Building Officials, Uniform Building Code, 1985 Edition, Whittier, CA., 1985.

31   International Conference of Building Officials, Uniform Building Code, 1988 Edition, Whittier, CA., 1988.

32   Japan Disaster Prevention Association, "Standard for Evaluation of Existing Reinforced Concrete Buildings," revised in 1990.

33   Japan Disaster Prevention Association, "Guidelines for Seismic Retrofitting of Existing Reinforced Concrete Buildings," revised in 1990.

34   Sugano, S., and T. Endo, "Seismic Strengthening of Reinforced Concrete Buildings in Japan," Strengthening of Building Structures - Diagnosis and Theory, IABSE Symposium, Venice, Italy, 1983, pp. 371-378.

35   Alcocer, S.M., and J.O. Jirsa, "Assessment of the Response of Reinforced Concrete Frame Connections Redesigned by Jacketing," Proceedings of Fourth U.S. National Conference on Earthquake Engineering, Vol. 3, pp. 295-304, May 20-24, 1990, Palm Springs, California.

36   Badoux, M.E., "Seismic Retrofitting of Reinforced Concrete Structures with Steel Bracing Systems," Ph.D. Dissertation, The University of Texas at Austin, May 1987.

37   Aoyama, H., et. al., "Strength and Behavior of Postcast Shear Walls for Strengthening Existing RC Buildings," Proc., 8WCEE, San Francisco, California, 1984.

38   Higashi, Y., and S. Kokusho, "The Strengthening Method of Existing RC Buildings," Proc., Review Meeting of U.S.-Japan Cooperative Research Program in Earthquake Engineering", Honolulu, Hawaii, 1975.

39   Higashi, Y., et al., "Experimental Study of Strengthening Reinforced Concrete Structures by Adding Shear Wall," Proc., 7WCEE, Istanbul, Turkey, 1980.

40   Sugano, S., and M. Fujimura, "Aseismic Strengthening of Reinforced Concrete

Buildings," Proc., 7WCEE, Istanbul, Turkey, 1980.

41   Higashi, Y., T. Endo, and Y. Shimizu, "Experimental Studies of Retrofitting of Reinforced Concrete Frames," Proc., 8WCEE, San Francisco, California, 1984.

42   Higashi, Y., M. Okubo, and K. Fujimata, "Behavior of RC Columns and Frames Strengthened by Adding Precast Concrete Panels," Proc., 6WCEE, New Delhi, India, 1977.

43   Sasaki, T., et al., "An Experimental Study on Earthquake Resistant Strengthening Work for Existing RC Buildings," Proc., Review Meeting of U.S.-Japan Cooperative Research Program in Earthquake Engineering", Honolulu, Hawaii, 1975.

44   Katsumata, H., and T. Takeda, "Study on Strengthening with Carbon Fiber for Earthquake Resistant Capacity of Existing Reinforced Concrete Columns," Proc., 9WCEE, Tokyo, Japan, 1988.

45   Arakawa, T., "Effects of Welded Band Plates on aseismic Characteristics of Reinforced Concrete Columns," Proc., 7WCEE, Istanbul, Turkey, 1980.

46   Aoyama, H., and T. Ichonise, "Experimental Study on Seismic Behavior of RC Subassemblages with Slitted Spandrel Walls," Proc., 8WCEE, San Francisco, California, 1984.

47   Bass, R.A., "Interface Shear Capacity of Concrete Surfaces Used in Strengthening Structures," PMFSEL Report No. 85-4, The University of Texas at Austin, December 1985.

48   Gaynor, P.J., "The Effects of Openings on the Cyclic Behavior of Reinforced Concrete Infilled Shear Walls," Master's Thesis, The University of Texas at Austin, August 1988.

49   Sugano, S., "Study of the Seismic Behavior of Retrofitted Reinforced Concrete Buildings," Proceedings of the Session Related to Seismic Engineering at Structures Congress, Seismic Engineering: Research and Practice, pp. 669-678, ASCE, New York, 1989.

VITA

Rodrigo Manuel Jordan was born in Santiago, Chile on May 24, 1955, the son of Alberto Jordan Jordan and Maria Elena Sainte-Marie Lizana.

In March, 1973, he entered the Universidad Catolica de Chile, where he graduated as Ingeniero Civil in April, 1978. After working five years in a consulting firm, he entered the Universidad Catolica de Chile as an assistant professor. In September, 1986, he entered the Graduate School of the University of Texas at Austin. Since then he has been working on his Ph.D. degree in the Department of Civil Engineering.

Rodrigo M. Jordan married Maria Teresa Gutierrez Navas on November 11, 1978 in Chile. They have three children, Paulina, born in 1980, Rodrigo, born in 1982, and Diego, born in 1985.

Permanent address: Universidad Catolica de Chile
                       Departamento de Ingenieria Estructural
                       Casilla 6177 - Correo 22
                       Santiago, Chile

This dissertation was typed by the author.